令和 5 年度修士論文

Environmental risk assessment for mine wastes originating from the Bor Copper mining region, Eastern Serbia

セルビア東部ボール銅鉱山地域の鉱業廃棄物の環境リスク評価

オラオツェ　オセニェング

OLAOTSE OSENYENG
6521102

秋田大学大学院
国際資源学研究科博士後期課程
資源学専攻

ACKNOWLEDGEMENTS

This study was conducted as part of the project "Research on the Integration System of Spatial Environment Analyses and Advanced Metal Recovery to Ensure Sustainable Resource Development" that belongs to SATREPS program, financed by the Japan International Cooperation Agency (JICA), Japan Science and Technology (JST) and the Government of the Republic of Serbia. Budget for the field survey was provided by the Society of Resource Geology of Japan and Akita University, so I would like to thank these organizations for the financial assistance.

First I would like to thank the Ministry of Education, Culture, Sports, Science and Technology of Japan (MEXT) for providing the scholarship my MSc and PhD studies at Akita University. Secondly, I would like to give my greatest gratitude to my supervisor, Professor Yasumasa Ogawa for his guidance, patience and teachings during my 5-year study period. I would also like to thank Professor Daizo Ishiyama for his enormous support in my research. Much gratitude is owed to my friends and family for their moral support and encouragement throughout the course of my stay in Japan. My colleagues and lab mates were also pivotal in making my stay here in Japan comfortable.

Abstract

Environmental risk assessment for mine wastes originating from the Bor Copper mining region, Eastern Serbia

Introduction

The exploitation of copper (Cu) in the Bor mining region, Eastern Serbia, has produced large volumes of mine wastes especially waste rock, overburden and flotation tailings which can generate acid mine drainage. Wastewaters discharged from the Bor metallurgical facilities and flotation tailings accidentally released from the Old Bor tailings dam and into the Bor River have caused severe contamination to the Timok River system. This thesis evaluates the risks of river water and riverbed sediments contamination including the environmental implications of efflorescent salts along the riverbanks and investigates the extractability of toxic elements from mine wastes.

Risk assessment of contamination of river water and riverbed sediments

In a river water system, arsenic (As) originating from the metallurgical wastewaters generally existed as a particulate species in the entire study area during both years and was widely removed from river waters by sorption onto the hydrous ferric oxides (HFO), whereas dissolved Cu was removed from river waters only at neutral pH conditions with hydrous aluminium oxides (HAO) and HFO at the downstream reservoir site of Timok River. Despite the similarity in Cu mobility during both years, the lower pH of river waters in 2019 than 2015 enabled dissolved Cu species to be transported farther downstream, resulting in a higher level of river water pollution. The contamination factor (CF) had higher values for Cu and As compared to other metals. The CF values of Cu were the highest in sediments near Bor metallurgical/smelting facilities and at downstream reservoir site, whereas the CF values of As were generally high in the entire research field. The sequential extraction test indicated that the predominant Cu species in sediments of the upstream region were oxidizable and residual, hosted by copper sulphides from the flotation tailings, suggesting a relatively low risk of Cu release from these sediments. However, at the downstream site, the contribution of acid-soluble Cu was 34.8 %, suggesting a higher risk of Cu release. The highest contributions of acid-soluble and reducible Cu (18 %) at the reservoir site were promoted by the effective settlement of Cu-sorbing HAO and HFO. The Cu contents of these two fractions were 0.86 wt.%, almost 3 times higher than that of Cu ore in Veliki Krivelj open pit mine, therefore an economically mineable Cu content.

Environmental implications of efflorescent salts along the Bor River banks

During the summer period, the evaporation of waters from the contaminated Bor River and the upward capillary migration of riverbanks pore waters leads to the precipitation of metal sulphates which provides a temporary storage of Fe, Cu and As. These metal sulphates consisted of: Fe^{2+} (melanterite, rozenite), mixed Fe^{2+}-Fe^{3+} (copiapite), Fe^{3+} (coquimbite) and Cu (chalcanthite). The dissolution test showed that a copiapite + coquimbite assemblage generated highest acidity (pH 1.8) owing to Fe^{3+} hydrolysis and released the highest concentrations of As (43.2 mg/L). Therefore, in the event of rainfall, copiapite and coquimbite could provide an instantaneous source of acidity and dissolved Fe and As to the Bor River waters whereas chalcanthite would provide source of Cu contamination. The flotation tailings covering the Bor riverbanks and floodplains could provide a source necessary for the continuous formation of efflorescent salts.

Extractability of toxic elements from waste rocks

The 4-step BCR sequential extraction procedure does not consider the underestimation of the oxidizable fraction due to the incomplete sulphide oxidation by hydrogen peroxide (H_2O_2) during Step 3. The current study proposes a 5-step modified BCR extraction test which includes a stronger oxidizing agent, the inverted aqua-regia ($3HNO_3$:1HCl), in Step 4 to decompose sulphides remaining after Step 3. The results showed that chalcopyrite oxidized easily in H_2O_2 to extract very high Cu contents in the oxidizable fraction (Step 3). On the other hand, covellite plus enargite exhibited difficult oxidation in H_2O_2 to extract a small fraction of Cu in Step 3, however were easily oxidized by inverted aqua-regia to extract very high Cu contents in the extreme-oxidizable fraction (Step 4). From the enargite-bearing sample, contents of As extracted during Step 4 were significantly higher than those in Step 3. Pyrite also exhibited difficult oxidation in H_2O_2 whereby the contents of Fe extracted in the oxidizable fraction were extremely lower than those in the extreme-oxidizable fraction. The new 5-step sequential extraction test is very useful in the determination of easy-oxidizing and difficult-oxidizing sulphides at natural atmospheric conditions. Additionally, the procedure can be used to estimate quantities of toxic elements expected to be released from mine wastes. For example, in fresh overburden, 39 000 t of Cu could easily be released into the environment; with 83 % Cu released by the oxidation of chalcopyrite-like sulphides, 10 % Cu released by reducing/ anoxic conditions and 7 % Cu released by rain/acidic water.

1. INTRODUCTION

1.1. METAL MINING AND THE ENVIRONMENT

Mining activities involves an array of processes, ranging from prospecting, exploration, mine construction, production to reclamation. Worldwide, copper (Cu) is principally mined from porphyry copper deposits (John et al., 2010; Khorasanipour et al., 2011) which are relatively low-grade, intrusion-related deposits commonly mined by open-pit operations (Berger et al., 2008). Mining activities such as extraction and mineral processing generate large quantities of waste materials, ranging from overburden, waste rock, flotation tailings to spent ore piles (Blowes et al., 2004; Nordstrom, 2011). Through blasting, crushing, grinding and milling processes, large surface areas of reactive sulphide minerals are exposed to the atmosphere and are oxidized to generate acidic and metal-rich waters. Shafts, tunnels and drifts created by underground mining operations expose sulphides contained in host rock to oxidizing conditions. Moreover, abandoned open pits tend to fill with water that reacts with the remaining sulphide ore. Therefore, mining significantly accelerates the oxidation of sulphide minerals, leading to the generation of acid mine drainage (Lottermoser, 2010; Sun et al., 2015).

1.2. RESEARCH PROBLEMS

The quality of river waters in the Bor Cu mining region has been investigated by several authors (Ishiyama et al., 2012; Đorđievski et al., 2018; Adamović et al., 2021). These researchers reported two sources of river water contamination; (1) acid mine drainage from mine waste dumps and (2) wastewaters originating from the metallurgical/smelting facilities. They also established that smelter wastewaters have the largest environmental impact and that the operating conditions at the smelter causes variation in the quality of river waters. However, studies on the mobility variations of toxic elements as a function of pH has not been carried

out. Also, a comparison in risk levels of river water contamination as a function of smelter operating conditions has not been performed.

The mineralogical and geochemical characteristics of the riverbed sediments in the Bor Cu mining region have been investigated by Đorđievski et al. (2018) and the results suggested two possible sources of sediments contamination; (1) flotation tailings accidentally released from impoundments and into the river system and (2) toxic elements chemically precipitated from the overlying river waters. This PhD thesis will contribute to that previous study by estimating the contamination level of the sediments using pollution indices and clarifying the origins of the contaminants using sequential extraction techniques.

In mine waste dumps such as overburden, sulphide minerals are usually present at the deeper parts. At these depths, sulphide oxidation is occurring, with the aid of sulphide oxidizing microorganisms, to generate solutions of high acidity and elevated concentrations of toxic elements. Some of these solutions seep out at the base of the overburden pile to accumulate into acid mine lakes or streams. Other solutions are transported to the surface by upward capillary migration. At the surface, high temperatures cause the evaporation of water, leading to the precipitation of hydrated metal sulphates. In this way, there are two mechanisms of acid generation and toxic metals release in overburden; namely sulphide oxidation and sulphate dissolution.

Based on these two mechanisms, during a Master's thesis, surface overburden samples were reacted with distilled water (pH 5.6) to investigate their acid generation potential. The investigation revealed that an acidic solution (pH ~3.3) was generated. However, that research was limited since the actual source of acidity was not detected by mineralogical investigations. Because of that, this PhD thesis will provide evidence that sulphate dissolution is the source of acidity in surface overburden.

Additionally, the chemical speciation of toxic elements in surface overburden and flotation tailings was investigated using the 4-step modified BCR sequential extraction procedure. However, since these waste materials generally contain low sulphide contents, the research in Master's thesis could not observe the incomplete oxidation of sulphides associated with this procedure. For this reason, this PhD thesis will use high-sulphide mine wastes to develop an optimized sequential extraction procedure that will consider the incomplete oxidation of sulphides observed in the 4-step modified BCR sequential extraction and therefore help distinguish between easy-oxidizing sulphides from difficult-oxidizing sulphides.

1.3. ACID MINE DRAINAGE (AMD)

The oxidation of sulphide minerals is a naturally occurring process involving the interaction of sulphide-containing rocks with oxygen and water and is referred to as acid rock drainage (ARD) (Egiebor and Oni, 2007). In an undisturbed environment, the ARD process is relatively slow. When mining is involved, an acid drainage generated is termed acid mine drainage (AMD) (Skousen et al.,1994; Komnitasas et al., 1995; Youngerand and Wolkersdorfer, 2004; Seal and Shanks, 2008; Nordstrom, 2011). AMD can be visually observed in different localities such as at the center of abandoned open-pits as an acid mine lake or at the base of overburden materials either as wastewater stream or pool. Depending on the predominant precipitated metal oxides/sulphates, AMD can show a variety of colors, mostly red which is a characteristic of iron oxides and green, which indicates that copper is dominant in the AMD.

AMD has been responsible for the acute contamination of water sources such as groundwater, streams and rivers. Examples of severe cases of acid mine drainage include; the AMD from the Richmond Mine (pH -3.6) in the Iron Mountain, California, USA (Nordstrom et al., 1999), AMD from Iron Duke mine (pH 0.5) in Zimbabwe (Williams and Smith, 2000), AMD of Apliki pit lake (pH 2.7-3.2) (Antivachis et al., 2016), AMD from overburden in mines of Old Bor (pH

2.6-3.4) and Veliki Krivelj (pH 3.3) in Eastern Serbia (Đorđievski et al., 2018), the Tinto River (pH 2.5) in Huelva, SW Spain (Sánchez-España et al., 2005; Olias et al., 2020), Kosva River basin (pH 2.3-4.3) in Russia (Ushakova et al., 2022).

1.4. SULPHIDE MINERAL OXIDATION

The process of sulphide mineral oxidation involves a complex array of factors, among which the most important include oxygen, ferric ion (Fe^{3+}), temperature, pH, Eh and the action of microorganisms (Nordstrom 1982; Weirsma and Rimstidt 1984). Pyrite (FeS_2) is ubiquitous in sulphur bearing ores and is therefore used to illustrate the chemical reactions involved in the generation of AMD. As mentioned above, mining processes tends to expose pyrite to the atmosphere, to react with oxygen and water through Reaction 1.1.

$$FeS_{2(s)} + 7/2O_{2(g)} + H_2O_{(l)} \rightarrow Fe^{2+}_{(aq)} + 2SO_4^{2-}{}_{(aq)} + 2H^+_{(aq)} \quad (1.1)$$

$$2Fe^{2+}_{(aq)} + ½\ O_{2(g)} + 2H^+_{(aq)} \rightarrow 2Fe^{3+}_{(aq)} + H_2O_{(l)} \quad (1.2)$$

$$Fe^{3+}_{(aq)} + 3H_2O_{(l)} \leftrightarrow Fe\ (OH)_{3(s)} + 3H^+_{(aq)} \quad (1.3)$$

$$FeS_{2(s)} + 14Fe^{3+}_{(aq)} + 8H_2O_{(l)} \rightarrow 15Fe^{2+}_{(aq)} + 2SO_4^{2-}{}_{(aq)} + 16H^+_{(aq)} \quad (1.4)$$

The dissolved ferrous iron (Fe^{2+}) and sulphate ions (SO_4^{2-}) produced cause an increase in the total dissolved solids in the water while hydrogen ions are indicative of acid generation (Lottermoser, 2008; Jennings et al., 2008). When there is sufficient dissolved oxygen in the reacting water, Fe^{2+} is further oxidized to Fe^{3+} through Reaction 1.2 (Jennings et al., 2008). This step is referred to as the rate-determining step for the overall reaction sequence under pH < 4 (Singer and Stumm, 1970). The rate of this reaction is usually accelerated by the role of Fe^{2+} oxidizing microorganisms (Udayabhanu and Prasad, 2010). When the pH increases to 3.5, Fe^{3+} will hydrolyze and precipitate as a solid ferric hydroxide, accompanied by the release of more protons into the solution (Reaction 1.3). The additional acidity generated will lower the pH of the waters, allowing more Fe^{3+} to stay in the solution (Lottermoser, 2010). When the

Fe^{3+}-laden solution comes in contact with pyrite, the direct oxidation of pyrite by Fe^{3+} would occur (Reaction 1.4). This reaction occurs at pH conditions below 3.5 (Udayabhanu and Prasad, 2010). This produces Fe^{2+} which can then be oxidized via reaction 2 to produce more Fe^{3+}. The Fe^{3+} will, in turn, oxidize pyrite via Reaction 1.4 which produces more Fe^{2+} and so on. In the presence of sufficient atmospheric oxygen, the produced Fe^{2+} continues the cycle of Reactions 1.2 and 1.3 (Younger et al., 2002).

Microorganisms are ubiquitously present in sulphide-containing mine wastes, accelerating the oxidation of sulphides. There are two mechanisms of microorganism's action in the oxidation of pyrite; (1) the direct mechanism, which involves the bacteria *Acidophilic sulfur* having physical contact with pyrite in Reaction 1.1 to yield Reaction 1.5; and (2) the indirect mechanism by the Fe^{2+}-oxidizing bacteria *Thiobacillus ferrooxidans* in Reaction 1.2 to yield Reaction 1.6 (Southam and Beveridge, 1992; Ledin and Pedersen, 1996; Kelly and Wood, 2000).

Acidophilic sulfur

$$FeS_{2(s)} + 3.5O_{(g)} + H_2O_{(l)} \longrightarrow Fe^{2+}{}_{(aq)} + 2SO_4{}^{2-}{}_{(aq)} + 2H^{+}{}_{(aq)} \quad (1.5)$$

Thiobacillus ferrooxidans

$$2Fe^{2+}{}_{(aq)} + ½\ O_{2(g)} + 2H^{+}{}_{(aq)} \rightarrow 2Fe^{3+}{}_{(aq)} + H_2O_{(l)} \quad (1.6)$$

2. STUDY AREA

2.1 Climate and hydrology

The Bor mining area is located in a town called ‘Bor’ in the Eastern Serbia and is characterized principally by a moderately continental climate. Cupać et al. (2014) reported that the minimum temperatures can be as low as -14 °C whereas the maximum temperatures can be as high as 35 °C. Snowfall usually starts in December to February, while snowmelt occurs in March to April. Rainfall is frequent in the months of May to mid-July, followed by the driest and hottest months of August and September where average daytime temperatures range from 26-30 °C and relative humidity range from 40-66%. The average annual precipitation is reported at 550 mm. The Bor mining region is found within the Timok river drainage system whose rivers consists of the Bor River, Krivelj River, Bela River, Ravna River and Timok River.

2.2 Geology

The Bor mining region lies within the Timok Magmatic Complex (TMC), an 85 km long complex extending from ‘Majdanpek’ village in the north to the ‘Bučje’ village in the south (Figure 2.1). The estimated radiometric age of the Timok magmatic complex is from 90 to 78 Ma (Clark and Ullrich, 2004; Von Quadt et al. 2005; Banješević, 2010). The geology of TMC is characterized by several magmatic suites for which the ones located in the eastern part, covering the Bor mining region, include the Bor clastites, Timok andesite (AT) and Metovnica epiclastite (EM) as indicated by Figure 2.1. These volcanic rocks were formed during the Upper Cretaceous.

The Timok andesite, predominantly amphibole andesite and high-potassium trachyandesites, occur in the eastern parts of the TMC, where they overlie Cenomanian and Turonian sediments and are covered by Senonian sediments and the Metovnica epiclastite (Banješević, 2015). These andesites are distinguished by the following facies: lava flows, lava domes, shallow

intrusions and various volcaniclastic rocks (Banješević, 2010). According to the high precision U/Pb, $^{40}Ar/^{39}Ar$ (Von Quadt et al. 2002 and Clark & Ullrich 2004), the Timok andesite age ranged from 89.0±0.6 to 84.26±0.67 Ma.

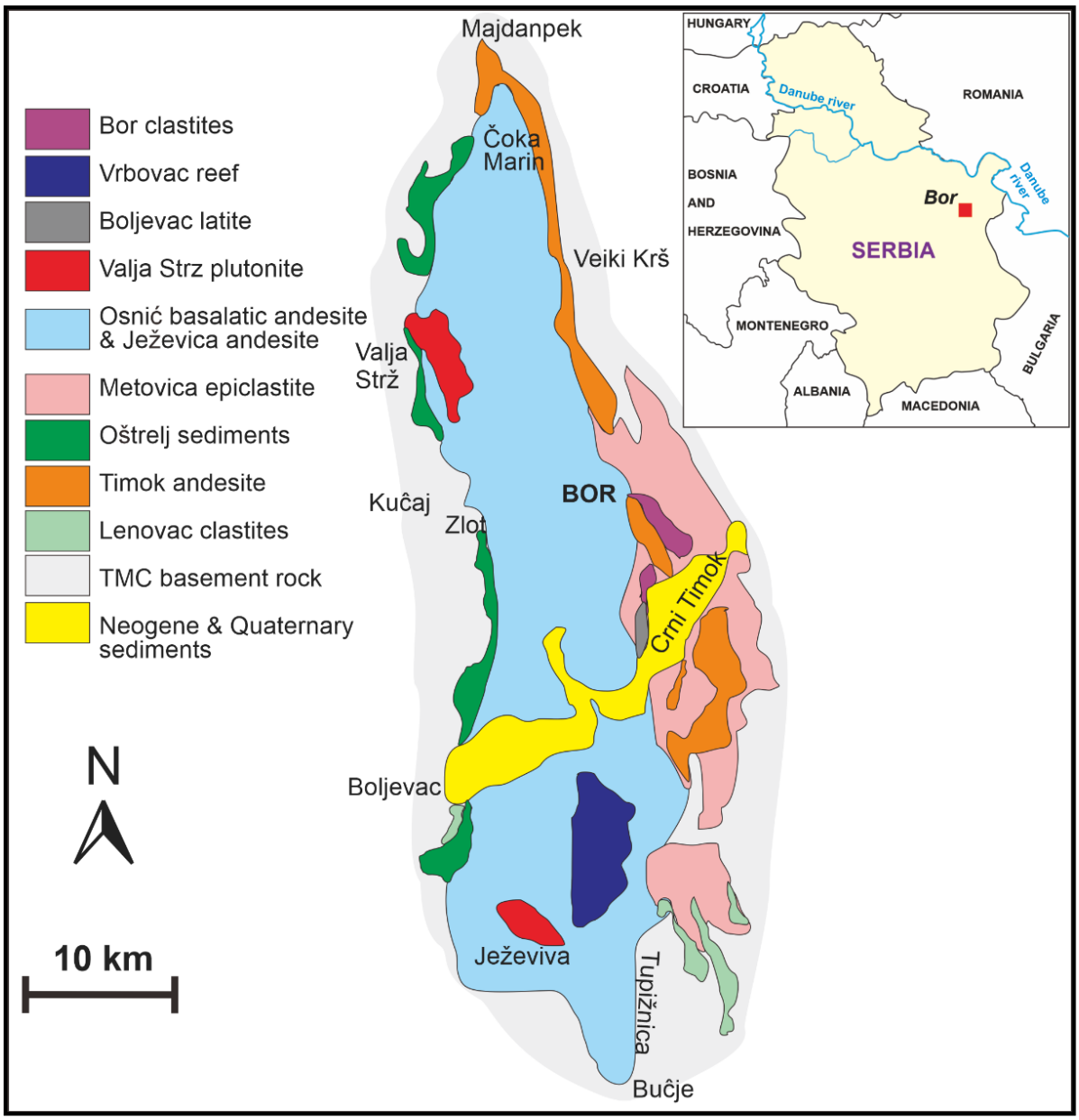

Figure 2.1 Simplified **g**eological map of the Timok Magmatic Complex (TMC), modified after Jelenković et al. (2016)

Metovnica epiclastite (EM) (Figure 2.1), also known as "pyroclastites or volcanoclastites" (Banješević, 2010) are found in the Metovnica village, south of Bor and near to the open-pit in Bor. Đorđević and Banješević (1997) reported that the EM developed in the eastern part of the

TMC in a shallow marine environment where they infill volcanic bedrocks. The rocks are coarse- to fine-grained, massive, coarsely banded, sometimes even laminated.

2.3 Mineralization

The mineralization in the Bor mining region consists of several ore fields such as the Bor, Veliki Krivelj, Cerova and Brestovac ore fields.

2.3.1 Bor ore field (Bor ore deposits)

There are two styles of mineralization in the Bor ore system; (1) the well-developed, sub-cropping massive, high sulphidation Cu-Au deposit on top (Armstong et al., 2005) and; (2) the porphyry copper deposit, known as the 'Borska Reka', located along the NW-SE striking Bor fault, below the massive sulphides (Simic and Mihajlović, 2006). These mineralization styles, continuously linked with one another, are hosted by the hydrothermally altered hornblende-biotite andesites and pyroclastites. Hydrothermal alterations in the Bor deposits are characterized by silicification, advanced argillic, propylitic (abundant illite and chlorite) and kaolinisation. Advanced argillic alteration and pervasive silicification marks transition zone between the high sulphidation and porphyry mineralization. The key sulphide minerals of the high sulphidation deposit consist of chalcocite, covellite, enargite, chalcopyrite and pyrite whereas mineral composition of the porphyry Cu deposit includes pyrite, chalcopyrite, bornite, chalcocite, covellite, magnetite and hematite (Kozělj, 2002; Janković, 1980; Armstong et al., 2005). Gangue minerals include neobiotite, gypsum, anhydrite, alunite, illite and chlorite.

2.3.2 Veliki ore field (Veliki Krivelj ore deposits)

The Veliki Krivelj porphyry Cu deposit is formed in the domain of dyke system above magmatic complexes and is hosted by the hydrothermally altered andesites and pyroclasts formed during the Upper Cretaceous (Armstrong et al., 2005). The mineral associations consist chalcopyrite and pyrite, minor hematite and magnetite, traces of covellite, enargite, bornite,

chalcocite and galena. Hydrothermal alterations comprise of biotitization, sericitization, silicification and pyritization. Gangue minerals are quartz and less often calcite, barite, siderite.

2.3.3 Cerova ore field

The Cerova is a small porphyry ore deposits located north of Old Bor mine. It is composed of sediments formed during the Lower Cretaceous as well the hydrothermally altered intrusive rocks and volcano-sedimentary units. The deposits show two distinctive zones: the oxidation zone and the secondary sulphide enrichment zone, which is exploited for Cu. The dominant minerals are chalcocite and covellite.

2.3.4 Brestovac ore field (Čukaru Peki Cu-Au deposit)

The mineralization identified at the Čukaru Peki deposit belongs to the epithermal and porphyry copper-gold types (Banješević and Large, 2014). The host rocks are the Upper Cretaceous hornblende and hornblende biotite andesites, andesite breccia and hydrothermal breccia. There are three styles of mineralization at Čukaru Peki deposit (1) High sulphidation Cu-Au massive-sulphides; (2) Porphyry Cu-Au deposits and (3) Transitional epithermal zone; located between the high sulphidation and porphyry Cu-Au mineralization.

2.4 History of mining

The exploitation of copper sulphide ores in the Bor mining region started in 1902 with underground operations at the 'Jama Bor' underground mine (Figure 2.2) which is still active. During that time, the copper ore content was 17 % (EJAtlas, 2016). In 1912, open-pit operations were initiated with the opening of 'Open-Pit Mine Bor' which was later closed in 1986. Currently, there are two active open-pit mines in the area, namely; Veliki Krivelj open-pit mine (opened in 1979) and Cerovo open-pit mine (opened in 1990). Stevanović et al. (2013)

and Stanković et al. (2015) reported that the current estimated copper content from the open-pit mines is around 0.3 %. The mining and mineral processing operations have been run by the state enterprise 'RTB-Bor'. However, in December 2018, a Chinese company 'Zijin Mining' bought and took over the mining and smelting operations and changed the name to 'Zijin Bor Copper'.

2.5 Smelting of Cu

The first smelting plant for metallurgical treatment of copper concentrate was commissioned in 1904 (Marković, 2014; Stirbanović et al., 2014). At this plant, the copper concentrate, produced by flotation techniques, is treated by pyro-metallurgical processes to obtain copper anode (Stevanović et al., 2013). This process generates two types of wastes: slag and sulphur dioxide which is the main source of air pollution in Bor (Urosĕvić et al., 2018). Stanojlović et al. (2014) reported the mineralogy of the smelting slag was dominated by fayalite (60 %) and magnetite (30 %) and contents of Fe and Cu were 38 and 0.87 wt%, respectively. Metallurgical/smelter facilities generate wastewaters that have been discharged directly into the Bor river without treatment (Ishiyama et al., 2012; Bugarin et al., 2013; Stevanović al., 2013; Đorđievski et al., 2018; Osenyeng et al., 2023).

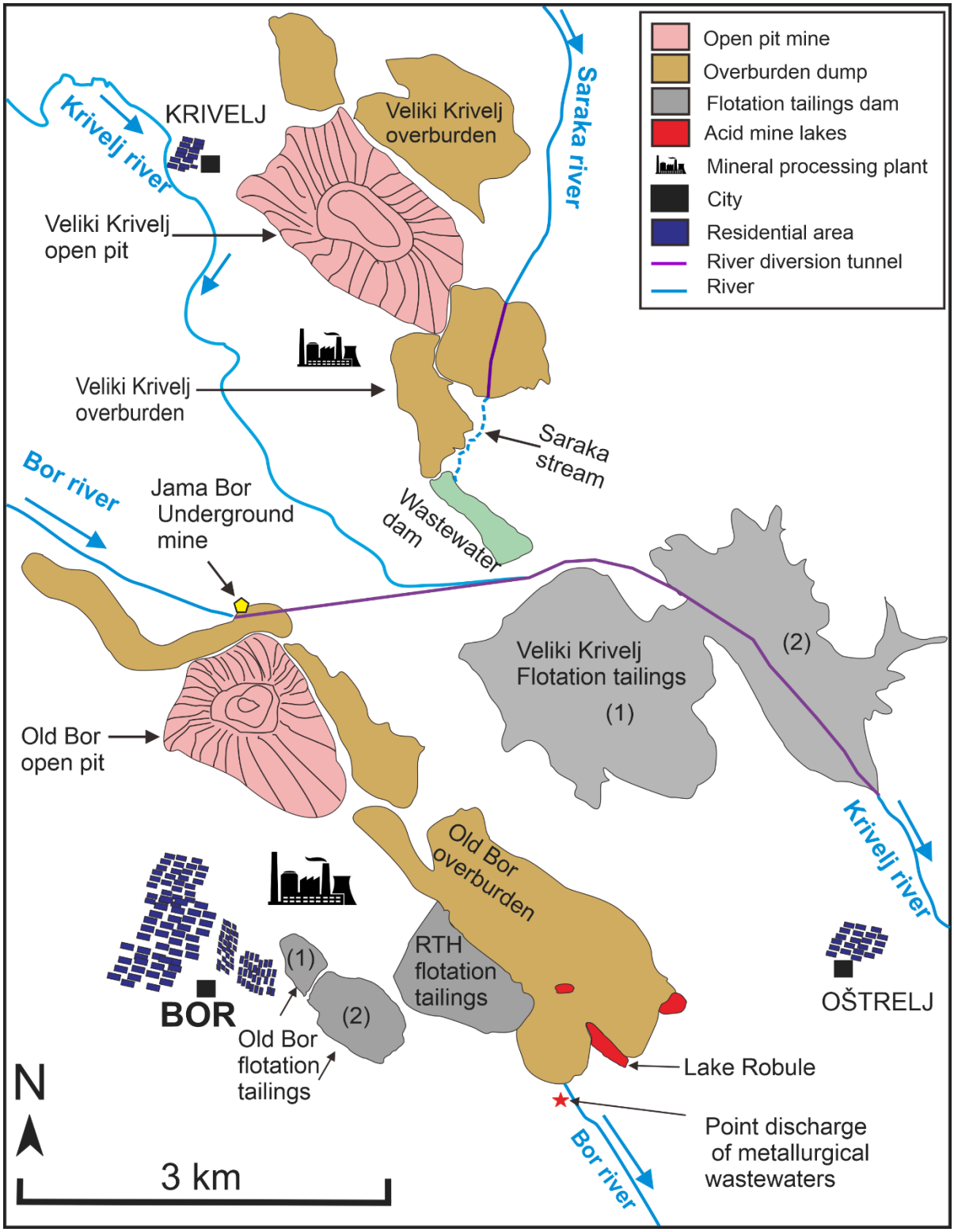

Figure 2.2 Map of the Bor copper mining region. Features such as open-pit, overburden heaps and flotation tailings dams were drawn using aerial photograms from Google Earth

2.6 Generated mine waste materials

Mining and mineral processing activities generate extremely large volumes of waste materials. Godin (1991) pointed out that an average mine immediately rejects 42% of the total mined material as waste rock, 52% of the ore is separated via the beneficiation processes (crushing, grinding, separation, flotation) as tailings, 4% leaves the smelter as slag, and only 2% is retained as the commodity for which the ore was extracted. In addition to the obvious aesthetic/visual pollution of the landscape, these voluminous mine wastes contain chemically reactive sulfide minerals that can generate acid mine drainage. In the Bor mining area, the extensive exploitation of copper ore has led to the generation of large volumes of overburden and flotation tailings (Figure 2.2). Bogdanović et al. (2011) and Marković et al. (2014) have estimated that, in total, there are about 700 Mt of overburden and flotation tailings around the Bor and Veliki Krivelj mines.

2.6.1 Overburden

Overburden is defined as any material (soil, rock and other rejects) that lies above the orebody and needs to be removed to access the deposit during open-pit operations (Prashant et al., 2010). Overburden materials are deficient in plant nutrients due to removal of biologically rich top soil (Maharana et al., 2015). The dissolution of sulphate minerals at the surface of the overburden and the oxidation of sulphide minerals at the deeper part of the overburden generate acid mine drainage, a significant environmental hazard. Indeed, during a Master's thesis, surface overburden from the Bor Cu mining area were tested for acid-generation potential by reacting with distilled water (pH 5.6) and the result indicated an acidic solution with pH ranging from 2.7 to 4.6 after 6 hours of reaction.

There are two overburden piles in the Bor Cu mining region; the Old Bor overburden, (Figure 2.3a) and Veliki Krivelj overburden (Figure 2.3b). The Old Bor overburden site is significantly

larger than the Veliki Krivelj overburden site (Figure 2.2). These materials are light reddish-brown and have been extensively weathered as evidenced by water erosion channels (Figure 2.3a and b) and have particle size ranging from fine sand to gravel size. The hydrological system of both overburden sites receive water mainly from rain. Stanojlović et al. (2014) sampled and performed geochemical analysis of Veliki Krivelj overburden and reported Fe and Cu contents as high as 4.97 and 0.23 wt %, respectively. Đorđievski et al. (2016) sampled an overburden material from Old Bor and reported that the Fe, Cu and As contents were 4.5, 0.06 and 0.012 wt%, respectively. During a Master's thesis, results from the geochemical analysis of surface overburden materials indicated values ranging from 28 000-55 000 mg/kg for Fe, 88-930 mg/kg for Cu and 7.6-108 mg/kg for As. Moreover, XRD analysis could not detect sulphide minerals, however, traces of pyrite were observed from all samples by reflected light optical microscopy.

2.6.2 Waste rocks/ discarded ore

Waste rock is an ore mined and transported out of the pit, however it is discarded or thrown out either due to very low contents of target metal or it contains minerals with undesirable elements (e.g. As). Waste rocks from Old Bor open-pit mine are found localized at the Old Bor overburden pile (Figure 2.3c) whereas from those from Veliki Krivelj mine are currently being dumped on Veliki Krivelj overburden (Figure 2.3d). Đorđievski et al. (2016) sampled a localized waste rock from the Old Bor overburden pile, performed mineralogical analyses using XRD and reported the presence of covellite, enargite and pyrite. The authors also performed XRF analysis of that sample and reported that the contents of Fe, Cu and As were 18.8, 21.9 and 1.6 wt%, respectively. Since mining in the Old Bor open-pit was started 1912 and ended in 1986, it is possible that this rock represents an ore that was discarded either due to lack of mining technology to separate covellite from enargite as well as Cu from As in enargite.

Compared to overburden materials, these waste rocks are present in very small volumes and therefore has infinitesimal environmental impact.

2.6.3 Flotation tailings

Flotation tailings are waste materials left after the beneficiation process, where the valuable ore have been separated from the uneconomic fraction. These are usually sand- and silt-sized particles and are disposed of by slurry-pumping to an impoundment. There are five flotation tailings ponds in the Bor mining area; the Old Bor Flotation Tailings Fields 1 and 2, 'RTH' Flotation Tailings pond and Veliki Krivelj Flotations Fields 1 and 2 (Figure 2.2, Figure 2.3.e and f). Conic et al. (2020) reported the contents of Al, Fe, Cu and As from the Old Bor tailings at 6.58, 7.78, 0.2 and 0.02 wt %, respectively. Stanojlović et al. (2014) were reported the contents of Fe and Cu from the Veliki Krivelj tailings at 5.18 and 0.8 wt %, respectively. The bulk chemical investigations of tailings conducted during a Master's thesis indicated contents ranging from 27 200-75 000 mg/kg for Fe, 51-1512 mg/kg for Cu and 1.9-121 mg/kg for As. Similar to overburden, XRD analysis of the tailings could not detect sulphide minerals, however, traces of pyrite were observed from all samples by reflected light optical microscopy. The Old Bor flotation tailings were also tested for acid-generating potential and the results showed an acidic pH ranging from 2.7 to 4.5

During the 1960s, heavy rains and dam technical failures led to the accidental release of fine-grained flotation tailings from the Old Bor flotation tailings pond into the Bor river (Paunović, 2010; Bogdanović et al., 2014; Stanojlović et al., 2014). These flotation tailings were transported by water downstream and contaminated riverbed sediments and floodplains of the Timok River system (Stevanović, 2012; Mikić et al., 2013; Đorđievski et al., 2018). The reported contents of toxic elements from the polluted riverbed sediments in the Timok River system ranged from 54 800-306 000 mg/kg for Fe, 264-16 300 mg/kg for Cu and 115-673 mg/kg for As (Đorđievski et al., 2018).

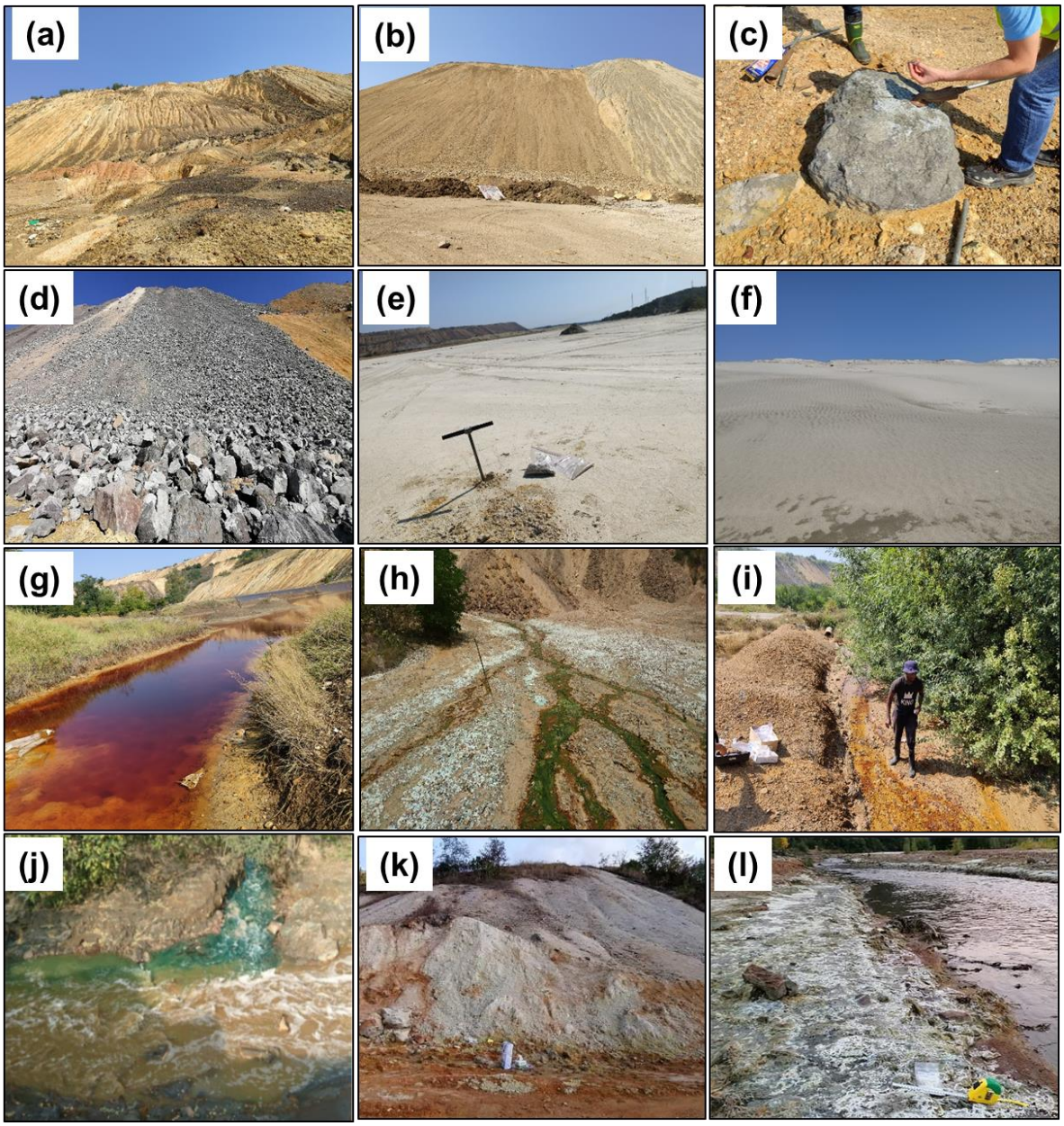

Figure 2.3 Photographs of the environmental signatures in the Bor Cu mining area. (a) Old Bor overburden, (b) Veliki Krivelj overburden, (c) Old Bor waste rock, (d) Veliki Krivelj waste rock, (e) Old Bor flotation tailings dam, (f) Veliki Krivelj flotation tailings dam, (g) Robule acid mine lake, (h) Veliki Krivelj overburden leakages, with efflorescent salts, (i) Jama Bor drainage water, (j) Bor metallurgical/smelter wastewaters, (k) Efflorescent salt at the base of Old Bor overburden, (l) Efflorescent salt along the Bor River

2.6.4 Wastewaters and acid mine drainages

Wastewaters in the Bor mining area are classified as: acid mine drainages from overburden, acid mine lakes, underground mine drainage waters, open-pit drainage waters, tailings pond drainage waters and metallurgical/smelter wastewaters. At the toe of Old Bor overburden, there is an extremely acidic, deep red-colored acidic mine lake 'Robule' (Figure 2.2 and 2.3g). At the base of Veliki Krivelj overburden, there is highly acidic green–colored wastewater stream 'Saraka' (Figure 2.3h). These acid mine drainages are accumulations of leached solutions generated by the oxidation of sulphide minerals in the Old Bor overburden and Veliki Krivelj overburden (Korać, 2006; Ishiyama et al., 2012; Gardić et al., 2015, 2017). There are also acidic and metal-loaded drainage waters originating from the 'Jama Bor' underground mine (Figure 2.3i). The blue-colored wastewaters generated at the Bor metallurgical/smelter facilities (Figure 2.3j) are discharged directly into the Bor River and have been reported to have large environmental impact on the Timok river system (Ishiyama et al., 2012; Bugarin et al., 2013; Stevanović al., 2013; Đorđievski et al., 2018; Osenyeng et al., 2023).

2.6.5 Evaporative salts

Colorful and popcorn-textured efflorescent salts are observed in several locations around the Bor mining area. These evaporative salts are abundant in the driest and hottest season, August and September. There is a plethora of these salts on the banks of Lake Robule, along the flow paths of leakages from Veliki Krivelj (Figure 2.3h) and North-Old Bor overburden (Figure 2.3k), Jama Bor drainages as well as on the banks of Bor River (Figure 2.3l). Since are highly soluble, they dissolve easily in rainwater to release acidic solutions with extremely high concentrations of toxic elements that can reach river waters, causing further contamination.

3. ENVIRONMENTAL RISK ASSESSMENT OF THE CONTAMINATION OF RIVER WATER AND SEDIMENTS FROM THE BOR MINING AREA, EAST SERBIA - SECONDARY CU ENRICHMENT AT THE RESERVOIR SITE

3.1 . INTRODUCTION

3.1.1 Contamination of river waters by the Bor Cu mining activities

Wastewaters originating from the Bor metallurgical/smelting facilities are the main source of contamination for the Bor River (Ishiyama et al., 2012; Bugarin et al., 2013; Stevanović al., 2013; Đorđievski et al., 2018). In fact, the Bor River presents a case of acute river pollution since its headwaters comprise solely of the untreated wastewaters from the metallurgical/smelting facilities, municipality and AMD leakages from the overburden. As a result, the Bor mining area represents a serious case of severe environmental pollution by the mining and processing of Cu from porphyry copper ore deposits.

The pH conditions of the Bor River and downstream environments change largely depending on the running conditions of the Bor metallurgical/smelter facilities. Indeed, river waters observed during this PhD thesis were more acidic compared to the previous research in 2015 (Đorđievski et al., 2018). However, the mobility of toxic elements as a function of pH variations in polluted rivers has not been studied. Also, the assessment of risk levels of river water contamination based on acidity and dissolved species of toxic metals (Ficklin et al., 1992; Plumlee et al.,1992) have not been performed in the Timok River system.

3.1.2 Mobility of toxic elements –formation of HFO and HAO

In a water column of AMD-impacted river systems, toxic metals and As are transported as either dissolved or fixed to the suspended particles (Montecino et al., 2020; Chikanda et al., 2021; Ye et al., 2022). Hydrous ferric oxides (HFOs) and hydrous aluminium oxides (HAOs) are the suspended particles with remarkable sorption properties, owing to their poor crystallinity, higher porosity and larger surface areas, therefore are very important in the

removal of toxic elements from contaminated waters (Montecinos et al., 2020; Chikanda et al., 2021; Lalinská-Voleková et al., 2022). Kaasalainen et al. (2019) and Lalinská-Voleková et al. (2022) noted that HFO include several minerals, such as schwertmannite and ferrihydrite. The formation of these particles is largely dependent on the pH of the surrounding waters, as well as temperature (Schemel et al., 2007; Ogawa et al., 2012). By extension, the adsorption of heavy metals and As onto HFO and/or HAO would also be pH-dependent (Lee et al., 2002).

3.1.3 Sorption of toxic elements onto HFO and/or HAO

In an acidic and oxidizing environment, the arsenate species [As(V)] is dominant over the arsenite species [As(III)]. The arsenate species forms an oxyanion ($HAsO_4^{2-}$) which tends to preferentially adsorb onto positively charged Fe^{3+} mineral surfaces such as schwertmannite (Regenspurg and Pfeiffer 2004; Acero et al. 2006; Espana-Sanchez et al., 2007; Cheng et al., 2009), thereby removed from the waters. Ogawa et al. (2012, 2013) reported higher contents of As originating from hot springs being sorbed onto HFO at pH 3.5 - 4.0. The role of the suspended particles in the removal of toxic elements from the river waters of the Timok river system has not been previously investigated.

Nordstrom and Alpers (1999) noted that divalent cations (Cu or Zn) can either be transported as dissolved species, fixed in other secondary phases such as sulphates, coprecipitate with and/or adsorbed to the hydrous iron oxides. Lee et al. (2002) and Acero et al. (2006) observed that at a low pH conditions, the adsorption of metals such as Cu, Mn and Zn is very limited. However, Montecinos et al. (2020, 2022) mentioned that HFO chemically fractionates Cu between the dissolved and the particulate state at pH > 5 while HAO promotes the physical removal of Cu-sorbing particles through gravitational settlement at pH ~ 7. Espana-Sanchez et al., 2007 Cu and Zn were only slightly sorbed onto HAO at pH > 5.

3.1.4 Contamination of riverbed sediments

Riverbed sediments act as natural sinks of contaminants from polluted rivers. The settlement of suspended materials from the contaminated river waters enriches the riverbed sediments, thereby causing serious pollution (Strzebońska et al., 2017; Wei et al., 2019; Sanchez et al., 2022; Iordache et al., 2022). The accumulation of toxic elements in riverbed sediments poses a direct threat to the benthic organisms and consequently other aquatic life forms via the transfer along the food chain (Ali and Khan, 2018; Mohammadi et al., 2020). The aggregation of suspended nanoparticles fills the openings/interstices in the riverbeds, thereby reducing the quality of habitats for aquatic flora and fauna. For example, Witters et al. (1996) postulated that in the river system, colloidal Al can be more toxic to fish than dissolved Al.

In the Bor mining area, researches on riverbed sediments focused mainly on bulk mineralogy and chemical composition (Filimon et al., 2013, 2016; Đorđievski et al., 2018). Therefore, the contribution of this PhD thesis will be estimating the contamination level of the riverbed sediments by using pollution indices such as contamination factor and ecological potential risk (Wei et al., 2019; Luo et al., 2020; Sakan et al., 2021; Zhuang et al., 2021; Sanchez et al., 2022). However, it is important to acknowledge that the use of bulk chemical composition of contaminants to evaluate the pollution of riverbed sediments is, in general, very limited with regards to chemical speciation, metal solubility and bioavailability (Ma and Rao, 1997). Furthermore, it is imperative to consider the fact that when the physicochemical conditions of the river system change, toxic elements will desorb and be released back into the water column, thus causing secondary water pollution (Xia et al., 2020; Miranda et al., 2021; 2022). For these reasons, this PhD thesis will use sequential extraction procedures to investigate the chemical fractionation of toxic elements in riverbed sediments thereby elucidating the strength of chemical bonds between the target elements and components in the riverbed sediments (Tessier et al., 1979; Ure et al., 1993; Filgueiras et al., 2002; Callender, 2003).

3.1.5 Sequential extraction techniques

The investigations of bulk mineralogy and chemical composition of solid materials are very limited in the assessment of availability and toxicity of toxic elements to the environment (Marin et al., 1997). The concept of sequential extraction primarily involves subjecting a solid material, such as waste rock, tailings, overburden, sediment and soil, to successive attacks by a series of progressively stronger reagents to dissolve increasingly resistant minerals. These schemes act as a simulation of the chemical reaction that could occur under different conditions in the natural environment. Sequential extraction tests are very important in water-rock environments as they provide information about the origin, mode of occurrence, physicochemical availability, biomobilization and transport of potentially toxic elements (Tessier et al., 1979; Ure et al., 1993; Filgueiras et al., 2002; Callender, 2003). Moreover, sequential extraction tests can effectively facilitate the evaluation and remediation strategies of areas contaminated with toxic metals.

3.1.5.1 BCR sequential extraction

The four-step BCR sequential extraction procedure was established by the Community Bureau of Reference (BCR) as a means of standardizing the sequential extractions schemes, thereby providing the means to compare the results worldwide and validate other procedures. Additionally, the BCR procedure provided the means to improve the quality of data obtained from the extractions of soils and sediments and has been performed successfully in several studies (Ure et al., 1993; Cappuyns et al., 2007; Alvarez-Valero et al., 2009; Pascaud et al., 2013; Zhai et al., 2014). In this procedure, there are four operationally defined steps: Step 1, acetic acid (0.11 mol/L, pH 2.9); Step 2, hydroxyl ammonium chloride (0.1 mol/L, pH 2); Step 3, hydrogen peroxide (8.8 mol/L, pH 2) with ammonium acetate (1 mol l/L, pH 2); and Step 4, aqua-regia ($1HNO_3$:3HCl).

3.1.5.2 Modified BCR sequential extraction

The main modification of the BCR sequential extraction procedure was intended to improve data reproducibility in the reducible fraction (Rauret et al., 1999; Filgueiras et al., 2002). This modification involved the increase in concentration of hydroxyl ammonium chloride from 0.1 to 0.5 mol/L and increasing the acidity of this reagent from pH 2 to pH 1.5 by the addition of nitric acid during the Step 2 extraction stage. This procedure has been used extensively in investigations of mine wastes (Yun-Guo et al., 2006; Alvarez-Valero et al., 2009; Kerolli-Mustafaet al., 2015; Zheng et al., 2018; Barcelos et al., 2020).

Several researches have reported that, during Step 3, the oxidation of organic matter and sulphide minerals by hydrogen peroxide is incomplete (Tessier et al., 1979; Forstner,1985; Campanella et al., 1995; Filgueiras et al., 2002; Galán et al., 2003; Sutherland et al., 2009; Favas et al., 2011). This leads to the underestimation of the oxidizable toxic metal contents and therefore, an underrate prediction of acid mine drainage generation.

3.1.5.3 Toxic elements speciation fractions

A description elemental targets or the retention fraction of the original and the modified BCR sequential procedure were provided by several authors (Tessier et al., 1979; Ure et al., 1993; Marin et al., 1997; Rauret et al., 1997).

3.1.5.3.1 Water, acid soluble and exchangeable fraction

The toxic elements extracted by acetic acid during this step include; water-soluble, exchangeable and acid-soluble contents. The water-soluble fractions include metals and As hosted by the hydrated metal sulphates such as melanterite ($FeSO_4 \cdot 7H_2O$), chalcanthite ($CuSO_4 \cdot 5H_2O$) etc. and can easily be released upon dissolution by rainwater or river waters. Exchangeable metals include those weakly adsorbed on surfaces of rocks, tailings or sediments by relatively weak electrostatic forces and will be released by ion-exchange processes. Acid-

soluble metals are those co-precipitated with carbonates and will be mobilized by acidic waters. When assessing metal mobility and bioavailability in soils and sediments, this fraction is the most important as the sequestrated toxic metals can easily be released into the environment.

3.1.5.3.2 Reducible fraction

These include metals and As bound to Fe^{3+} and Mn oxides/hydroxides through processes such as adsorption and co-precipitation. Metal contents sequestrated by aluminium oxides can also be released in this step (Harrison et al., 1981; Hickey and Kittrick, 1984). Due to the instability of Fe and Mn oxides/hydroxides under reducing conditions, changes in the redox potential (from oxic to anoxic conditions) could largely influence adsorption-desorption reactions, leading to their dissolution and consequent release of adsorbed toxic metals. Kaasalainen et al. (2019) noted that the well crystalline and therefore, more resistant oxides such as jarosite and hematite will require stronger reducing conditions to be dissolved.

3.1.5.3.3 Oxidizable fraction

This fraction comprises of metal sulphides and metals bound to the organic matter including humified materials, living organisms and organic detritus (Hamilton et al.,1984; Kersten and Forstner, 1989; Gomez and Ruiz, 2023). There is usually less or no organic matter in mine wastes such as waste rock, tailings or overburden, therefore, the oxidizable fraction could exclusively contain metal sulphides. The oxidative weathering of metal sulphides such as pyrite, chalcopyrite etc. could release metals to the environment.

3.1.5.3.4 Residual fraction

This fraction contains naturally occurring minerals, hosting trace metals within their crystalline matrix. Under the existing and normal environmental conditions, the metals bound in this fraction are highly unlikely to be released. They include detrital silicate minerals, resistant

sulphides and oxide minerals with well crystalline such as hematite and magnetite (Tessier, 1979; Rauret et al., 1997; Anju and Banerjee, 2010; Dold, 2003).

3.1.6 Enrichment mechanism of economical secondary metal contents in riverbed sediments

Hydraulic structures such as dams decreases the flow velocity of a river and consequently promotes the settling of suspended particles such as silt, clay or Fe and Al oxides/hydroxides onto the upstream bed sediments (Jeong et al., 2014; Shim et al., 2015; Zhao et al., 2021). In consequence, metal(loids) fixed onto these suspended particles tend to accumulate in the sediments, leading to enrichment. Ogawa et al. (2013) observed that total loads of Indium (In) originating from acidic thermal waters decreased markedly at sites upstream of Tamagawa dam, leading to the enrichment of high contents of In on the reservoir sediments. Shim et al. (2015) reported that the enrichment of riverbed sediments with metals such as Cu and Zn originating from wastewaters of an industrial complex was promoted by the low flow velocity of the river induced by a dam. Đorđievski et al. (2018) mentioned that the Cu content in reservoir sediment was 5 times higher than the Cu ore grade at the Veliki Krivelj open pit mine. The contribution of this PhD thesis will be to clarify the Cu enrichment mechanism compared to As, based on pH-dependent Cu and As mobility in the contaminated rivers as well as Cu speciation in sediments.

3.2 METHODOLOGY

3.2.1 Description of the river system

The Bor Cu mining area belongs to the Timok river drainage system. This river system includes the Bor River which flows and mixes with the Krivelj River to form the Bela River which in turn flows into the Timok River (Figure 3.1 and Figure 3.2). There is a natural tributary, named

the Ravna River, which flows into the Bela River. The Bor River is solely made up of untreated wastewaters originating from the metallurgical/smelter facilities (Figure 3.3a), municipality, as well as AMD from the Old Bor overburden (Gardić et al., 2015; Đorđievski et al., 2018). The Krivelj River receives wastewaters originating from the Veliki Krivelj overburden (Figure 3.3b) and flotation tailings as well as drainage waters from the Veliki Krivelj open-pit and the Jama Bor underground mine (Korać and Kamberović, 2007; Gardić et al., 2015, 2017). In the 1950s, there was an accidental release of fine-grained flotation tailings from the Old Bor flotation tailings dam directly into the Bor river (Paunović, 2010; Bogdanović et al., 2014) as indicated by Figure 3.2. These flotation tailings were transported by water through the Bela River to the Timok River, resulting in elevated concentrations of toxic elements on the riverbed sediments (Đorđievski et al., 2018).

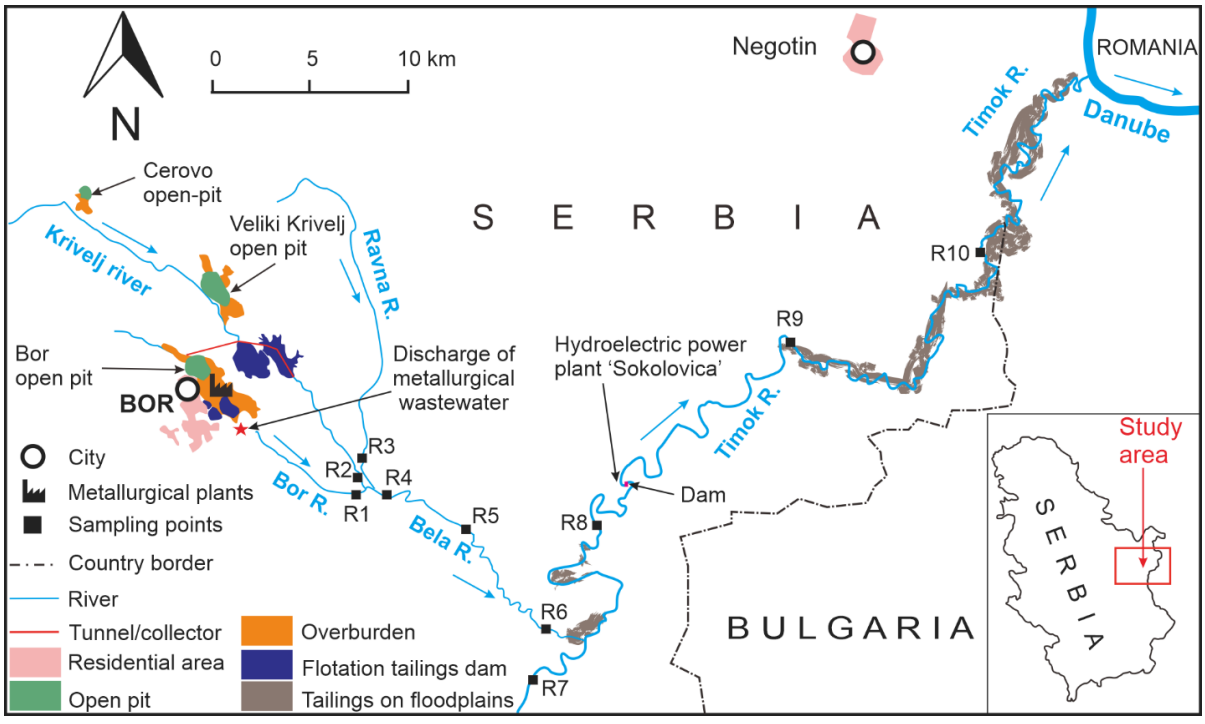

Figure 3.1 Map of the study area with sampling locations (modified from Đorđievski et al., 2018). The point locations represent both river water and sediment sample. For example, R1 represent RW1 (water sample) and RS1 (sediment sample)

3.2.2 River water sampling

In August 2019, a field survey was conducted around the Bor mining area to collect river waters. The sampling procedures and analyses followed in this study were the same as those adopted by Đorđievski et al. (2018). At each sampling site, temperature, pH and ORP values were measured using a combined hand-handled ION/pH meter (model IM-32P TOA DKK). Sample locations are presented in Figure 3.1, schematic diagram of the study area is presented in Figure 3.2 while field observations of rivers are provided in Table 3.1 and Figure 3.3. Three samples were collected at each site, two of which were filtered via cellulose acetate hydrophilic filters with a pore size of 0.2 μm and the other was left unfiltered. The samples were stored in 50 mL pre-washed polypropylene bottles. The unfiltered samples and one set of the filtered samples were acidified with 5 % volume nitric acid (HNO_3) to prevent precipitation of metals, growth of bacteria and to prevent adsorption to walls of polypropylene bottles and later analysed for Al, Fe, Cu, Zn, Pb, Ni, Mn, Cd and As using inductively coupled plasma mass spectrometry (ICP-MS; Perkin Elmer NexION), where Indium (In) was used as an internal standard. Atomic absorption spectroscopy (AAS; Agilent 240FS AA) was used to determine concentrations of Na, K, Mg and Ca from the filtered and acidified samples. Ion Chromatography (TOSO IC-2001) was used to analyse SO_4^{2-}, Cl^-, F^- and NO_3^- concentrations from filtered and non-acidified samples. The concentrations of bicarbonate ions (HCO_3^-) were determined by charge balance calculations between major cations (Na^+, K^+, Mg^{2+}, and Ca^{2+}) and major anions (F^-, Cl^-, SO_4^{2-} and NO_3^-). To evaluate the limits of detection for elements by ICP-MS, a blank solution was also analysed and the values were 2 μg/L for Al, 20 μg/L for Fe, 0.1 μg/L for Cu, 0.3 μg/L for Zn, 0.04 for Pb, 0.05 μg/L for Ni, 0.1 μg/L for Mn, 0.02 μg/L for Cd and 0.05 μg/L for As.

3.2.3 Treatment of the riverbed sediments

The riverbed sediments samples were obtained from the 2015 field survey and their locations are shown in Figure 3.1. They were collected at every respective point beneath the river water sampling location using a stainless steel shovel. The samples were then dried overnight at ambient temperatures and sieved to obtain < 180 μm fraction. Đorđievski et al. (2018) performed X-ray diffraction (XRD) analysis and acid digestion on these samples to obtain the mineralogical and bulk geochemical characteristics, respectively. In this study, we newly conducted the observation of the sediment samples by optical microscopy (outlined in Section 5.2.2.5) and 4 step modified BCR sequential extraction procedure described below.

Table 3.1 Sample locations and field descriptions of river waters

Sample ID	Sampling date	Location	Field observations
RW1	23/08/2019	Bor river, downstream Slatina	Dirty brown waters, efflorescent salts covering riverbanks
RW2	23/08/2019	Krivelj river, Zagradje	Grey colored waters
RW3	23/08/2019	Ravna river	Clear waters
RW4	23/08/2019	Bela river, Zagradje	Brown waters with an orange-yellow precipitate
RW5	23/08/2019	Bela river, Rgotina	Brown waters with a light brownish-yellow precipitate
RW6	23/08/2019	Bela river, Vrazogrnac	Yellow orange precipitate on the riverbed
RW7	23/08/2019	Timok river, before confluence with Bela River	Clear waters
RW8	23/08/2019	Timok river, after confluence with Bela River	Clear waters

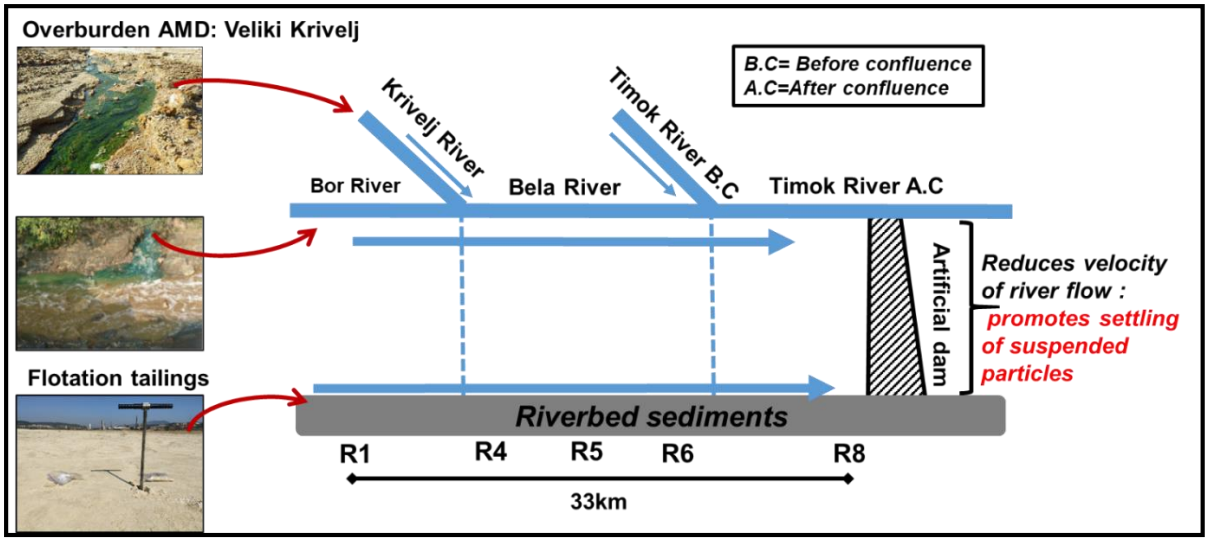

Figure 3.2 Schematic illustration for the contamination of the Timok river water system

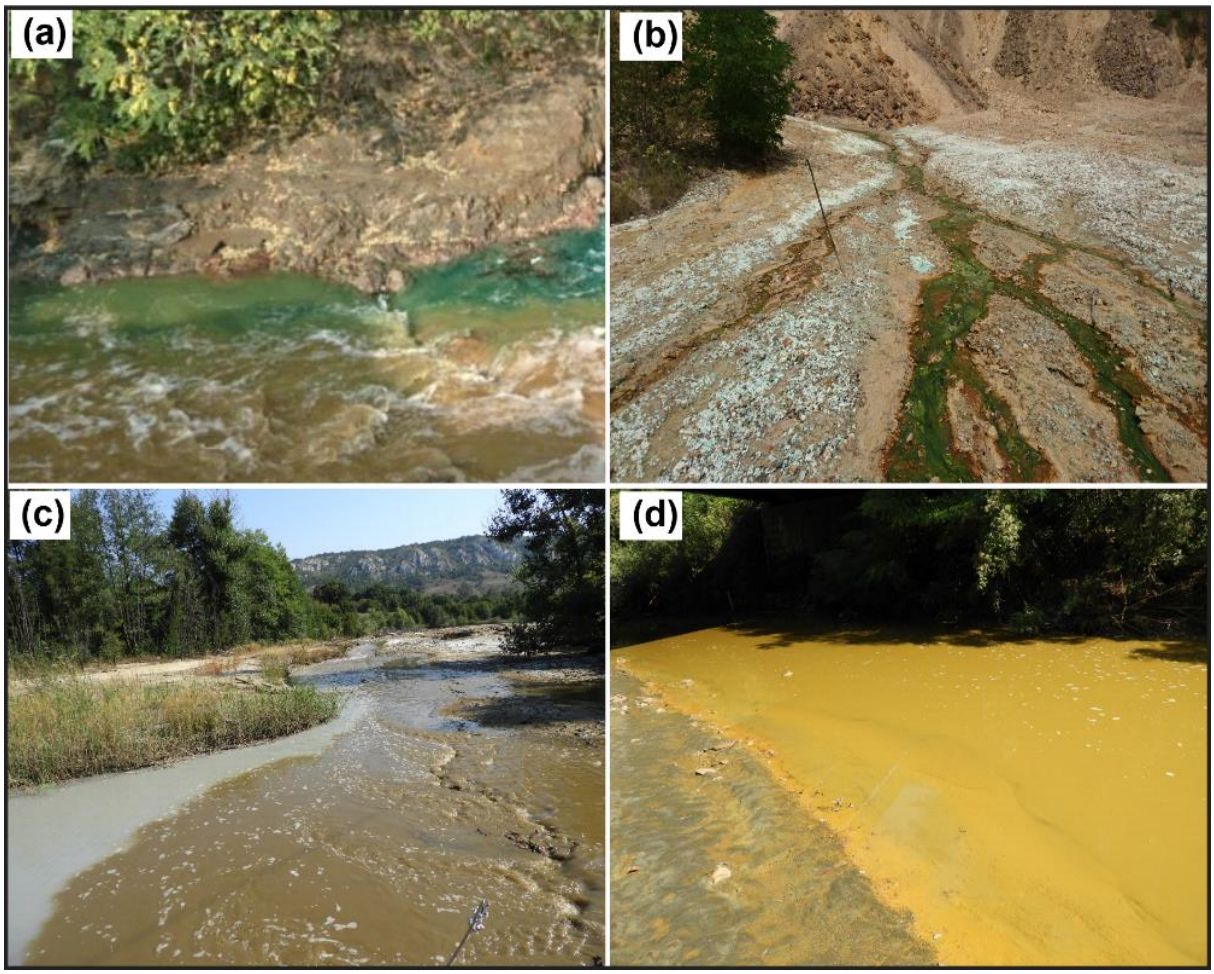

Figure 3.3 Field photographs of wastewaters and polluted rivers. (a) discharge of metallurgical/smelter wastewaters (Bluish-green color) into the Bor River (Brownish color) (Đorđievski et al., 2018). (b)Veliki Krivelj overburden leakage. (c) mixing of Bor River (right) and Krivelj River (left). (d) Upstream Bela River

3.2.4 The 4-step modified BCR sequential extraction

The modified four-step BCR sequential extraction procedure used for the investigation of riverbed sediments was similar to the one adopted by Rauret et al. (1999) and is summarised in Table 3.2. In brief, Step 1 comprises water-soluble, acid-soluble (carbonates) and exchangeable fractions, Step 2 involves the reducible fraction (oxides and hydroxides of Fe and Mn) whereas Step 3 includes the oxidizable fraction (sulphides and organic matter). In this study, the residual fraction was determined by the subtraction of the sum of the three steps from the bulk chemical compositions. The pH values of the reagents were measured using a pH meter (HM-25R TOA DKK) and are presented in Table 3.2. This test was applied for all riverbed sediments and the initial weight of the sample used was 0.5 g (<75 μm).

Table 3.2 The modified BCR sequential extraction procedure, adapted from Rauret et al. (1999)

Fraction code	Fraction name	Targets	Sample	Reagents	Extraction temperature (°C)	Agitation conditions
Step 1	Water soluble +Acid soluble +Exchangeable	Weakly adsorbed on materials	0.5 g, dry	0.11 M CH_3COOH *(pH 2.9)*	25	16 hours, 80 rpm
Step 2	Reducible	Fe, Mn oxides and hydroxides	Step 1 Residue	0.5 M $NH_2OH.HCl$ *(pH 1.5)*	25	16 hours, 80 rpm
Step 3	Oxidizable	Organic matter, sulphides	Step 2 Residue	8.8 M H_2O_2 (x2) *(pH 2.0)*	85	16 hours, 80 rpm
				1 M NH_4COOCH_3 *(pH 2.0)*		
Step 4	Residual	Sulphides, silicates and crystalline structures	Bulk composition - Σ (Step 1+2+3)			

3.2.5 Assessment of river water and sediment pollution levels

3.2.5.1 River water toxicity classification

Ficklin et al. (1992) devised a classification scheme primarily for the mine wastewaters using sample pH and concentrations of dissolved base metals (Cu + Zn + Cd + Co + Ni + Pb). In Ficklin diagrams, sample pH is plotted against the respective concentration sum of 6 dissolved base metals. The AMD-impacted and unpolluted rivers in the Bor mining area can be classified by the combination of two parameters: (1) pH - dependency, ranging from 'near- neutral' to 'ultra-acid' and (2) dissolved base metal - dependency, ranging from 'low metal' to ultra-metal' (Plumlee et al., 1992). Therefore, a sample could be classified as 'high acid/extreme metal', 'high acid/high metal', 'acid/high metal', 'near-neutral/high metal', 'near-neutral/low metal' etc.

3.2.5.2 Contamination factor (CF)

The contamination factor was adopted in this study to assess the pollution or enrichment of the riverbed sediments with toxic metals (Cu, Zn, Pb, Co and Ni) and As. The CF values are calculated using Equation 3.1 proposed by Hakanson (1980)

$$CF = C^i / C^i_{background} \quad (3.1)$$

where C^i represents the concentration of a specific metal (loid) in riverbed sediments and $C^i_{background}$ is the background abundance of that metal (loid). In this study, values used for $C^i_{background}$ are the contents of the upper continental crust (Rudnick and Gao, 2003) provided in Table 3.3. According to Hakanson (1980), the CF values can estimate the degree of pollution in sediments via the following categories: $CF < 1$ (low contamination), $1 \leq CF < 3$ (moderate contamination), $3 \leq CF < 6$ (considerable contamination), $CF \geq 6$ (very high contamination).

Table 3.3 Background contents of toxic elements used to calculate contamination factor

Background levels	Cu (mg/kg)	Zn (mg/kg)	Pb (mg/kg)	Co (mg/kg)	Ni (mg/kg)	As (mg/kg)
Upper continental crust	28	67	17	17.3	47	4.8
Ravna River (unpolluted)	11.8	9.8	6.6	3.2	4.4	1.7
Timok River (unpolluted)	9.4	15.4	9.9	4.8	5.1	1.4

3.2.5.3 Ecological potential risk index (Er)

Hakanson (1980) also proposed the ecological potential risk which combines the contamination factor (CF) of a specific metal (loid) with its respective toxic response factor (T_r) into Equation 3.2.

$$E_r = CF \times T_r \quad (3.2)$$

The T_r value account for two principles: (1) toxicity, providing information on the threat to humans and aquatic life due to a toxic substance and (2) sensitivity of an organism to the said substance and is calculated from the bio-production index (BPI) values (Hakanson, 1980). The T_r values of metal (loids) used in this study were: Zn=1, Cu=Ni=Co=Pb=5 and As=10 (Hakanson, 1980). The ecological potential risk is described by the following terminology: $CF < 40$ (low potential ecological risk), $40 \leq CF < 80$ (moderate potential ecological risk), $80 \leq CF < 160$ (considerable potential ecological risk), $160 \leq CF < 320$ (high potential ecological risk), $CF \geq 320$ (very high potential ecological risk).

3.2.6 Thermodynamic data calculations

The field evidence of the suspended particles in a river water column are obtained from the filter membrane during sampling of the river waters. The mineralogical characteristics of these suspended materials will then be investigated through XRD or SEM-EDS. However, in this

study, such physical evidence was not available. Instead, a geochemical model based on the pH and Eh data of the river waters was used to predict what minerals should be stable under equilibrium conditions (Alpers and Nordstrom, 1999). The thermodynamic data used was obtained from Majzlan et al. (2004) and is presented in Table 3.4.

Table 3.4 Thermodynamic data (Majzlan et al., 2004) used to construct the pH vs Eh diagram

Phases/boundaries	**Line equations and equilibrium constants**	**Calculations**
H_2	$2H^+ + é \rightleftharpoons 3H_2$, *logK=0*	Eh= -0.0591pH
O_2 vs H_20	$4H^+ O_2 + é \rightleftharpoons 2H_2O$, *logK=83*	Eh=1.23-0.0591pH
Fe^{2+} vs Fe^{3+}	$Fe^{2+} \rightleftharpoons Fe^{3+} + é$, *logK=13*	Eh=0.769V
Fe^{3+} vs schwertmannite	$Fe_8O_8(SO_4)(OH)_{6(s)} + 22H^+_{(aq)} \rightleftharpoons 8Fe^{3+}_{(aq)} + SO_4^{2-}{}_{(aq)} + 14H_2O_{(l)}$, *logK=9.6*	pH =1.23
Fe^{2+} vs schwertmannite	$Fe_8O_8(SO_4)(OH)_{6(s)} + 22H^+_{(aq)} + 8é = 8Fe^{2+}_{(aq)} + SO_4^{2-}{}_{(aq)} + 14H_2O_{(l)}$, *logK=113.6*	Eh= 0.969-0.163pH
$Fe(OH)_3$ vs schwertmannite	$Fe_8O_8(SO_4)(OH)_{6(s)} + 10H_2O_{(l)} = 8Fe(OH)_{3(s)} + SO_4^{2-}{}_{(aq)} + 2H^+$, *logK=-17.6*	pH =8.05
Pyrite vs schwertmannite	$8FeS_{2(s)} + 78H_2O_{(aq)} = Fe_8O_8(SO_4)(OH)_{6(s)} + 15SO_4^{2-}{}_{(aq)} + 120é + 150H^+$, *logK=-799.2*	Eh= 0.383-0.0739pH
Fe^{2+} vs Pyrite	$FeS_{2(s)} + 8H_2O_{(aq)} = Fe^{2+}_{(aq)} + 2SO_4^{2-}{}_{(aq)} + 16H^+ + 14é$, *logK=-85.7*	Eh= 0.341-0.0676pH
$Fe(OH)_3$ vs Pyrite	$FeS_{2(s)} + 11H_2O_{(aq)} = 15é + Fe(OH)_3 + 2SO_4^{2-}{}_{(aq)} + 19H^+$, *logK= -103.6*	Eh= 0.397-0.0749pH

log[Fe]=-2.0 or -2.3, Log[SO_4^{2-}]=-1.5 or -1.8, Eh(V)= 0.05914pe, log(é)= -pe, log(H^+)= -pH

The diagram was constructed for the 2019 and 2015 sampling period, each using the maximum Fe and SO_4^{2-} concentrations, which was the Bor River data. The constructed plots suggested that in the high acidity and SO_4^{2-} concentrations waters from the Bor Cu mining region, schwertmannite ($Fe_8O_8(SO_4)(OH)_6$) should be the iron hydroxide mineral stable under equilibrium conditions thereby a major constitution to the suspended particles.

3.3 RESULTS

3.3.1 pH variations of river waters

The summary of physicochemical characteristics of river waters, including pH, are provided in Appendices 1 and 2. The pH variations of river waters in 2015 and 2019 are presented in Figure 3.4. Except for site RW2, samples collected in 2019 were highly acidic compared to those collected in 2015.

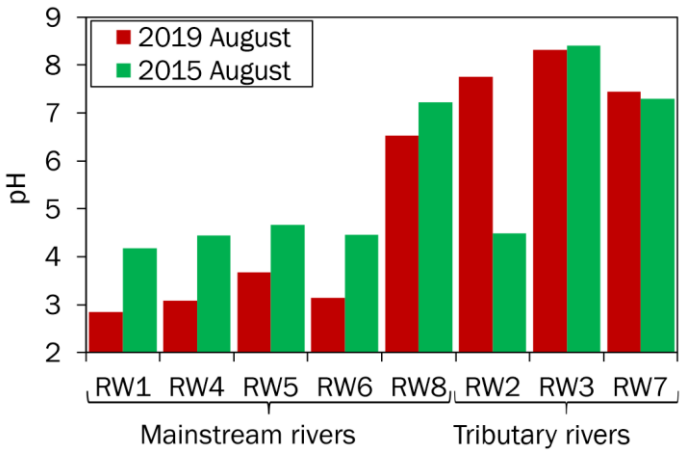

Figure 3.4 pH variations of river waters between the 2015 and 2019 sampling periods. Mainstream refers to those impacted by Bor metallurgical/smelter wastewaters. Tributaries are not impacted by such wastewaters

The Bor River (RW1) was the most acidic, with a pH value of 2.9 in 2019 and 4.2 in 2015. The Bela River (RW4-RW6) had a pH ranging from 3.1 to 3.7 in 2019 and from 4.5 to 4.7 in 2015. Before the confluence with the Bela River, the Timok River (RW7) had a neutral pH of 7.3 and

7.5 in 2015 and 2019, respectively. However, after mixing with the Bela River, the Timok River (RW8) had a pH value of 7.2 and 6.5, respectively in 2015 and 2019. During the 2015 sampling period, the tributary Krivelj River (RW2) was acidic, with a pH value of 4.5 whereas, in 2019, waters from the Krivelj River were neutral (pH=7.8). Ravna River (RW3) was weakly alkaline in both sampling periods, with pH values of 8.4 and 8.3 in 2015 and 2019, respectively.

3.3.2 Major component variations

The 2019 results showed that the dissolved concentrations of major cations had values ranging from 5.5-94.9 mg/L for Na, 2.7-9.0 mg/L for K, 61.-112.5 mg/L for Mg and 76.9-554 mg/L for Ca while dissolved concentrations of SO_4^{2-} ranged from 8.2 to 2830 mg/L. Although these values are generally higher than those obtained in 2015, there are no wide variations between the two sampling periods (Figure 3.5). The concentrations of Na, K, Mg and SO_4^{2-} decreased downstream, from the Bor River through the Bela River to the Timok River. The Krivelj and Ravna Rivers, which were not affected by acid mine drainages (AMDs), had high HCO_3^- concentrations at 134.1 and 243.8 mg/L, respectively. The highest concentration of bicarbonate ions (HCO_3^-) was observed in the weakly alkaline Black Timok River (RW7=359.6 mg/L), which is also not influenced by AMD. However, after mixing with the Bela River, this HCO_3^- dropped to 170.6 mg/L in the Timok River (site RW8).

The concentrations of major anions and cations (including Al^{3+}, Fe^{2+} and Cu^{2+}) were plotted in stiff diagrams (Figure 3.5) to compare the chemical compositions of river waters in two respects; from upstream to downstream and between the 2015 and 2019 sampling periods. The stiff diagrams of waters from the Bor and Bela Rivers in both sampling periods had a similar polygon (Figure 3.5), reflecting similar concentrations of Na+K and Cl^- and the lack of bicarbonate ions due to acidic conditions upstream (Figure 3.5). In 2019, concentrations of Ca+Mg at every site were higher than in 2015. To determine the water types at each site, the

highest concentration value of a cation and an anion were used and it was revealed that the waters of the Bor and Bela Rivers were Ca^{2+}- SO_4^{2-} type.

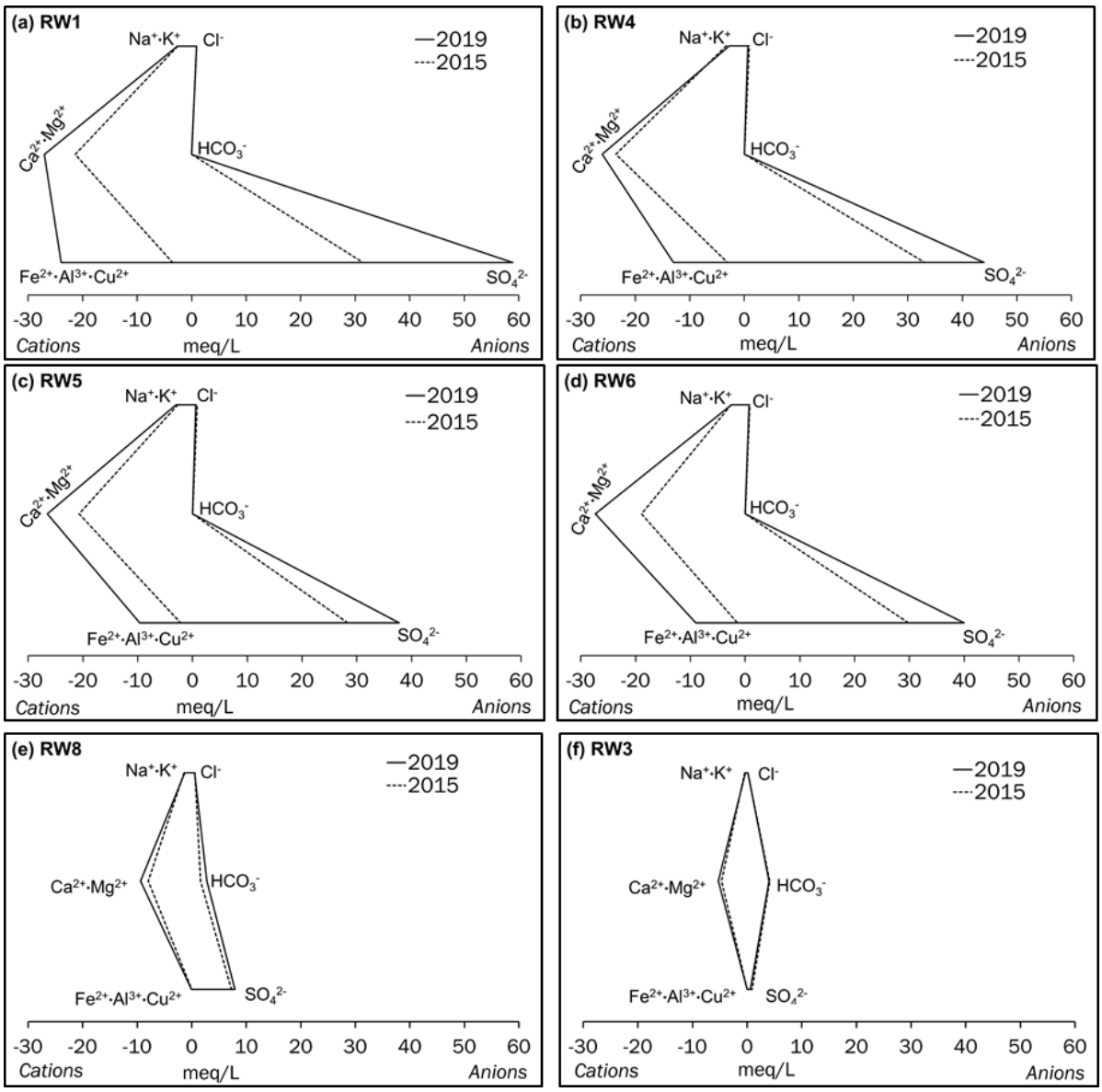

Figure 3.5 Stiff diagrams showing variations in the chemistry of river waters during the 2015 and 2015 sampling periods

Responding to the pH variations at upstream sites (Figure 3.4), stiff diagrams have shown that concentrations of Al, Fe and Cu were higher in 2019 than in 2015 (Figure 3.5). For example, at downstream Bela River (site RW6), the dissolved Al, Fe and Cu were almost completely

removed from the water in 2015 whereas, in 2019, these metals remained in the water column (Figure 3.5d).

At the downstream site (RW8), the concentrations of HCO_3^- ions were high both in 2015 (100.4 mg/L) and 2019 (170.6 mg/L). Although the pH value at site RW8 was lower in 2019 than in 2015 (Figure 3.4), the observed higher HCO_3^- ions in 2019 were due to the input from the tributary Black Timok River (RW7) whose HCO_3^- ion concentrations in 2019 (359.6 mg/L) were higher than in 2015 (254 mg/L). The Bor mining area is dominated by limestone (Kozelj, 2002; Jelenkovic et al., 2016) whose dissolution by groundwater has input high concentrations of HCO_3^- into river waters, providing higher buffering capacity (Đorđievski et al., 2018; Adamović et al., 2021). These bicarbonate ion levels are extremely higher than those in surface waters (HCO_3^- =70.3-92 mg/L) from a region whose limestone is limited to surface exposure (Oyarzún et al., 2013) as well as the estimated world average content of HCO_3^- ions (58.4 mg/L) reported by Levinson (1974).

The dissolution of calcite detected from the riverbed sediments of the Timok River by Đorđievski et al. (2018) is another source of HCO_3^- ion in the water column. Regardless of the variations in pH at regions upstream, the presence of high concentrations of HCO_3^- ions at site RW8 has resulted in very small concentrations of Al, Fe and Cu in both sampling periods. These dissolved metal concentrations were also similar in both years, as indicated by the almost same-shaped stiff diagram (Figure 3.5e). This shape is also almost similar to the stiff diagrams of unpolluted tributary Ravna River (Figure 3.5f).

3.3.3 Variations in concentrations of toxic elements in river waters

The statistical summaries of metals and arsenic concentrations in filtered and non-filtered river water samples collected in 2019 and 2015 are provided in Appendices 3 and 4, respectively.

The dissolved concentrations of metals and As in the 2019 sampling period were significantly higher than those in 2015, as a response to the higher acidity (Figure 3.4). In 2019, the concentrations of dissolved metals and As from the Bor River and Bela River had values ranging from 46.3-97.7 mg/L for Al, 39.7-270 mg/L for Fe, 51.1-109 mg/L for Cu and 0.02-0.65 mg/L for As. On the other hand, in 2015, the dissolved concentrations ranged from 7.6-16 mg/L for Al, 0.24-26.4 mg/L for Fe, 17.2-24.2 mg/L for Cu and 0.002-0.03 mg/L for As. Moreover, at the downstream site (RW8), the dissolved concentrations of Al and Cu in 2019 (pH 6.5) were 0.2 mg/L and 1.6 mg/L, respectively whereas, in 2015 (pH 7.2), Al and Cu concentrations were 0.05 and 0.11 mg/L.

A wide variation in the concentrations of dissolved toxic elements from the Bor River was observed between the two sampling periods. In 2019, when the pH of site RW1 was 2.9, the dissolved concentrations of Fe, Al, Cu and As were 270 mg/L, 97.7 mg/L, 109 mg/L and 0.65 mg/L, respectively. However, in 2015 when the pH was 4.2, the dissolved metal and As concentrations were comparatively lower (Fe: 26.4 mg/L, Al: 16 mg/L, Cu: 24.2 mg/L, As: 0.02 mg/L). With regard to the Krivelj River (RW2), in 2015 (pH 4.5), the dissolved concentrations of Al, Cu and Fe were 29.2 mg/L, 30.5 mg/L and 12.2 mg/L, respectively. However, their dissolved concentrations in 2019 (pH 7.8) were significantly lower (Al: 0.26 mg/L, Cu: 0.074 mg/L, Fe: < 0.1 mg/L).

3.3.4 Mineralogy of the riverbed sediments

The mineralogical characteristics of the riverbed sediments were studied by Đorđievski et al. (2018) using the XRD technique. In summary, pyrite was the only sulphide mineral detected and was present only in the mainstream sediments (RS1, RS4-RS6 and RS8). Other Fe-rich minerals detected from these sediments included magnetite and fayalite, products of the smelting process at the Bor mine. The full XRD data can be found in Appendix 5.

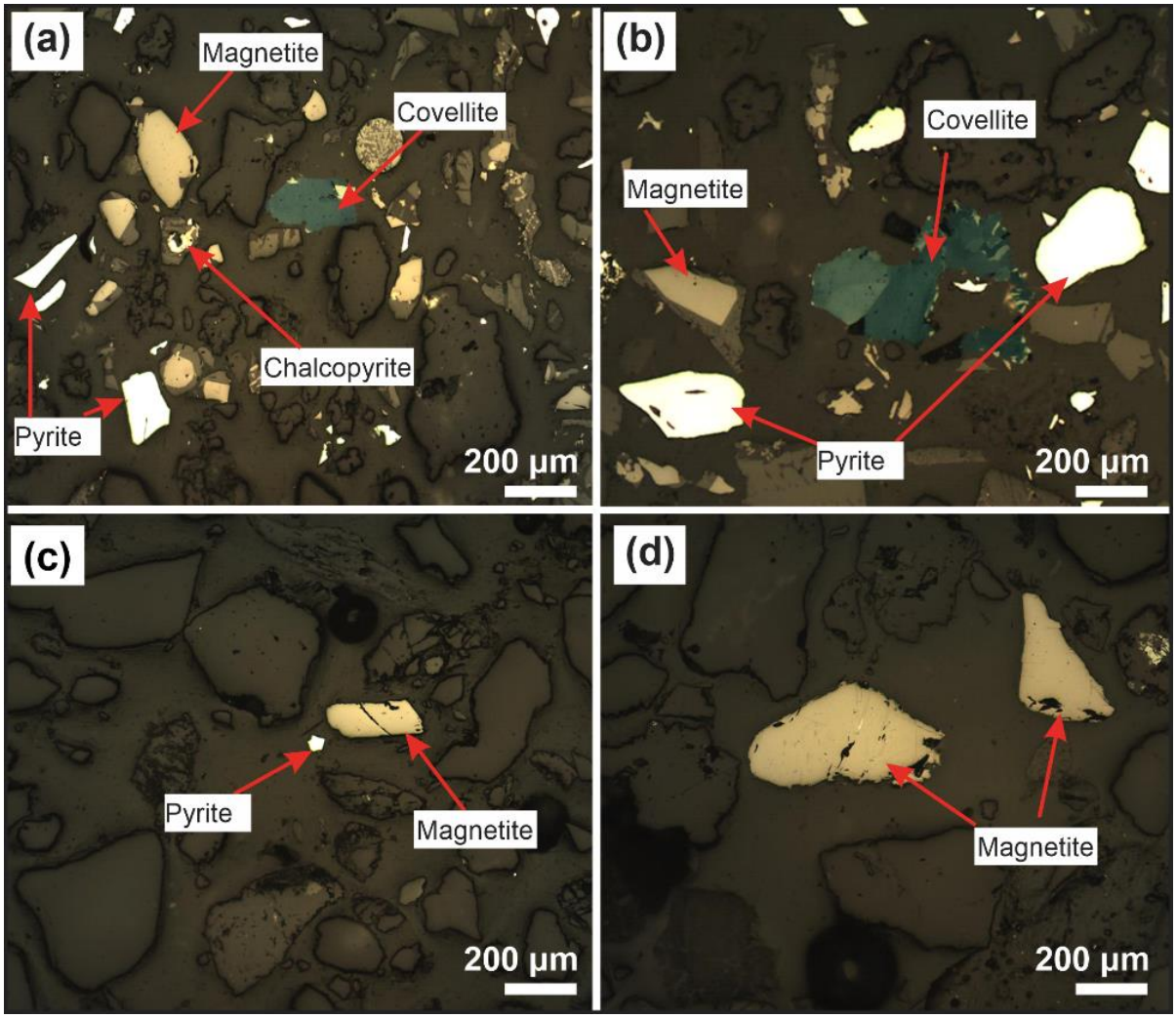

Figure 3.6 Photomicrographs in reflected light microscope showing sulphide and oxide minerals from riverbed sediments. (a) and (b), RS1: pyrite, covellite, chalcopyrite and magnetite. (c), RS4: pyrite and magnetite. (d), RS8: magnetite

A polished section of a sample obtained at the most upstream site (RS1) was observed under a microscope (Figure 3.6a and 3.6b) and the key minerals observed included pyrite, magnetite, chalcopyrite and covellite. In addition, magnetite and pyrite were observed in the Bela River sediments (Figure 3.6c) while magnetite was observed in the Timok River sediments (Figure 3.6d).

3.3.5 Sequential extraction of Cu and As from the riverbed sediments

A summary of the results from the modified BCR sequential extraction is depicted in Figure 3.7 as extraction percentages, reflecting the individual content of an element sequestered in a specific fraction against the total contents of said element. The results of other toxic metals can be found in Appendix 21.

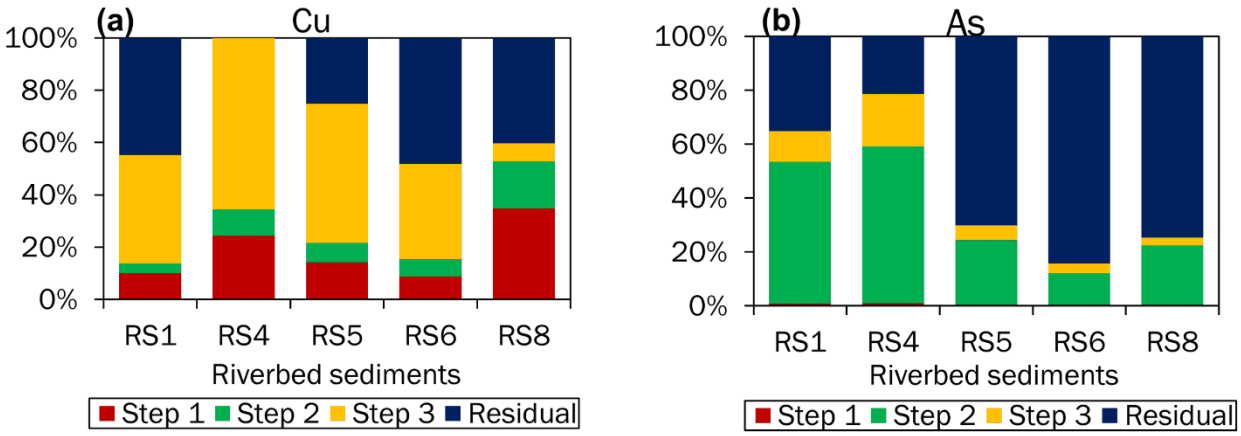

Figure 3.7 BCR sequential extraction of (a) Cu and (b) As from the mainstream riverbed sediments

The water-soluble, acid-soluble and exchangeable fraction (Step 1) had Cu contents ranging from 8.9 to 24.3 % between RS1 and RS6, but the contribution at RS8 reached 34.8 % of total Cu. The reducible (Step 2) Cu contents were fairly small at upstream sites (RS1 and RS4-RS6), with values ranging from 3.7 to 10.2 % (Figure 3.7a). However, at the downstream site (RS8), the amount of reducible Cu was significant, reaching 18 %. The oxidizable fraction (Step 3) had high Cu contents, ranging from 36.2 to 65.6 % of total Cu contents in the Bor and Bela riverbed sediments (Figure 3.7a). The Cu contents in the residual fraction ranged from 0 to 48 %. With regards to As, the reducible fraction (Step 2) sequestered considerably high contents of As, ranging from 12 to 58 %, with the most upstream sites (RS1 and RS4) having the highest contents (Figure 3.7b). Across all samples, the oxidizable (Step 3) forms of As ranged from 2.9 to 19.7 % whereas contents of residual As ranged from 21.3 to 84.2 %.

3.4 DISCUSSION

3.4.1 Mobility behaviour of metals and arsenic in river waters

The concentrations of metals and As (Appendices 3 and 4) were converted into fluxes by multiplying with respective river discharges. Since the 2015 and 2019 sampling trips were carried out during the summer season (month of August), the values of discharge used in this study were assumed to be the same as those measured and reported by Đorđievski et al. (2018). Figure 3.8 shows the upstream-downstream pH variations with total (sum of particulate and dissolved fluxes), dissolved and particulate fluxes of Al, Fe, As and Cu, because of their higher fluxes. Fluxes for other metals are presented in Appendix 6. Just as mentioned in Section 1, there are essentially two major river water pollution sources in the Bor mining area; (1) the metallurgical/smelter wastewaters (Figure 3.3a), located upstream of the Bor River and (2) Krivelj mine overburden leakages (Figure 3.3b), located upstream of the Krivelj River (Korać and Kamberović, 2007; Ishiyama et al., 2012; Filimon et al., 2016; Gardić et al., 2015, 2017; Đorđievski et al., 2018; Adamović et al., 2021).

3.4.1.1 Variations in Al mobility and the formation of HAO

Loads of dissolved Al discharged into the Bor River from the metallurgical/smelter wastewaters are represented by the closest receiving site, RW1. The dissolved fluxes of Al at site RW1 were higher in 2019 (3.42 kg/min) than in 2015 (0.56 kg/min). In 2019, Al existed primarily as dissolved species in the Bor and Bela Rivers (pH 2.9-3.7) as indicated by the indistinguishable fluxes of total and dissolved Al (Figure 3.8a).

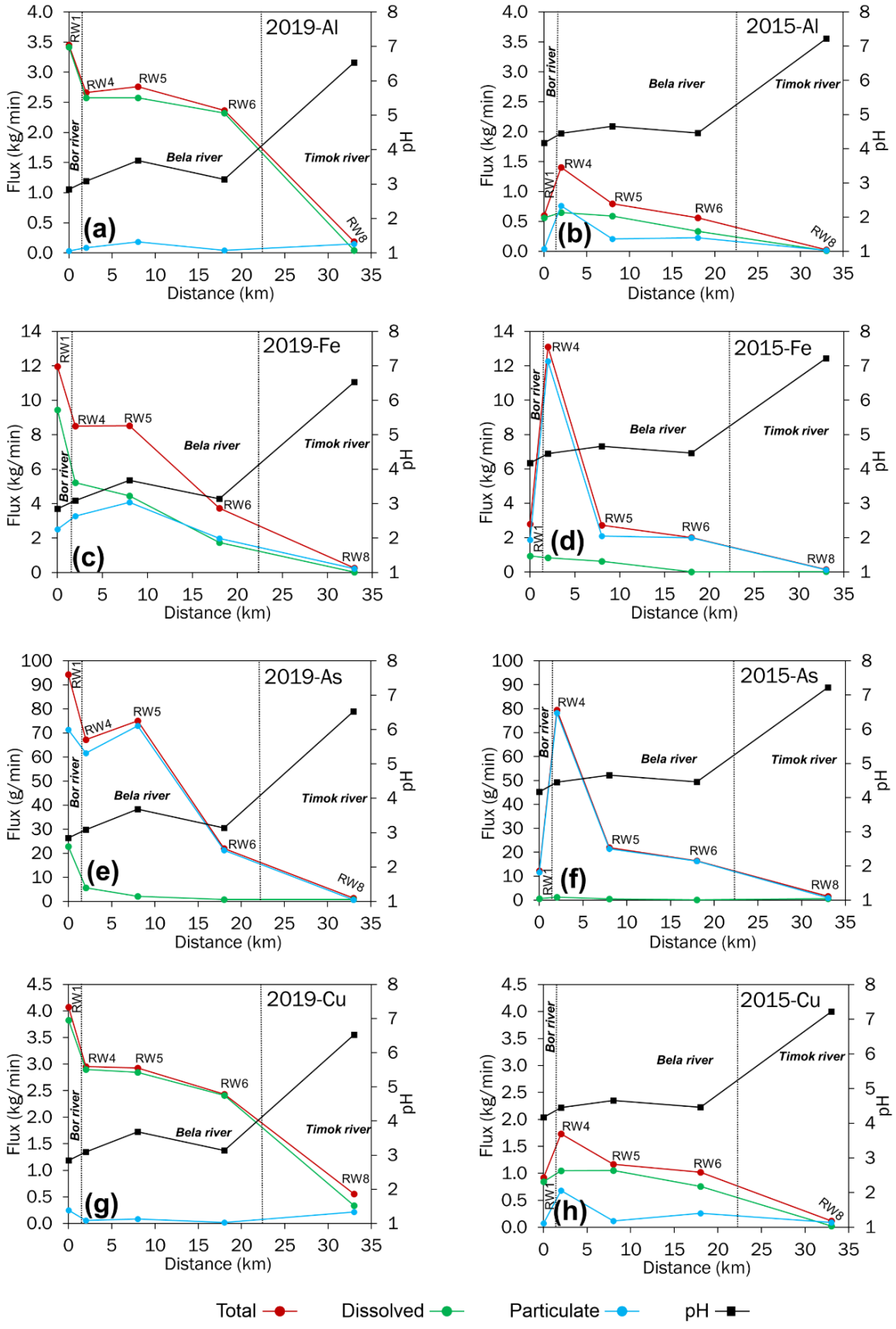

Figure 3.8 Upstream-downstream variations in mobility of metals and As during the 2019 and 2015 sampling campaigns

The solubility diagram of $Al(OH)_3$ (Figure 3.9a) shows that the data for the acidic river waters plot away from the Al^{3+} saturation line, consistent with the insignificant contents of particulate Al species in Figure 3.8a. However, as pH increased at the downstream site (RW8: pH 6.5) there was a larger amount of particulate Al species (79 % of total Al: obtained by subtracting dissolved species from total species).

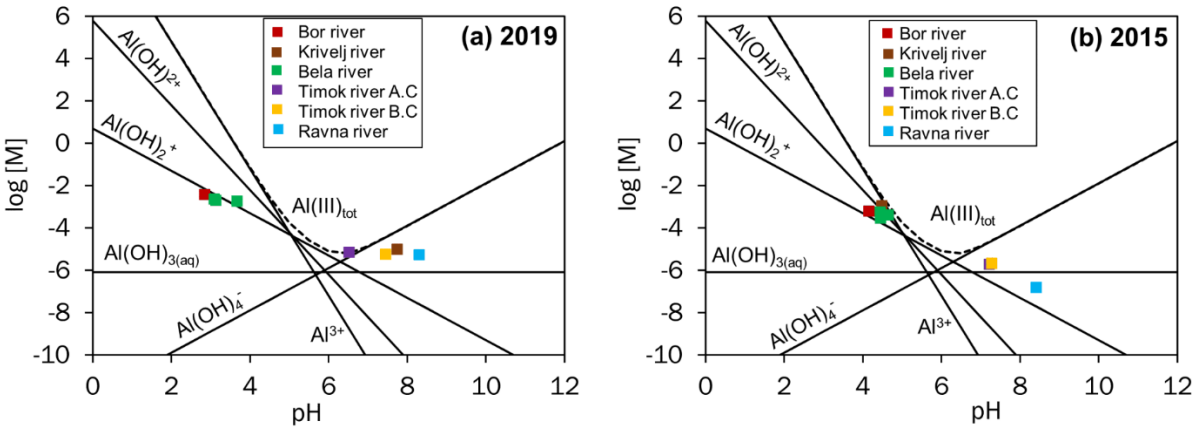

Figure 3.9 Thermodynamic diagram showing the solubility of $Al(OH)_3$ with plotted concentration data of Al^{3+} obtained in the 2019 (a) and 2015 (b) sampling campaigns. B.C and A.C in the legends refers 'before confluence' and 'after confluence', respectively with Bela River

In 2015, there were significant contents of particulate Al species in the Bela and Timok Rivers (pH 4.5-7.2), ranging from 26 to 58 % of total Al (Figure 3.8b). The highest contents of the suspended species of Al at site RW4 (Figure 3.8b) could be explained by the high input of Al from the Krivelj River into the Bela River. These suspended Al particles are commonly known as hydrous aluminium oxides (HAO) and have been reported to form in conditions of pH greater than 4.6 (Schemel et al., 2000; 2007, Gammons et al., 2005). The solubility diagram of $Al(OH)_3$ (Figure 3.9b) shows that in 2015, Al^{3+} concentration data plotted very close to the Al^{3+} saturation line, thus supporting the assertion of the formation of HAO. The decrease of total Al from upstream to downstream sites (Figures 3.8a and b) suggests that as the pH

increased, HAO precipitated and settled under gravity onto the riverbed, especially at site RW8, thus effectively removing Al from the water column.

3.4.1.2 Variations in Fe mobility and the formation of HFO

Loads of dissolved Fe discharged into the Bor River (site RW1) were extremely higher in 2019 (9.45 kg/min) compared to 2015 (0.92 kg/min). In 2019, the dissolved Fe fluxes were dominant in the acidic waters of the Bor River and decreased through the Bela River to the Timok River as pH increased (Figure 3.8c). However, 21 % of total Fe represented the particulate Fe species in the acidic Bor River (pH 2.9). This content increased at Bela River to values of 39 and 48 %, respectively at sites RW4 (pH 3.1) and RW5 (pH 3.7). Figure 3.10a (Majzlan et al., 2004), constructed using thermodynamic data in Table 3.4, shows that the pH and Eh data for the Bor and Bela Rivers plot within the schwertmannite stability field. In this way, the abundance of suspended Fe particles in the Bor and Bela Rivers indicated by Figure 3.8c could be related to schwertmannite. From site RW6 to RW8, total Fe fluxes decreased to almost zero values (Figure 3.8c), suggesting that at the most downstream site (RW8: pH 6.5), Fe was effectively removed from the water column.

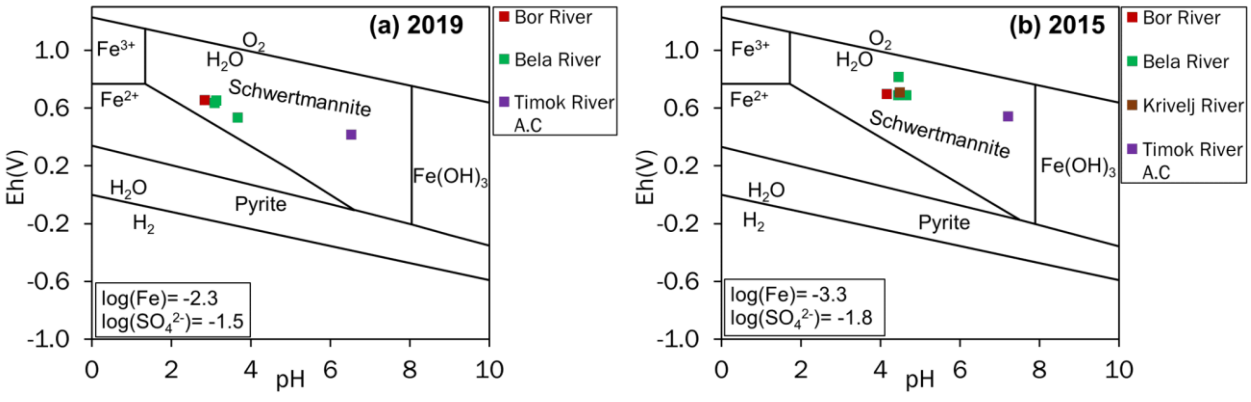

Figure 3.10 Eh vs pH diagram for the Fe-O-S-H_2O system at 25 °C (Majzlan et al., 2004) with plotted values of Eh and pH obtained in the 2019 (a) and 2015 (b) sampling campaigns. A.C in the legends refers to 'after confluence' with Bela River

In 2015, the higher pH values of the Bor and Bela Rivers (pH 4.2-4.7) provided the optimum conditions for the formation of the suspended hydrous iron oxides (HFO) (Gammons et al., 2005; Parker et al., 2008; Ogawa et al., 2012, 2013). The particulate species of Fe predominated the waters of the Bor River up to the Timok River as indicated by Figure 3.8d. The Eh-pH diagram (Figure 3.10b) shows that the 2015 data plotted in the stability field of schwertmannite, thus supporting the suggestion of HFO formation. The particulate Fe species at the Bor River (RW1) accounted for 67 % of total Fe whereas, in the Bela River (RW4-RW6), particulate Fe fluxes ranged from 77 to 99 % of total Fe fluxes. It was further observed that after the confluence of the Bor and Krivelj Rivers (Figure 3.2, Figure 3.3c), the HFO were the highest (site RW4), showing the Krivelj River acting as a pollution source for the Bela River. Then, particulate Fe decreased drastically at site RW5 (Figure 3.8d) due to precipitation and settlement onto the riverbed. These observations indicate that in 2015 when pH was higher, the hydrous iron oxides (HFO) were formed even at upstream sites, transported downstream as suspended particles and were nearly completely removed from waters at site RW8 via settling onto the riverbed.

3.4.1.3 Variations in As mobility

The loads of dissolved As discharged into the Bor River (RW1) during the 2019 and 2015 sampling periods were 22.9 and 0.62 g/min, respectively. The mobility of As is controlled by the pH variations as well as the amount of HFO present in the water column (Ogawa et al., 2013, 2018; Chikanda et al., 2021; Lalinská-Voleková et al., 2022). Figures 3.8e and f, respectively, indicate that for both 2019 and 2015, As existed as a particulate species even at upstream sites. From the Bor and Bela Rivers, the contents of particulate forms of As in 2019 and 2015 ranged from 75 to 96 % and 95 to 99 %, respectively, of the total As. This indicates that As was effectively sorbed onto the suspended HFO (Ogawa et al., 2012; Chikanda et al., 2021; Lalinská-Voleková et al., 2022; Ye et al., 2022). In fact, for the 2015 data, the flux pattern

of As was similar to that of Fe (Figure 3.8d) which implies that As have been adsorbed onto or co-precipitated with the HFO and settled onto the riverbed. The model showing this mobility is illustrated by Figure 3.11.

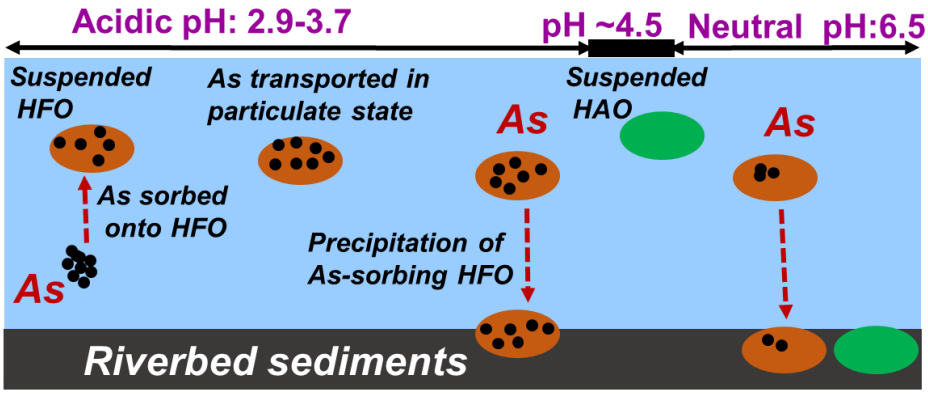

Figure 3.11 Detailed illustration of the mobility of As in acidic waters (2019 sampling period), involving removal by hydrous ferric oxides (HFO)

Since the HAO generally forms at conditions of pH > 4.6 (Gammons et al., 2005; Schemel et al., 2007), they did not have a significant role in controlling the mobility of As from the Bor and Bela Rivers, especially during the 2019 sampling period. It was observed that in 2015, the acidic Krivelj River (pH 4.5) input significant fluxes of As into the Bela River and downstream environments. However, in 2019, there was no pollution input from the neutral Krivelj River (pH 7.8). Despite this variation, the total flux of As in the Bela River was much higher in 2019 than in 2015. This highlights the severity of the contamination that wastewaters from the Bor metallurgical/smelting facilities have on the Timok River system.

3.4.1.4 Variations in Cu mobility

The dissolved fluxes of Cu discharged from the Bor metallurgical/smelter facilities into the Bor River in 2019 (Cu: 3.83 kg/min) were significantly higher than in 2015 (Cu: 0.82 kg/min). Contrary to As, Cu was transported primarily as a dissolved species in the entire study area during the 2019 sampling period (Figure 3.8g), similar to Al. In 2015, Cu also existed mainly as a dissolved species, however, there were considerable contents of particulate Cu species (Figure 3.8h), also analogous to Al. Additionally, the total Cu flux decreased from upstream to downstream in a similar pattern to Al and Fe (Figures 3.8b and d). This suggests that, especially in 2015, Cu may have been adsorbed onto the suspended HAO and/or HFO and later precipitated and settled onto the riverbed. The model showing this mobility is illustrated by Figure 3.12. It is important to note that due to the pH variations at site RW8 (Figure 3.4), the amount of Cu sorbed onto HAO and/or HFO in 2015 (79 % of total Cu) was higher than in 2019 (39 % of total Cu) as indicated by Figures 3.8g and h. Montecinos et al. (2020) reported that at pH ~7, most of the Cu contents are sorbed onto the hydrous Al oxides.

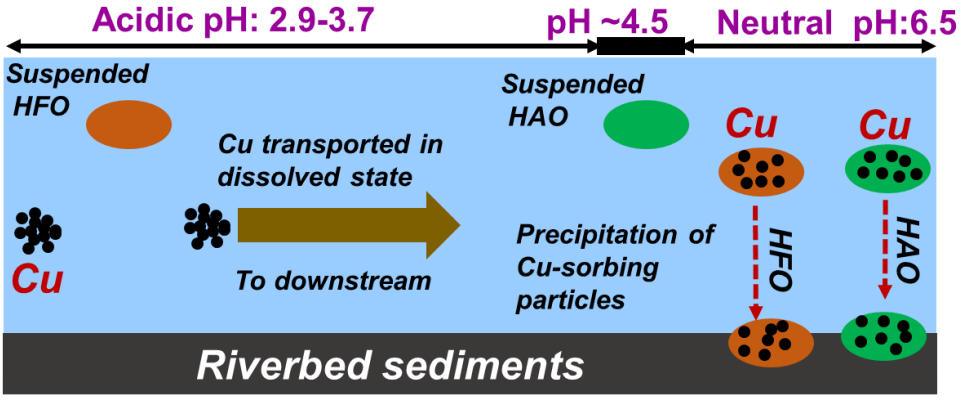

Figure 3.12 Detailed illustration of the mobility of Cu in acidic and neutral waters (2019 sampling period), involving removal by hydrous ferric oxides (HFO) and hydrous aluminium oxides (HAO)

3.4.2 Risk assessment of river water contamination

The discharge of wastewaters from the Bor metallurgical/smelting facilities directly into the Bor River (Figure 3.2, Figure 3.3a) represents a major anthropogenic environmental contamination source to the Timok River system (Korać and Kamberović, 2007; Ishiyama et al., 2012; Filimon et al., 2016; Šerbula et al., 2016; Gardić et al., 2017; Đorđievski et al., 2018; Adamović et al., 2021). Figures 3.13a and b respectively show the 2019 and 2015 river water data plotted in the Ficklin diagrams to evaluate the variations in river water contamination.

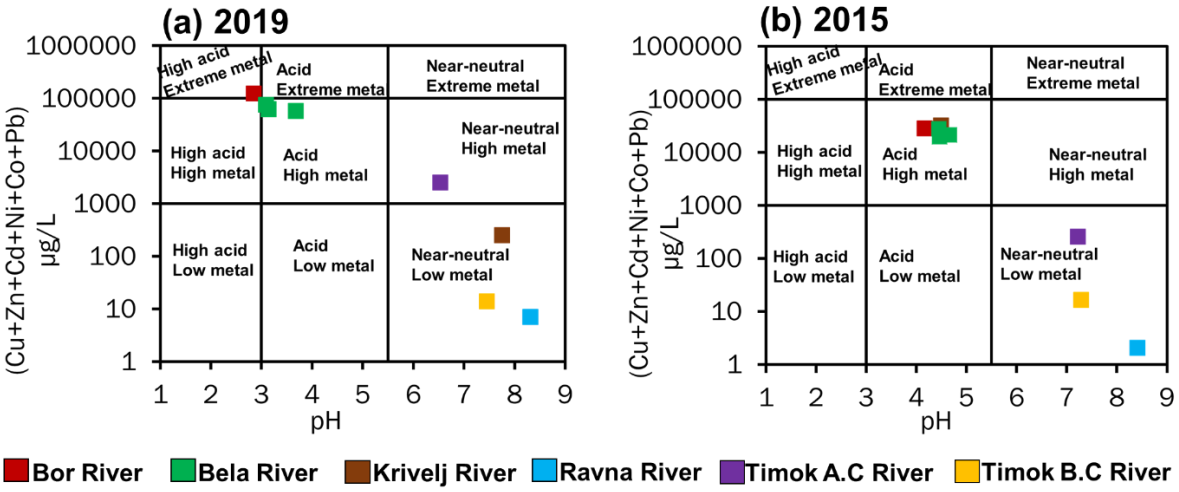

Figure 3.13 Ficklin diagrams of 2019 (a) and 2015 (b) sampling periods. B.C and A.C in legends refers to 'before confluence' and 'after confluence' with Bela River

For the 2019 sampling period, data for the Bor River and Bela River were plotted near the boundary of the 'high acid and extreme metal' and 'acid and high metal' regions, respectively (Figure 3.13a). However, in 2015, the data for the two rivers was plotted in the 'acid and high metal' region (Figure 3.13b). The variation in the plotting regions was caused by the more acidic conditions of the Bor and Bela Rivers in 2019 (pH 2.9-3.7) than in 2015 (pH 4.2-4.7). The dissolved Cu contributed the most toxicity to the waters of the Bor and Bela Rivers in both

2019 (Figure 3.14a) and 2015 (Figure 3.14b), with values ranging from 87 to 89 %. This is linked to the predominance of dissolved Cu species in the Bor and Bela Rivers (Figures 3.8g and h).

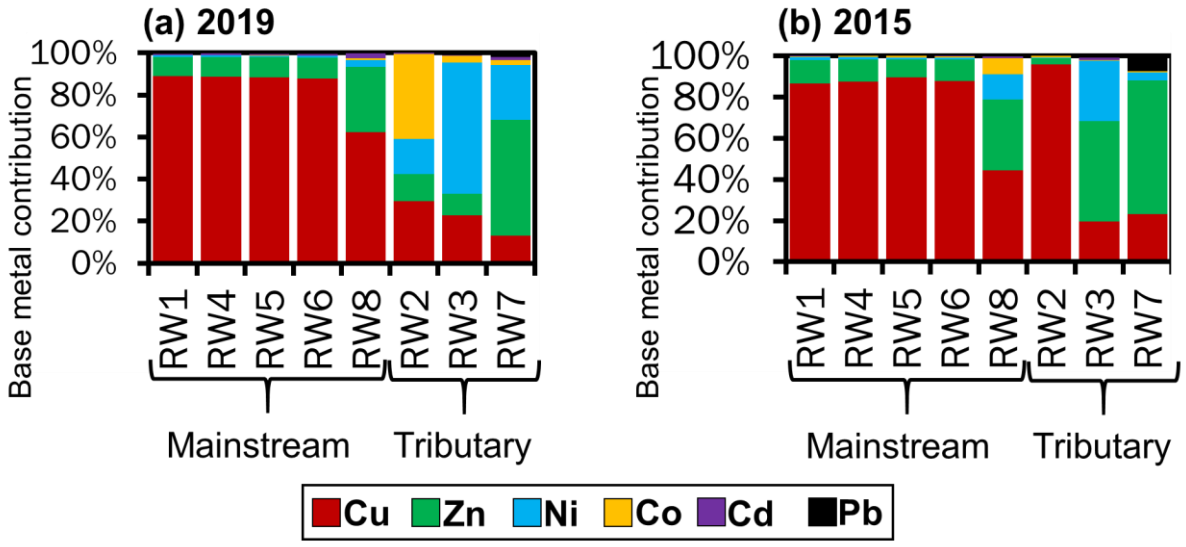

Figure 3.14 Dissolved metal toxicity contributions during the 2019 (a) and 2015 (b) sampling periods. Mainstream and Tributary rivers refers to those impacted and non-impacted, respectively by Bor metallurgical/smelter wastewaters

The tributary Krivelj River (RW2) was plotted in the 'acid and high metal' region for the 2015 sampling period whereas, in 2019, the data was plotted in the 'neutral and low metal' region. The water chemistry results of the Krivelj River (RW2) indicated that the contents of dissolved Cu in 2015 (pH 4.5) were 412 times higher than in 2019 (pH 7.8). In consequence, the Cu toxicity contribution in 2015 was as high as 96 % (Figure 3.14b) whereas, in 2019, the Cu contribution was only 30 % (Figure 3.14a). Therefore, it should be highlighted that in 2015, the Krivelj River also acted as a serious pollution source to the Bela River and downstream environments.

For the most downstream site (RW8), the 2015 and 2019 data were plotted in the 'neutral and low metal' and 'neutral and high metal' regions, respectively. This variation was caused mostly by the higher contents of dissolved Cu species in 2019 (Figure 3.8g) than in 2015 (Figure 3.8h).

Consequently, the Cu toxicity contribution in 2019 was as high as 62 % (Figure 3.14a) whereas, in 2015, the Cu contribution was only 44 % (Figure 3.14b). Despite the Krivelj River acting as a pollution source to the Bela River and downstream areas in 2015, site RW8 plotted in a region of higher risk in 2019 than in 2015. This further highlights the severity of water contamination by the Bor metallurgical/smelter facilities observed during the 2019 sampling campaign.

The quality of the Bor River is controlled primarily by wastewaters originating from the Bor metallurgical/smelting facilities (Đorđievski et al., 2018; Adamović et al., 2021). So, changes in the acidity and loads of dissolved toxic elements in the Bor River could be linked directly to changes in the operating conditions of the facilities. Therefore, it can be speculated that the facilities discharged wastewaters with much higher acidity and dissolved toxic elements into the Bor River in 2019 than in 2015, which were then transported downstream (Figure 3.8), posing a higher risk of river water contamination as suggested by Figure 3.13.

3.4.3 Environmental risk assessment of riverbed sediments contamination

The upstream-downstream distribution of heavy metals and As concentrations in the riverbed sediments is illustrated in Figure 3.15. Based on the results of optical microscopy (Figure 3.6) and XRD (Appendix 5), the mineralogy of the riverbed sediments is primarily controlled by the flotation tailings released from the mineral processing plant in the 1950s into the Bor River and transported through the Bela River to the Timok River (Paunović, 2010; Bogdanović et al., 2014; Đorđievski et al., 2018).

In addition to this, heavy metals and As originating from wastewaters of the Bor metallurgical/smelting facilities and Veliki Krivelj mine overburden could also be possible sources of pollution to the riverbed sediments as suggested by the mobility behaviour of As (Figures 3.8e and f) and Cu (Figures 3.8g and h) in river waters as well as their chemical

speciation in riverbed sediments (Figure 3.7). In this section, we assess the level of pollution in riverbed sediments through contamination factor (CF) and ecological risk potential (Er), focusing on the bulk chemical composition of As and Cu and relating it to their mobility in river waters (Figures 3.8e to h).

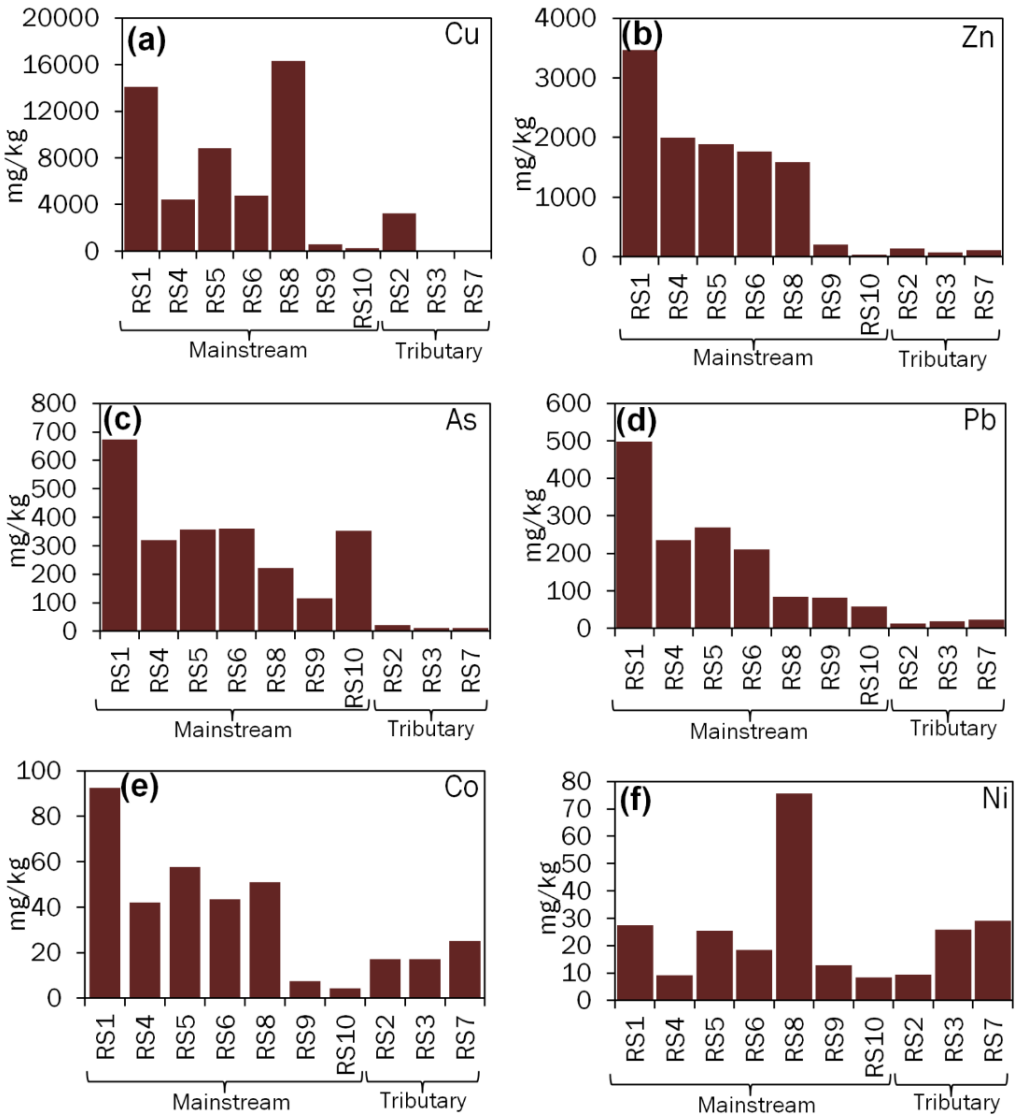

Figure 3.15 Bulk chemical compositions of riverbed sediments. Mainstream sediments refers to those impacted by flotation tailings and the Bor metallurgical/smelter wastewaters while Tributary sediments are impacted by neither. Data obtained from Đorđievski et al. (2018)

3.4.3.1 Contamination factor (CF)

Figure 3.16 depicts the distribution of the contamination factor index (CF) values of Cu, As, Zn, Pb, Co and Ni in the riverbed sediments.

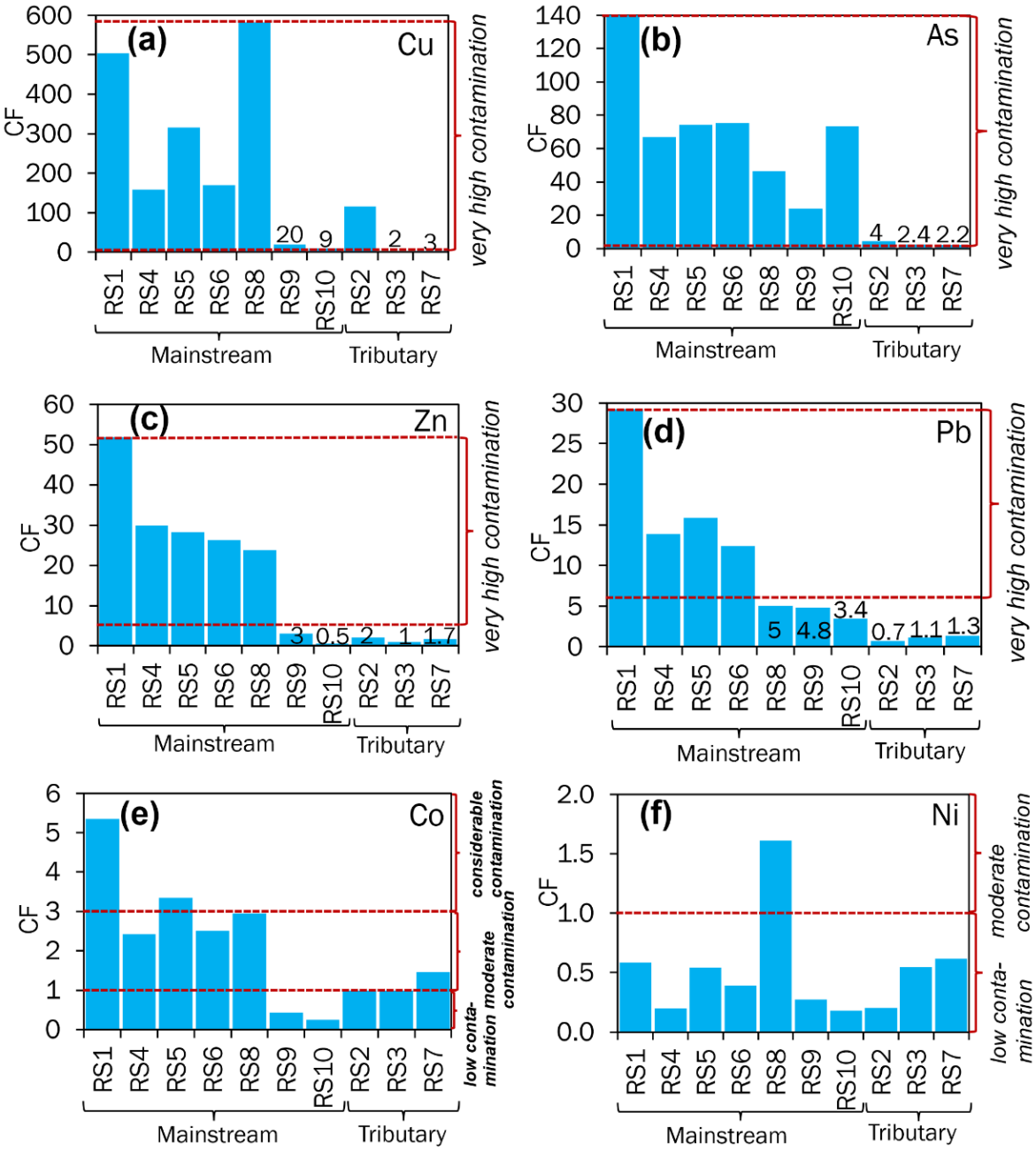

Figure 3.16 Variations in the contamination factor index (CF) of metals and As from the riverbed sediments. Mainstream sediments refers to those impacted by flotation tailings and the Bor metallurgical/smelter wastewaters. Tributary sediments are not impacted by either

According to Figure 3.16a to d, the CF values from the mainstream sediments (RS1, RS4-RS6 and RS8) were the highest for Cu and As, ranging from 159-582 and 46-140, respectively whereas the CF values of other metals ranged from 24-52 for Zn and 5-29 for Pb. According to Hakanson (1980), a CF value ≥ 6 indicates a 'very high contamination' level of the riverbed sediments. It was observed that the CF values of Cu (Figure 3.16a) were the highest at the downstream reservoir sediments (RS8; CF=582) and near the Bor metallurgical/smelting facilities near (RS1; CF=504), suggesting a very high contamination level.

The CF value of Cu at site RS8 could be related to the effective removal of Cu from the Timok River waters (RW8) through the precipitation of Cu-sorbing HFO and HAO as suggested by Figure 3.8h. The CF values of As were especially high in sediments of the Bor River (CF=140) and Bela River (CF= 69-75) and could be attributed to the widely distributed removal of As through sorption by HFO and settlement onto the riverbed (Figures 3.8e and 3.8f).

3.4.3.2 Ecological risk potential (Er)

Figure 3.17 depicts the distribution of the ecological risk potential index (E_r) values for Cu, As, Zn, Pb, Co and Ni in the riverbed sediments. From the mainstream sediments (RS1, RS4-RS6 and RS8), the Er values of Cu and As ranged from 793-2911 and 463-1402, respectively. According to Hakanson (1980), the Er value ≥ 320 indicates a 'very high ecological risk' level to the riverbed sediments. Based on Figure 3.17, the Er values of Cu were the highest in sediments at the downstream (RS8; Er=2911) and upstream sites (RS1; Er=2518), suggesting a very high ecological potential risk level. On the other hand, the Er value of As was very high at the upstream (RS1) and midstream sites (RS4-RS6), which could be attributed to the precipitation of As-sorbing HFO from the Bor River (RW1) and Bela River (RW4-RS6), similar to the CF values.

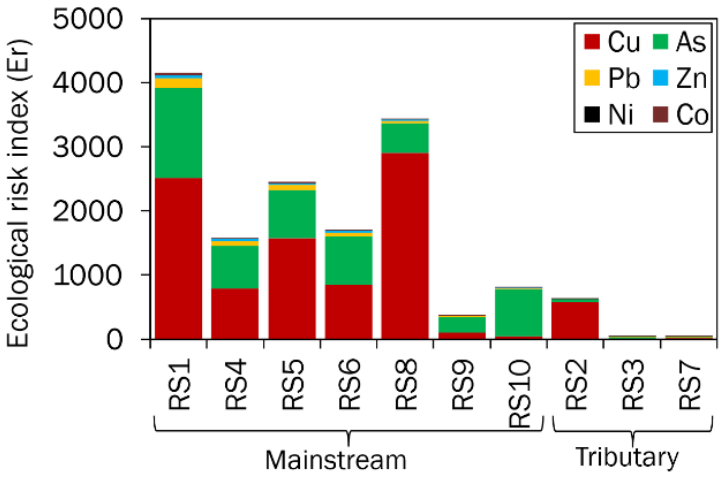

Figure 3.17 Variations in the ecological risk potential (Er) of metals and As from the riverbed sediments. Mainstream sediments refers to those impacted by flotation tailings and the Bor metallurgical/smelter wastewaters. Tributary sediments are not impacted by either

3.4.4 Chemical states of Cu and As in riverbed sediments and their origins

The CF and Er values of Cu and As were much higher than those of other metals. These values could be divided into two constituents; (1) those yielded by Cu and As precipitated from river waters through sorption onto HFO and/or HAO (Figures 3.8e to h) and; (2) those yielded by Cu and As originating from flotation tailings. It is very important to note that the Cu and As sequestrated by HFO and/or HAO can easily be released back into the river waters (Marin et al., 1997), meaning a high risk of mobilization. On the other hand, Cu and As in sulphide minerals are relatively resistant to dissolution, suggesting a lower risk of release. In this section, we elucidate both the origins of Cu and As and the risk of mobilization based on the sequential extraction test (Figure 3.7).

3.4.4.1 Speciation of Cu

The Cu contents liberated in Step 1 (Figure 3.7a), probably weakly adsorbed onto the surfaces of suspended particles such as hydrous oxides (Marin et al., 1997), were the highest at the downstream site (RS8). The reducible Cu contents released in Step 2 were also higher at site RS8, possibly related to the Cu sorbed onto and/or co-precipitated with HAO and/or HFO in

neutral waters (Montecinos et al., 2020). On the other hand, the high contents of oxidizable Cu observed from upstream riverbed sediments (Figure 3.7a) are hosted by the Cu sulphide minerals such as covellite and chalcopyrite (Figures 3.6a and b), originating from the flotation tailings. Owing to the incomplete digestion of sulphide minerals in Step 3, most of the residual Cu could also be related to the sulphides (Filgueiras et al., 2002; Galán et al., 2003; Dold and Fontboté, 2001; Khorasanipour et al., 2011).

The contents of Step 1 + Step 2 forms of Cu (8610 mg/kg) at site RS8 constituted a CF value of 307 (Figure 3.18a) and an Er value of 1537 (Figure 3.19a) which according to Hakanson (1980), indicates a 'very high contamination' level and a 'very high ecological risk' level, respectively, of the Timok River sediments by Cu precipitated from the overlying river waters. It is very important to observe that these CF and Er values make up 53 % of those observed in Figures 3.18a and 3.19a, implying that the contribution of polluted river waters in the contamination of downstream sediments is slightly higher than that of flotation tailings (oxidizable and residual fractions).

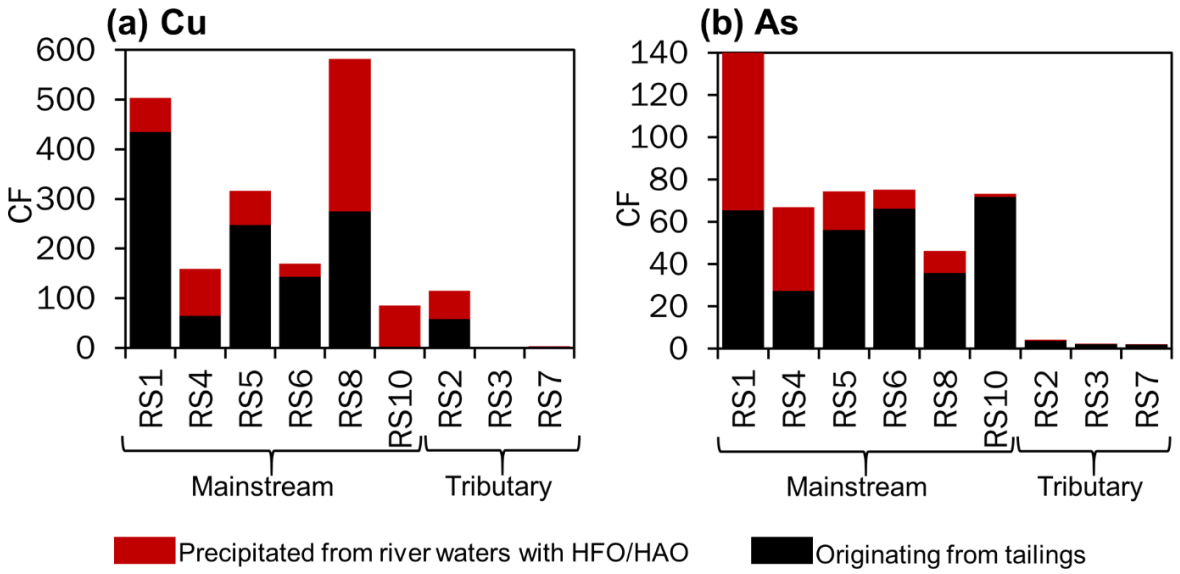

Figure 3.18 Contamination factor (CF) of Cu (a) and As (b) modified by the sequential extraction data to clarify sources riverbed sediments contamination. Mainstream sediments refers to those impacted by flotation tailings and the Bor metallurgical/smelter wastewaters. Tributary sediments are not impacted by either

According to Figure 3.18a and Figure 3.19a, the Step 1+ Step 2 forms of Cu (1922 mg/kg) at site RS1 respectively constituted a CF value of 69 and an Er value of 343, also suggesting a 'very high contamination' and 'very high ecological risk' of the Bor River sediments. However, these CF and Er values only account for 14 % of those observed in Figures 3.16a and 4.17, suggesting that Cu contamination of the sediments near the Bor metallurgical/smelting facilities is mainly contributed by the flotation tailings. Although the CF values (Figure 3.16a) and Er values (Figure 3.17) were the highest at both sites (RS8 and RS1), the risks of Cu mobilization are very different. The risks of Cu release from the sediments of the Timok River into the waters are very high while the risks of Cu mobilization from sediments of the Bor River into the waters are very low.

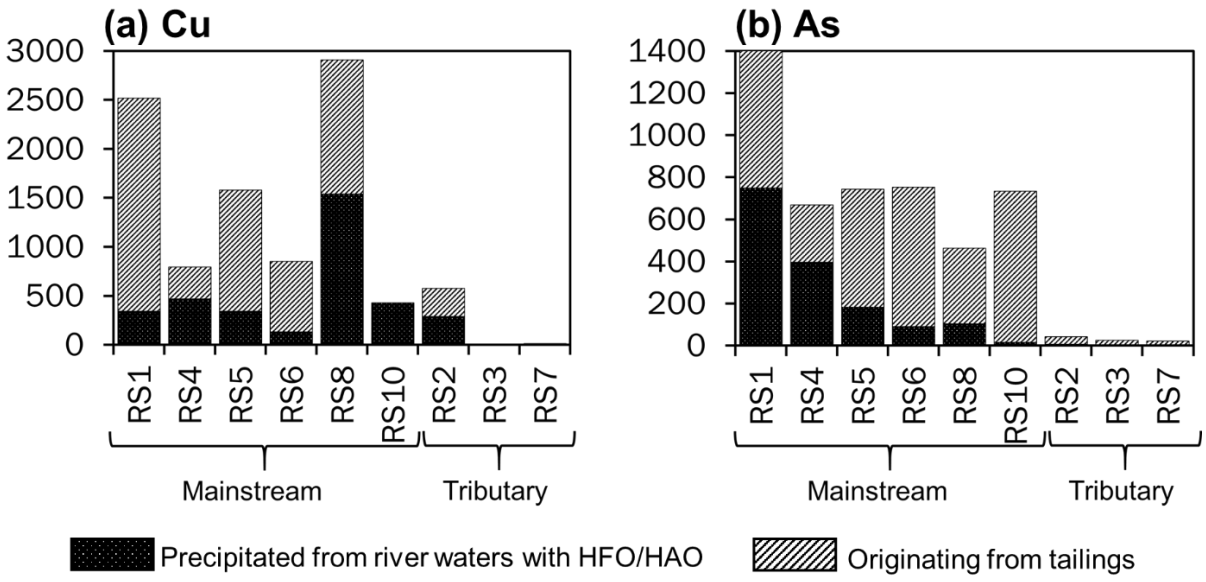

Figure 3.19 Ecological risk potential (Er) of Cu (a) and As (b) modified by the sequential extraction data to clarify sources riverbed sediments contamination. Mainstream sediments refers to those impacted by flotation tailings and the Bor metallurgical/smelter wastewaters. Tributary sediments are not impacted by either

3.4.4.2 Speciation of As

The high contents of reducible As observed in upstream sediments (Figure 3.7b) is in agreement with the As flux patterns (Figures 3.8e and f), where particulate As species, sorbed onto the suspended HFO, are dominant in the entire study reach and have eventually settled to enrich the riverbed sediments. The photograph of site RW4 (Figure 3.3d) could provide field evidence of the abundance of HFO (possibly with sorbed As) in the Bela River as seen by the yellow coatings on the riverbed. The collective contents of As extracted from the oxidizable (Step 3) and residual fractions were also high (Figure 3.7b). Considering the high total As contents (Figure 3.15), it can be assumed that these fractions are majorly associated with the sulphide minerals, especially pyrite (Deditius et al., 2011; Reich et al., 2013; Franchini et al., 2015).

The contents of reducible As at sites RS1 (354 mg/kg) and RS4 (186 mg/kg) constituted CF values of 74 and 39 (Figure 3.18b), respectively, suggesting a 'very high contamination' level of the sediments near the Bor metallurgical/smelter facilities by As precipitated by with HFO. It is imperative to note that these CF values are 53 % (RS1) and 58 % (RS4) of those observed in Figure 3.16b, which implies that upstream sediments are slightly more contaminated with As from the river waters than from the flotation tailings. Consequently, the risks of As release from sediments of the Bor and Bela Rivers into the waters are very high.

3.4.5 Sediment enrichment by economically mineable Cu from wastewaters

Artificial dams generally slow down the speed of a river flow, and in doing so, promote the gravitational settling of suspended materials sorbing several metals and metalloids at sites upstream of the said dam. Ogawa et al. (2012, 2013, 2018) have observed that the reservoirs sometimes act as sinks for rare metals such as Ga and In originating from acidic thermal waters. Similar behaviour leading to the accumulation of high Cu contents was observed in this

research area. In fact, out of a total Cu content of 16,300 mg/kg at site RS8, this process is responsible for the collective 53 % (Step 1 + Step 2) (Figure 3.7a) through Figure 3.20.

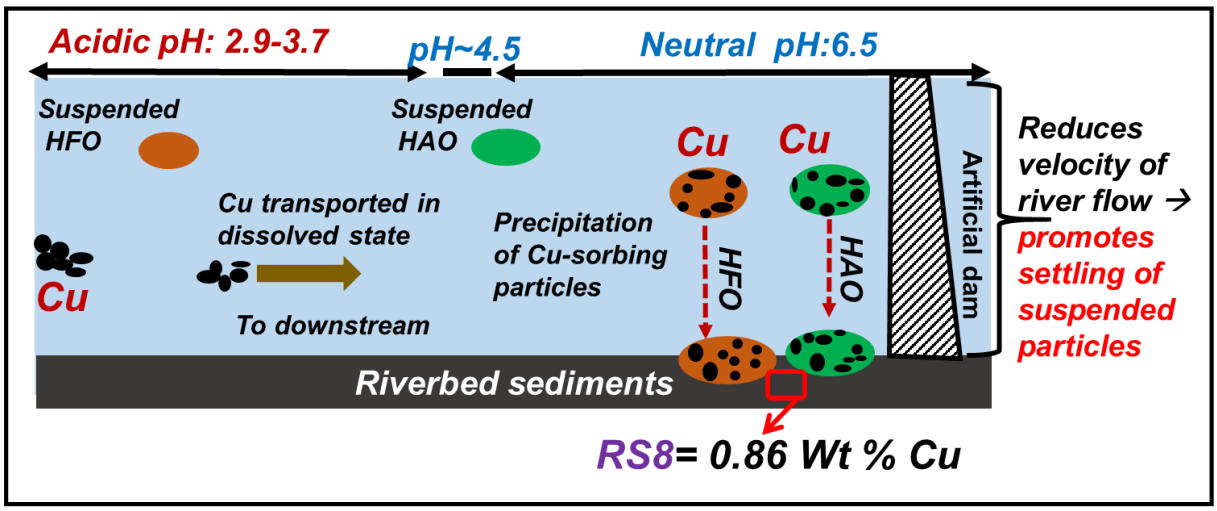

Figure 3.20 Schematic diagram showing the enrichment mechanism of Cu on the dam/reservoir sediments

This amount to 0.86 wt % Cu and is higher than the Cu ore grade (0.3 wt %) at the Veliki Krivelj open pit mine reported by Stanković et al. (2015). The remaining Cu at RS8 mainly originates from the flotation tailings released from the Bor mineral processing plant. Despite the high risk of Cu release as suggested by the modified BCR extraction procedure (Figure 5a), this implies that with respect to mining and metal recovery, this site could provide a secondary Cu deposit.

In 2019, the total concentrations of Cu and As at site RW1 were 116 mg/L and 2.7 mg/L, respectively, giving a Cu/As mole ratio of 51. The chemical fractionation of Cu and As occurs during river transport. According to Figures 3.8e and f, particulate As tends to be widely distributed during transport to site RW8, whereas Cu precipitates effectively between sites RW6 and RW8 (Figures 3.8g and h). At site RS8, the contents of Cu and As released from Step 1 + Step 2 were 8610 mg/kg and 49.9 mg/kg, respectively (Figure 3.7), giving a Cu/As mole ratio of 203. Assuming that these Cu and As contents originate from Bor metallurgical/smelting facilities, Cu is preferentially concentrated in sediments at RS8 compared to river water at RW1,

rather than As. This fact means the effective accumulation of economically useful metals excluding toxic elements in the reservoir sediment (Figure 3.20).

3.5 CONCLUSIONS

The Bor and Bela Rivers were highly acidic in 2019 than in 2015 and consequently had extremely higher dissolved concentrations of Al, Fe, Cu and As, suggesting the severity of river water contamination by the Bor metallurgical/smelting facilities in 2019. The risk assessment of river water contamination was evaluated in a Ficklin diagram for the two sampling periods and it was established that in 2015, the Bor River and Bela River plotted in the 'acid/high metal' region. However, in 2019, the Bela River plotted in the 'acid/high metal' region whereas the Bor River plotted in the 'high acid/extreme metal' region. The dissolved Cu species contributed the most toxicity to the waters of Bor and Bela Rivers. Also, due to the long transport of Cu as a dissolved species under more acidic conditions, the downstream site (RW8) plotted in a region of higher risk during the 2019 sampling period.

Fe existed in form of the suspended hydrous ferric oxides (HFO) in upstream regions and its removal from the water column by settlement onto the riverbed was widely distributed in the study area. Arsenic was sorbed onto the HFO and removed from the water column via settlement. Al and Cu existed primarily as dissolved species in the entire study area, especially in 2019. Cu fluxes decreased markedly at neutral pH conditions with suspended hydrous Al oxide (HAO).

Responding to the settling of the As-sorbing HFO, As in the riverbed sediments existed mainly as a reducible form at upstream sites (RS1 and RS4) whereas at downstream sites, the contents of reducible As were only considerable. The settling of Cu-sorbing HAO and/or HFO at the downstream site is consistent with high contents of acid-soluble and reducible Cu at site RS8.

However, at upstream sites, the higher Cu contents were associated with Cu sulphide minerals originating from the tailings.

The contamination factor index (CF) indicated that all mainstream sediments exhibit a very high contamination level by Cu and As. The As precipitated with HFO from the overlying river waters contributed 54 and 22 % to the CF values of As in sediments of the Bor River and Timok River, respectively. On the other hand, the Cu precipitated with HAO and HFO contributed 14 and 53 % to the CF values of Cu in sediments of the Bor River and Timok River, respectively. The ecological risk potential index has shown that Cu and As pose a very high ecological risk to the sediments of the Bor River, Bela River and Timok River.

The reduced flow velocity of the Timok River induced by an artificial dam promoted the gravitational settling of the suspended Cu-sorbing particles, thereby enriching the riverbed sediments with economically mineable Cu contents. The amount of Cu originating from the flotation tailings, released from the mineral processing plant in the 1950s into the Bor River, was 0.77 wt %. On the other hand, the Cu settled with suspended HFO and/or HAO, which mainly originated from the metallurgical/smelter wastewaters, in the reservoir sediment was 0.86 wt % and is higher than the Cu ore grade (0.3 wt %) at the Veliki Krivelj open pit mine.

4. OCCURRENCES AND ENVIRONMENTAL IMPLICATIONS OF EFFLORESCENT SALTS ALONG THE BOR RIVER CONTAMINATED BY COPPER MINING ACTIVITIES IN EASTERN SERBIA

4.1 INTRODUCTION

Efflorescent salts, composed mostly of hydrated metal sulphates, are very important secondary minerals in mine environments. Investigations of their occurrence, spatial distribution, mineralogy, paragenetic evolution and dissolution behaviour are crucial as these minerals tend to act as both solid transients of toxic trace elements and sources of water and soil contamination (Nordstrom, 2009; Dold, 2014, Pi-Puig et al., 2020).

4.1.1 Formation of hydrated metal sulphates

The evaporation of acid mine drainage during hot and dry seasons produces colorful blooms of efflorescences, consisting of a variety of hydrated metal sulphates (Alpers et al. 1994, Jambor et al. 2000). Additionally, the upward capillary migration of pore waters from mine wastes has been known to cause the precipitation of hydrated metal sulphates at the surface (Romero et al., 2006; Arranz-González et al., 2020). Efflorescent salts have been observed at different hydrogeological locations: on the banks of AMD-impacted rivers (Buckby et al., 2003; Romero et al., 2006; Cánovas et al., 2008;2010; Fosso-Kankeu et al., 2017; Cala-Rivero et al., 2018; Nordin et al., 2018); on the surface of the flotation tailings or waste-rock piles (Dold, 2003; Murray et al., 2014; Khorasanipour, 2015; Grover et al., 2016; Biagioni et al., 2020; Pi-Puig et al., 2020; D'Orazio et al., 2021; Loredo-Jasso et al., 2021; Islam et al., 2021; Gerding et al., 2021); on the mine benches and rims of abandoned open-pits (Valente et al., 2013; Buzatu et al., 2016; Antivachis et al., 2017), within mine-workings (Nordstrom and Alpers, 1999; Onac et al., 2003; Jamieson et al., 2005) and along the stream of flowing mine

waters (Valente and Gomes, 2009; Hammarstrom et al., 2005; Basallote et al., 2019; Newman et al., 2020; Nieva et al., 2021).

The hydrated metal sulphates with divalent cations ($Me^{2+}SO_4 \cdot nH_2O$) are the most dominant mineral types (Jambor et al., 2000, Romero et al., 2006) and are usually the first to form during the evaporation of acidic, metal and sulphate loaded waters through Reaction 4.1.

$$Me^{2+}_{(aq)} + SO_4^{2-}{}_{(aq)} + nH_2O_{(l)} \rightleftharpoons Me^{2+}SO_4 \cdot nH_2O_{(s)} \quad (4.1)$$

where *Me* = Fe, Mg, Cu, Ca n = 1 to7

4.1.2 The role of climate on the precipitation hydrated metal sulphates

Temperature and humidity are the primary climate variables controlling evaporation (Nordstrom, 2009). In semiarid to arid climates, evaporation drastically reduces the amount of water, promoting the concentration of solutes to a point of mineral saturation (Basallote et al., 2019). Seal and Piatak (2012) reported that, because of the concentrating effect of evaporation, acidity and metal concentrations in AMD are typically several orders of magnitude greater in dry seasons than rainy seasons in arid environments. However, in temperate and wet climates, constant rains continually dilute acid and metal-laden mine waters to benign contents, thereby inhibiting the supersaturation of metals and sulphate concentrations (Seal and Piatak, 2012).

4.1.3 Groups of hydrated metal sulphates

4.1.3.1 Melanterite group

The general formula of minerals in the monoclinic melanterite group is represented $M^{2+}SO_4 \cdot 7H_2O$ and include common end members such as melanterite (*M*=Fe^{2+}), boothite (*M*=Cu), zinc-melanterite (*M*=Zn, Cu) and mallardite (*M*=Mn). Melanterite ($Fe^{2+}SO_4 \cdot 7H_2O$) is the first Fe sulphate mineral to form from the evaporation of Fe^{2+} and SO_4^{2-} rich mine effluents

(Bigham and Nordstrom 2000; Jambor et al., 2000; Jerz and Rimstidt, 2003; Hammarstrom et al. 2005; Sanchez-Espana et al., 2008). The color of melanterite ranges from pale blue to green-blue (Hammarstrom et al., 1999, 2005; Jerz and Rimstidt, 2003; Valente and Gomes, 2009; Antivachis et al., 2016; D'Orazio et al., 2021). Onac et al. (2003) reported that upon exposure to dry air, melanterite can turn white-yellowish. Melanterite has been known to sequester high contents of Zn and Cu in its solid solution (Alpers et al., 1994; Frau, 2000; Jambor et al., 2000; Bucky et al., 2003; Hammarstrom et al., 2005; D'Orazio et al.,2021), due to the homovalent substitution between Fe^{2+} and Cu^{2+} or Zn^{2+}.

4.1.3.2 Epsomite group

The general formula of minerals in the orthorhombic epsomite group is represented $M^{2+}SO_4 \cdot 7H_2O$ and include common end members such as epsomite (M=Mg), morenosite (M=Ni) and goslarite (M=Zn). Minerals in the epsomite group are usually white colored (Antivachis et al., 2016; Loredo-Jasso et al., 2021). Epsomite can include only very small amounts of substitution for Mg by Fe, Cu or Co (Jambor et al., 2000). Romero et al. (2006) realized that epsomite contained significant contents of Mn (1 wt. %) and Zn (0.5 wt. %) in its solid solution.

4.1.3.3 Hexahydrite group

The general formula of minerals in the monoclinic hexahydrite group is represented $M^{2+}SO_4 \cdot 6H_2O$ and include common end members such as hexahydrite (M=Mg), ferrohehydrite (M=Fe) and bianchite (M=Zn). They commonly occur as white slat blooms (Valente et al., 2013). In hexahydrite, the substitution of Mg for Ni has been reported (Janjic et al. 1980). Bucky et al. (2003) observed that hexahydrite sequester relatively low contents of trace elements compared to melanterite.

4.1.3.4 Chalcanthite group

The general formula of minerals in the triclinic chalcanthite group is represented $M^{2+}SO_4 \cdot 5H_2O$ and include common end members such as chalcanthite (*M*=Cu), pentahydrite (*M*=Mg) and siderotil (*M*=Fe). Chalcanthite has a characteristic deep blue color (Hammarstrom et al., 2005; Valente et al., 2013; Antivachis et al., 2016; Loredo-Jasso et al., 2021). A mutual Cu-Fe substitution has been observed in several studies (Jambor and Traill 1963; Antivachis et al., 2016). With regards to pentahydrite, substitution for Mg by Cu and Zn have been reported by Palache et al. (1951).

4.1.3.5 Rozenite group

The general formula of minerals in the monoclinic rozenite group is represented $M^{2+}SO_4 \cdot 4H_2O$ and include common end members such as rozenite (*M*=Fe), starkeyite (*M*=Mg) and ilesite (*M*=Mn). Rozenite usually has a white color (Hammarstrom et al., 1999; Jerz and Rimstidt, 2003; Valente and Gomes, 2009; Paramanick et al., 2021).

4.1.3.6 Copiapite group

The general formula of minerals in copiapite group is represented $AR_4(SO_4)_6(OH)_2 \cdot 20H_2O$, where *R* is dominated by Fe^{3+} in all members and *A* is usually Fe^{2+} (copiapite) or Al^{3+} (aluminocopiapite). Copiapite is a golden yellow mineral (Nordstrom and Alpers, 1999; Jerz and Rimstidt, 2003; Hammarstrom et al., 2005; Jamieson et al., 2005; Valente et al., 2013; Paramanick et al., 2021).

$$Fe^{2+}_{(aq)} + 3Fe^{3+}_{(aq)} + 6SO_4{}^{2-}_{(aq)} + 22H_2O_{(l)} \rightleftharpoons Fe^{2+}(Fe^{3+})_3(SO_4)_6(OH)_2 \cdot 20(H_2O)_{(s)} + H^+_{(aq)} \quad (4.2)$$

The formation of copiapite requires warm temperatures, oxidizing conditions and low pH environments. It can form from the oxidation of Fe^{2+} sulphates such as melanterite or rozenite or precipitate directly from Fe^{2+}-Fe^{3+}– acid rich solutions according Reaction 4.2 (Buckby et

al. 2003). Theoretically, copiapite contains about 80 % of Fe^{3+} and 20% of Fe^{2+} in its solid solution. Copiapite has been reported to store Zn, Cu and As (Jamieson et al, 2005) in its solid structure.

4.1.3.7 Coquimbite group

The general formula of minerals in the coquimbite group is represented $A_2(SO_4)_3 \cdot nH_2O$, where A is usually occupied by Fe^{3+} or Al^{3+}, and n ranges from 6 to 17. Chou et al. (2002) reported that coquimbite ($Fe_2(SO_4)_3 \cdot 6H_2O$) and alunogen ($Al_2(SO_4)_3 \cdot 17H_2O$) are the most commonly occurring trivalent hydrated sulphate minerals. Coquimbite is usually purple to violet in color whereas alunogen is colorless (D'Orazio et al., 2021). Alpers et al. (1994) observed that coquimbite is intimately associated with copiapite in gossan deposits and mine workings. Coquimbite has been reported to be enriched with high contents of As (Romero et al., 2006; D'Orazio et al., 2021; Nieva et al., 2021), which is owed to the sorption by the Fe^{3+} phase.

4.1.3.8 Halotrichite group

The general formula of minerals in the halotrichite group is represented by $AR_2(SO4)_4 \cdot 22(H_2O)$, where *R* is always Al^{3+} or Fe^{3+} and *A* is Mg, Fe^{2+}, Mn^{2+}, Co^{2+}, or Zn^{2+}. The common end members of this group include halotrichite ($Fe^{2+}Al_2(SO4)_4 \cdot 22H_2O$), pickeringite ($MgAl_2(SO4)_4 \cdot 22H_2O$) and apjohnite ($MnAl_2(SO4)_4 \cdot 22H_2O$) (Martin et al. 1999). According to Blowes et al. (2004) and Hammarstrom et al. (2005), the crystallization of minerals in the halotrichite group is paragenetically later than that of Fe, Mg and Cu salts. This is attributed to the fact that during the formation of such minerals, divalent cations (Fe^{2+}, Cu^{2+}, Mg^{2+}) are removed from waters, thereby enriching waters with Al which will eventually form halotrichite (Jerz and Rimstidt, 2003).

4.1.4 Paragenetic evolutions of sulphate minerals

Paragenesis refers to the sequence of mineral formation and alteration that occurs as hydrous metal sulphates form and continue to evolve with time. The precipitation and evolution of evaporative sulphates is controlled primarily by the dehydration and oxidation reactions brought about by changes in acidity, oxidation conditions, relative humidity and temperature (Frau, 2000; Jambor et al., 2000; Jerz and Rimstidt, 2003; Jamieson et al., 2005). Nordstrom and Alpers (1999) noted that a typical paragenetic sequence of mineralogical maturation of Fe sulphates follow a trend: melanterite > rozenite > szomolnokite > copiapite > coquimbite > rhomboclase > halotrichite.

4.1.4.1 Dehydration

An increase in temperature or a decrease in humidity can transform hydrous metal sulphates from high hydration state to low hydration state. Hammastrom et al. (2005) mentioned that exposure of melanterite to ambient conditions will dehydrate to rozenite through Reaction 4.3. Other minerals with varying hydration level in the $FeSO_4$-H_2O systems include ferrohexahydrate ($FeSO_4 \cdot 6H_2O$), siderotil ($FeSO_4 \cdot 5H_2O$), and szomolnokite ($FeSO_4 \cdot H_2O$). The dehydration product is also controlled by solid solution composition. For example, Jambor and Traill (1963) observed that Cu-bearing melanterite dehydrated to siderotil (Reaction 4.4) whereas Cu-free melanterite dehydrated to rozenite under the same conditions (Reaction 4.3). Antivachis et al. (2016) also reported the transformation of melanterite into siderotil, occurring on the exposed surfaces of Cu-pyrite mineralization.

$$Fe^{2+}SO_4 \cdot 7H_2O_{(s)} \rightarrow Fe^{2+}SO_4 \cdot 4H_2O_{(s)} + 3H_2O_{(l)} \quad (4.3)$$

$$Fe^{2+}SO_4 \cdot 7H_2O_{(s)} \rightarrow (Cu,Fe^{2+})SO_4 \cdot 5H_2O_{(s)} + 3H_2O_{(l)} \quad (4.4)$$

4.1.4.2 Oxidation

Fe^{3+} minerals are usually formed through the oxidation of the Fe^{2+} phases under warm temperatures, highly acidic and oxidizing environments (Frau 2000; Jerz and Rimstidt 2003). The oxidation of rozenite in acidic pore waters forms copiapite which in turn can transform into coquimbite through Reactions 4.5 and 4.6, respectively (Chou et al., 2013).

$$5Fe^{2+}SO_4 \cdot 4H_2O_{(s)} + H_2SO_{4(l)} + O_{2(g)} \rightleftharpoons Fe^{2+}Fe^{3+}{}_4(SO_4)_6(OH)_2 \cdot 20(H_2O)_{(s)} \quad (4.5)$$

$$2Fe^{2+}Fe^{3+}{}_4(SO_4)_6(OH)_2 \cdot 20H_2O_{(s)} + \tfrac{1}{2}O_{2(g)} + 3H_2SO_{4(l)} \rightarrow \quad 5Fe^{3+}{}_2(SO_4)_3 \cdot 9(H_2O)_{(s)} \quad (4.6)$$

The general trend for the simple hydrous sulfate salts is that the Fe^{2+} minerals form first, followed by the mixed Fe^{2+}-Fe^{3+} minerals, and then the Fe^{3+} minerals (Jambor et al., 2000). The newly formed secondary minerals are more stable and resistant to redissolution compared to their precursors. Also, the continued exposure of these minerals to oxidizing conditions could lead to the formation of less soluble hydroxide and oxyhydroxide minerals, such as schwertmannite, jarosite, ferrihydrite and goethite (Nordstrom, 1982; Levy et al., 1996).

4.1.5 Transient of toxic elements from contaminated waters

Through coprecipitation, minor contents of toxic metals are incorporated into the main crystal matrix (through substitution) as an impurity thereby removed from AMD waters (Jambor et al., 2000). Additionally, hydrated metal sulphates have large surface areas, providing them with remarkable abilities to adsorb high quantities of trace elements, thereby immobilizing toxic metals from mine effluents and AMD-bearing river waters (Lin, 1997; Nordstrom and Alpers, 1999; Berger et al., 2000). Essentially, efflorescent salts are a solid form of AMD, temporarily stored until the next rainstorm or snowmelt event.

4.1.6 Dissolution behavior of efflorescent salts

Efflorescent salts are highly soluble and provide an instantaneous source of acidic water upon dissolution occurring during first rainfall event (Nordstrom, 1982; Cravotta, 1994), resulting in the increased acidity and metals loadings in the receiving rivers or streams (Keith et al., 2001; Smuda et al., 2007; Valente and Gomes 2009). The instantaneous spike in dissolved element concentrations is referred to as 'first flush' AMD (Dagenhart 1980; Jambor et al., 2000; Nordstrom, 2009). Valente et al. (2003) dissolved hydrated metal sulphates in distilled water (20g/L ratio) and reported different pH values for chalcanthite + halotrichite assemblage (pH 4.3), copiapite + szomolnokite + halotrichite assemblage (pH 2.5) and copiapite + rhomboclase assemblage (pH 2.0-2.1). This PhD thesis will demonstrate the environmental significance of hydrated metal sulphates formed on the banks of the acutely contaminated Bor River as sources of acidity and toxic elements.

4.2 METHODOLOGY

4.2.1 Sample descriptions

A variety of colourful evaporative salts were observed along the banks of the Bor River (Figure 4.1 and 4.2) during the summer season (August and September). The salts were carefully sampled with a stainless steel spatula to separate the salts from substrate (soil/ rock). The sample were air-dried overnight at ambient temperatures. Immediately after drying, the efflorescent salts were sealed off in airtight Ziplocs, to avoid hydration or dehydration of the mineral phases. At each site, the coordinates were obtained by a GARMIN global positioning system (GPS). Field observations such as color, moisture and texture were also made and recorded appropriately.

A descriptive summary of salt sampling dates and field observations is provided in Table 4.1. Briefly, evaporative salts were sampled from two locations on the banks of the Bor River (Figure 4.1); upstream samples (EF1- EF3, Figure 4.2a, b and c) were obtained in August 2017 and downstream samples (EF4 - EF6, Figure 4.2d, e and f) were collected in September 2021. Site EF1 was located 30m from the point discharge of the Bor metallurgical/smelter wastewaters whereas EF2 and EF3 were close to each other and 70 m downstream of EF1(Figure 4.1). The downstream samples were located 8 km from the point discharge of the Bor metallurgical/smelter wastewaters; site EF4 was very close to the waters of the Bor River while EF5 and EF6 were 3 and 10 m, respectively, away from the waters, towards the outer edge of the river bank (Figure 4.1).

Table 4.1 Sample locations and field descriptions of efflorescent salts along the Bor River

Sample ID	Sample date	Field observations and descriptions
EF1	08/08/2017	Yellowish precipitates of Bor river, after metallurgical wastewaters
EF2	08/08/2017	Pale blue precipitate, 80 m downstream of EF1
EF3	08/08/2017	Pale yellow precipitate, 80 m downstream of EF1
EF4	14/09/2021	Yellowish blue precipitate of downstream Bor river
EF5	14/09/2021	Faint blue precipitate along Bor river, 3m south of EF4
EF6	14/09/2021	Golden yellow/faint purple precipitate of Bor river,10m south of EF4

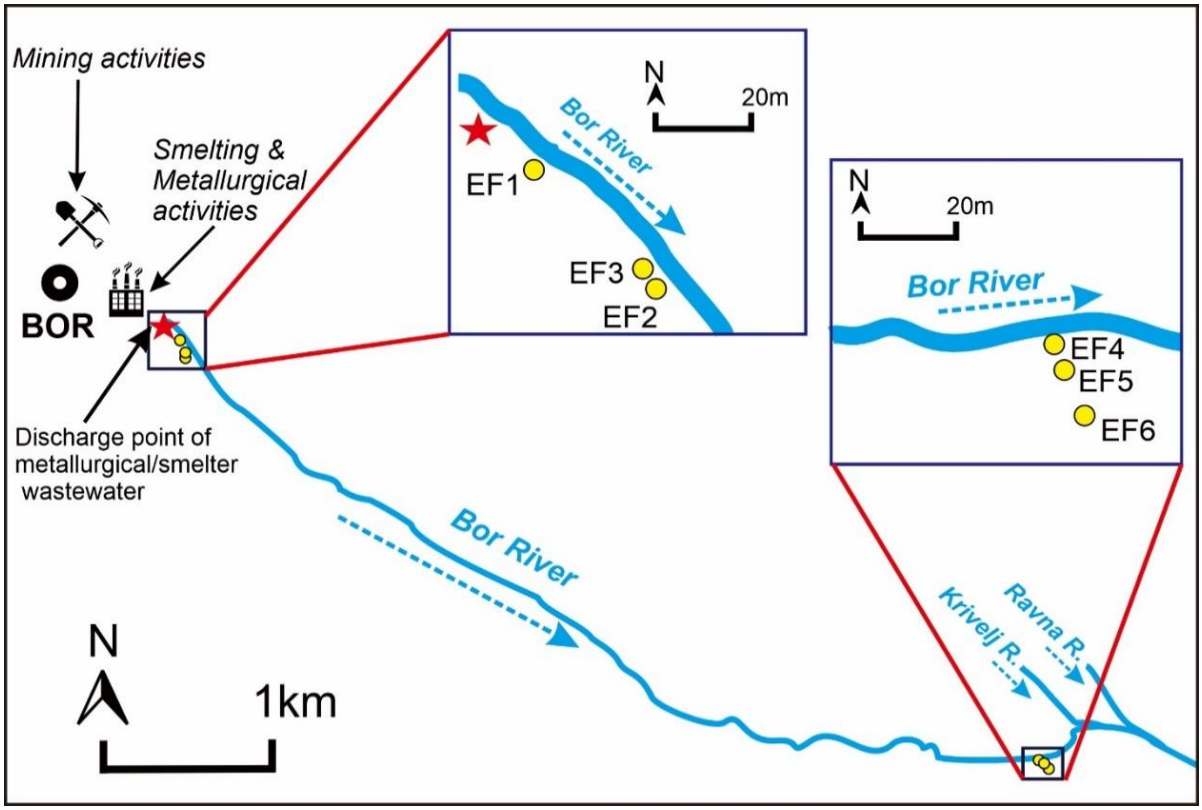

Figure 4.1 Map of the study area with efflorescent salt sampling locations

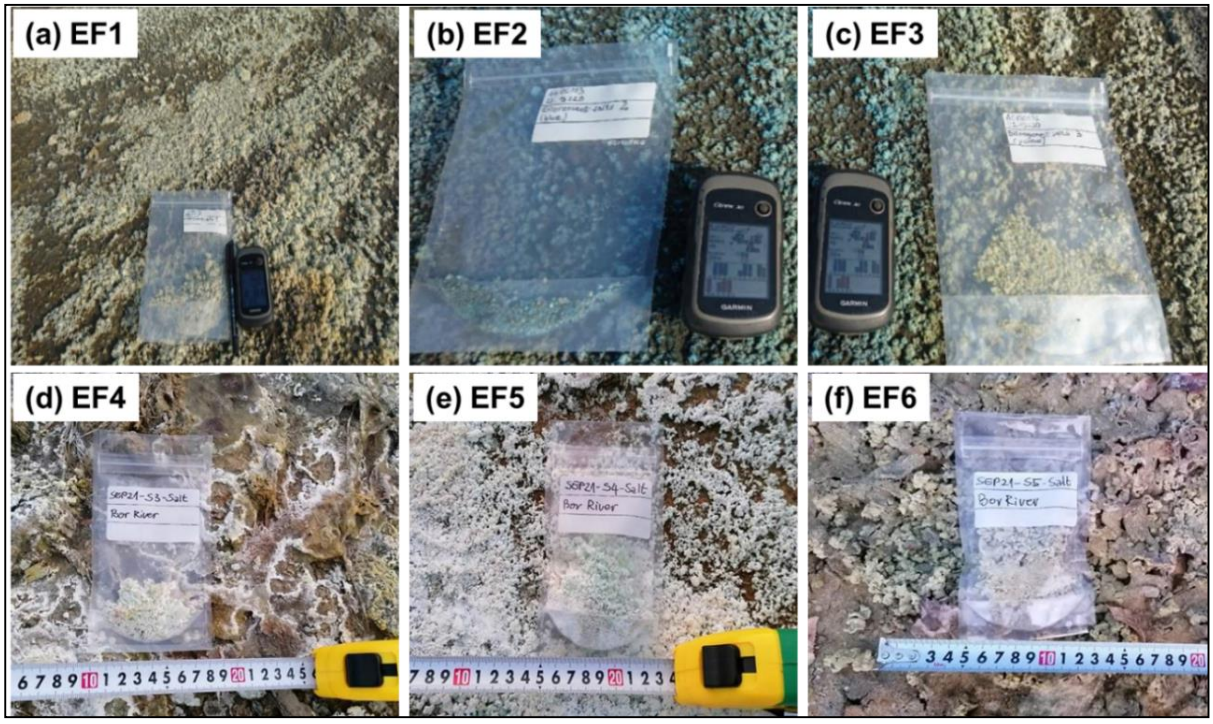

Figure 4.2 Field photographs of efflorescent salts along the banks of the Bor River in August 2017 (a, b and c) and September 2021 (d, e and f)

4.2.2 Treatment of samples

The samples collected in the August 2017 campaign (EF1-EF3) were analyzed by XRD technique for bulk mineralogical characterization immediately after collection using the procedure outlined in Section 5.2.2.1. The samples were then stored at ambient air temperatures and humidity. These samples were re-analyzed in September 2021 using the same analytical procedure. This was done to observe any mineralogical changes (aging effects) or transformation of mineral types during the 4 years' storage time and make comparisons with the 2017 data. The samples obtained in the September 2021 survey (EF4-EF6) were analyzed immediately after collection, therefore, the mineralogy obtained represent an assemblage of mineral phases in the field.

4.2.3 Scanning Electron Microscope-Energy Dispersive spectra (SEM-EDS)

Pulverized efflorescent salt samples were mounted on a glass slide using a carbon tape and were carbon-coated two times to ensure complete coverage on the whole sample. The samples were analysed by a Field Emission Scanning Electron Microscope (JSM-7800F) combined with an energy dispersive system (SEM-EDS) to study the morphological and compositional characteristics (Figure 4.3). The operating settings for SEM-EDS were: accelerating voltage of 20.0 kV, emission current of 90 μA and electron beam diameter of < 1μm. This analysis was conducted at Akita university.

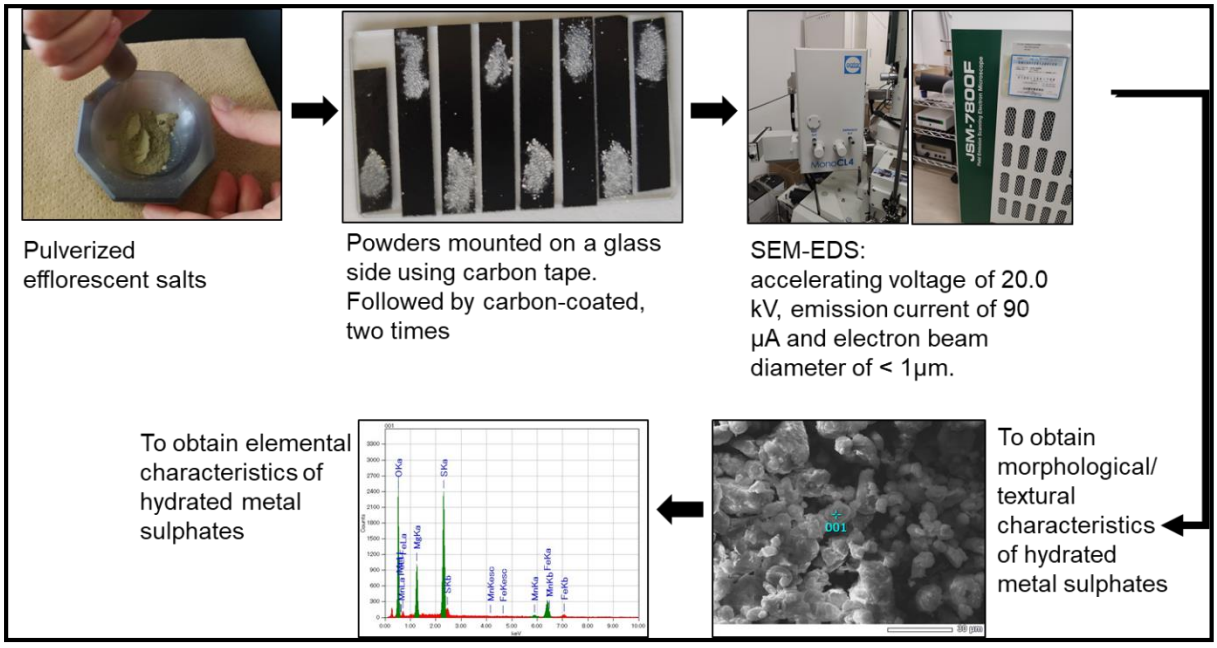

Figure 4.3 Schematic diagram of salt sample preparation for SEM-EDS analysis

4.2.4 Dissolution of efflorescent salts

This test simulated the dissolution of efflorescent salts occurring during the interaction with first rainwater after prolonged dry period, leading to the release of acidity and toxic elements into the environment. The test was carried for all collected salts samples. A 2.0 g dried sample, with no particle size reduction, was mixed with 20 mL distilled water (pH 5.6), simulating rainwater in the Bor town. The mixtures were agitated in 50 mL polypropylene centrifuge tubes for 2 hours at a speed of 200 rpm (Recipro Shaker, model SR-2W) as indicated in Figure 4.4. After agitation, centrifugal force (Himac centrifuge, model CT6EL) was applied to the mixtures at a speed of 3000 rpm for 20 minutes to separate the supernatant from the solid residue. The leachate was then filtered using cellulose acetate hydrophilic filters with a pore size of 0.2 µm.

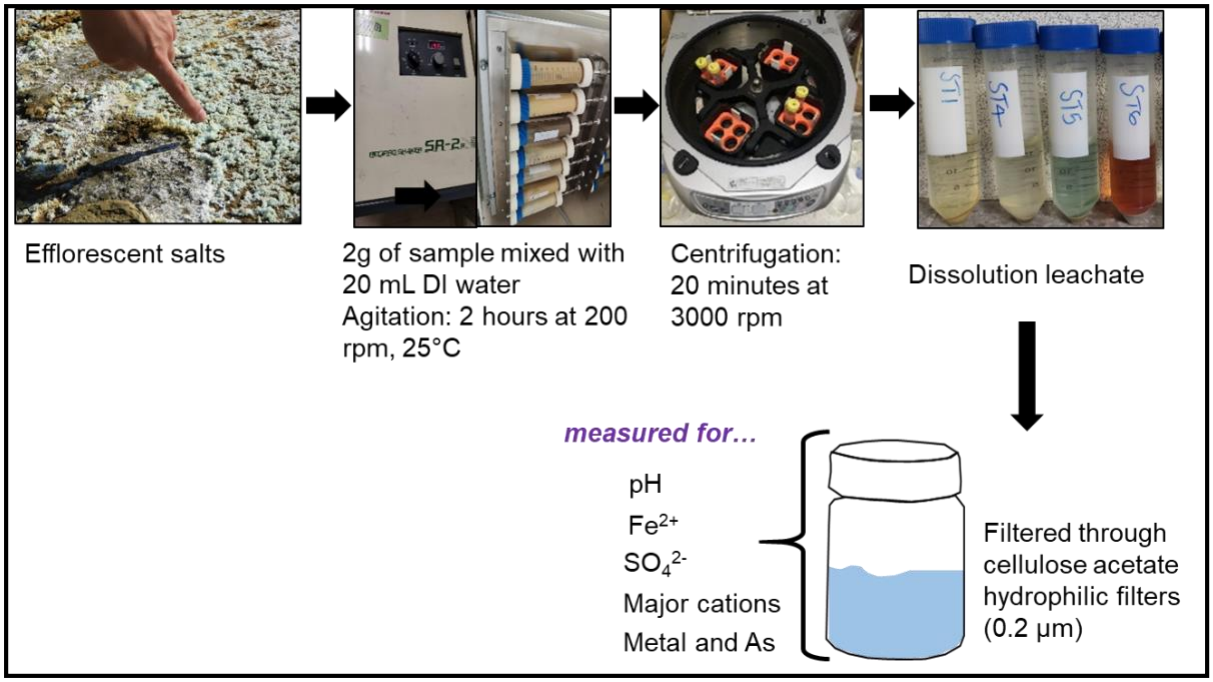

Figure 4.4 A detailed schematic diagram of the salt dissolution procedure

An aliquot of the leachate was measured for pH using a desktop pH meter (model HM-25R). Another split of the leachate was analysed for SO_4^{2-} concentrations using ion chromatography (IC). The remainder was acidified with 1% volume HNO_3 acid and later analysed for heavy metals using ICP-MS and analysed for major cations using Atomic absorption spectroscopy (AAS) based on the methods described in Section 5.2.4.1 and 5.2.4.2, respectively. This test was also applied for all the overburden materials (< 2mm) to assess the dissolution of soluble secondary sulphate minerals that may be present in the surface overburden materials. In this case, the agitation period was increased to 6 hours while other conditions were kept the same.

4.2.5 Fe speciation analysis-spectrophotometry

After the dissolution of evaporative salts (Figure 4.4), an aliquot of filtered sample (0.2µm filter size) was subjected to analysis by a spectrophotometer to obtain concentrations of dissolved Fe^{2+} (Figure 4.5). Due to the expected high concentrations of Fe in the leachates of

hydrated metal sulphates, the solutions were first diluted 1000 or 10,000 fold with distilled water, to ensure that Fe concentration did not exceed calibration.

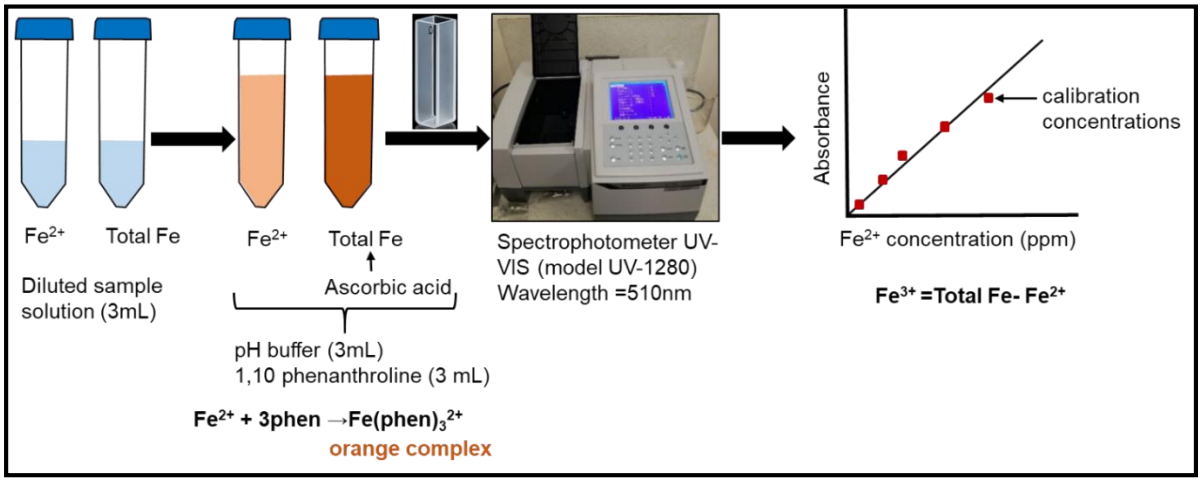

Figure 4.5 A detailed schematic diagram of the analysis of Fe^{2+} and Fe^{3+} using the colorimetric analysis technique

A 3mL of the diluted solution was added to two separate 15 mL polypropylene centrifuge tubes labelled "Fe^{2+}" and "Total Fe". On the "Total Fe" sample, enough amount (small laboratory stainless steel spatula) ascorbic acid, a reducing agent, was added to the sample to reduce the ferric iron (Fe^{3+}) to ferrous iron (Fe^{2+}). Then 3 mL of sodium acetate, a pH buffer solution, was added to both samples to maintain a constant pH at 3.2-3.5. Next, 3mL of 1,10 phenanthroline solution was added to both samples. Fe^{2+} reacts with 1,10-phenanthroline to form an orange coloured complex in direct proportion to the Fe^{2+} concentration (Method 3500-Fe B;1997). This is illustrated by the Equation 4.7.

$$Fe^{2+} + 3phen \rightarrow Fe(phen)_3^{2+} \quad (4.7)$$

The determination of the Fe^{2+}-phen complex was carried out with a UV-VIS spectrophotometer (model UV-1280) at a fixed wavelength of 510 nm using external calibration based on iron standard solutions (Fe= 10 ppm, 5 ppm, 3 ppm, 2 ppm, 1ppm and 0 ppm). The concentrations of Fe^{2+} were calculated from the measured absorbance/intensity using a calibration curve. The

concentration of Fe^{3+} was then obtained by subtracting Fe^{2+} from total dissolved Fe concentrations.

4.3 RESULTS

4.3.1 The mineralogy of efflorescent salts

The mineralogy of the evaporative salts from the banks of the Bor River (Table 4.2 and Figure 4.6) consisted of simple hydrated metal sulphates with divalent cations, trivalent cations and mixed divalent-trivalent cations. It is important to note that the salts from the Bor River were characterized by an assemblage of mineral phases and that single phases were not observed.

Table 4.2 X-ray diffraction mineralogical characterization of efflorescent salts

Hydrated sulphate minerals		2017 analysis			2021 analysis					
		EF1	EF2	EF3	EF1	EF2	EF3	EF4	EF5	EF6
Name	Formula									
Melanterite	$Fe^{2+}SO_4 \cdot 7H_2O$	O		O				O	O	
Rozenite	$Fe^{2+}SO_4 \cdot 4H_2O$				O		O		O	
Alpersite	$(Cu,Mg)SO_4 \cdot 7H_2O$		O							
Chalcanthite	$CuSO_4 \cdot 5H_2O$					O				
Epsomite	$MgSO_4 \cdot 7H_2O$	O	O							
Hexahydrite	$MgSO_4 \cdot 6H_2O$			O	O			O		
Pentahydrite	$MgSO_4 \cdot 5H_2O$				O		O			
Starkeyite	$MgSO_4 \cdot 4H_2O$					O				
Halotrichite	$FeAl_2(SO_4)_4 \cdot 22H_2O$							O		
Gypsum	$CaSO_4 \cdot 2H_2O$		O		O	O	O			
Copiapite	$Fe^{2+}Fe^{3+}{}_4(SO4)_6(OH)_2 \cdot 20(H_2O)$									O
Coquimbite	$Fe^{3+}{}_2(SO4)_3 \cdot 9(H_2O)$									O

4.3.1.1 Upstream Bor River efflorescent salts (EF1-EF3)

2017 XRD analysis

The results of the 2017 mineralogical analysis are presented in Table 4.2 and they represent the assemblages of the hydrated sulphates that prevailed on the banks of the Bor River in the 2017 August field survey. EF1 salt was whitish-yellow to pale blue (Figure 4.2a) and dominated by melanterite ($Fe^{2+}SO_4 \cdot 7H_2O$) with few epsomite ($MgSO_4 \cdot 7H_2O$) and gypsum ($CaSO_4 \cdot 2H_2O$) as indicated by Figure 4.6a. EF2 salt was blue (Figure 4.2b) and dominated by alpersite [$(Cu,Mg)SO_4 \cdot 7H_2O$], followed by epsomite and few gypsum (Figure 4.6b) while EF3 was whitish-yellow (Figure 4.2c) and dominated by melanterite with traces of hexahydrite ($MgSO_4 \cdot 6H_2O$) as shown in Figure 4.6c.

2021 XRD analysis

Due to the prolonged storage time (4 years), the mineralogical characterization of the evaporative salts detected in the 2021 analysis could represent an assemblage of mineral phases formed due to the aging effects, especially dehydration, of the evaporative salts sampled in 2017. This suggestion is supported by Hammastrom et al. (2005) who asserted that minerals sensitive to relative humidity such as melanterite will dehydrate at ambient laboratory conditions unless preserved in a special way.

Salt EF1 was predominated by rozenite ($Fe^{2+}SO_4 \cdot 4H_2O$), pentahydrite ($MgSO_4 \cdot 5H_2O$), hexahydrite ($MgSO_4 \cdot 6H_2O$) and gypsum ($CaSO_4 \cdot 2H_2O$). In Salt EF2, chalcanthite ($CuSO_4 \cdot 5H_2O$) dominated the mineralogy, followed by a few gypsum and starkeyite ($MgSO_4 \cdot 4H_2O$). The mineralogy of EF3 salt was dominated by both rozenite and pentahydrite, with traces of gypsum.

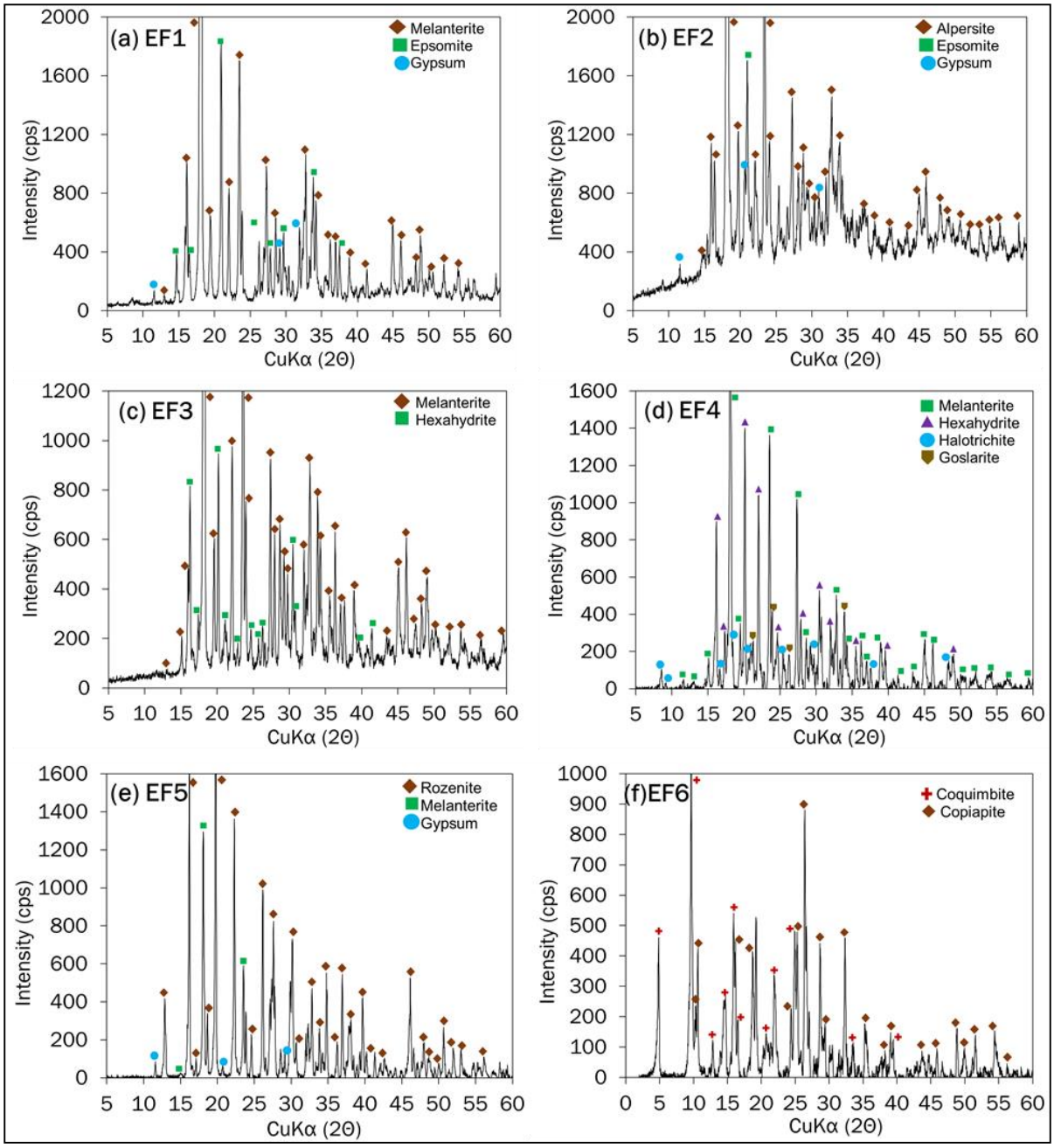

Figure 4.6 XRD patterns showing mineralogy of the efflorescent salts immediately after sampling

4.3.1.2 Downstream Bor River efflorescent salts (EF4-EF6)

Salt EF4 had yellowish-blue color (Figure 4.2d) and was dominated by melanterite, followed by hexahydrite and a few halotrichite ($FeAl_2(SO_4)_4 \cdot 22H_2O$) as indicated by Figure 4.6d. Salt EF5 had a faint-blue color (Figure 4.2e) and its mineralogy was dominated by the both rozenite

and melanterite (Figure 4.6e). In this sample, the contents of rozenite were significantly than melanterite. Salt EF6 had a pale yellow/faint-purple color (Figure 4.2f) and its mineralization was characterized by coquimbite ($Fe^{3+}_2(SO4)_3 \cdot 9(H_2O)$) and copiapite ($Fe^{2+}Fe^{3+}_4(SO4)_6(OH)_2 \cdot 20(H_2O)$) as shown in Figure 4.6f. The contents of coquimbite were higher than copiapite.

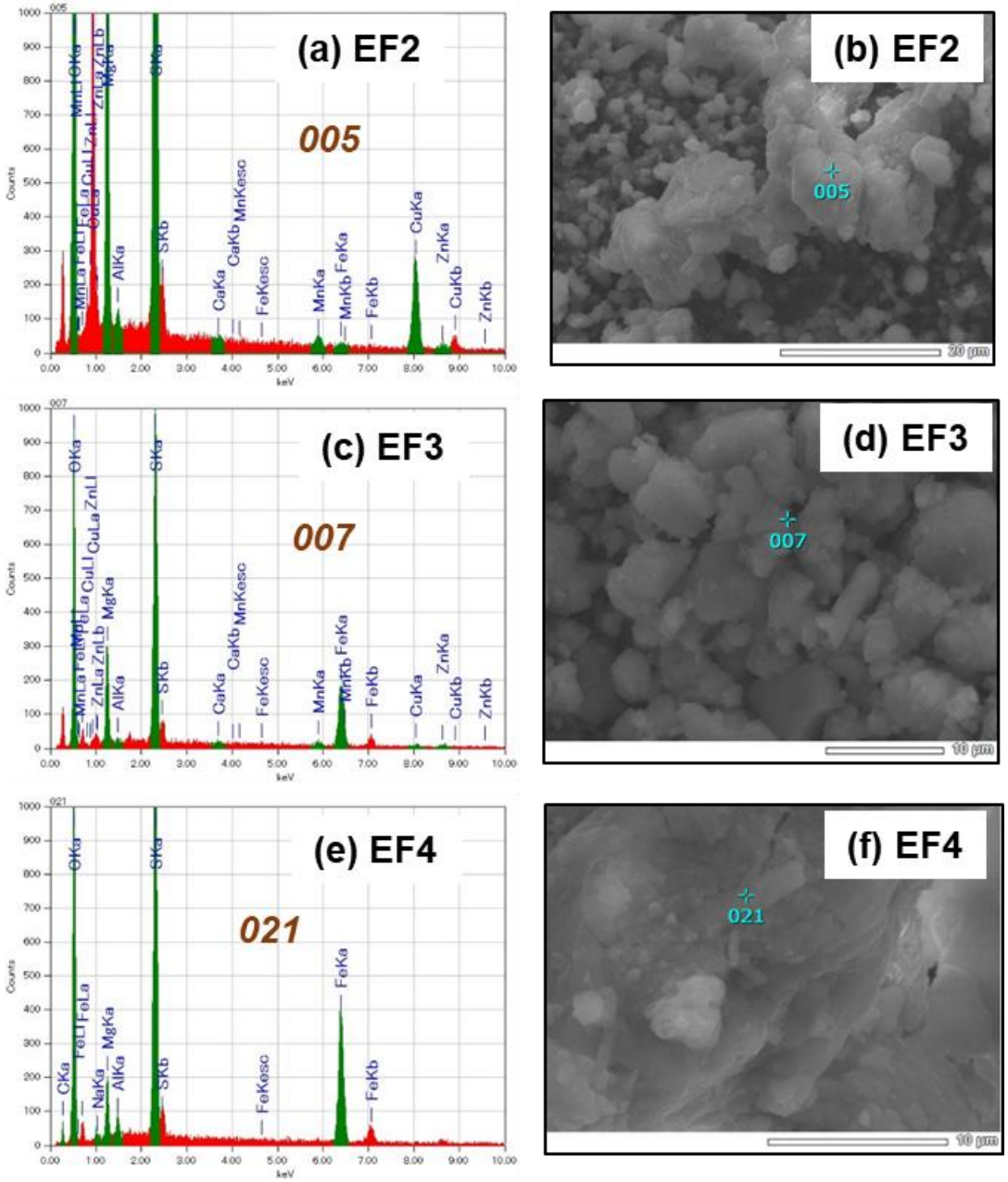

Figure 4.7 SEM-EDS results of the efflorescent salts. Back scattered electron (BSE) images on the right with corresponding EDS spectra on the left, showing elements present in the salts

The results of tentative SEM-EDS investigations of the salts are presented in Figure 4.7, providing a chemical characterization and crude estimate of the elements present in the mineralogical make-up of the hydrated metal sulphates.

4.3.2 Physico-chemical characteristics of the salt leachates

After 2 hours of water-salt interaction, the leachates obtained very distinct colors as indicated in Table 4.3 and Figure 4.8. Leachates of salts EF1, EF4 and EF5 were pale yellow (Figure 4.8a, d and e) while the leachate of EF3 was whitish-yellow with a faint blue (Figure 4.8c). The leachate of EF2 was pale blue (Figure 4.8b) while that of EF6 was reddish brown (Figure 4.8f). The final pH of the leachates from the Bor River evaporative salts ranged from pH 1.8 to 4.4, with EF6 generating the most acidic solution and EF2 generating least acidic solution.

Table 4.3 Physico-chemical characteristics of the salt leachates after 2-hour dissolution with distilled water (pH 5.6)

Sample ID	Color of the leachate	pH	Ca	Mg	Na	K	SO_4^{2-}
	Unit	-	mg/L	mg/L	mg/L	mg/L	mg/L
EF1	Yellowish	2.78	8.2	5320	209	1.0	47,600
EF2	Pale blue	4.41	7.6	5290	120	0.5	45400
EF3	Light yellowish blue	3.29	18	5030	20.5	1.3	51,800
EF4	Light yellowish white	3.00	107	2930	286	0.9	47,100
EF5	Light yellowish white	3.17	33.2	1280	149	0.8	42,800
EF6	Reddish brown	1.76	3.0	131	32.7	43.6	52,600

4.3.2.1 Variations in the concentrations of released elements

The dissolution of efflorescent salts released extremely high contents of major cations and sulphate ions: Na (20.5-286 mg/L), K (0.8-43.6 mg/L), Mg (131-5320 mg/L) and SO_4^{2-}

(42,800-52,600mg/L). The results of the concentrations of toxic elements released during the dissolution of evaporative salts are presented in Figure 4.9.

The elements had very high concentrations: Al (25-835 mg/L), Fe (99-17,959 mg/L), Cu (2.1-4870 mg/L), Zn (33.3-1070 mg/L), Mn (9.4-512 mg/L), Ni (0.58-11.75 mg/L), Co (2.1-25.6 mg/L), As (0.02-43.2 mg/L), Pb (0.02-0.93 mg/L), Cd (0.03-0.95 mg/L). The highest Fe concentrations were released from EF5 (melanterite + rozenite), followed by EF6 (copiapite + coquimbite) as shown in Figure 4.9a. The highest Cu concentrations were released from EF2 (alpersite). The concentration of released As was exceptionally high in the EF6 (coquimbite + copiapite) leachate (Figure 4.9f).

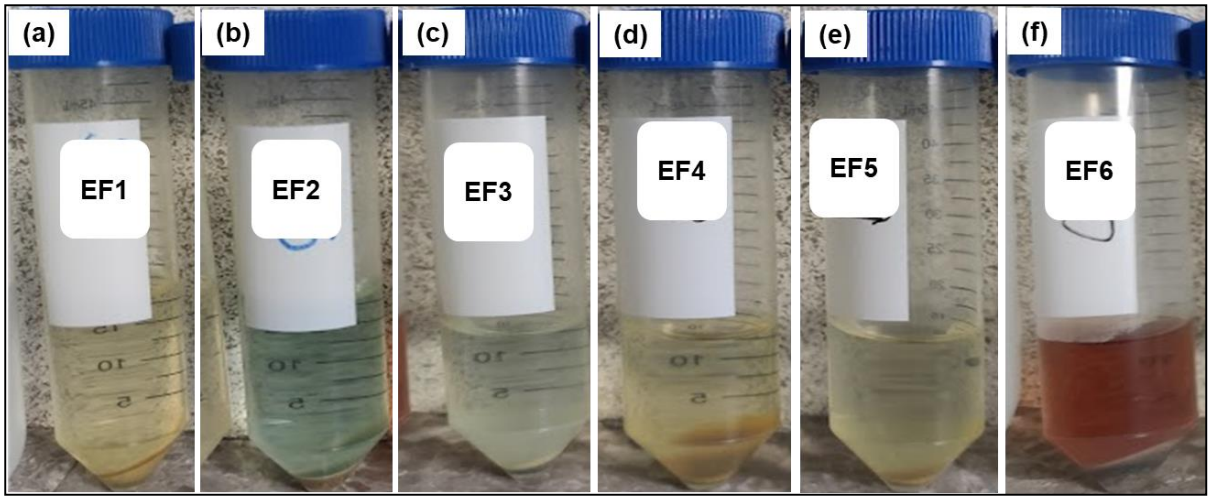

Figure 4.8 Experimental photographs showing variations in the color of leachates after 2 hours of interaction with distilled water

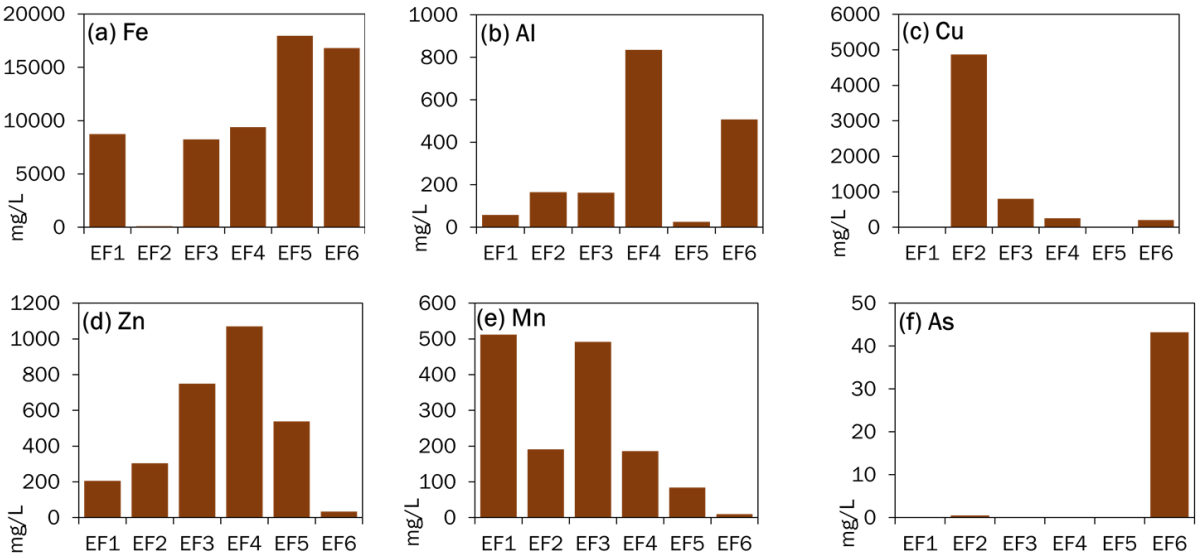

Figure 4.9 Variations in the concentrations of dissolved metals and As released during salt dissolution

4.3.2.2 Variations in the released Fe species

Figure 4.10 show that, as expected, Fe^{2+} dominated the Fe concentration released from salts containing melanterite and rozenite. The concentrations of Fe^{2+} in EF1 and EF3 were 8240 and 8060 mg/L, respectively while Fe^{2+} concentrations in EF4 and EF5 were 9090 and 17,680 mg/L, respectively. From these Fe^{2+} sulphates, the concentrations of released Fe^{3+} accounted for only 1.5 to 5.9 % of total released Fe (Figure 4.10), with EF1 containing the most Fe^{3+} (510 mg/L). On the other hand, at site EF6, Fe^{3+} was predominant (14,280 mg/L) whereas Fe^{2+} only reached (2540 mg/L) (Figure 4.10). At site EF2, the released concentration of total Fe was the lowest (99 mg/L; Figure 4.9) with Fe^{2+} being dominant (87 mg/L) over Fe^{3+} (12 mg/L).

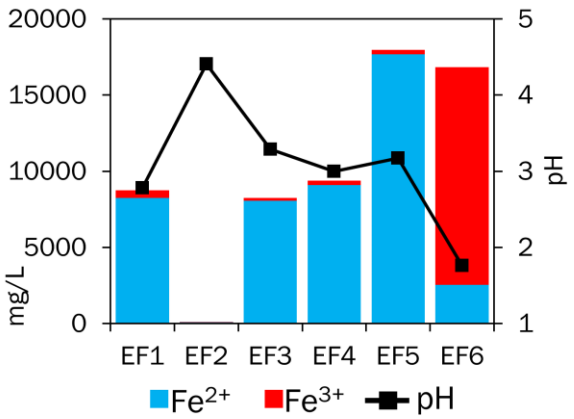

Figure 4.10 Variations in the pH and concentrations of dissolved Fe^{2+} and Fe^{3+} released during salt dissolution

4.4 DISCUSSION

4.4.1 Formation of simple hydrous divalent cation sulphates on the banks of Bor River

The Bor River is acutely contaminated by wastewaters from the Bor metallurgical/smelter facilities and overburden leakages, resulting in high acidity and elevated concentrations of dissolved metals and sulphate (Korać and Kamberović, 2007; Ishiyama et al., 2012; Filimon et al., 2016; Šerbula et al., 2016; Gardić et al., 2017; Đorđievski et al., 2018; Adamović et al., 2021; Osenyeng et al., 2023). The hot and dry period experienced during August and September (sampling periods) resulted in the evaporation of river waters from the Bor River and allowed for the generation of colorful blooms of evaporative salts on the banks of the Bor River (Figure 4.2). The upward capillary migration of the pore waters from the tailings-covered riverbanks and floodplains could have also led to the precipitation of metal sulphates on the surfaces of the river banks (Nordstrom and Alpers, 1999; Nordstrom, 2009).

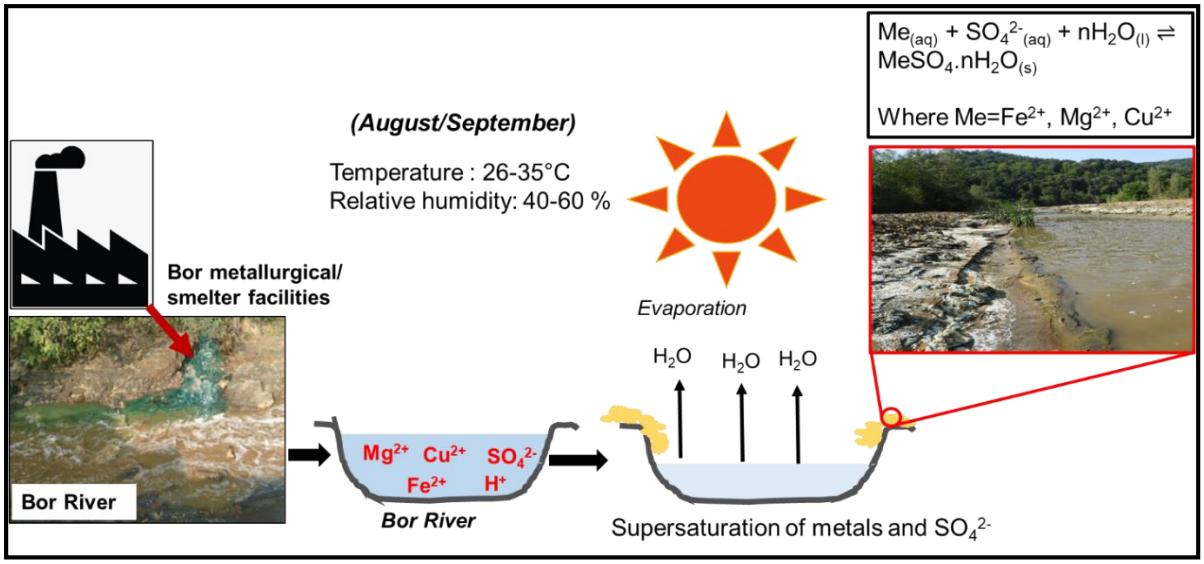

Figure 4.11 Schematic diagram showing the formation of efflorescent salts from the Bor River

For example, as a response to intense evaporation (Figure 4.11), Fe^{2+} and SO_4^{2-} combined to form melanterite observed at sites EF1 (Figure 4.6a) and EF3 (Figure 4.6c) and at sites EF4 (Figure 4.6d) and EF5 (Figure 4.6e) through Reaction 4.8. Similarly, for Mg-sulphates, epsomite detected in salts EF1 and EF2 (Figure 4.6a and b) formed by the combination Mg^{2+} and SO_4^{2-} through Reaction 4.9

$$Fe^{2+}_{(aq)} + SO_4^{2-}{}_{(aq)} + 7H_2O_{(aq)} \rightleftharpoons FeSO_4 \cdot 7H_2O_{(s)} \quad (4.8)$$

$$Mg^{2+}_{(aq)} + SO_4^{2-}{}_{(aq)} + 7H_2O_{(aq)} \rightleftharpoons MgSO_4 \cdot 7H_2O_{(s)} \quad (4.9)$$

Alpersite [$(Mg,Cu)SO_4 \cdot 7H_2O$] detected in EF2 (Table 4.2 and Figure 4.6b) belong to the melanterite group ($Me^{2+}SO_4 \cdot 7H_2O$), meaning it has similar crystal structure with such minerals. For this reason, it is usually overlooked since it is similar in color and other physical properties to Cu-bearing melanterite [$(Fe,Cu)SO_4 \cdot 7H_2O$] and chalcanthite ($CuSO_4 \cdot 5H_2O$). Peterson et al. (2006) mentioned that after the dissolution of Fe^{2+} sulphates such as melanterite or rozenite by rainwater, the released Fe^{2+} will oxidize to Fe^{3+} and hydrolyze to form iron oxides, thereby removing Fe from the solution. The authors further postulated that if contents of Mg are significantly higher than Cu in the Fe^{2+}-depleted solution, alpersite might form with epsomite.

This observation is consistent with the mineral assemblage in EF2 (Table 4.2, Figure 4.6b). The chemical formula of alpersite provided by XRD analysis of EF2 was [$(Mg_{0.7},Cu_{0.3})SO_4 \cdot 7H_2O$], implying that indeed contents of Mg were significantly higher than Cu in the Fe^{2+}-depleted waters.

4.4.2 Paragenesis of hydrated metal sulphates

In this thesis, the paragenesis will be discussed into 2 aspects; (1) mineralogical changes of upstream salts (EF1- EF3) observed between the 2017 and the 2021 analysis and; (2) mineralogical changes of downstream salts (EF4- EF6) precipitated sequentially further from the waters of the Bor River (Figure 4.1).

4.4.2.1 Mineralogical evolution of upstream salts (EF1- EF3) during the 2017 and 2021 analysis

Melanterite is the first Fe sulphate mineral to precipitate from acidic wastewaters with extremely high Fe and SO_4^{2-} concentrations via Reaction 4.8 (Jerz and Rimstidt, 2003). During the 2017 XRD analysis of the evaporative salts, melanterite ($Fe^{2+}SO_4 \cdot 7H_2O$) was detected in EF1 and EF3 samples (Table 4.2, Figure 4.6a and c). However, during the 2021 analysis, this mineral was not detected from those samples. Instead, rozenite ($Fe^{2+}SO_4 \cdot 4H_2O$) dominated the mineralogy (Figure 4.12a and c). Owing to the aging effects brought by sample storage at ambient temperature conditions for 4 years before the 2021 analysis, the melanterite present in the 2017 analysis have dehydrated to form rozenite via Reaction 4.10. Hammastrom et al. (2005) mentioned that unless preserved in a special way, melanterite will dehydrate at ambient laboratory conditions.

$$Fe^{2+}SO_4 \cdot 7H_2O_{(s)} \rightarrow Fe^{2+}SO_4 \cdot 4H_2O_{(s)} + 3H_2O_{(l)} \quad (4.10)$$

$$MgSO_4 \cdot 7H_2O_{(s)} \rightarrow MgSO_4 \cdot 6H_2O_{(s)} + H_2O_{(l)} \quad (4.11)$$

Similarly, epsomite ($MgSO_4 \cdot 7H_2O$) detected in the 2017 analysis (Table 4.2) could have dehydrated to the lower hydrated phases such as hexahydrite ($MgSO_4 \cdot 6H_2O$), pentahydrite ($MgSO_4 \cdot 5H_2O$) and starkeyite ($MgSO_4 \cdot 4H_2O$) (Table 4.2). According to Chou and Seal (2003, 2007), the formation of magnesium sulphates, and the transition from one phase to another, as a function of changing humidity, follows the Reaction 4.11.

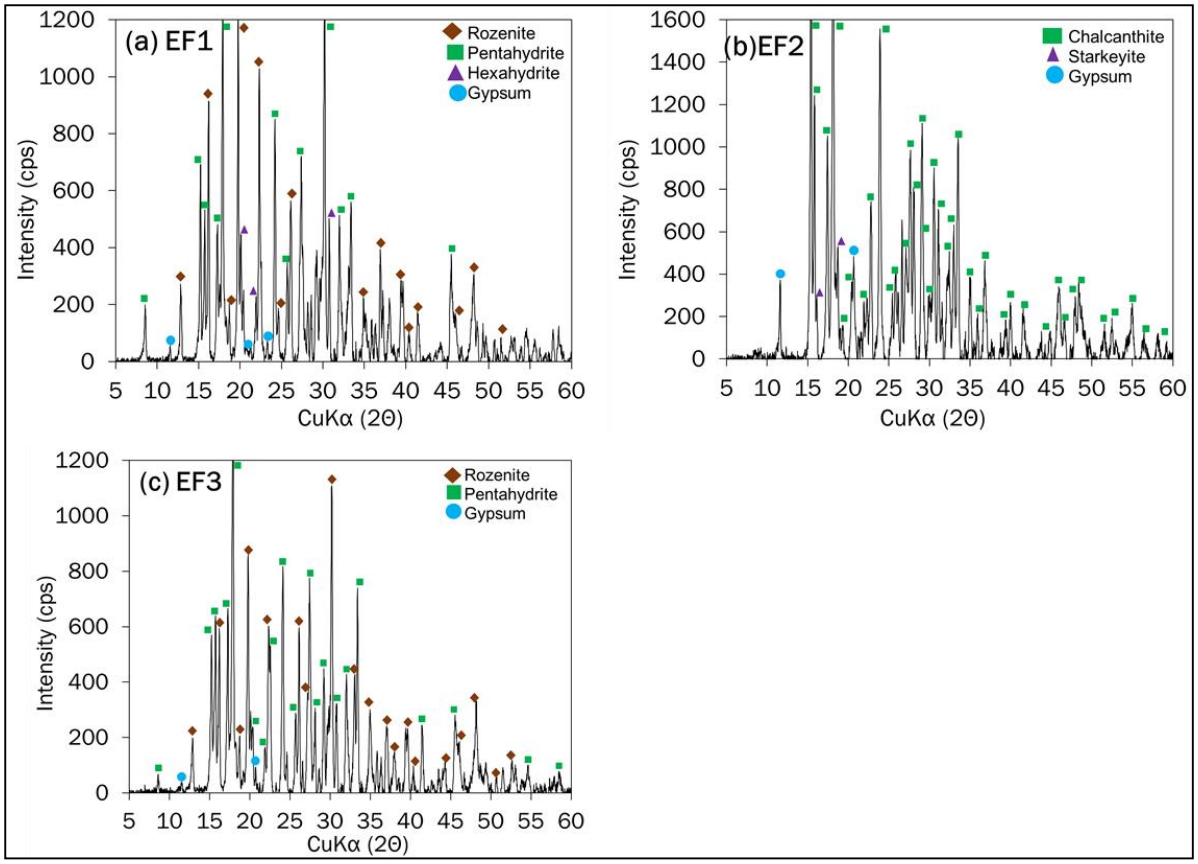

Figure 4.12 XRD patterns showing the mineralogy of the efflorescent salts after 4 years of storage at ambient conditions

The 'magnesian' Chalcanthite [$(Mg_{0.4}Cu_{0.6})SO_4 \cdot 5H_2O$] detected in EF2 (Figure 4.12b) in the 2021 analysis could be a dehydration product of alpersite (Figure 4.6b). This assertion could

be supported by Peterson et al. (2006), who reported that alpersite dehydrate to cuprian pentahydrite [(Mg,Cu)$SO_4 \cdot 5H_2O$], a member of the chalcanthite group ($Me^{2+}SO_4 \cdot 5H_2O$). It is imperative to note that 'magnesian' chalcanthite and cuprian pentahydrite are isostructural.

4.4.2.2 Mineralogical evolutions in the downstream Bor River evaporative salts (EF4-EF6)

In this section, a discussion on the sequence of mineral formation and alteration that occurs as Fe-sulphates form and evolve with time will be made. Given that during evaporation, the edges of a water basin/river banks will desiccate first (Figure 4.11), it can be assumed that evaporative salts on the outermost edges of the Bor River are mature whereas those formed closest to the waters of the Bor River are the newest to form from river water evaporation.

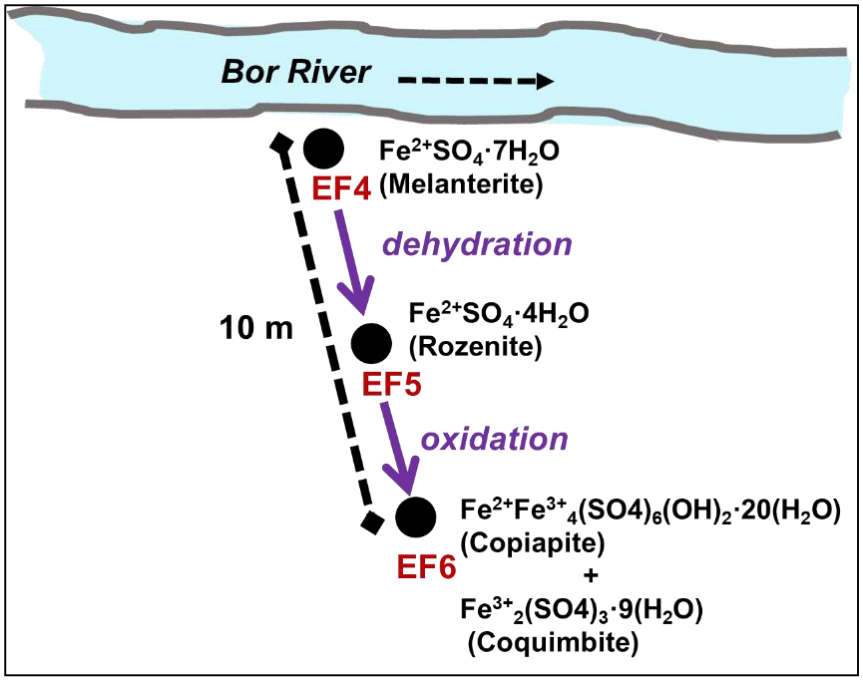

Figure 4.13 Schematic diagram showing the paragenetic sequence of Fe sulphates along the Bor River

Melanterite detected at site EF4 is a precursor mineral for other Fe sulphate minerals (Bigham and Nordstrom 2000; Hammarstrom et al. 2005; Jambor et al. 2000; Komnitsas et al. 1995). The salts at site EF5 are mature than those in EF4, therefore the existence and dominance of rozenite over melanterite at site EF5 is indicative of the dehydration processes, transforming melanterite into rozenite (Chou et al., 2002; 2013) via Reaction 4.10. This process is illustrated in Figure 4.13. The process of oxidation also played a vital role in the evolution of Fe sulphate minerals.

$$Fe^{2+}SO_4 \cdot 4H_2O_{(s)} + H_2SO_{4(l)} + O_{2(g)} \rightarrow Fe^{2+}Fe^{3+}{}_4(SO4)_6(OH)_2 \cdot 20(H_2O)_{(s)} \qquad (4.12)$$

Through oxidation, copiapite might have formed from transformation of rozenite through Reaction 4.12. Coquimbite [$Fe^{3+}{}_2(SO_4)_3 \cdot 9(H_2O)$] at site EF5 (Figure 4.6f) is said represent a more advanced stage in the oxidation sequence of the Fe^{2+} sulphates (Jambor et al., 2000) as illustrated by Figure 4.13

4.4.3 Environmental implications of the dissolution of hydrated metal sulphates

4.4.3.1 Generation of acidity

The lowering of the pH of distilled water during salt dissolution is due to 2 main processes; (1) hydrolysis of Fe^{3+} in the Fe^{3+} sulphates and; (2) hydrolysis of Al^{3+} in the Al-bearing phases (Cravotta, 1994; Jambor et al., 2000; Nordstrom and Alpers, 1999; Jerz and Rimstidt, 2003; Hammarstrom et al., 2005; Frau, 2011; Valente et al., 2013). Additionally, some authors have suggested that the Fe^{2+} in the Fe^{2+} sulphates might oxidize into Fe^{3+} during the dissolution experiment and thus generate acidity (Reaction 4.13) (Frau, 2011). To clarify the variations in the acid generation potential of evaporative salts in the Bor River, the results were classified according to the mineral assemblage phases.

$$Fe^{2+}_{(aq)} + ¼O_{2(g)} + 2.5H_2O_{(aq)} \rightleftharpoons Fe^{3+}_{(aq)} + 4H^{+}_{(aq)} \quad (4.13)$$

$$Fe^{3+}_{(aq)} + 3H_2O_{(aq)} \rightleftharpoons Fe(OH)_{3(s)} + 3H^{+}_{(aq)} \quad (4.14)$$

$$Al^{3+}_{(aq)} + 3H_2O_{(l)} \rightleftharpoons Al(OH)_{3(s)} + 3H^{+}_{(aq)} \quad (4.15)$$

i. Chalcanthite + Gypsum + Starkeyite (EF2)

The assemblage generated a leachate with pH 4.4 (Figure 4.10). This result is consistent with another study which revealed that chalcanthite-rich sample had lower acid producing potential, with a final pH of 4.3 (Valente et al., 2013). The hydrolysis of Al^{3+} (Figure 4.9b) could have provided more acidity to the leachate of EF2 salt through Reaction 4.15 (Valente and Gomes, 2009). The very low concentrations of released Fe^{3+} (Figure 4.10) might not have been sufficient enough to lower pH of the waters during dissolution. Gypsum and starkeyite are not acid-forming mineral phases, and did not contribute to acidity generation (Bucky et al., 2003).

ii. Melanterite + Rozenite (EF1, EF3, EF4, EF5)

The assemblage generated leachates with pH ranging from 2.8 to 3.3. The significant amounts of Fe^{3+} measured from the leachates of the melanterite and/or rozenite (Figure 4.10) could suggest that Fe^{3+} have hydrolyzed to generate acidity (Reaction 4.14). Frau (2011) proposed that even small amounts of Fe^{3+} in a Fe^{2+} sulphate may promote a decrease in the solution pH. It is important to observe that among the Fe^{2+} sulphates, salts with higher Fe^{3+} contents (Figure 4.10) generated leachates with higher acidity compared to those with lower higher Fe^{3+} contents. Indeed, this acid generating potential could provide proof that sulphates may have been present on the surface overburden material, even at trace contents, and are responsible for the acidity observed in the Masters' thesis.

iii. Copiapite + Coquimbite (EF6)

This assemblage generated a leachate with pH 1.8. Through hydrolysis, the predominance of Fe^{3+} in EF6 (Figure 4.10) is responsible for the very low in the pH of the leachate via Reaction 4.14. Nordstrom and Alpers (1999) reported a highly acidic copiapite solution, with negative pH values in acid drainages.

4.4.3.2 Release of toxic metals into the Bor River

The results of the dissolution experiments demonstrated the role of the hydrated metal sulphates as sources of secondary contamination of the Bor River during the first rains that immediately follow a prolonged dry period. In the Bor mining area, the first rains usually occur in September/October, causing a dissolution of the soluble salts, leading to a sharp increase in the acidity and concentrations toxic metals and metalloids of the Bor River as illustrated by Figure 4.14. Dagenhart (1980) observed a spike in the concentrations of Al, Fe, Cu and Zn occurring during the first rainfall at Contrary Creek drainage basin (Virginia) which dissolved evaporative salts.

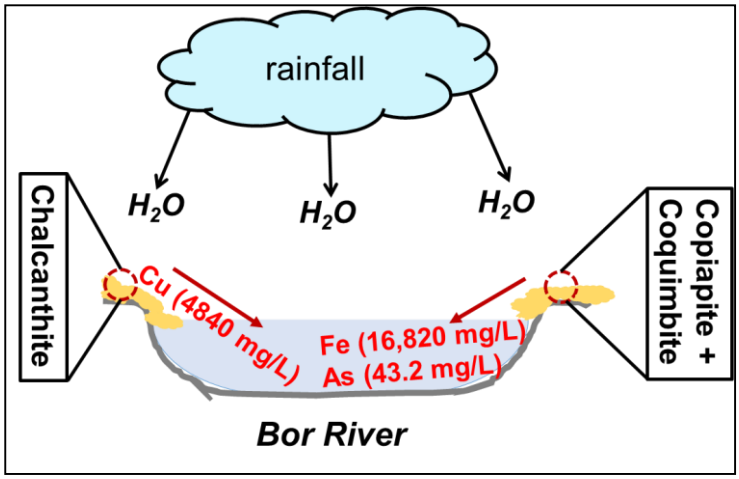

Figure 4.14 Schematic diagram showing the dissolution of metal sulphates along the Bor River

The dissolution of the Fe^{2+}-bearing sulphates (melanterite and rozenite) released exceptionally high concentrations of Fe (Figure 4.8a). Indeed, these Fe concentrations are extremely higher than the dissolved Fe concentrations usually reported from the waters of Bor River (Đorđievski et al., 2018; Adamović et al., 2021; Osenyeng et al., 2023). The release of high concentrations of Cu, Zn and Mn from the Fe^{2+} sulphates is consistent with the fact that these metals are usually incorporated into melanterite and/or rozenite solid solution by the substitution of Fe^{2+} (Giere et al., 2003; Jambor et al., 2000). Chalcanthite released the highest Cu concentrations (Figure 4.9b and Figure 4.14). This Cu concentration is several orders of magnitude higher than total Cu concentrations reported from the Bor River (Đorđievski et al., 2018; Adamovic et al., 2021; Osenyeng et al., 2023) as well as those originating from the Bor metallurgical/smelter facilities (Đorđievski et al., 2018). On the other hand, it released the lowest Fe contents compared to other mineral assemblages.

The dissolution of copiapite + coquimbite in EF6 released extremely high concentrations of Fe, dominated by Fe^{3+} (85 % of total Fe). This sample released the highest As concentration (43.2 mg/L) in the entire study area (Figure 4.14). The enrichment of As in the Fe^{3+} bearing sulphates and its subsequent release have been reported in other studies (Giere et al., 2003; Jamieson et al., 2005; Romero et al., 2006; Nieva et al., 2021). D'Orazio et al. (2021) speculated that it is very likely that As enters the crystal structure of coquimbite as As^{5+}, replacing S^{6+}.

4.5 CONCLUSION

The continental climate of the Bor mining region, Eastern Serbia, enabled the precipitation of hydrated Fe, Mg and Cu sulphates in August and September. An inventory of mineralogy and chemical composition of these sulphates and their spatial distribution is very important for the

development of effective strategies to improve water quality in regions contaminated by mining activities.

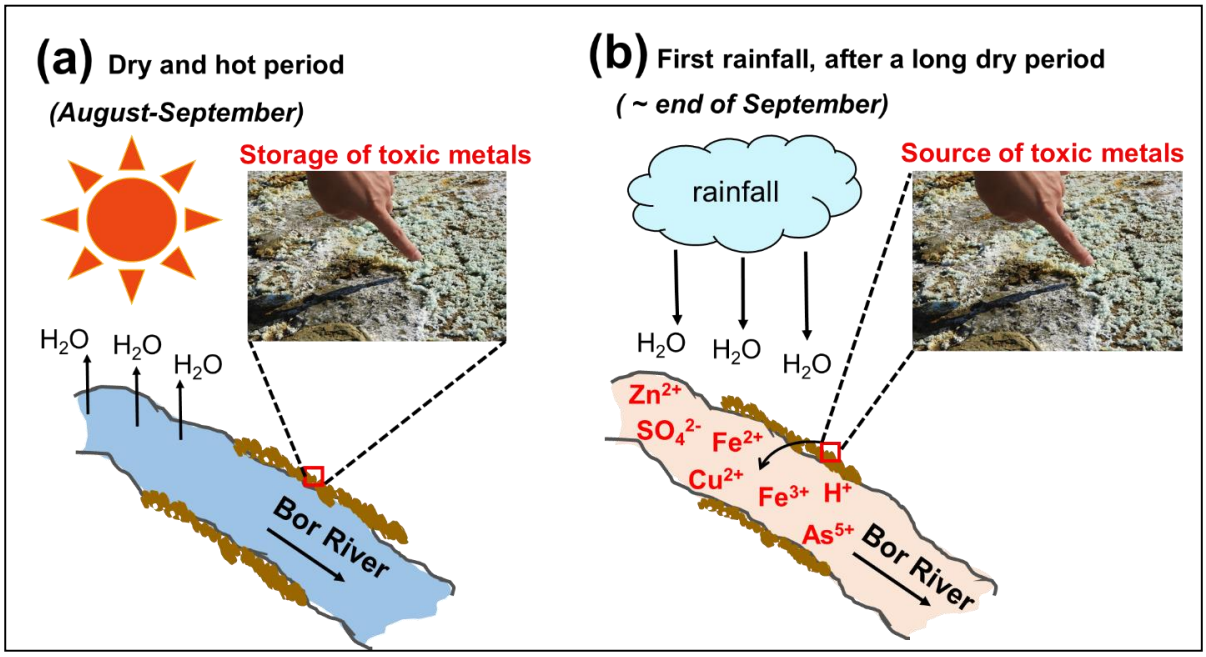

Figure 4.15 Schematic diagram showing a summary of the precipitation and dissolution of efflorescent salts

These minerals acted a temporary storage of toxic metals and As during the dry and hot season (Figure 4.15). However, being very soluble, these minerals acted as secondary contamination to the Bor River waters through the release of acidic and metal loaded solution. This instantaneous spike in acidity and toxic element contents will only last for a short period since a continued rainfall will lead to dilution of acidity and metal contents to benign concentrations. Moreover, although its contribution is significantly lower than wastewaters originating from the Bor metallurgical/smelting facilities, the flotation tailings covering the Bor riverbanks and floodplains could suggest a long term source of toxic metals and acidity necessary for the continuous precipitation of hydrated metal sulphates each year during the dry and hot periods.

5. CHEMICAL EXTRACTABILITY OF METALS AND AS IN WASTE ROCKS FROM THE BOR CU MINING REGION, EASTERN SERBIA

5.1 INTRODUCTION

Several researchers have reported that in the 4-step modified BCR sequential extraction procedure, there is an incomplete oxidation of sulphide minerals by hydrogen peroxide during Step 3 (Tessier et al., 1979; Forstner,1985; Campanella et al., 1995; Filgueiras et al., 2002; Galán et al., 2003; Sutherland et al., 2009; Favas et al., 2011). This leads to the underestimation of the oxidizable fraction and therefore to the underrate interpretation of risks of metal release from sulphides during natural oxidation.

During a Master's thesis, mine wastes such as surface overburden and flotation tailings were investigated using the 4-step modified BCR sequential extraction procedure outlined in Section 3.2.4. However, since these waste materials generally contain very low sulphide contents, that research could not observe the incomplete oxidation of sulphides associated with this procedure. For example, the XRD mineralogical investigation of the residues after reaction with H_2O_2 could not be investigated. For this reason, this PhD thesis will use high-sulphide mine wastes to develop an optimized sequential extraction procedure that will consider the incomplete oxidation of sulphides observed in the 4-step modified BCR sequential extraction and therefore help distinguish between easy-oxidizing sulphides from difficult-oxidizing sulphides.

5.1.1 Oxidation of metal sulphides with hydrogen peroxide (H_2O_2)

Hydrogen peroxide (H_2O_2) is known to be an excellent oxidizing agent of metal sulphides (Antonijevic et al.,1997; Dimitrijević et al., 1999; Petrović et al., 2018). The oxidizing strength of H_2O_2 is attributed to its high value of oxidation-reduction potential according to the oxidative action (Reaction 5.1).

For example, the dissolution of pyrite by H_2O_2 in acidic solutions and very acidic solutions, respectively, is illustrated by Reaction 5.2 and Reaction 5.3.

$$H_2O_{2(l)} + 2H^+_{(aq)} + 2e^- \rightarrow 2H_2O_{(l)} \qquad E^\circ = 1.77\ V \qquad (5.1)$$

$$FeS_{2(s)} + 7.5H_2O_{2(l)} \rightarrow Fe^{3+}_{(aq)} + 2SO_4^{2-}{}_{(aq)} + H^+_{(aq)} + 7H_2O_{(l)} \qquad (5.2)$$

$$FeS_{2(s)} + 7.5H_2O_{2\ (l)} + H^+_{(aq)} \rightarrow Fe^{3+}_{(aq)} + 2HSO_4^-{}_{(aq)} + 7H_2O_{(l)} \qquad (5.3)$$

The use of H_2O_2 is extensive in sequential extraction tests as a reagent simulating the oxidation conditions of sulphide minerals when exposed to the atmospheric conditions (Tessier et al., 1979; Ure et al., 1993; Rauret et al., 1997; Marin et al., 1997; Filgueiras et al., 2002; Callender, 2003). For example, Ferrer et al. (2021) tested the leaching capability of H_2O_2 by performing a partial extraction of a concentrate containing pyrite using 35% H_2O_2 for 1 h at 80 $^\circ$C and reported that 70 % of pyrite was dissolved.

5.1.2 Oxidation of metal sulphides with Nitric acid (HNO_3)

The oxidation and dissolution of metal sulphides by nitric acid (HNO_3) has been studied by several authors (Kadioğlu et al., 1995; Habashi, 1999; Gao et al., 2009; Narangarav et al., 2014; Rogozhnikov et al., 2019; Dizer et al., 2022; Teimouri et al., 2022). The NO_3^- ions possesses very strong oxidant abilities, enabling nitric acid to achieve pseudo-total oxidation of sulphides and the transfer of valuable metals into a solution (Gao et al., 2009). The strong oxidative action of NO_3^- ions in acidic solutions is based on Reactions 5.4 giving a high standard electrode potential (Gao et al., 2009; Tsogtkhankhai et al., 2011; Narangarav et al., 2014).

$$NO_3^-{}_{(aq)} + 4H^+_{(aq)} + 3e^- \rightarrow NO_{(g)} + 2H_2O_{(l)} \qquad E^\circ = 0.96\ V \qquad (5.4)$$

Miroslav et al. (2009) reported that, depending on the leaching conditions, pyrite could be oxidized by the NO_3 acid to simultaneously generate both elemental sulphur and sulphate, according to Reaction 5.5. Gao et al. (2009) observed small contents of elemental sulfur

suspended in the solution during pyrite oxidation. However, due to the excessive amount of HNO_3, all the elemental sulphur was oxidized to sulphate as the reaction progressed to completion.

$$FeS_{2(s)} + 8HNO_{3(aq)} \rightarrow Fe^{2+}_{(aq)} + SO_4^{2-}{}_{(aq)} + S^0_{(s)} + 8NO_{2(g)} + 4H_2O_{(aq)} \qquad (5.5)$$

5.1.3 Oxidation of metal sulphides with inverted aqua-regia ($3HNO_3$ + 1HCl)

Usually, metal sulphide that could not dissolve easily in an acidic solution will first need to be oxidized. Also, some sulphides will form an oxide layer protecting them from an acid attack, a process called passivation. Aqua regia ($1HNO_3$ + 3HCl) has an excellent combination of oxidizing agent and chlorine, with enough HNO_3 to oxidize sulphides and enough HCl to produce a metal chloride salts from which the metals can be dissolved.

On the other hand, reversing the ratio from $1HNO_3$:3HCl to $3HNO_3$:1HCl, means there is lot more oxidizing agent in a solution and this will ensure pseudo-total oxidation of the sulphides especially those that would passivate easily. It is usually used to dissolve sulphides in Cu concentrates. Based on this description, it can be observed that inverted aqua regia is much stronger oxidizing agent, compared to hydrogen peroxide.

5.2 METHODOLOGY

5.2.1 Sample description and collection

For the development of the sequential extraction procedure that clarifies the incomplete oxidation of sulphides by hydrogen peroxide, high-sulphide mine wastes will be required. These will allow the observations of sulphide mineralogy before and after reaction with hydrogen peroxide. To do this, the ore that was discarded, either due to very low contents of target metal or because it contained minerals with undesirable elements, was obtained from the Bor Cu mining area. This discarded ore is referred to as 'waste rock' in this entire PhD thesis.

Waste rocks from the Old Bor overburden dump site (R1-R3) were collected in August 2019 whereas waste rocks from the Veliki Krivelj overburden dump site (R4-R6) were collected in September 2021. At each site, the sample coordinates were obtained by a GARMIN global positioning system (GPS) and plotted in the location map (Figure 5.1). Field observations of outcrops such as colour and naked-eye identification of minerals were recorded and are summarised in Table 5.1. Since were recently dumped, the Veliki Krivelj rocks (Figure 5.2c and 5.2d) are assumed to be fresh/new compared to Old Bor rocks (Figure 5.2a and 5.2b). Samples were either handpicked or chipped with geological hammer from a larger boulder and stored in airtight Ziplocs.

Table 5.1 Sample locations and field descriptions of waste rocks in the Bor mining region

Sample ID	Sample date	Location	Locations and field observations
R1	27/08/2019	Old Bor overburden dump	Dark grey rock with indigo-blue and brass yellow minerals observed on the surface
R2	27/08/2019	Old Bor overburden dump	Dark grey rock, shiny-brass yellow mineral observed on the surface
R3	27/08/2019	Old Bor overburden dump	Reddish black rock, covered with a brown material
R4	05/10/2021	Veliki Krivelj overburden dump	Dark grey rock with a faint green
R5	05/10/2021	Veliki Krivelj overburden dump	Grayish green rock
R6	05/10/2021	Veliki Krivelj overburden dump	Dark grey rock, shiny brass yellow mineral observed on the surface

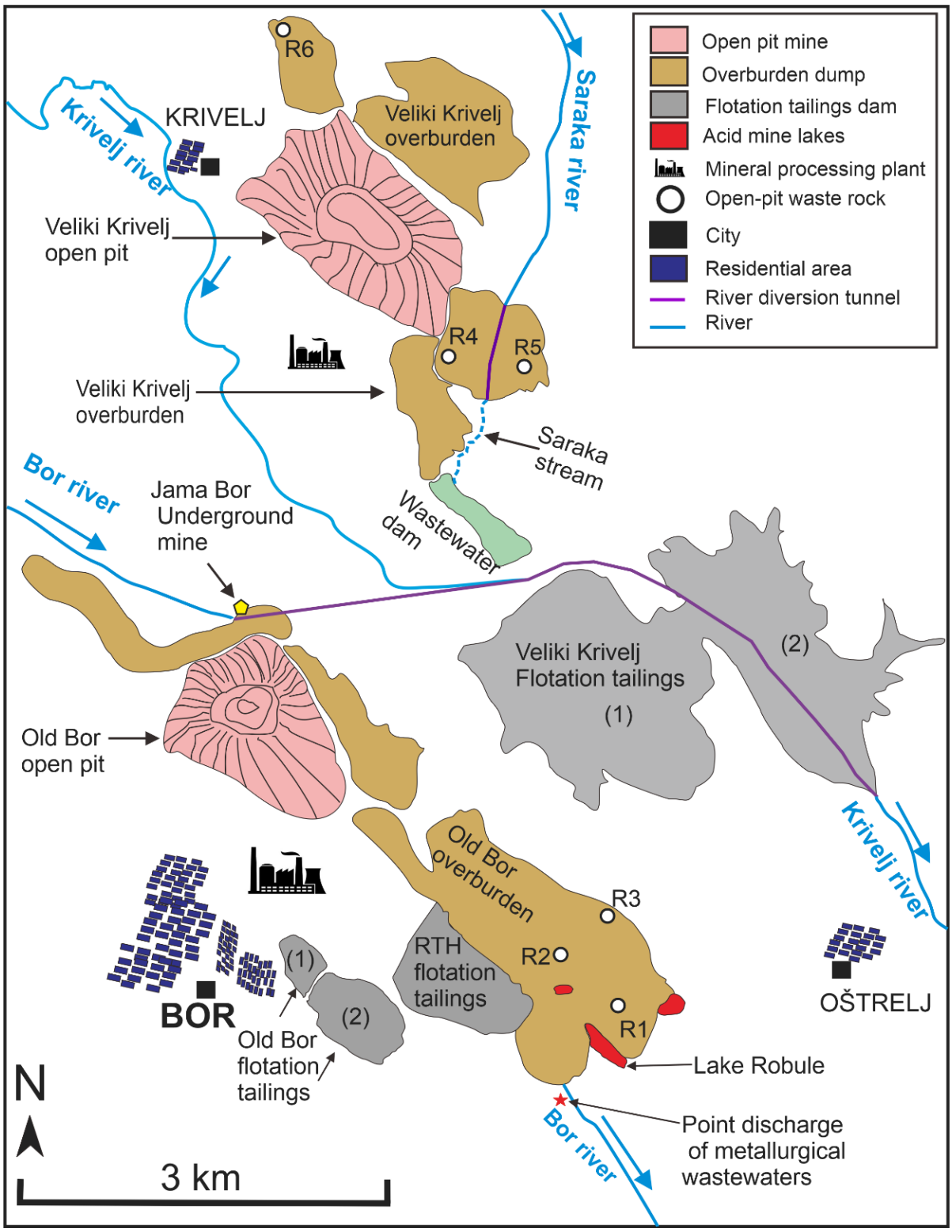

Figure 5.1 Map of the study area with waste rock sampling locations

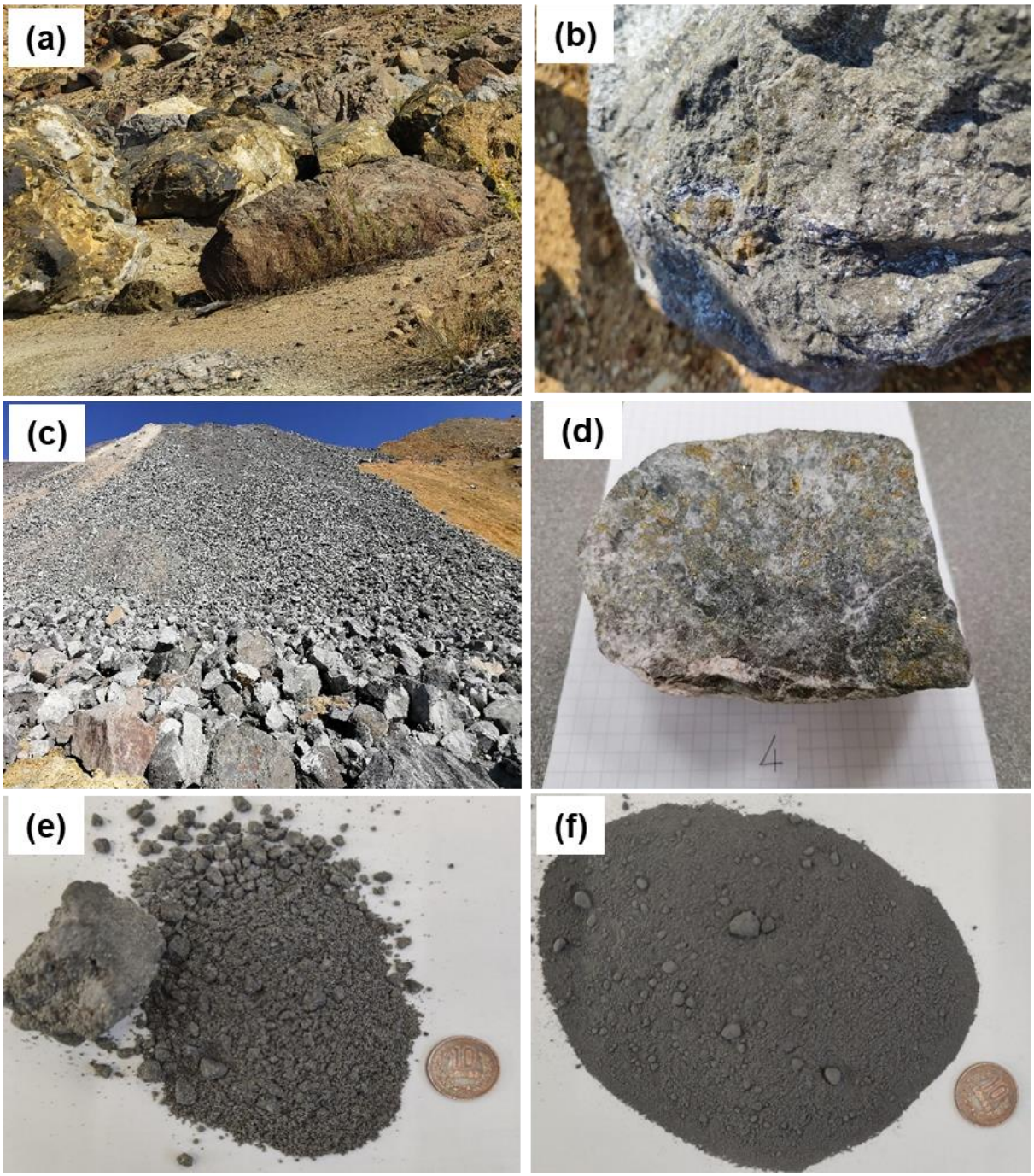

Figure 5.2: Field photographs of waste dumps from the Bor mining region **(a)** and **(b)** Old Bor open-pit waste rocks; (**c)** and **(d)** Waste rocks of Veliki Krivelj open-pit. (**e)** and **(f)** Photographs of sampled discarded ore/ waste rock

5.2.2 Mineralogy characterization techniques

5.2.2.1 X-ray diffraction analysis (XRD) - Bulk

To investigate their mineral compositions, all solid samples were pulverized to a fine powder (<63 μm) using a pestle and mortar and analysed by X-ray diffraction (XRD). Small drops of ethanol were added to the sample to pulverize detrital particles to a powder. As indicated by Figure 5.3, the sample powders were loosely pressed/mounted in round aluminium holders (2mm thickness, 24 mm inner diameter) using a clean glass slide. The bulk mineralogical determination was carried out using a Rigaku MiniFlex II desktop X-ray diffractometer equipped with a graphite monochromator (CuKα target, λ=1.5418 Å) x-ray tube operating at an output voltage of 30Kv and output current of 15mA. Samples were analysed within a scan range (2θ) of 2-60° and in a continuous scan mode with a scan speed of 2°/min. To identify the individual crystalline phases, the diffractograms were interpreted by a search/match software called Integrated X-Ray Powder Diffraction (PDXL), equipped with a database called the International Centre for Diffraction Data (ICDD). In addition to the qualitative determination of minerals, a combination of peak positions (CuKα=2θ) and peak intensity (Cps) were used to tentatively estimate the mineral abundances in each sample. All analyses were carried out the Graduate School of International Earth Resource Sciences, Akita University.

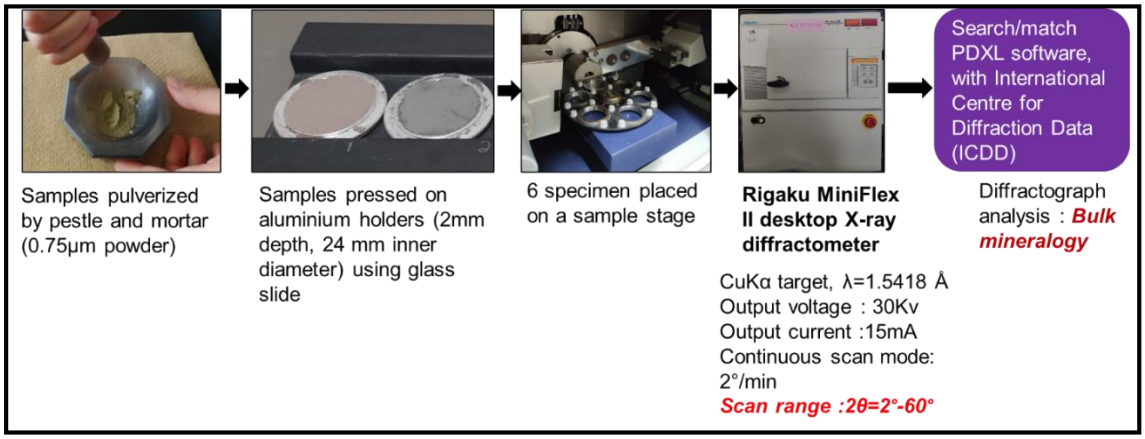

Figure 5.3 Detailed illustration of the bulk XRD analysis of waste rocks and efflorescent salt samples

5.2.2.2 XRD analysis - Clay minerals

Clay minerals in waste rocks were analysed from oriented powders of waste rocks prepared by mixing pulverised sample with distilled water to make a suspension. The mixture was shaken vigorously and allowed to stagnate for 10 seconds until the high density minerals such as silicates and sulphides have settled/precipitated (Figure 5.4). An adequate amount (1.5-2.0 mL) of the suspension (containing clay minerals) was pipetted onto a glass disc (Figure 5.4), placed in an incubator and dried overnight at 35° C. The dried samples were analysed within a scan range (2θ) of 2-40° for the identification of clay minerals.

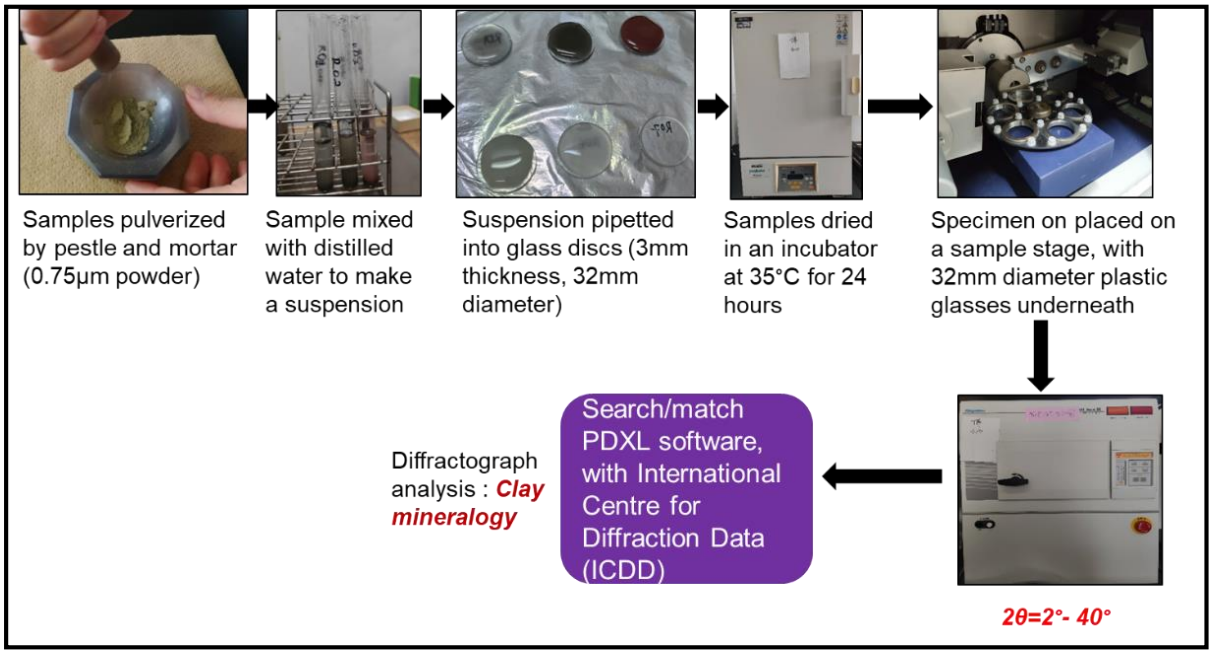

Figure 5.4 Detailed illustration of the analysis of oriented powders by XRD to determine clay mineralogy

Ethylene glycol- confirmation for the presence of montmorillonite

After the oriented-powder samples have been analysed, peaks suspected to be montmorillonite needed to be verified. To do this, the sample was sprayed with small amounts of ethylene glycol (3-4 squirts) and left to dry for 30 minutes at room temperature. The sample was then re-

analysed following the same settings as above (Figure 5.4). If montmorillonite is confirmed present, the peaks would shift in the x-axis (2θ).

5.2.2.3 XRD analysis- after Step 3 and Step 4 of the sequential extraction

The solid residues of Step 3 and Step 4 of the sequential extraction procedure were also subjected to the bulk mineralogical analysis to primarily identify the residual sulphides. The amount of the sample remaining after the Step 3 and Step 4 extraction stage was very small to analyse by the normal XRD bulk analysis procedure (Figure 5.3). However, a solution was prepared by mixing the solid residue with small amount of distilled water, ensuring the complete suspension of all minerals. The solution (including sulphides, oxides, silicates and clays) was immediately pipetted onto a glass disc and dried overnight at 35° C in an incubator. The dried samples were analysed within a scan range (2θ) of 2-60° for the identification of the remaining sulphide and oxide minerals as illustrated by Figure 5.5.

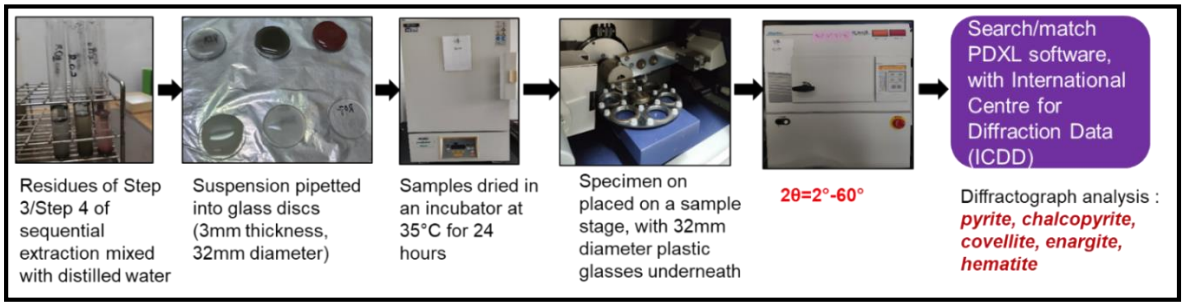

Figure 5.5 Detailed illustration of the analysis of the Step 3 and Step 4 sequential extraction residues by XRD to determine residual mineralogy

5.2.2.4 Preparation of standard polished sections

Standard sections were prepared from non-pulverized waste rock and riverbed sediments by pouring a mixture of Petropoxy 154 resin and a curing agent (mixing ratio; 10mL: 1 mL) to

aggregate loose particles, especially in riverbed sediments as shown in Figure 5.6. This was prepared in a round-folded aluminium foil (22 mm diameter of the bottom surface) and heated on a hotplate at 105°C for 1 hour or until complete dryness. The aggregated material was fitted to the bottom of a yellow caplug (20 mm depth, 28 mm diameter) and was then fixed to a mixture of hardener and polyester resin (Type: No.105; JP-21111001) and left to dry overnight (at approximately 37-40 °C). The dried sample was polished with Black Waterproof Silicon Carbide sandpapers of particle sizes #220 followed #320, each for 2 minutes, after which the sample was polished with Black Silicon Carbide powder of particle sizes #800 followed by #1000, each for 2 minutes. Next, the sample was polished with White Fused Alumina powder of particle sizes #2000 followed by #3000, each for 5 minutes.

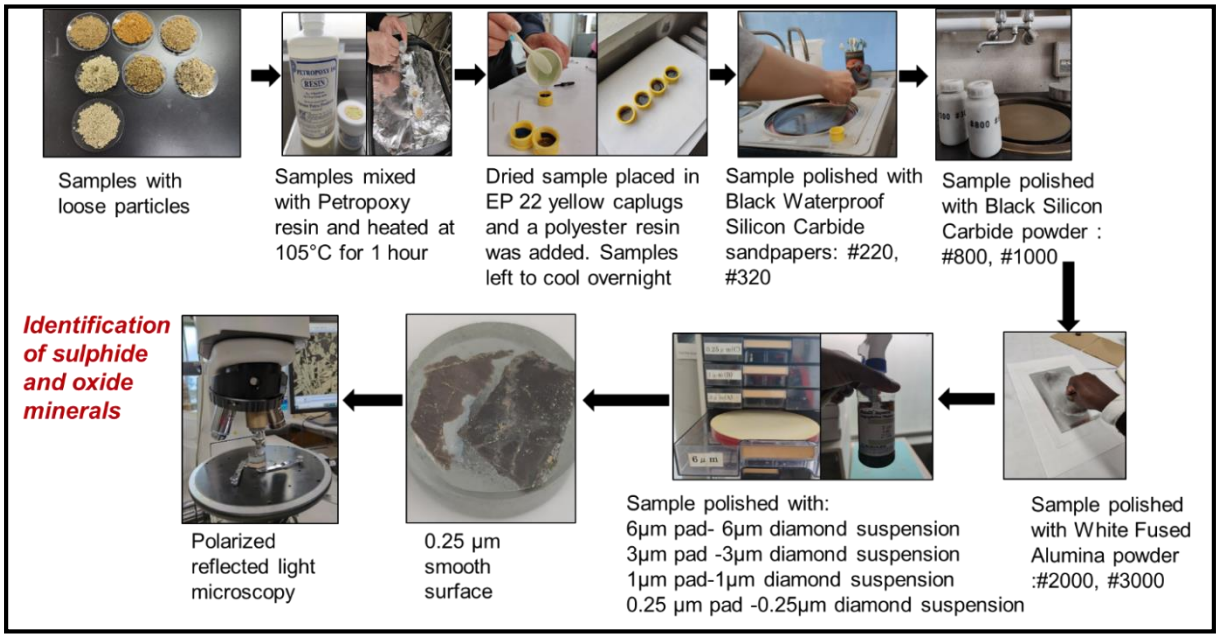

Figure 5.6 Detailed illustration of the preparation of polished sections for optical microscopy analysis

The sample was then placed in an ultrasonic cleaner filled with distilled water to remove the residual polishing powders. The final polishing involved the use of diamond polishing plates: 6 µm, 3 µm, 1 µm and 0.25 µm fixed onto a Buehler AutoMet 250 grinder-polisher. Polycrystalline diamond suspensions, with particle sizes: 6 µm, 3 µm, 1 µm and 0.25 µm, were

added to the respective diamond polishing plates and polishing was done (5 minutes for each plate) until 0.25 μm smooth surface of the sample was achieved. This experiment was carried out for all collected waste rocks and riverbed sediments.

5.2.2.5 Optical microscopy

To define ore mineralogy in waste rocks and riverbed sediments, reflected-light microscopy was adapted. Specifically, this technique was used to verify XRD mineral identifications, resolve overlapping data and identify minerals undetected by XRD due to either low content or poor crystallinity (Dold, 2003). The prepared polished sections were observed under a Nikon Eclipse 50i POL polarised light microscope (Figure 5.6) to identify minerals, especially sulphides and oxides. The microscope was connected to a computer equipped with Motic Images Plus 2.3S software that enabled the observation of images on a computer monitor and the capturing of photomicrographs. The tentative estimation of percentage composition was carried out by observing the sulphide mineral, particularly pyrite crystals in the microscope field of view (2X magnification) and comparing that to the chart prepared by Terry and Chilingar (1955). This analysis was carried out for all samples and was conducted at the Graduate School of International Earth Resource Sciences, Akita university.

5.2.2.6 Electron probe micro-analyser (EPMA)

In preparation of EPMA analysis, a spot to be analysed was first selected by drawing a circle around the area of mineralogical interest in the sample using the objective ‘draw’ function in the microscope (Figure 5.7). A pencil-sketch of the spot location was drawn on a notebook and labelled appropriately. A photomicrograph of the selected spot was captured, printed and labelled accordingly to allow easy identification during EPMA analysis. The sample was then subjected to carbon-coating.

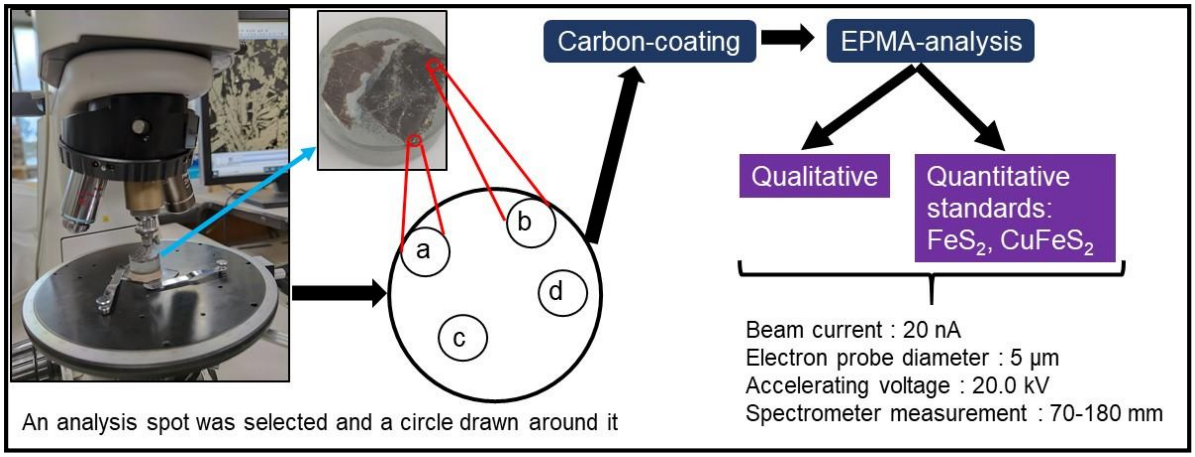

Figure 5.7 Schematic diagram of sample preparation for EPMA analysis

The polished, carbon- coated sections of waste rock samples were analysed with Electron probe micro-analyser (EPMA; JEOL 733 Electron Microprobe), to qualitatively characterise chemical composition of the identified sulphide minerals. The technique was also used to confirm the composition of small crystal of minerals that could not be clearly identified by optical microscopy. EPMA quantitative analysis was conducted to obtain the geochemical characteristics of the identified the sulphide minerals i.e. to determine contents of S, Fe, Cu, As, Zn and Pb. Pyrite and chalcopyrite were used as internal standards. This analysis was conducted at Akita university. From a total of 6 waste rock samples and 3 riverbed sediment samples, 35 spots were selected for the analysis. The operating settings for EPMA were: beam current of 20 nA, electron probe diameter of 5 μm, accelerating voltage of 20.0 kV and spectrometer measurement between 70 and 180 mm.

5.2.2.7 EPMA elemental mapping

This analysis was conducted on a selected sample to verify the results obtained by the spot qualitative and quantitative analysis. Specifically, this analysis was conducted due to the observed inconsistency between the optical microscopy (colour of the enargite mineral) and EPMA data. The operating settings for EPMA elemental mapping were: accelerating voltage

of 20.0 kV, beam current of 20 nA and electron probe diameter of 1μm and image pixel size of 200.

5.2.3 Geochemical investigation techniques

5.2.3.1 Bulk chemical composition analysis

For the analysis of bulk chemical compositions, 0.1 g of pulverised samples (<75 μm) were decomposed using a conventional hotplate digestion technique involving a concentrated acid mixture of 0.4 mL Hydrofluoric acid (HF: 46 % conc.), 0.4 mL Perchloric acid ($HClO_4$: 60 % conc.) and 1 mL Nitric acid (HNO_3: 61% conc.) in 15 mL volume Teflon bottles as illustrated in Figure 5.8. This technique provides near-total concentrations of elements from mine wastes. Analysis of a blank control was used to determine limits of detection (LODs) and the certified reference materials, CRM (JA-2 and JR-2, provided by the Geological Survey of Japan) were used to assess the accuracy of measurements of elements in digested samples. The ratio of measured values of CRMs against the recommended values ranged from 92 to 127 %. the All reagents were of analytical grade and all solutions were prepared using ultrapure water. Moreover, all glassware and Teflon bottles were pre-cleaned with diluted Nitric acid (HNO_3) for at least 2 days, then rinsed with ultrapure water three times to ensure no residual metal contamination. The digestion solutions were diluted 100-fold and analyzed by ICP-MS with Indium as a standard solution.

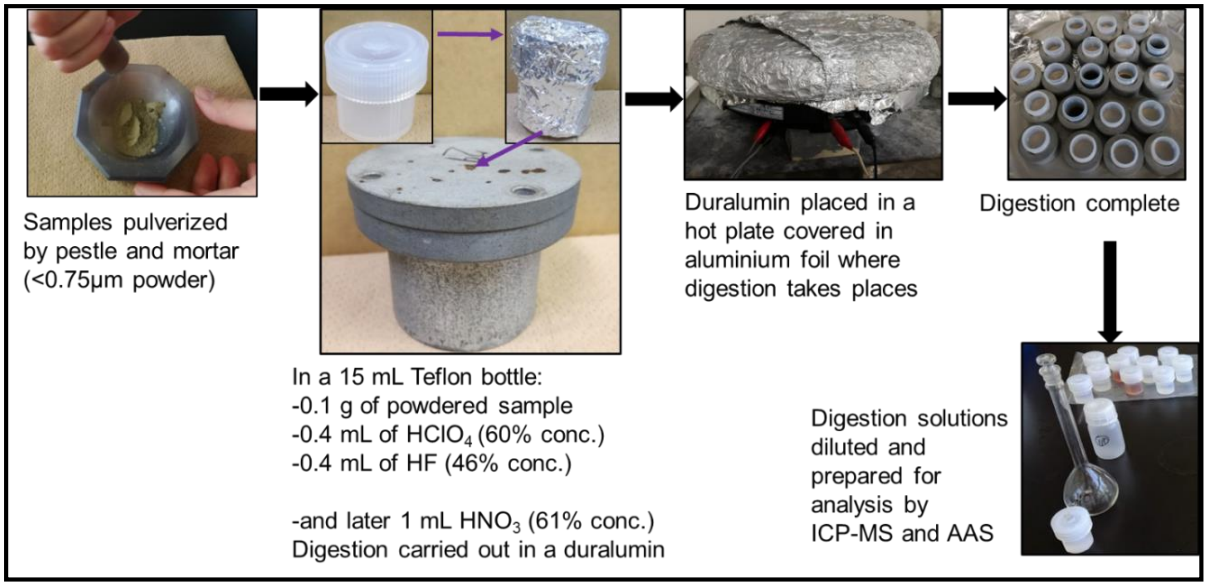

Figure 5.8 Schematic diagram of a conventional hot plate, mixed acid digestion

5.2.3.2 The 5-step procedure (Optimised-modified BCR sequential extraction)

Responding to the problem of incomplete oxidation of organic matter and sulphide minerals by hydrogen peroxide during Step 3 of the 4-step modified BCR sequential extraction procedure (Rauret et al., 1999), the current study will optimize it by including a very strong oxidizing agent to dissolve the resistant sulphides remaining after the Step 3 extraction stage. Table 5.2 provides a detailed summary of the procedure.

Step 1: Accurately weighed 0.5 g of a pulverized sample was added to a 50 mL centrifuge tube with 20 mL of 0.11 M acetic acid (CH_3COOH, pH 2.9) and agitated for 16 hours at a speed of 80 rpm at room temperature. The mixture was then centrifuged at 3000 rpm for 20 minutes, followed by filtration using 0.2 µm cellulose acetate hydrophilic filters. The solid residue was thoroughly washed with distilled water and stored in a freezer (-30 °C) for later use. The water-washes were added to the extraction solution to prevent sample loss. The supernatant was collected in a 100 mL volumetric flask, acidified with 5% v/v of HNO_3 acid, later diluted 10 fold and analyzed by ICP-MS for the determination of Al, Fe, Cu, Zn, Mn, As and Pb

concentrations. The elements extracted in this step corresponds to the water-soluble, acid soluble and exchangeable phases.

Table 5.2 The 5-step sequential extraction procedure, modified from Rauret et al. (1999)

Phase code	Phase name	Target	Sample	Reagents	Extraction temperature (°C)	Agitation conditions
Step 1	Exchangeable, Water/acid soluble	Sulphates, weakly absorbed on materials	0.5 g, dry	0.11 M CH_3COOH *(pH 2.9)*	25	16 hours, 80 rpm
Step 2	Reducible	Mn and Fe oxides	Step 1 Residue	0.5 M $NH_2OH.HCl$ *(pH 1.5)*	25	16 hours, 80 rpm
Step 3	Oxidizable	Organic matter, metal sulphides	Step 2 Residue	8.8 M H_2O_2 (x2), *(pH 2.0)* 1 M NH_4COOCH_3 *(pH 2.0)*	85	16 hours, 80 rpm
Step 4	Extreme-oxidizable	Sulfides that could not be decomposed by H_2O_2	Step 3 Residue	Inverted aqua-regia HNO_3: HCl 3:1	160	-
Step 5	Residual	Silicate minerals and well crystalline structures	Step 4 residue	HNO_3+ $HClO_4$ +HF (mixing ratio; 1:1:2.5) (x2)	135	-

Step 2: A 20 mL aliquot of freshly prepared 0.5 M hydroxyl ammonium chloride ($NH_2OH.HCl$), adjusted to pH 1.5 by HNO_3 acid, was added to the residue of Step 1. The mixture was agitated for 16 hours at a speed of 80 rpm at room temperature. The mixture was then centrifuged at 3000 rpm for 20 minutes, followed by filtration using 0.2 µm cellulose acetate hydrophilic filters. Filtration, sample handling and analysis were carried out in a similar way to Step 1, however extraction solutions were diluted 100 fold before analysis by ICP-MS.

The elements obtained from this step are bound to the reducible minerals such as Fe and Mn oxide/ hydroxides.

Step 3: A 5 mL (in 1 mL increments) of 8.8 M Hydrogen Peroxide (H_2O_2), adjusted to pH 2.03 by acetic acid, was added to the Step 2 residue in a centrifuge tube placed in a beaker filled with cold water, to control exothermic reactions. The samples were then placed in a hotplate and heated at 85 °C for an hour or until the complete evaporation of H_2O_2. After cooling, a second 5 mL split of H_2O_2 was added to the mixture and the same procedure was repeated. A 20 mL of 1.0 M of ammonium acetate solution (NH_4COOCH_3) was then added to the cool residue. The centrifuge tube was then agitated at 80 rpm for 16 h, followed by centrifugation at 3000 rpm for 20 minutes. The sample filtration and handling were the same as that of Step 2. The elements dissolved in this step are retained in metal sulfides and organic matter. The washed residue was analyzed by XRD to identify remaining sulphide and oxide minerals, following the procedure outlined in Section 5.2.2.3.

Step 4: After XRD analysis, the Step 3 residue was transferred to a 100 mL beaker and the inverted aqua-regia (3 mL HNO_3 : 1 mL HCl) was added. The mixture was heated in a hotplate at 160°C for 3 hours to achieve complete evaporation/dryness. The dried residue was mixed with 2.5 mL of HNO_3 acid and reheated at 160°C to complete dryness. A 9 mL of ultrapure water and 1 mL HNO_3 acid were added to the cooled sample and heated again at 160°C for 3 hours. The mixture was then transferred back to the centrifuge tube and centrifuged at 3000 rpm for 20 minutes. The sample filtration and preparation procedure was the same as that of Step 2 and Step 3. The elements bound to this fraction are usually considered as residual (Filgueiras et al., 2002; Galán et al., 2003; Dold and Fontboté, 2001; Khorasanipour et al., 2011). In this study, however, the elements dissolved during this step primarily correspond to sulphide minerals that could not be dissolved by H_2O_2. Additionally, a combination of HNO_3 and HCl acids can partially attack and decompose silicate minerals (Tessier et al., 1979;

Element, 2007). The washed residue was analyzed by XRD to identify remaining sulphide and oxide minerals, following the procedure outlined in Section 5.2.2 3.

***Step 5*:** After the XRD analysis, the Step 4 residue was decomposed by a conventional hotplate digestion technique with a concentrated mixture of acids: 0.4 mL HNO_3, 0.4 mL $HClO_4$ and 1 mL HF in 15 mL Teflon bottles and heating at 135 °C overnight or to complete dryness. After cooling, a second split of acids, in the same volumes, were added and the digestion was conducted the same as for bulk chemical composition analysis in Section 5.2.3.1. This fraction contains elements hosted within detrital silicate minerals and well crystalline oxides as hematite.

The sources of errors in the sequential extraction experiments could originate from sample loss during the washing process between the steps, sample transfer to a different vessel and during XRD analysis of residues of Step 3 and Step 4. Therefore, there is a critical need to validate the analytical results of the sequential extraction tests. The accuracy was evaluated by summing the contents of a specific element in each fraction and dividing the sum by total contents of the said element obtained by total decomposition as illustrated in Equation 3.1. From all the analyzed waste rocks, the recovery values ranged from 80-89 % for Al, 80-101 % for Fe, 77-89 % for Cu, 81-93% for As, 91-133 % for Zn, 85-128 % for Pb and 87-98 % for Mn. The average recovery values reported from the previous researches range from 76 to 138 % (Marin et al., 1997; Sutherland et al., 2000; Anju and Banerjee, 2010; Khorasanipour et al., 2011), therefore, the recoveries of the current study are within the acceptable range.

$$\text{Recovery (\%)} = \Sigma\,(\text{Step 1} + \text{Step 2} + \text{Step 3} + \text{Step 4} + \text{Step 5})/\text{Total contents}) \times 100 \qquad (5.1)$$

5.2.4 Chemical analyses

5.2.4.1 Inductively coupled plasma mass spectrometry (ICP-MS)

The concentrations of metals (Al, Fe, Cu, Zn, Mn, As, Pb, Ni, Cd) and arsenic (As) were determined by Inductively coupled plasma mass spectrometry (ICP-MS; Perkin Elmer NexION) at Tohoku University. The solutions were prepared in 15 mL centrifuge tubes, dilutions were made by ultrapure water and an internal standard used was Indium (1 ppm), prepared from a reagent Cat#: XSTC-13. A filtered aliquot of river water, total digestion solutions and Step 2 to Step 5 sequential extraction solutions were diluted 100 fold, salt leachates were diluted 1000 and 10 000 fold, Step 1 sequential extraction solutions were diluted 10 fold. In each analytical solution, 0.1 mL of Indium standard solution and 0.5 mL of HNO_3 acid (61 % conc.), making a total volume of 10 mL analytical solution. A blank solution was also analysed and results were used to determine limits of detection.

5.2.4.2 Atomic absorption spectroscopy (AAS)

The concentrations of major cations (Ca, K, Mg, Na) were determined by Atomic absorption spectroscopy (AAS; Agilent 240FS AA) at Akita University. The solutions were prepared in 15 mL centrifuge tubes and all dilutions were made with ultrapure water. Four calibration solutions: 10 ppm, 5 ppm, 2 ppm and 1 ppm each for Na and Mg were prepared from separate Na (1000 ppm) and Mg (1000 ppm) standard solutions. A 10 ppm calibration solution was prepared from 1000 ppm K standard solution while 100 ppm, 10 ppm and 0 ppm Ca was prepared from a separate Ca (1000 ppm) standard solution. A 1 mL of prepared Strontium solution (Sr) was added to the Ca calibration solutions. Aliquots of filtered river water and salt leachates were diluted 10 and 100 fold. In each analytical solution, 0.5 mL of HNO_3 acid (61 % conc.) was added and in separate solutions for Ca determinations, 1 mL of Sr was added, making a total volume of 10mL.

5.2.4.3 Sequential extraction analytical considerations

Before use, all the glassware, Teflon digestion vessels and polypropylene bottles were pre-cleaned with dilute HNO_3 acid for at least 3 days and rinsed with ultrapure water three times to ensure no residual metal contamination. The distilled water was prepared from an Automatic Water Distillation Apparatus (Advantec GS-2000) and ultrapure water (18.2 MΩ·cm resistivity) was prepared using the Simplicity ® Water Purification System. The concentrations of acids used in this research were: HNO_3 (61%), $HClO_4$ (60 %), HF (46 %), and HCl (36 %). The 0.11 M acetic acid used for Step 1 was prepared from a 17.47 M glacial CH_3COOH acid and the 0.5 M Hydroxyl ammonium chloride used in Step 2 was prepared by dissolving 34.745 g of $NH_2OH.HCl$ crystals in 1L of distilled water. To achieve the 5 mL of 8.8 M H_2O_2 used in Step 3 of the modified sequential extraction (Rauret et al., 1999), a 4.35 mL of H_2O_2 was calculated from 31 wt % H_2O_2 while the 1.0 M of ammonium acetate solution was prepared from dissolving 77.08 g of CH_3COONH_4 in 1L distilled water. Agitation was carried out using an SR-2W Recipro Shaker while centrifugation was achieved in a Hitachi Himac CT6EL tabletop centrifuge.

5.2.4.4 Map creation and acquisition

A study area location map (Figure 2.2) was prepared using a CorelDraw 2020 software (64-bit) based on desktop reconnaissance and field survey of the Bor mining area. Aerial photographs from Google earth showing features including open-pits, overburden dumps, flotation tailings dams, mine lakes and rivers, with plotted sample locations, were pasted on CorelDraw. A trace function was then used to draw these features to scale. The location map in Figure 4.1 was modified from Đorđievski et al (2018) through CorelDraw. The modifications include: location spot for the discharge of wastewaters from metallurgical/smelter facilities into the Bor River and the spot location of the dam on the gorge of the Timok River. The geological

map in Figure 2.1 was modified from Jelenković et al. (2016) using CorelDraw. Figure 7.1 is an aerial photograph obtained from Google Earth on November 2023 and modified by Microsoft PowerPoint (PPT) to delineate waste dumps and sample locations.

5.3 RESULTS

5.3.1 XRD mineralogical characterization

A summary of the results from the XRD analysis is presented in Table 5.2, where the semi-qualitative mineral contents are marked as: abundant (□), moderate (○) and few (Δ). The representative XRD patterns of waste rocks showing bulk mineralogy are illustrated in Figure 5.9.

Table 5.2 Mineralogical characteristics of the waste rocks obtained by X -ray diffraction.

		R1	R2	R3	R4	R5	R6
Silicate minerals	Quartz	□	□	□	□	□	□
	Plagioclase				□	□	□
	Tremolite				○	Δ	
Clay minerals	Illite			Δ	Δ		□
	Kaolinite	Δ		Δ			
	Clinochlore				○	□	Δ
	Pyrophyllite		Δ				Δ
Fe-rich minerals	Pyrite	□	□	Δ	Δ	Δ	Δ
	Hematite			□			
Cu-rich minerals	Chalcopyrite			Δ			○
	Covellite	Δ					
	Enargite	Δ					
Secondary sulphates	Gypsum			□			Δ

According to Table 5.2, the waste rocks are characterized by an assemblage of silicate minerals; quartz (SiO_2) ± Plagioclase ($NaAlSi_3O_8$) ± tremolite ($Ca_2Mg_5Si_8O_{22}(OH)_2$), clay minerals; illite ($(K,H_3O)(Al,Mg,Fe)_2(Si,Al)_4O_{10}[(OH)_2,(H_2O)]$) ± kaolinite ($Al_2Si_2O_5(OH)_4$) ± clinochlore [$(Mg,Fe)Si_3Al_2O_{10}(OH)_8$] ± pyrophyllite ($Al_2Si_4O_{10}(OH)_2$), sulphide minerals; pyrite (FeS_2) ± chalcopyrite ($CuFeS_2$) ± covellite (CuS) ± enargite (Cu_3AsS_4) and oxide minerals; hematite (Fe_2O_3).

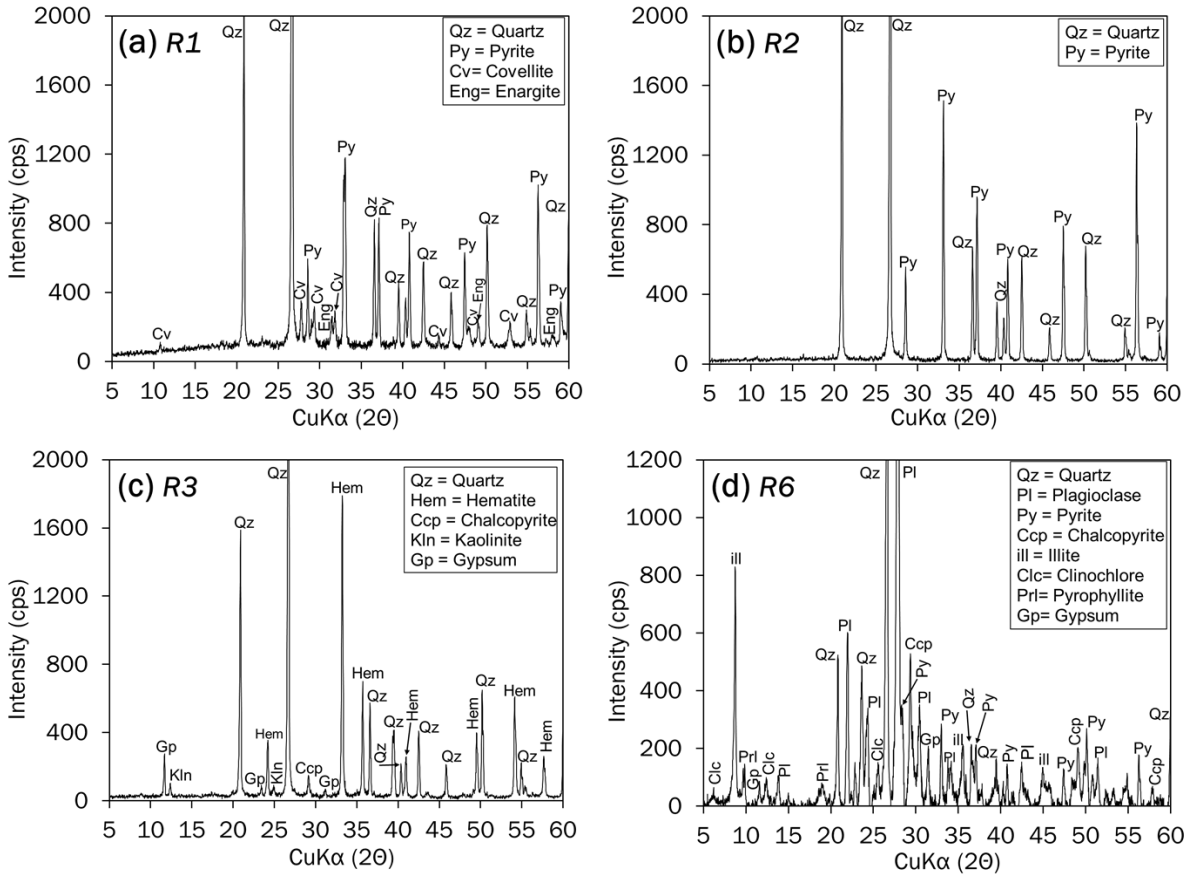

Figure 5.9 XRD patterns showing bulk mineralogy of mine waste rocks. Abbreviations after Whitney and Evans (2010): Qz, quartz; Pl, Plagioclase; Ccp, chalcopyrite; Cv, covellite; Eng, enargite; Py, pyrite; Hem, hematite

Plagioclase was very abundant in Veliki Krivelj rocks but was undetected in Old Bor rocks (Table 5.2). On the other hand, pyrite was ubiquitous in Old Bor rocks, especially R1 (Figure 5.9a) and R2 (Figure 5.9b) whereas only a few peaks of pyrite were detected in Veliki Krivelj rocks. Small contents of covellite and enargite were detected from rock R1 (Figure 5.9a).

Chalcopyrite was detected from R3 (Figure 5.9c) and R6 (Figure 5.9d), with the R6 rock containing higher contents. The mineralogy of rock R3 was dominated by quartz and hematite (Figure 5.9c).

5.3.2 Optical microscopy investigations

The results from optical microscopy verified those of XRD analysis, specifically in the detection of sulphide minerals and hematite. Also, minerals with small contents that could not be detected by XRD techniques due to the detection limit problem (Dold, 2003) were identified under reflected light microscopy. On the surfaces of polished sections of R1, R2 and R6 rocks, a shiny gold/brass-yellow colored mineral (Table 5.1 and Figure 5.2f), assumed to be pyrite was visible to the naked eye.

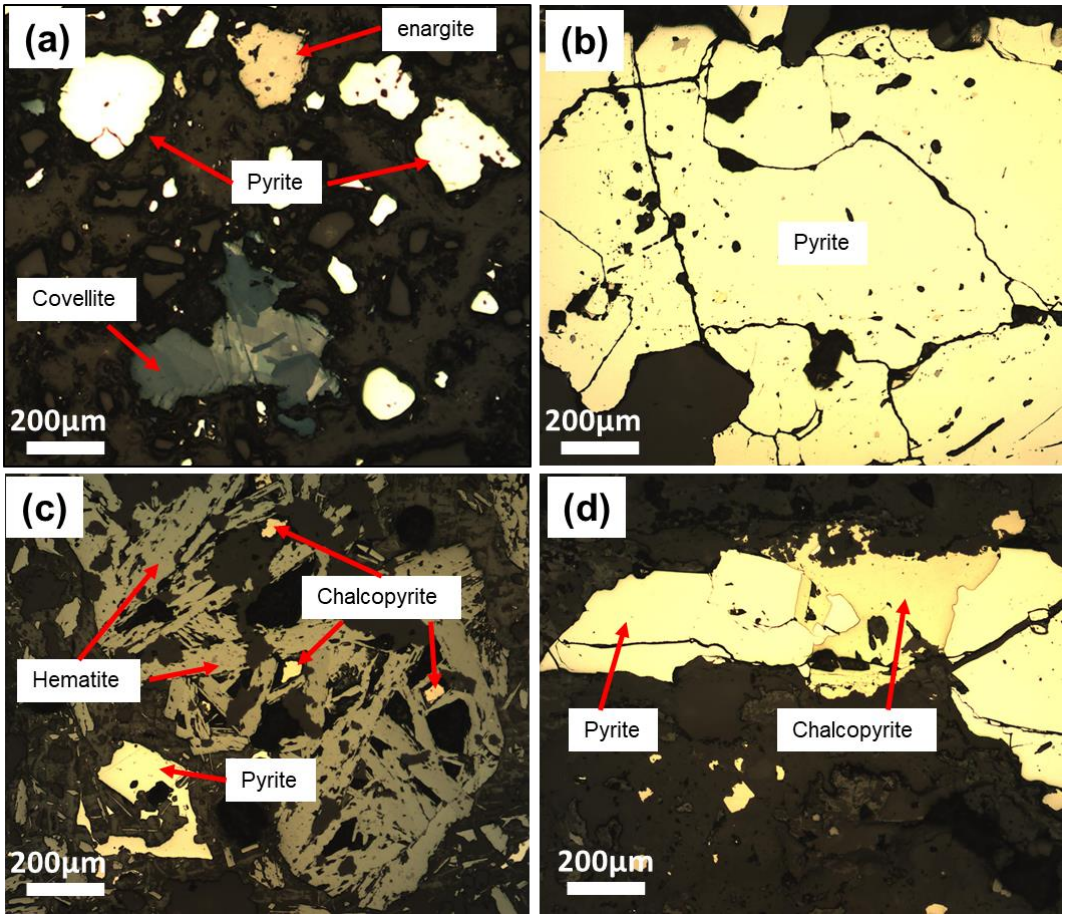

Figure 5.10: Photomicrographs in reflected light microscope showing sulphide and oxide minerals from waste rocks. **(a)** R1: pyrite, covellite and enargite **(b),** R2: pyrite. **(c)**, R3: pyrite, chalcopyrite and hematite. **(d),** R6: pyrite and chalcopyrite

Indeed, pyrite was identified in all waste rocks by optical microscopy (Figure 5.10) and its abundance was tentatively estimated based on the chart proposed by Terry and Chilingar (1955). The estimations revealed that pyrite contents ranged from 25-30 % in R1 (Figure 5.10a), 40-50 % in R2 (Figure 5.10b), 1-3% in R3 (Figure 5.10c) and 5-7 % in R6 (Figure 5.10d). In the outcrop (Figure 5.2d) and polished section of R1, both under a hand magnifying glass (LOUPE RUPER-10X), small crystals of a blue colored mineral were observed. Indeed, under a reflected light microscopy, an indigo-blue covellite and yellow-brown enargite were observed in R1 (Figure 5.10a). From rock R3, hematite was observed as a tabular, elongated and brownish grey mineral while chalcopyrite and pyrite were observed as yellow and whitish yellow minerals (Figure 5.10c), respectively.

5.3.3 Chemical characteristics of sulphide minerals from waste rocks

The results of the quantitative EPMA spot analysis (Table 5.3) provide the chemical composition of the identified sulphide minerals (pyrite, chalcopyrite, covellite and enargite) and hematite from the waste rocks. The results were converted from weight percent (wt %) to atomic percent (at %) such that the ratios are in agreement with the chemical formulae. The contents of Fe and S in the analyzed pyrite averaged 33.1 and 66.9 at %, respectively. In chalcopyrite, contents of Fe, Cu and S averaged 23.6, 25.6 and 50.8 at %, respectively while Fe and O contents in hematite were 34.7 and 65.3 at %. The chemical composition of covellite was characterized by 48.1 at % Cu and 51.8 at % S whereas enargite was made up of 35.9 at % Cu, 52.1 at % S, 11.4at % As and traces of Fe (0.5 at %). Indeed, these results are in agreement with the common chemical formulae of sulphides. For example, the atomic % ratio of Cu and S in covellite gives $Cu_{0.9}S$, which is similar to CuS. Also, the atomic % ratio of Fe and S in pyrite gives $Fe_{0.5}S$, which is FeS_2, thereby verifying the accuracy and validity of the analysis.

Table 5.3 Quantitative EPMA mineralogical characteristics of the waste rocks

Sample name	Mineral analyzed	Formula	Cu	Fe	Zn	Pb	As	S	O	Total
			at %	at%	at%	at%	at%	at%	at %	at %
R1	Covellite	CuS	48.1	0.1	0.0	0.0	0.0	51.8	0.0	100
	Enargite	Cu_3AsS_4	35.9	0.5	0.1	0.0	11.4	52.2	0.0	100
	Pyrite	FeS_2	0.1	32.8	0.0	0.0	0.0	67.1	0.0	100
R2	Pyrite	FeS_2	0.0	33.2	0.0	0.0	0.0	66.8	0.0	100
R3	Chalcopyrite	$CuFeS_2$	23.4	25.8	0.0	0.0	0.0	50.8	0.0	100
	Pyrite	FeS_2	0.0	32.8	0.0	0.0	0.0	67.2	0.0	100
	Hematite	Fe_2O_3	0.0	34.7	0.0	0.0	0.0	0.0	65.3	100
R4	Pyrite	FeS_2	0.0	33.3	0.0	0.0	0.0	66.7	0.0	100
R5	Pyrite	FeS_2	0.0	33.8	0.0	0.0	0.0	66.2	0.0	100
R6	Pyrite	FeS_2	0.0	32.9	0.0	0.0	0.0	67.1	0.0	100
	Chalcopyrite	$CuFeS_2$	23.8	25.5	0.0	0.0	0.0	50.7	0.0	100

5.3.4 Bulk chemical composition of waste rocks

A summary of the total contents of metals and As obtained from the total acid-digestion of waste rocks is presented in Table 5.4. The Al contents in Veliki Krivelj waste rocks (90,900-99,300 mg/kg) were extremely higher than in Old Bor waste rocks (Al: 1090-9340 mg/kg). On the other hand, the contents of Fe (273,000-305,000 mg/kg), Cu (663- 51,740 mg/kg) and As (24.9-6167 mg/kg) were comparatively higher in Old Bor rocks than in Veliki Krivelj rocks (Fe: 59,900-74,000 mg/kg, Cu: 150- 12,500 mg/kg, As: 6.6-9.2 mg/kg). The contents of other metal ranged from 34.4-1944 mg/kg for Mn, 57.3-816 mg/kg for Zn, 4.1-120 mg/kg for Pb, 4.7-76.8 mg/kg for Ni and 7.8-48.2 mg/kg for Co as shown in Table 5.4.

Table 5.4 Total concentrations of metals and arsenic from waste rocks

	Al	Fe	Cu	Mn	Zn	Co	Ni	Pb	As
Unit	mg/kg	mg/kg	mg/kg	mg/kg	mg/kg	mg/kg	mg/kg	mg/kg	mg/kg
R1	1090	237,000	51,800	34.4	86.7	41.1	7.6	120	6167
R2	1200	322,000	663	36.5	816	44.8	16	39.7	25
R3	9340	305,000	1405	49.4	45.0	7.8	4.7	9.0	33
R4	92,700	59,900	150	1944	674	16.1	61.5	17.6	6.6
R5	99,300	61,500	249	1546	349	17.5	10.3	20.6	8.2
R6	90,900	74,000	12,500	322	57.3	48.2	76.8	4.1	9.2

5.3.5 Sequential extraction of waste rocks

Figure 5.11 depict a summary of the results from the 5-step optimized 'modified BCR sequential extraction' as percentages, reflecting the individual content of an element extracted in a specific fraction against the sum of the 5 fractions. The contents of metals and As extracted in Step 3 were dissolved by a weaker oxidizing agent (hydrogen peroxide) whereas those extracted Step 4 were dissolved by a stronger oxidizing agent (inverted aqua-regia)

Al existed mainly in the residual fraction (Step 5), with contents ranging from 35.4 to 79.8 % of total Al across all samples (Figure 5.11a). The Al contents from the extreme-oxidizable fraction (Step 4) were higher in Veliki Krivelj rocks (32.4-53.3 %) than in Old Bor rocks (13.6-20.7 %). The reducible forms of Al (Step 2) were only significant in Veliki Krivelj rocks, ranging from 4.5 to 5.4 %. In spite of low total contents (Table 4), Old Bor rocks contained higher acid-soluble and exchangeable forms of Al (1.6-21.5 %) than Veliki Krivelj rocks (1.2-2.1 %) as indicated by Figure 5.11a.

Fe was hosted primarily in the extreme-oxidizable fraction (Step 4), with contents ranging from 19.3 to 88.6 % of total Fe across all samples (Figure 5.11b). The oxidizable forms of Fe (Step

3) in Old Bor rocks and Veliki Krivelj rocks ranged from 1.4 to 29.3 % and 5.3 to 12.5 %, respectively. The reducible forms of Fe were only significant in Veliki Krivelj rocks, ranging from 2.5 to 8.3 %. The residual fraction (Step 5) was especially important in rock R3, where it hosted 78.9 % of total Fe (Figure 5b). From other rocks, residual Fe contents ranged from 3.4 to 15.4 % of total Fe.

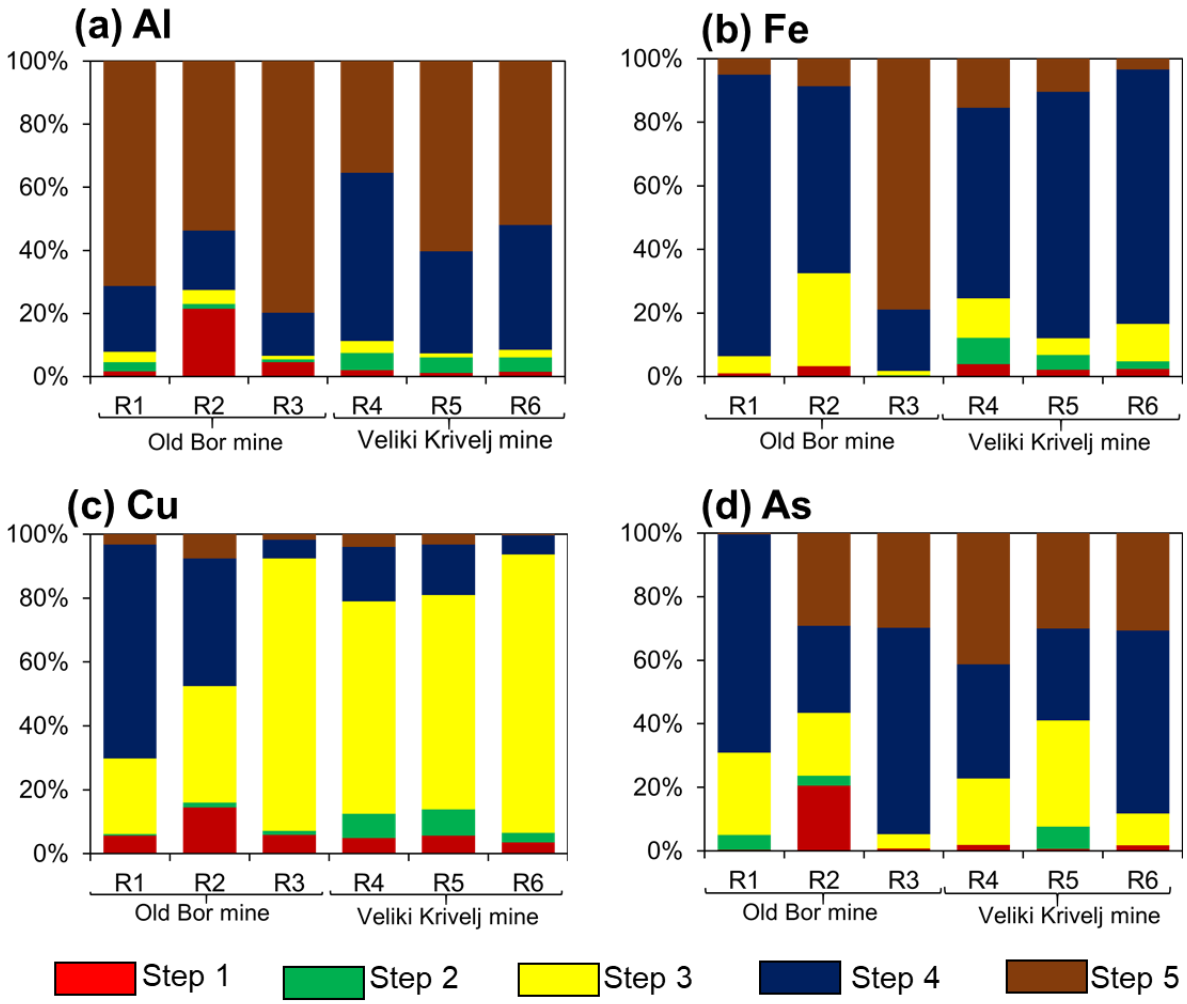

Figure 5.11: The 5-step modified BCR sequential extraction of Al (**a);** Fe **(b);** Cu **(c)** and As **(d)** from the waste rocks

According to Figure 5.11c, Cu existed primarily in the oxidizable fraction (Step 3), with contents ranging from 23.6 to 87.1 % of total Cu contents across all rocks. It is important to observe that the highest oxidizable Cu was extracted from rock R6 followed by R3 (Figure

5.11c). The highest contents of extreme-oxidizable Cu (Step 4) was extracted from rock R1 with contents reaching 67.0 % of total Cu. The acid-soluble and exchangeable forms of Cu ranged from 3.6 to 14.4 %, with contents from the Old Bor rocks generally higher than those from Veliki Krivelj rocks. On the other hand, the reducible Cu was only significant in Veliki Krivelj rocks, with contents ranging from 3.0 to 8.2 % of total Cu (Figure 5.11c).

The total content of As was extremely high at site R1 (Table 5.4), with 26.0 and 68.6 % total As extracted from the oxidizable fraction (Step 3) and extreme-oxidizable fraction (Step 4), respectively (Figure 5.11d). In addition, only 4.6 % of total As existed in the reducible phase. Despite the comparatively low total As contents from other waste rocks (Table 5.4), the contents of oxidizable As ranged from 4.5 to 33.3 % while contents of extreme-oxidizable As ranged from 27.4 to 64.9 % of total As (Figure 5.11d). The residual fraction was also important in these low As content-bearing rocks, with contents ranging from 29.1 to 41.3 % of total As.

5.4 DISCUSSION

5.4.1 Mineralogy and geochemical characteristics of waste rocks

Mine waste rock is essentially an ore, however, with very low contents of the target metals for economic recovery. Therefore, the mineralogical characterization of waste rocks in the Bor Cu mining region (Table 5.2 and Figure 5.9) is consistent with the mineralization of the massive, high sulphidation Cu deposit and the porphyry Cu deposit reported in the region (Jankovic, 1980; 1990; Kozělj, 2002; Armstong et al., 2005; Simic and Mihajlović, 2006; Jelenkovic et al., 2016)

The mineralogy of the waste rocks controlled the chemical composition. According to Table 5.2, plagioclase, an Al-rich silicate mineral was abundantly present in the Veliki Krivelj rocks (R4-R6) and has resulted in extremely high contents of Al (Table 5.4) in these rocks. On the

other hand, the absence of plagioclase in Old Bor rocks (R1-R3) has led to comparatively lower contents of Al in these rocks. This pattern suggest that plagioclase is the principal mineral controlling Al contents. To a lesser extent, clay minerals also contributed to the contents of Al. The dominance of pyrite in the mineralogy of rocks R1 and R2 (Table 5.2) is responsible for the extremely high total Fe contents (Table 5.4). Moreover, variations in the contents of pyrite between R1 and R2 (Figure 5.10) caused differences in the observed Fe contents. According to the EPMA quantitative results (Table 5.3), the contents of Fe from pyrite was about 33.1 at%. In rock R3, the extremely high total Fe contents is associated with the predominance of hematite (Table 5.2 and Figure 5.10c), which is made up of 34.7 at % Fe (Table 5.3).

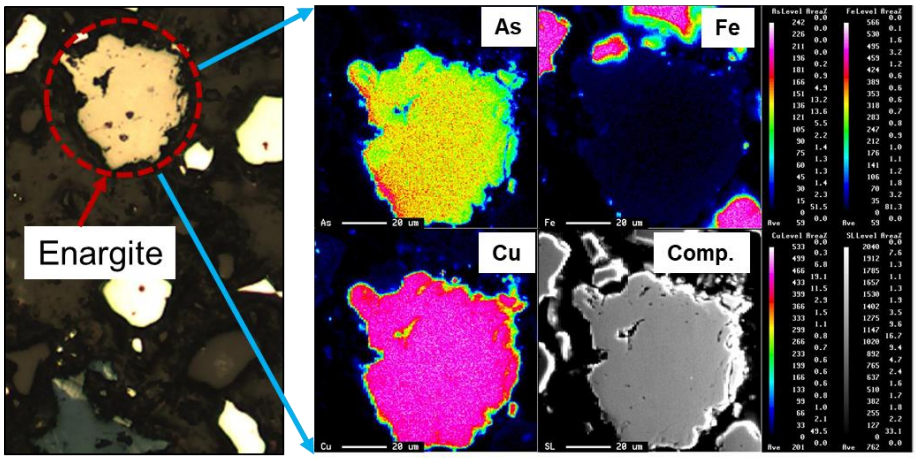

Figure 5.12 EPMA elemental mapping of As, Fe and Cu composition from a possible enargite mineral

The presence of Cu-sulphides, covellite and enargite in rock R1 (Figure 5.10a and Table 5.2), is responsible for the highest total Cu contents (Table 5.4). Based on Table 5.3, the contents of Cu in covellite and enargite was 48.1 and 35.9 at %, respectively. This, combined with the fact that contents of covellite were slightly higher than enargite (Figure 5.9a and Figure 5.10a), could suggest high Cu contribution from covellite than enargite. The variations in the Cu contents in rocks R3 and R6 are attributed to the differences in the contents of chalcopyrite (Table 5.2), which contains around 23.6 at % Cu. According to the results of EPMA (Table

5.3), enargite contains around 11.4 at % As and is therefore responsible for the highest total As contents observed in rock R1. Indeed, this content of As is comparable to the 12.3 at % As reported by Adiwidjaja and Lohn (1970) through EPMA analysis of enargite obtained from Bor, Serbia. This is also supported by the high composition in the As mapping of enargite (Figure 5.12).

5.4.2 Extractability of metals and As

5.4.2.1 Al fractionation

The extraction of high contents of Al in the residual fraction (Figure 5.11a) is consistent with the fact that Al is hosted by plagioclase ($NaAlSi_3O_8$ — $CaAl_2Si_2O_8$), a silicate mineral which decomposes by mixture of strong acids ($HClO_4$ + HF + HNO_3). Moreover, the decomposition of clay minerals (Table 5.2) could have also contributed to the contents of residual Al. The significant contents of Al extracted in the extreme-oxidizable fraction (Figure 5.11a) proves that a mixture of HNO_3 acid and HCl acid partially attacks and decompose silicate minerals as mentioned by Tessier et al. (1979) and Element (2007). The difference in the contents Al extracted in Step 4 between the Veliki Krivelj rocks and the Old Bor rocks could be attributed to the higher contents of plagioclase (Table 2) and consequently, high total Al contents (Table 5.4) in the former than the latter. The notable contents of reducible Al observed from Veliki Krivelj rocks (Figure 5.11a) could be attributed to associations with the amorphous Fe and Mn oxy-hydroxides. The 21.5% of Al dissolved by acetic acid (Step 1) in rock R2 (Figure 5.11a) correspond to the Al either weakly adsorbed on the rock surface by relatively weak electrostatic interaction, co-precipitated with the carbonates or hosted by water-soluble secondary minerals. (Marin et al.1997; Filgueiras et al. 2004).

5.4.2.2 Fe fractionation

The low contents of oxidizable Fe (Figure 5.11b) from the pyrite-bearing waste rocks (Table 2 and Figure 5.9) suggest that pyrite exhibited difficult-oxidation by hydrogen peroxide. Nonetheless, the highest contents of oxidizable Fe observed from rock R2 (29.3 %) is attributed the predominance of pyrite in its mineralogy (Figure 3b and Figure 4b). According to Figure 5.13, after the digestion of waste rocks with H_2O_2 followed by subjecting the solid residues to the bulk XRD analysis, pyrite was still detected. This incomplete digestion of sulphide minerals in mine wastes by H_2O_2 has been mentioned in several studies (Filgueiras et al., 2002; Galán et al., 2003; Dold and Fontboté, 2001; Khorasanipour et al., 2011).

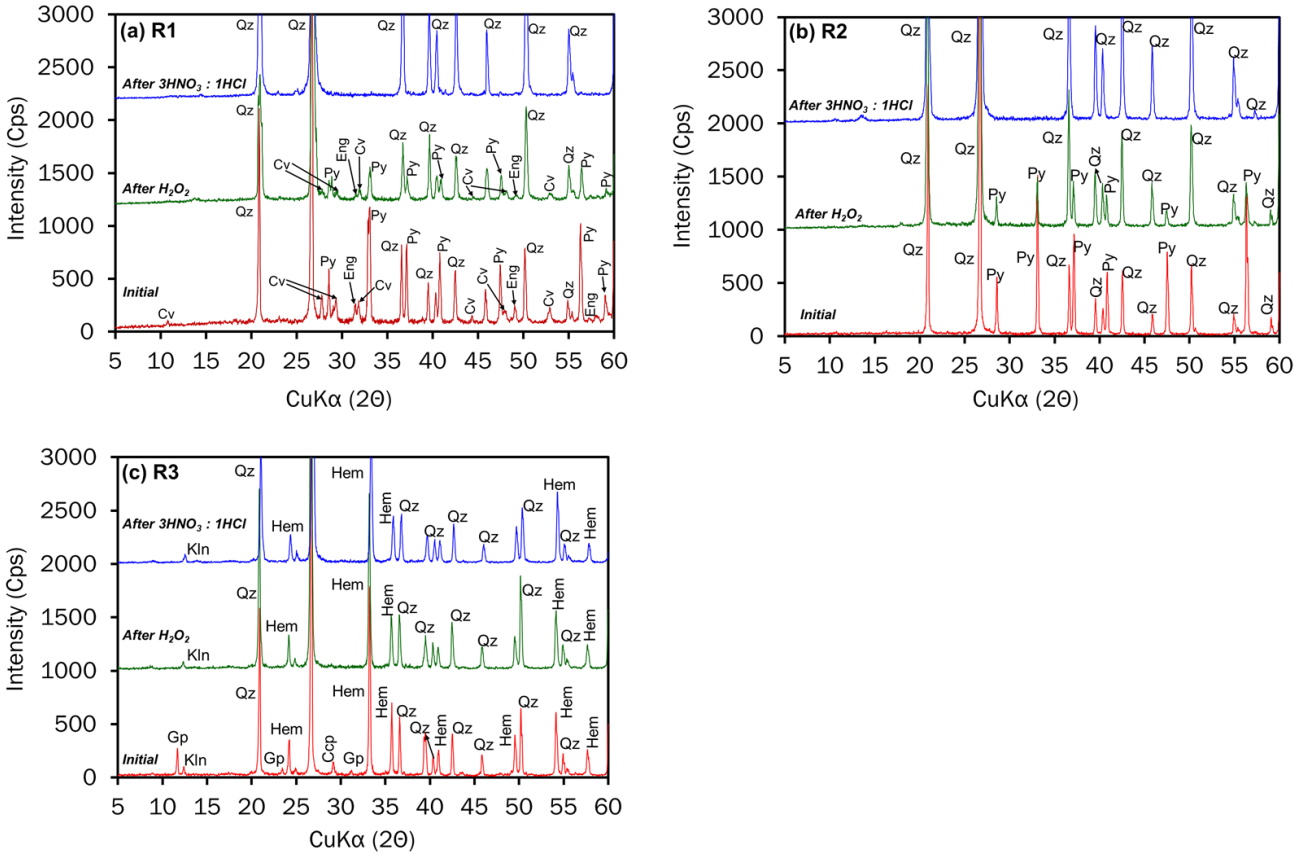

Figure 5.13: XRD Diffraction of waste rocks and their residues after reaction with hydrogen peroxide (H_2O_2) and inverted-aqua regia ($3HNO_3$: 1HCl). Abbreviations after Whitney and Evans (2010): Qz, quartz; Ccp, chalcopyrite; Cv, covellite; Eng, enargite; Py, pyrite; Hem, hematite; Kln, kaolinite; Gp, gypsum

The high contents of the extreme-oxidizable Fe (28,800-176,000 mg/kg) observed across all samples suggest that inverted aqua-regia is a powerful oxidizing agent, in comparison to hydrogen peroxide (Tsogtkhankhai et al., 2011). Figure 5.13 shows that all Fe-bearing sulphide minerals were undetected after treating the solid residues of Step 3 with 3 mL HNO_3 acid and 1 mL HCl acid, hence the complete oxidation and dissolution of pyrite and chalcopyrite. Indeed, after the reaction, the supernatant of the pyrite-dominated rock (R2) was yellowish, which could indicate extremely high concentrations of Fe transferred into a solution through the complete oxidative dissolution of pyrite (Figure 5.10b). Based on the established fact that a mixture of HNO_3 acid and HCl acid can partially decompose silicate minerals (Tessier et al., 1979; Klock et al.,1986; Element, 2007), it should be acknowledged that the Fe-bearing silicates could have contributed to the contents of extreme-oxidizable Fe, however to a lesser extent.

The low contents of residual Fe (Figure 5.11b), except for rock R3, is consistent with the absence of either pyrite or chalcopyrite in the solid residues of Step 4 (Figure 5.13). This further highlights the total digestion of Fe-sulphides by inverted aqua-regia. Additionally, the residual Fe contents could be underestimated by the partial decomposition of Fe-bearing silicates during the preceding extraction (Step 4), however to a lesser extent. The extremely high residual Fe contents observed from rock R3 (Figure 5.11b) is attributed to the well crystalline hematite which predominated the mineralogy of this sample (Figure 5.9c). According to Figure 7.7c, hematite persisted in the sample from Step 1 to Step 4 extraction stages, suggesting that it was not digested by the reagents. Hematite is known to be one of the oxides minerals hosting Fe in the residual fraction, owing to its well crystalline structure (Tessier, 1979; Rauret et al., 1997; Anju and Banerjee, 2010; Dold, 2003). Moreover, according to Schwertmann and Taylor (1989), hematite is the most stable, relatively insoluble mineral. Similar to Al (Figure 5.11a),

the notable contents of reducible Fe observed only from Veliki Krivelj rocks could be attributed to Fe oxy-hydroxides.

5.4.2.3 Cu fractionation

The high contents of oxidizable Cu (Figure 5.11c) suggest that it is extracted from the Cu-sulphide minerals. The 24.7 % (10,900 mg/kg) observed from R1 correspond to the partial oxidative dissolution of covellite and enargite (Figure 5.10a). Based on Figure 5.13a, small peaks of covellite and enargite were detected in the solid residue of R1 after digestion with H_2O_2. This incomplete digestion of could be supported by Ferrer et al. (2021) who reported that only 10 and 15% of covellite and enargite, respectively were dissolved by 35% H_2O_2 after 1 hour of reaction at 80 °C. Sasaki et al. (2010) noted that the oxidation rate of enargite is much slower than that of other Cu sulphides such as chalcopyrite and covellite, especially in acidic pH. On the other hand, the oxidizable Cu contents of 87.1 % (8,353 mg/kg) and 85 % (929 mg/kg) observed from rocks R6 and R3 (Figure 5.11c), respectively, suggest the almost complete digestion of chalcopyrite (Figure 5.10c and d) by hydrogen peroxide. This is supported by the absence of chalcopyrite peaks after treatment with H_2O_2 (Figure 5.13c). Indeed, after the total evaporation of H_2O_2, a blue precipitate was observed from R6 sample, which could indicate a Cu sulphate formed from the oxidation of chalcopyrite (Tsogtkhankhai et al.,2011; Sokic et al., 2019). This suggests that in H_2O_2, chalcopyrite dissolves easily in H_2O_2 than covellite and enargite. Ferrer et al. (2021) tested the leaching ability of hydrogen peroxide by performing a partial extraction of concentrate containing chalcopyrite using 35% H_2O_2 for 1 h at 80 $^{\circ}$C and reported that 60 and 10 % of Cu and Fe, respectively, were released from chalcopyrite.

The highest contents of extreme-oxidizable Cu observed in rock R1 (Figure 5.11c; 30,854 mg/kg) suggest that inverted aqua-regia completely digested covellite and enargite (Figure

5.10a). To support this assertion, Figure 5.13a shows that after treating rock R1 with a mixture of HNO_3 acid and HCl acid, the solid residue did not show peaks of these Cu-sulphides. Indeed, after the reaction, the filtered supernatant of R1 was bluish-green, which could indicate extremely high concentrations of Cu transferred into a solution through the complete oxidative dissolution of covellite and enargite. This color of the supernatant is consistent with the greenish-blue color of hydrated copper chloride which can be generated by reaction of Cu sulphides with a mixture of HNO_3 and HCl acids.

Similar to Al (Figure 5.11a) and Fe (Figure 5.11b), notable contents of reducible Cu observed only from Veliki Krivelj rocks could be attributed to Fe oxy-hydroxides. The higher contents of Cu in the water-soluble, acid-soluble and exchangeable fraction in Old Bor rocks, especially R2 (Figure 5.11c) correspond to the Cu either weakly adsorbed on the rock surface by relatively weak electrostatic interaction, co-precipitated with the carbonates or hosted by water-soluble secondary minerals, similar to Al (Figure 5.11a).

5.4.2.4 As fractionation

The highest contents of oxidizable As extracted from R1 (1494 mg/kg) correspond to the partial digestion of the As-bearing enargite (Figure 5.10a). Based on Figure 5.13a, a small peak of enargite was detected in the residue after treatment with H_2O_2. The treatment of the Step 3 residue with inverted aqua-regia led to the total digestion of enargite and the transfer of As into a solution, accounting for the observed 68.6 % (3943 mg/kg) of total As contents. The enhanced significance of As in the water-soluble, acid-soluble and exchangeable fraction in rock R2 (Figure 5.11c; 20.6 %) correspond to the As either weakly adsorbed on the rock surface by relatively weak electrostatic interaction, co-precipitated with the carbonates or hosted by water-soluble secondary minerals, similar to Al (Figure 5.11a) and Cu (Figure 5.11c)

5.4.3 Environmental implications of the oxidation behaviour of sulphides

The newly developed 5-step modified sequential extraction procedure simulate the chemical reactions that could occur under different conditions in the natural environment. Therefore, the reaction of sulphide-bearing waste rocks with hydrogen peroxide mimic the natural oxidation of these sulphides which involves interaction with atmospheric oxygen, water and the action of microorganisms to generate acid mine drainage (AMD) as indicated by Figure 5.14. On the other hand, the stronger oxidizing power and reaction temperature of inverted-aqua simulate a much harsher condition that is not represented by the natural environment. Therefore, it could represent a slow rate of sulphide oxidation in the natural environment. It also very important to note that the laboratory experiments conducted for sequential extractions did not include microorganisms/bacteria, the test result might be different from the natural oxidation processes.

5.4.3.1 Easy oxidation-high environmental impact

The release of 87.1 % of total Cu from a chalcopyrite-bearing rock (R6) when reacted with H_2O_2 suggest that this sulphide mineral is easily oxidized under natural atmospheric conditions. The easy-oxidation pattern of chalcopyrite by H_2O_2 was also observed from rock R3, where 85 % of total Cu was chalcopyrite-dissolution. This Cu speciation behaviour could suggest that chalcopyrite-like sulphides could pose a high environmental impact with regards to contamination (Figure 5.14a). Mine wastewaters such as the green-colored Saraka stream (Figure 2.3h) might have formed by the easy oxidative dissolution of chalcopyrite.

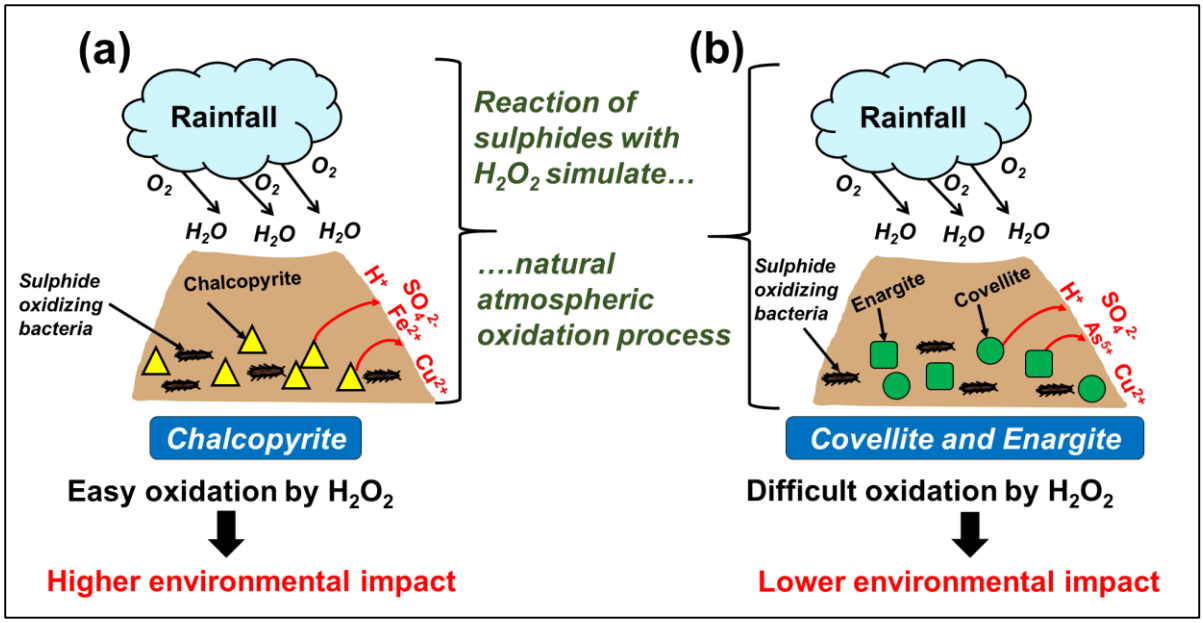

Figure 5.14 A detailed model simulating the easy-oxidation of chalcopyrite and difficult-oxidation of covellite and enargite under natural atmospheric oxidation conditions

5.4.3.2 Difficult oxidation - low environmental impact

The release of 24.7 % of total Cu from a rock containing covellite and enargite upon reaction with H_2O_2 could suggest that these sulphides exhibit difficult oxidation under natural atmospheric conditions (Figure 5.14b). This might imply that these sulphide have a low environmental impact with regards to contamination. However, it should be noted that the contents of Cu and As easily released by H_2O_2 from covellite and enargite are significant enough to pose risk to the environment. Additionally, the contents of Cu and As dissolved by stronger oxidizing reagent suggest that covellite and enargite will be available in mine wastes for a longer period and therefore presenting a long-term source of AMD.

5.5 CONCLUSION

A comprehensive mineralogical investigation of mine wastes using a combination of tools such as XRD, optical microscopy, electron probe micro-analyzer and sequential extraction is very useful in the predicting the contamination potential of mine wastes, thereby helping in the mitigation and remediation plans of both active and abandoned mine waste storages. The current study optimized 'the 4-step modified BCR sequential extraction procedure' and included inverted aqua-regia, a very strong oxidizing agent, to dissolve the resistant sulphides remaining after the treatment with H_2O_2. Despite the abundance of pyrite in waste rocks, low Fe contents were extracted in the oxidizable fraction and this was associated with difficulty of pyrite oxidation by H_2O_2. The residual pyrite was completely decomposed by inverted aqua-regia to extract very high contents of Fe in the extreme-oxidizable fraction. Covellite and enargite also exhibited difficult oxidative dissolution in H_2O_2 to extract small contents of Cu (and As) in the oxidizable fraction, however were easily dissolved by inverted aqua-regia to release highest contents Cu (and As) in the extreme-oxidizable fraction. On the other hand, chalcopyrite dissolved easily in H_2O_2 and released the highest Cu contents in oxidizable fraction. The newly developed 5-step sequential extraction test is very useful in the distinguishing ease-oxidizing sulphides and difficult-oxidizing sulphides and therefore enabled the interpretation of environmental impacts from the sulphides. It can be used to infer the presence of small particles (1 μm) of sulphides in overburden and flotation tailings when conventional mineralogical characterization techniques such as XRD or optical microscope are unable to detect such minerals. It can be applied to a large-scale estimation of quantities of toxic elements expected to be released into the environment under different conditions.

6. APPLICATIONS OF THE SEQUENTIAL EXTRACTION DATA – A FIELD SCALE ESTIMATION OF RELEASED QUANTITIES OF TOXIC ELEMENTS

6.1 INTRODUCTION

The interpretation of sequential extraction data in regards to environmental assessment is usually based on the absolute risk obtained by simple laboratory experiments which uses a very small sample weight. This is very limited since it does not associate the extraction data with the field volume of mine waste materials to give a mass-ordered relative risk of potential contamination. In this PhD thesis, an application of the sequential extraction data will be demonstrated by estimating the quantities of toxic elements (Fe, Cu and As) that are susceptible to be released from mine wastes at a large scale. This will be achieved by combining the sequential extraction results with the estimated mass/volume of mine wastes. The estimated quantities could then be useful in monitoring strategies of mine wastes storages.

6.2 Estimation of mass/volume of overburden and flotation tailings

There are 2 identified overburden wastes generated by the Old Bor open-pit mine; North and South-eastern overburden (Figure 6.1). There is also Veliki Krivelj overburden generated from Veliki Krivelj open-pit mine (Figure 6.1). The volume of Old Bor Flotation Tailing Fields 1 and 2 (Figure 6.1) were estimated by analysis of satellite images. On the other hand, the volume of Veliki Krivelj flotation tailings were actual volumes recorded each time during deposition into the impoundments. The mass of overburden was estimated by satellite image analysis for volume estimations. The density values of mine wastes were provided by the Mining and Metallurgy Institute Bor; overburden and flotation tailings was estimated at 1.8 and 1.3 g/cm^3, respectively.

By using the provided density and estimated volume, the mass of mine wastes was calculated using Equation 6.1. The estimated mass was then converted into tonnes and megatons as indicated in Table 6.1.

$$\text{Mass (g)} = \text{Volume (cm}^3\text{)} \times \text{Density (g/cm}^3\text{)} \quad (6.1)$$

According to Figure 6.1 and Table 6.1, the Veliki Krivelj Flotation Tailings Field 1 and 2 has the largest mass of flotation tailings at 166 and 116 Mt, respectively. RTH dam (60 Mt) has the third largest mass of tailings followed by Old Bor Flotation Tailings Field 2 has (19 Mt). The Veliki Krivelj overburden has the largest mass (200 Mt), followed by South-East Old Bor (150 Mt) and North – Old Bor (57 Mt).

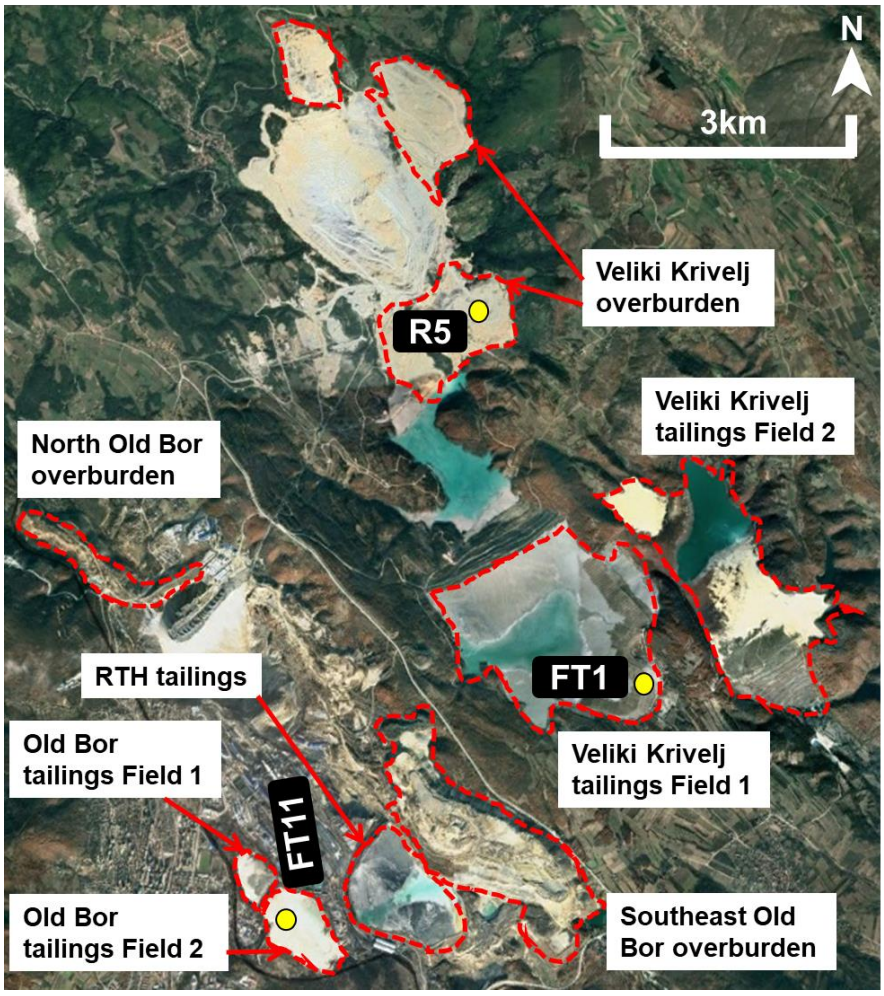

Figure 6.1 Aerial photograph showing deposition sites of overburden and flotation tailings generated by Bor mining activities. The photograph was acquired on

Table 6.1 Estimated volume and mass of overburden and flotation tailings originating from the Bor Cu mining region

Mine waste	Location	Estimated volume (cm^3)	Density (g/cm^3)	Mass (kg)	Mass (t)	Mass (Mt)
Flotation tailings	Veliki Krivelj Field 1	1.28×10^{14}	1.3	1.66×10^{11}	1.66×10^{8}	166.4
	Veliki Krivelj Field 2	8.94×10^{13}	1.3	1.16×10^{11}	1.16×10^{8}	116.2
	Old Bor Field 1	2.21×10^{12}	1.3	2.87×10^{9}	2.87×10^{6}	2.87
	Old Bor Field 2	1.46×10^{13}	1.3	1.90×10^{10}	1.9×10^{7}	19.0
	RTH dam	3.33×10^{13}	1.3	4.33×10^{12}	4.33×10^{7}	43.3
Overburden	Old Bor-North	1.11×10^{13}	1.8	1.99×10^{10}	1.99×10^{7}	19.9
	Old Bor-South East	8.33×10^{13}	1.8	1.50×10^{11}	1.49×10^{8}	149.9
	Veliki Krivelj	1.11×10^{14}	1.8	2.00×10^{10}	2.00×10^{8}	200
Σ Veliki Krivelj Flotation tailings mass					2.83×10^{8}	283
Σ Old Bor Flotation tailings mass					2.19×10^{7}	21.9
Σ Overburden mass					3.70×10^{8}	370

6.3 Estimation of quantities of Cu, Fe and As from mine wastes – a large scale environmental risk evaluation

Three samples; one representing fresh and deeper overburden material (R5); one representing surface Veliki Krivelj flotation tailings (FT1); and the other representing surface Old Bor flotation tailings (FT11) were selected to demonstrate the application of the 5-step sequential extraction in estimating quantities of toxic metals expected to be released from mine wastes. It is important to note that the Old Bor tailings are very old, weathered and were generated by less effective ore beneficiation processes. On the other hand, Veliki Krivelj tailings are relatively new, fresh and were generated through ore beneficiation technologies with high Cu recovery.

According to Figure 6.2, contents of Cu, Fe and As hosted in the water-soluble + acid-soluble + exchangeable fraction (Step 1), reducible fraction (Step 2) and oxidizable fraction (Step 3) can be easily released into the environment by dissolution and oxidation. Therefore, the sum of these three fractions can be used to infer a 'total environmental impact'. Based on this assumption, Cu (Figure 6.2a) poses higher threat of release than Fe (Figure 6.2b) and As (Figure 6.2c). On the other hand, quantities of Cu, Fe and As hosted in the extreme-oxidizable fraction (Step 4) will be released at a very slow rate while those hosted in the residual fraction (Step 5) are highly unlikely to be released into the environment.

Table 6.2 Results of the 5-Step modified BCR sequential extraction from overburden and flotation tests

		Step 1 + Step 2 + Step 3 (mg/kg)	*Step 4* (mg/kg)	*Step 5* (mg/kg)	*Bulk composition* (mg/kg)
	Fe	7428	48,029	6444	61,499
R5	Cu	172	33.4	6.9	249
	As	2.7	1.9	2.0	8.2
FT1	Fe	5832	18,946	12,490	37,268
	Cu	724	51	0	775
	As	1.7	0.2	0	1.9
	Fe	5671	55,253	14,468	75,392
FT11	Cu	552	227	180	960
	As	0.2	82.7	38.9	122

Table 6.2 shows the actual values from the newly developed 5-step modified BCR sequential extraction procedure. Since 0.5g weight of the sample was used in the experiment, quantities of Cu, Fe and As per 0.5 g of the mine wastes were calculated. Next, the obtained quantities were multiplied by the estimated mass (Table 6.1) to achieve the mass-ordered relative risk of contamination (Table 6.3). These calculations are demonstrated below in Section 6.3.1.

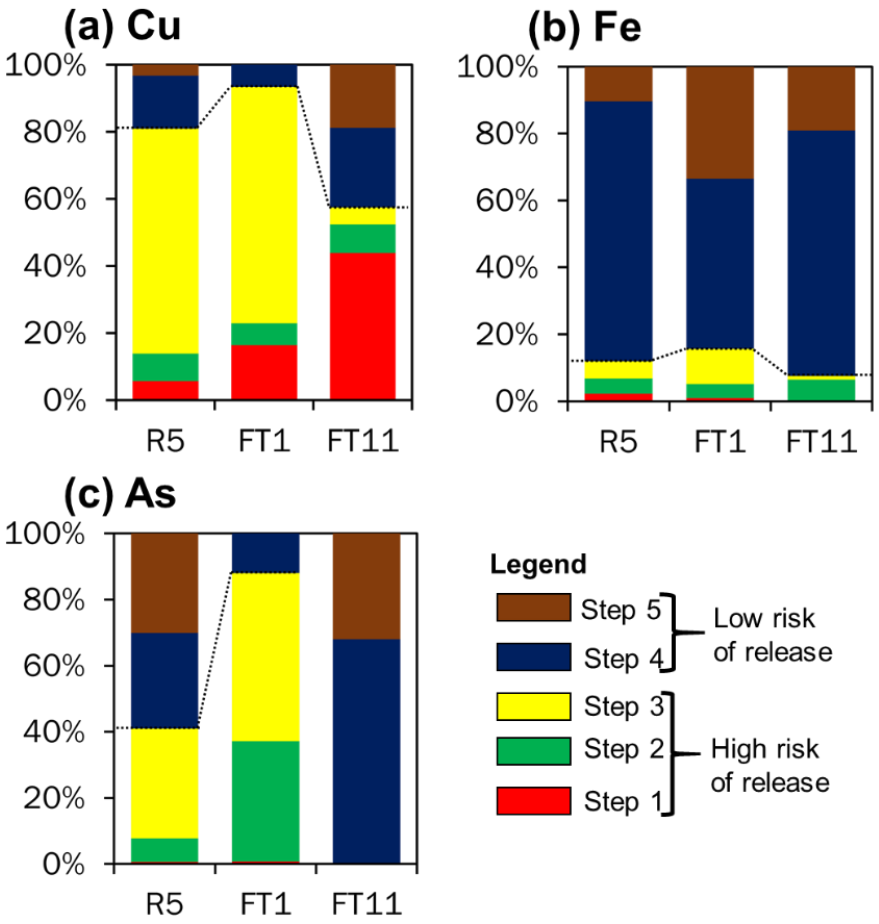

Figure 6.2 Chemical speciation of Cu, Fe and As in overburden and flotation tailings

6.3.1 Quantities of Cu

The sum of Step 1 + Step 2 + Step 3 forms of Cu extracted from overburden sample (R5) were 172 mg/kg (Table 6.2). This value is read as "172 mg of Cu in 1 kg of the R5 overburden material". However, the sequential extraction test only used 0.5 g of a sample. Therefore, quantities of Cu released from 0.5 g of a sample was calculated as;

172 mg of Cu: 1 kg sample

χ of Cu: 0.5 g of sample

where χ was calculated as: $172\ \text{mg} \times \frac{g}{1000\ mg} \times \frac{1}{1000 g} \times 0.5\ \text{g} = 8.6 \times 10^{-5}\ \text{g of Cu}$ (6.2)

Therefore;

0.5g of sample: 8.6×10^{-5} g of Cu

3.70×10^{8} t of total overburden: γ t of Cu

γ was calculated as: $\frac{8.6 \times 10^{-5} \text{ g of Cu}}{0.5\ g\ of\ sample} \times 3.70 \times 10^{8}$ t of overburden = 64,000 t of Cu

(6.3)

This value represents the 'total environmental impact' of Cu release from the deeper Overburden (Table 6.3). However, it is very important to determine the contributions of the acid-soluble, reducible and oxidizable fractions to the easily released quantities of Cu (Table 6.3). From the total of 64,000 t of Cu, the acid-soluble fraction constituted 7%, meaning that 4500 t of Cu is bioavailable and would be released during the interaction of overburden with rainwater or acidic river waters (Figure 6.3a). Additionally, 10 % was contributed by the reducible phase, implying that 6400 t of Cu would be released upon the exposure of overburden to reducing/anoxic conditions (Figure 6.3a). The oxidizable fraction constituted 83 %, implying that the oxidation of chalcopyrite-like sulphides would be required for the release of 53,000 of Cu from the overburden (Figure 6.3a), thereby representing a greater threat of Cu contamination. On the other hand, 12,000 t of Cu (Table 6.3) would be released very slowly under the natural atmospheric conditions whereas 2600 t of Cu contributed by the residual materials is highly unlikely to be released into the environment.

From the flotation tailings, 1600 and 1200 t of Cu represents the total environmental impact of Cu release from Veliki Krivelj and Old Bor impoundments, respectively (Figure 6.3b). Rainwater or acidic water will be required for the release of 2800 t Cu (17.5 %) and 9200 t Cu (77 %) from the Veliki Krivelj tailings and Old Bor tailings, respectively. This variation suggests that, upon interaction with rainwater/acidic waters, Old Bor tailings could pose a higher risk of Cu release than Veliki Krivelj tailings and overburden materials. The reducing/anoxic conditions will easily release 1100t Cu (6.9 %) and 1800t Cu (15 %) from the Veliki Krivelj tailings and Veliki Krivelj tailings and Old Bor tailings, respectively. However, the oxidation of chalcopyrite-like sulphides will release 12,000 t Cu (75 %) and 1100 t Cu (9.2 %) from the Veliki Krivelj tailings and Old Bor tailings, respectively. This variation is congruent with the fact that tailings from Veliki Krivelj are general new and fresh and may still contain sulphide minerals.

Table 6.3 Estimated quantities of Fe, Cu and As inferred by the 5-step modified sequential extraction test and mass of overburden an tailings

			Step 1 + Step 2 + Step 3 (Easily released)	***Step 4 (Difficult to release)***	***Step 5 (Not released)***
Total estimated mass of mine wastes (t)			Estimated quantities from mine wastes (t)		
Overburden	370,000,000	Fe	2,800,000	18,000,000	2,400,000
		Cu	64,000	12,000	2600
		As	1000	710	740
Veliki Krivelj Tailings	283,000,000	Fe	128,000	415,000	274,000
		Cu	16,000	1100	0
		As	37	5	0
Old Bor Tailings	21,900,000	Fe	124,000	1,200,000	317,000
		Cu	12,000	5,000	4,000
		As	4	1,800	850

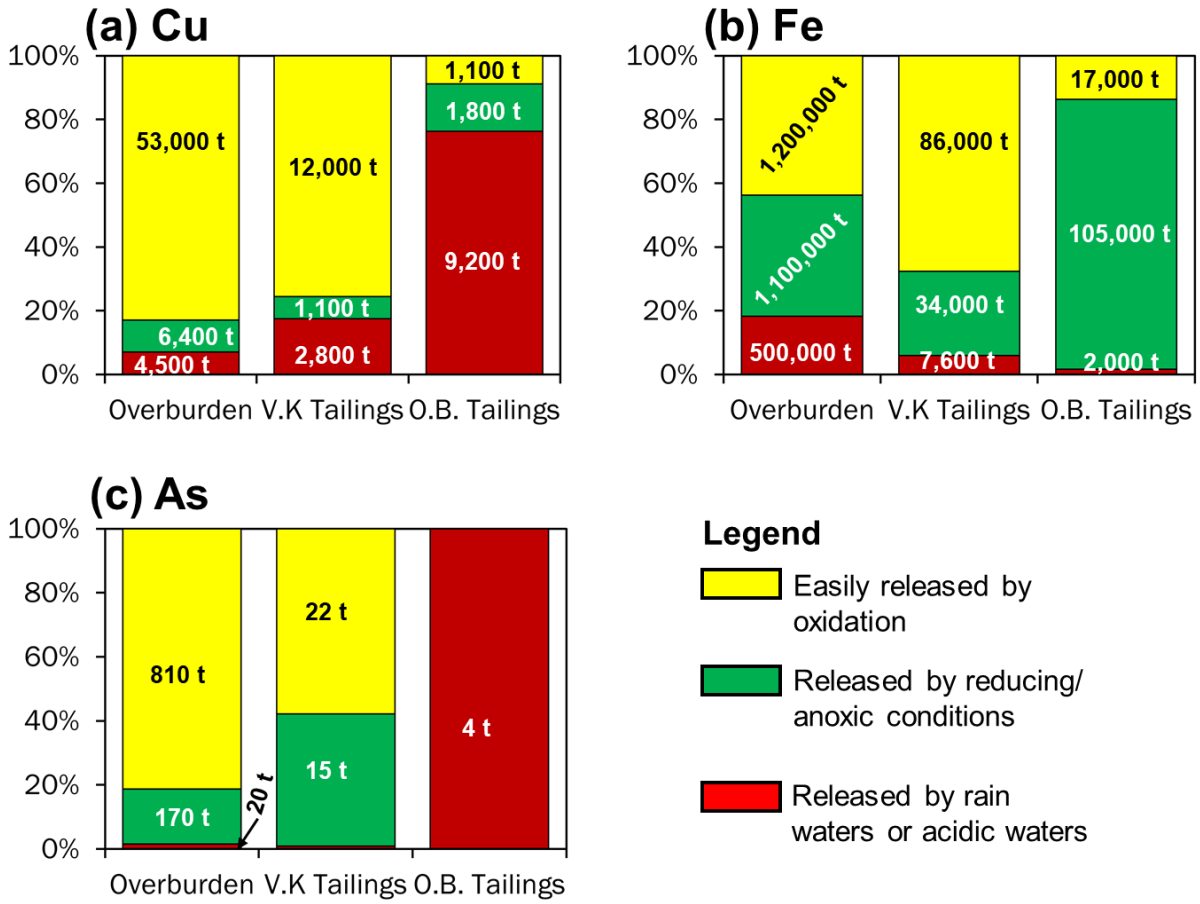

Figure 6.3 The contribution of acid-soluble (Step 1), reducible (Step 3) and oxidizable fraction (Step 3) to the total environment impact (easily released) posed by Cu, Fe and As. The terms 'V.K' and 'O.B' refers to Veliki Krivelj and Old Bor, respectively

6.3.2 Quantities of Fe

According to Table 6.3, the estimated quantities of Fe that would be easily released from overburden, Veliki Krivelj flotation tailings and Old Bor tailings are 2,800,000 t Fe, 128,000 t Fe and 124,000 t Fe, respectively. Figure 6.3b shows that the easy-oxidation of Fe-sulphides will release 1,200,000 t Fe (44 %) from overburden; 86,000 t Fe (67 %) from Veliki Krivelj tailings; and 17,000t Fe (14 %) from Old Bor tailings. The reducing/anoxic conditions will release 1,100,000 t Fe (38 %) from overburden; 34,000 t Fe (27 %) from Veliki Krivelj tailings; and 105,000t Fe (85 %) from Old Bor tailings. The high quantities of reducible Fe in Old Bor tailings is in agreement with the fact that these materials are very old and have been exposed

to weathering conditions for a prolonged period. Rainwater or acidic water will interact with mine wastes to release 500,000 t Fe (19 %) from overburden; 7600 t Fe (6 %) from Veliki Krivelj tailings; and 2000t Fe (2 %) from Old Bor tailings.

6.3.3 Quantities of As

According to Table 6.3, the estimated quantities of As that would be easily released from overburden, Veliki Krivelj flotation tailings and Old Bor tailings are 1000 t, 37 t and 4t, respectively. Based on Figure 6.3c, all of the 4t of As in Old Bor tailings will be easily released by either rainwater or acidic waters. However, a reducing condition will be required for the release of 15 t and 170t of As from Veliki Krivelj tailings and overburden, respectively. Additionally, easy-oxidation of sulphides (containing As) will be needed for the release of 22 t and 810t As from Veliki Krivelj tailings and overburden, respectively.

6.4 Estimation of quantities of Cu, Fe and As from weathered tailings during interaction with rainwater

During a Master's thesis, the estimation of quantities of toxic elements expected to be released from weathered tailings was evaluated by reacting with distilled water to simulate rainwater interaction. The concentrations of Fe, Cu and As (mg/L) obtained from the tailings leachates were converted into mg/kg based on the 1:10 tailings-water mixing ratio. Next, quantities of Cu, Fe, As in 3 g of sample were calculated following Equation 6.2, followed by multiplying with total mass of tailings (Table 6.1) to achieve mass-ordered relative risk of potential contamination. It is imperative to note that these quantities are mostly from the metal sulphates that may be present, even at trace contents, on the surface tailings. In this PhD thesis, a

comparison will be made between the quantities obtained from Step 1 fraction (Figure 6.3) and the water-dissolution test (Figure 6.4).

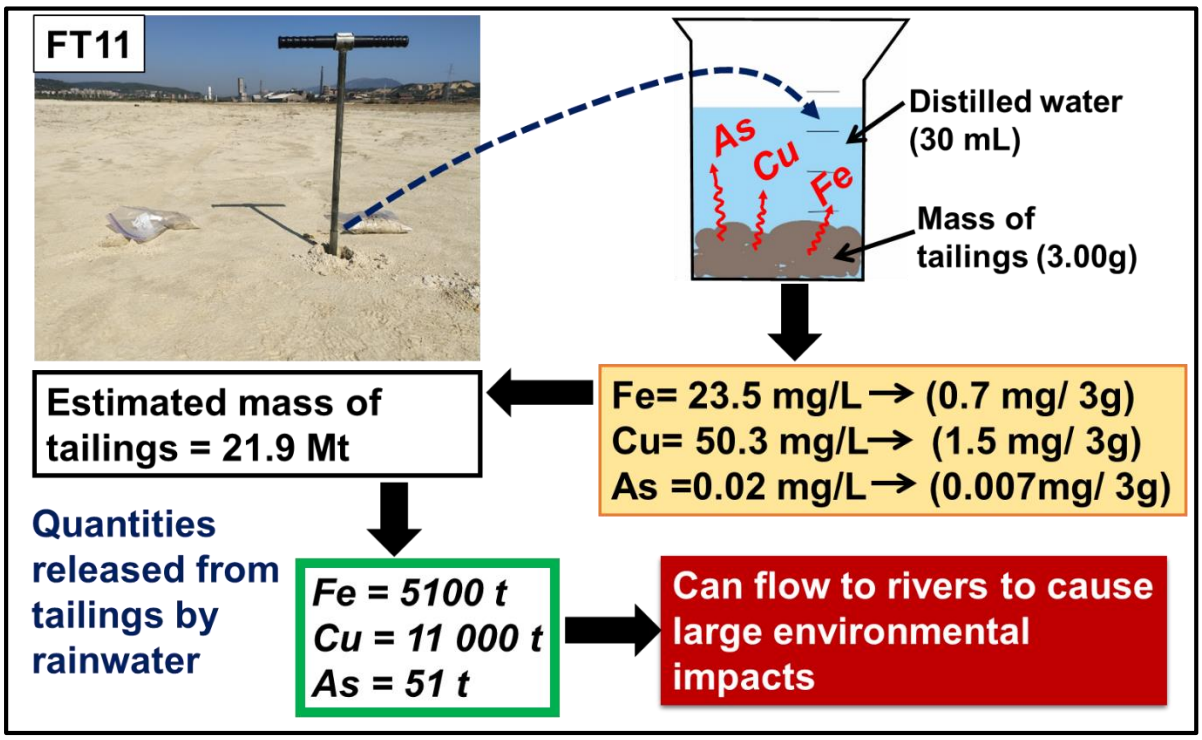

Figure 6.4 Quantities of Cu, Fe and As expected to be released from the surface Old Bor tailings upon interaction with rainwater

According to Figure 6.4, the quantities of Cu, Fe and As expected to be released from tailings upon interaction with rainwater are 11 000, 5100 and 51 t, respectively. Interestingly, the quantities of Cu released by rainwater (Figure 6.4) is similar to the ones released during Step 1 of the sequential extraction (Figure 6.3). This proves that the hydrated metal sulphates present in tailings poses a higher risk of Cu and As contamination than sulphide minerals.

7. SUMMARY

The Bor Cu mining region presents a case of acute contamination of the environment by mining activities. These potential risks of pollution have been observed in both mine wastes systems and river systems (Figure 7.1).

In mine waste systems, sulphide minerals are usually present at the deeper parts of overburden dumps. At these depths, sulphide oxidation is occurring, with the aid of sulphide oxidizing microorganisms, to generate solutions of high acidity and elevated concentrations of toxic elements. According to the newly developed 5-step modified BCR sequential extraction procedure, chalcopyrite will easily dissolve under simulated natural oxidizing conditions, causing a higher impact to the environment. On the other hand, covellite and enargite will exhibit difficulty in dissolving under simulated natural oxidizing conditions, causing a lower impact to the environment. At the surface of the overburden dumps, there are usually sulphate minerals, formed by upward capillary migration of pore waters of the weathered materials. Since are highly soluble, these metal sulphates dissolve easily by rainwater to release acidic and metal loaded solutions. Both solutions formed by sulphide oxidation and sulphate dissolution can either accumulate into streams or acid mine lakes or flow into river waters, causing contamination.

In the river system, at upstream and acidic conditions, As was sorbed onto and removed from the water column by the suspended HFO through precipitation onto the riverbed sediments, consequently enriching the upstream riverbed sediments with contents of As. On the other hand, at downstream and neutral conditions, Cu was sorbed onto and removed from the water column by the suspended HFO and HAO through the gravitational settlement onto the riverbed sediments, consequently enriching the downstream riverbed sediments with contents of Cu. The enrichment of Cu at the downstream site was also aided by the artificial dam which

decreased the river velocity, thereby promoting the precipitation of the Cu-sorbing HAO/HFO. Additionally, the artificial dam has very important environmental significance as it prevents the downstream transportation of toxic elements. Based on the BCR sequential extraction results, the As-sorbing HFO and the Cu-sorbing HAO/HFO could be dissolved when the riverbed sediments are exposed to anoxic conditions, causing the release of Cu and As into the environment. Also, the chalcopyrite-like sulphides observed at upstream sediments could be easily oxidized to release Cu into the river system.

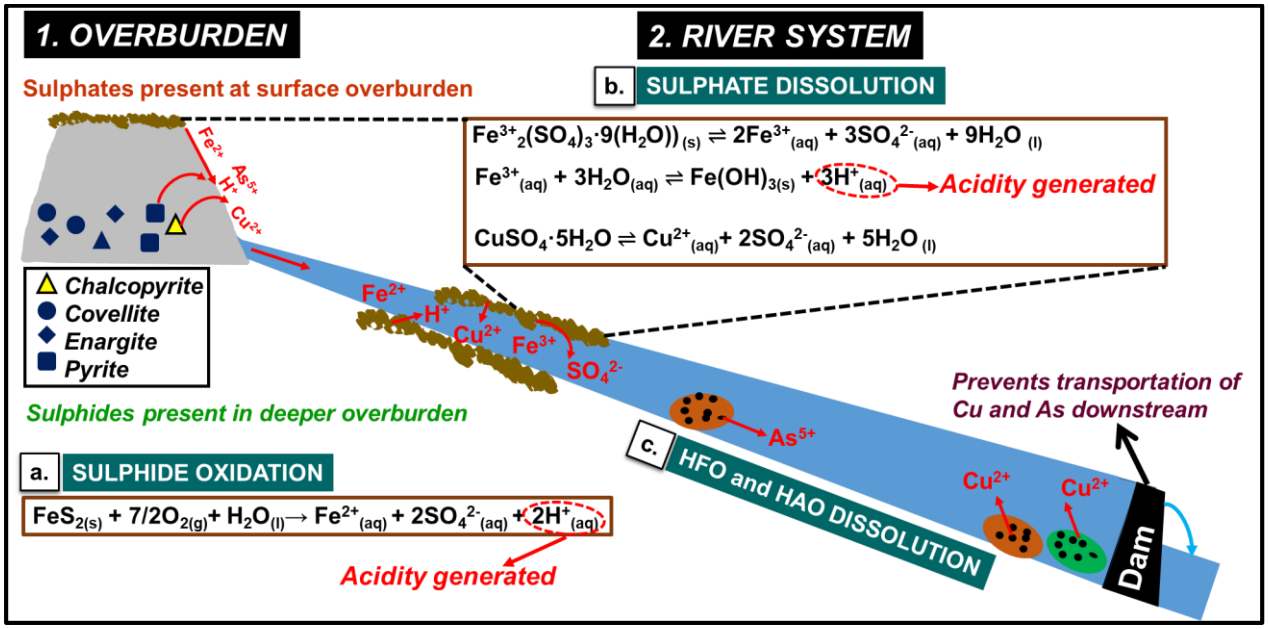

Figure 7.1 A schematic diagram summarizing environmental risks associated with mining activities in the Bor Cu mining region

On the banks of the acutely contaminated Bor River, there are Fe^{2+}, Fe^{3+}, Cu^{2+} and Mg^{2+} sulphates that form during the summer period either by evaporation of waters from the Bor River or by upward capillary migration of pore waters of the tailings-covered riverbanks. These sulphates are temporary storage of toxic elements from river waters. However, since are highly soluble, they will release acidity and toxic metal contents upon interaction with water, providing further contamination to the river system.

7.1 EFFECTS OF CLIMATE CHANGE ON SUSTAINABLE MINE WASTE MANAGEMENT

The projected trends in climate change suggest an increase of land and ocean temperatures; drier summer periods and torrents/floods in winter periods. This makes investigations of the systematic management of water resources increasingly important. Additionally, the understanding of contaminants transport from upstream to downstream in different climates is very important. The general expected change in climate in the Bor mining region is increased and decreased rainfall in the winter and summer, respectively. This means that in the winter season, due to higher rains, floods could occur and thereby transport pollutants from the mining sites by the river system, causing further contamination to the downstream areas. There could also be a second case of the accidentally release of flotation tailings from the impoundments into the Bor river system, causing contamination to sediments and floodplains. Higher rains could also suggest higher chances sulphide oxidation from the mine wastes, hence higher probability of acid mine drainage and metal release. On the other hand, drier and hotter summer periods, means lack of water resource. It also means the precipitation of hydrated metal sulphates, hence removal of toxic elements from the watercourses.

7.2 APPLICATION OF THE PhD THESIS

This PhD thesis has global applications in the fields ranging from Water and Soil Resource Management, Mine Waste Management, Environmental Geochemistry, Environmental Impact Assessment (EIA) as well as Exploration Geochemistry. Since it is generally focused on different tools and techniques of assessing and evaluating the risks of contamination from mine wastes, it can easily be applied in every study area where there is mining activities and influence of waste materials in the environment.

For example, there is plethora of mines in Botswana extracting resources such as diamond, copper, nickel, gold, coal etc. These mining activities have generated voluminous amounts of waste materials such as overburden, tailings, waste rock and slag, similar to these generated in the Bor Cu mining region. In spite of this, there are no thorough geochemical investigation on these mine wastes to determine their potential as sources of acid mine drainage. Moreover, despite the fact that Botswana has shortage of surface water due to lack of rains, there are no systemic studies that focus on the quality of water bodies in the vicinity of mining sites to determine pollution levels. Therefore, this PhD thesis will provide me with the ability to investigate the environmental risks for mine waste generated by the Cu, Ni, Au or coal mines in Botswana as well evaluating the river water and groundwater quality.

REFERENCES

Adamović, D., Ishiyama, D., Đorđievski, S., Ogawa, Y., Stevanović, Z., Kawaraya, H., Sato, H., Obradović, L., Marinković, V., Petrović, J. and Gardić, V. (2021) Estimation and comparison of the environmental impacts of acid mine drainage-bearing river water in the Bor and Majdanpek porphyry copper mining areas in Eastern Serbia. *Resource Geology*, 71, 123–143. https://doi.org/10.1111/rge.12254

Alpers, C.N., Blowes, D.W., (1994). Secondary iron-sulphate minerals as sources of sulphate and acidity. Environmental Geochemistry of Sulphide Oxidation, C.N. Alpers and D.W. Blowes (Eds.), Am. Chem. Soc. Series 550, pp. 345-364.

Alpers, C.N. and Nordstrom, D.K. (1999) Geochemical modeling of water–rock interactions in mining environments. In G.S. Plumlee and M.J. Logsdon, Eds., The Environmental Geochemistry of Mineral Deposits. Part A. Processes, Methods, and Health Issues. Society of Economic Geologists, Reviews in Economic Geology, 6A, 289–323.

Alpers, C.N., Jambor, J.L, and Nordstrom, D.K. (Eds.) (2000) Sulfate Minerals—Crystallography, Geochemistry, and Environmental Significance, 40, 608 p. Reviews in Mineralogy and Geochemistry, Mineralogical Society of America, Chantilly, Virginia. ISBN: 0-939950529

Álvarez-Valero, A.M., Pérez-López, R., Matos, J.M.A., Capitán, A., Nieto, J.M., Sáez, R., Delgado, J., Caraball, M., (2008). Potential environmental impact at São Domingos mining district (Iberian Pyrite Belt, SW Iberian Peninsula): evidence from a chemical and mineralogical characterization. Environ. Geol. 55, 1797–1809.

Álvarez-Valero, A. M., Sáez, R., Pérez-López, R., Delgado, J., & Nieto, J. M. (2009). Evaluation of heavy metal bio-availability from Almagrera pyrite-rich tailings dam (Iberian Pyrite Belt, SW Spain) based on a sequential extraction procedure. Journal of Geochemical Exploration, 102(2), 87-94.

Anju, M., & Banerjee, D. K. (2010). Comparison of two sequential extraction procedures for heavy metal partitioning in mine tailings. *Chemosphere*, *78*(11), 1393-1402. https://doi.org/10.1016/j.chemosphere.2009.12.064

Antivachis, D. N., Chatzitheodoridis, E., Skarpelis, N., & Komnitsas, K. (2017). Secondary sulphate minerals in a Cyprus-type ore deposit, Apliki, Cyprus: Mineralogy and its implications regarding the chemistry of pit lake waters. Mine Water and the Environment, 36(2), 226-238.https://doi.org/10.1007/s10230-016-0398-0

Armstong, R., Koželj, D. and Herrington, R. (2005) The Majdanpek Cu-Au Porphyry Deposit of Eastern Serbia: A Review. In: Porter, T. M. (Ed.) *Super Porphyry Copper & Gold Deposits*: *A Global Perspective*, Vol. 2. Adelaide: PGC Publishing, pp. 453–466

Arribas Jr., A., (1995). Characteristics of high sulfidation epithermal deposits and their relation to magmatic fluid. Mineral Assoc. Can. Short Course 23, 419–454.

Bandy M.C (1938) Mineralogy of three sulphate deposits at Northern Chile. In: Nordstrom DK (ed) The Effect of sulphate on aluminium concentrations in natural waters: Some stability relations in the system Al2O3–SO3–H2O at 298 K. Geochim Cosmochim Acta, vol 4, pp 681–692

Banješević, M., Đorđević, M., Ljubović-Obradović, D., & Đokić, B. (1997) The composition and age of bor clastites from the b2 drill hole at čukaru peki.

Banješević, M. (2010): Upper Cretaceous magmatic suites of the Timok Magmatic Complex. Annales géologiques de la Peninsule balkanique, 71, 13–22. https://doi.org/10.2298/GABP1071013B

Banješević, M. and Large, D. (2014) Geology and mineralization of the new copper and gold discovery south of Bor Timok magmatic complex. In *Proceedings of the XVI Serbian Geological Congress, Serbian Geological Society, Donji Milanovac* (pp. 739-741).

Banješević, M. (2015): Geološka karta Republike Srbije (Kartografska građa) [Geological Map of the Republic Serbia (Cartographic composition, Zaječar 1 – 1:50000)], Zaječar 1 – 1:50000. – Geološki zavod Srbije, Beograd.

Barcelos, D. A., Pontes, F. V., da Silva, F. A., Castro, D. C., Dos Anjos, N. O., & Castilhos, Z. C. (2020). Gold mining tailing: Environmental availability of metals and human health risk assessment. *Journal of Hazardous Materials*, *397*, 122721. https://doi.org/10.1016/j.jhazmat.2020.122721

Basallote, M.D., Cánovas, C.R., Olías, M., Pérez-López, R., Macías, F., Carrero, S., Ayora, C., & Nieto, J.M. (2019). Mineralogically-induced metal partitioning during the evaporative precipitation of efflorescent sulfate salts from acid mine drainage. *Chemical Geology*, *530*, 119339.

Berger, B.R., Ayuso, R.A., Wynn, J.C., Seal, R.R., (2008). Preliminary Model of Porphyry Copper Deposits: U.S. Geological Survey Open-file Report 2008-1321 (55 p.).

Biagioni, C.; D'Orazio, M.; Vezzoni, S.; Dini, A.; Orlandi, P. (2013) Mobilization of Tl-Hg-As-Sb-(Ag,Cu)-Pb sulfosalt melts during low-grade metamorphism in the Alpi Apuane (Tuscany, Italy). Geology, 41, 747–750.

Biagioni, C.; Mauro, D.; Pasero, M. (2020**)** Sulfates from the pyrite ore deposits of the Apuan Alps (Tuscany, Italy): A review. Minerals, 10, 1092.

Bigham JM, Nordstrom DK (2000) Iron and aluminium hydroxysulfates from acid sulfate waters. In: Alpers CN, Jambor JL, Nordstrom DK (Eds), Sulfate Minerals: Crystallography, Geochemistry, and Environmental Significance, Reviews in Mineralogy & Geochemistry, 40, MSA, Washington DC, p351—403

Bigham, J.M., Schwertmann, U., Traina, S.J., Winland, R.L., Wolf, M., (1996). Schwertmannite and the chemical modeling of iron in acid sulfate waters. Geochim. Cosmochim. Acta 60, 2111–2121.

Blowes, D.W., Reardon, E.J., Cherry, J.A., Jambor, J.L., (1991). The formation and potential importance of cemented layers in inactive sulfide mine tailings. Geochim. Cosmochim. Acta 55, 965–978.

Blowes DW and Jambor JL (1998). Modern approaches to ore and environmental mineralogy. Mineralogical Association of Canada. p. 27.

Blowes DW, Ptacek CJ, Jambor JL,Weisener CG (2003). The geochemistry of acid mine drainage. Elsevier, 149p.

Blowes, D.W., Ptacek, C.J., Jambor, J.L., Weisener, C.G., Paktunc, D., Gould, W.D., Johnson, D.B., 2014. The geochemistry of acid mine drainage. In: Reference Module in Earth Systems and Environmental SciencesTreatise on Geochemistry, Second edition, 11, pp. 131–190. https://doi.org/10.1016/B978-0-08-095975-7.00905-0.

Bogdanović, G., Trumić, M., Trumić, M. and Antić, D.V. (2011) Mining waste management – genesis and possibility of processing. *Recycling and Sustainable Development*, Vol. 4, 37–43 (in Serbian, English abstract)

Bogdanović, D., Obradović, L. and Miletić, S. (2014) Selection of the optimum method of rehabilitation the degraded areas around the Bor river downstream from the flotation tailing dump Bor. *Mining and Metallurgy Institute Bor*, 4, 137–156

Bogdanović G D, Stanković V D, Trumić M S, Antić D V, Trumić M Ž. (2016) Leaching of low-grade copper ores: A case study for "Kraku Bugaresku-Cementacija" Deposits (Eastern Serbia) [J]. Journal of Mining and Metallurgy A, 52: 45−56.

Buckby, T., Black, S., Coleman, M.L., Hodson, M.E., (2003). Fe-sulphate-rich evaporative mineral precipitates from the Rio Tinto, southwest Spain. Mineral. Mag. 67, 263–278.

Bugarin, M., Jonović, R., Avramović, L., Ljubojev, M., Stevanović, Z. and Marinković, V. (2013) Integrated Treatment of Waste Water and Solid Mining Waste. *Journal of TTEM-Technics Technologies Education Management*, 8, 423–429.

Buzatu, A., Dill, H.G., Buzgar, N., Damian, G., Maftei, A.E., & Apopei, A.I. (2016). Efflorescent sulfates from Baia Sprie mining area (Romania)--Acid mine drainage and climatological approach. *The Science of the total environment, 542 Pt A*, 629-41 .

Cala-Rivero, V., Arranz-González, J.C., Rodríguez-Gómez, V., Fernández-Naranjo, F.J., & Vadillo-Fernández, L. (2018). A preliminary study of the formation of efflorescent sulfate salts in abandoned mining areas with a view to their harvesting and subsequent recovery of copper. Minerals Engineering.

Callender, E. (2003) Heavy metals in the environment - Historical trend. In: Holland, H.D. and Turekian, K.K. (Ed.) *Treatise on Geochemistry*, Vol. 9. Elsevier, pp. 67-105.

Cánovas, C.R., Olías, M., Nieto, J.M., Sarmiento, A.M., & Cerón, J.C. (2007). Hydrogeochemical characteristics of the Tinto and Odiel Rivers (SW Spain). Factors controlling metal contents. *The Science of the total environment, 373 1*, 363-82 .

Cánovas, C.R., Olías, M., Nieto, J.M., & Galván, L. (2010). Wash-out processes of evaporitic sulfate salts in the Tinto river: Hydrogeochemical evolution and environmental impact. *Applied Geochemistry, 25*, 288-301.

Cappuyns, V., Swennen, R., & Niclaes, M. (2007). Application of the BCR sequential extraction scheme to dredged pond sediments contaminated by Pb–Zn mining: a combined geochemical and mineralogical approach. *Journal of geochemical exploration*, *93*(2), 78-90.

Carlson, L., Bigham, J.M., Schwertmann, U., Kyek, A., Wagner, F., (2002). Scavenging of As from acid mine drainage by schwertmannite and ferrihydrite: a comparison with synthetic analogues. Environ. Sci. Technol. 36, 1712–1719.

Chikanda, F., Otake, T., Koide, A., Ito, A. and Sato, T. (2021) The formation of Fe colloids and layered double hydroxides as sequestration agents in the natural remediation of mine drainage. *Science of The Total Environment*, 774. https://doi.org/10.1016/j.scitotenv.2021.145183

Chou, I.M., Seal, R.R., II, and Hemingway, B.S. (2002) Determination of melanterite-rozenite and chalcanthite-bonattite equilibria by humidity measurements at 0.1 MPa. American Mineralogist, 87, 108–114

Chou, I.M., Seal, R.R. (2003). Determination of epsomite–hexahydrite equilibria by the humidity buffer technique at 0.1 MPa with implications for phase equilibria in the system MgSO4–H2O. Astrobiology 3 (3), 619–630.

Chou I-M, Seal RR II (2007) Magnesium and calcium sulphate stabilities and the water budget of Mars. J Geophys Res 112(E11):10

Chou, M., Seal, R.R., Wang, A., (2013). The stability of sulfate and hydrated sulfate minerals near ambient conditions and their significance in environmental and planetary sciences. J. Asian Earth Sci. 62, 734–758.

Clark, A. H., & Ullrich, T. D. (2004). 40 Ar-39 Ar age data for andesitic magmatism and hydrothermal activity in the Timok Massif, eastern Serbia: implications for metallogenetic relationships in the Bor copper-gold subprovince. Mineralium Deposita, 39, 256-262.

Cody AD, Grammer TR (1979) Magnesian halotrichite from White Island. New Zealand. J. Geol. Geophys 22(4):495–498

Conić, V., Stanković, S., Marković, B., Božić, D., Stojanović, J., & Sokić, M. (2020). Investigation of the optimal technology for copper leaching from old flotation tailings of the copper mine bor (Serbia). *Metallurgical and Materials Engineering*, *26*(2), 209-222.

Consani, S., Ianni, M.C., Dinelli, E., Capello, M., Cutroneo, L., Carbone, C. (2019). Assessment of metal distribution in different Fe precipitates related to Acid Mine Drainage through two sequential extraction procedures. J. Geochem. Explor. 196, 247–258. https://doi.org/10.1016/j.gexplo.2018.10.010.

Courtin-Nomade, A., Bril, H., Neel, C., Lenain, J., (2003). Arsenic in iron cements developed within tailings of a former metalliferous mine – Enguialès, Aveyron, France. Appl. Geochem. 18, 395–408.

Cravotta, C.A., (1994). Secondary iron-sulfate minerals as sources of sulfate and acidity: geochemical evolution of acidic groundwater at a reclaimed surface coal mine in Pennsylvania. In: Alpers, C.N., Blowes, D.W. (Eds.), Environmental Geochemistry of Sulfide Oxidation. American Chemical Society, Washington DC., pp. 345–364 (Symposium Series 550).

Crowley, J.K., Williams, D.E., Hammarstrom, J.M., Piatak, N.M., Chou, I.M., Mars, J.C., (2003). Spectral reflectance properties (0.4–2.5 Am) of secondary Fe-oxide, Fe-hydroxide, and Fe-sulphate-hydrate minerals associated with sulphide-bearing mine wastes. Geochem. Explor. Environ. Anal. 3, 219–228.

Dagenhart, T.V. Jr., (1980). M.S. thesis, University of Virginia.Charlottesville.

Deditius, A.P., Utsunomiya, S., Reich, M., Kesler S.E., Ewing, R.C., Hough, R. and Walshe, J. (2011) Trace metal nanoparticles in pyrite. *Ore Geology Reviews*, 42, 32–46. https://doi.org/10.1016/j.oregeorev.2011.03.003

Dimitrijević, M.; Kostov, A.; Tasić, V.; Milosević, N. (2009) Influence of pyrometallurgical copper production on the environment. *J. Hazard. Mater. 164*, 892–899

Dold, B., (1999). Mineralogical and geochemical changes of copper flotation tailings in relation to their original composition and climatic setting—implications for acid mine drainage and element mobility. Terre Environ. 18, 1–230.

Dold, B., Fontbote, L., (2001). Element cycling and secondary mineralogy in porphyry copper tailings as a function of climate, primary mineralogy, and mineral processing. J. Geochem. Explor. 74, 3–55. https://doi.org/10.1016/S0375-6742(01)00174-1.

Dold, B., Fontbote, L., (2002). A mineralogical and geochemical study of element mobility in sulfide mine tailings of Fe oxide Cu–Au deposits from the Punta del Cobre belt, northern Chile. Chem. Geol. 189, 135–163. https://doi.org/10.1016/S0009-2541 (02)00044-X.

Dold, B., (2003). Speciation of the most soluble phases in a sequential extraction procedure adapted for geochemical studies of copper sulfide minewaste. J. Geochem. Explor. 80, 55–68. https://doi.org/10.1016/S0375-6742(03)00182-1.

D'Orazio, M.; Mauro, D.; Valerio, M.; Biagioni, C. (2021) Secondary Sulfates from the Monte Arsiccio Mine (Apuan Alps, Tuscany, Italy): Trace-Element Budget and Role in the Formation of Acid Mine Drainage. Minerals, 11, 206. https://doi.org/10.3390/min11020206

Đorđievski S., Petrović J., Krstić V., Stevanović Z., Marković R., Jonović R., Avramović L. (2016) Comparative XRD and XRF analysis of selected mine waste samples from Oštreljski Planir dump (Bor, Serbia). Recycling and sustainable development, 9, 21–27 (in Serbian, English abstract).

Đorđievski, S., Ishiyama, D., Ogawa, Y. and Stevanovic, Z. (2018) Mobility and natural attenuation of metals and arsenic in acidic waters of the drainage system of Timok River from Bor copper mines (Serbia) to Danube River. *Environmental Science and Pollution Research*, 25, 25005–25019. https://doi.org/10.1007/s11356-018-2541-x

Doulati Ardejani, F., Karami, G.H., Assadi, A.B., Dehghan, R.A., (2008). Hydrogeochemical investigations of the Shour River and groundwater affected by acid mine drainage in Sarcheshmeh porphyry copper mine. 10th International Mine Water Association Congress, Karlovy Vary, Czech Republic, pp. 235–238.

Egiebor, N. O., and Oni, B. (2007). Acid rock drainage formation and treatment: a review. *Asia-Pacific Journal of Chemical Engineering*, *2*(1), 47-62.

EJATLAS (2016). Environmental Justice Atlas: Over a century of pollution from the Bor mines, Serbia [accessed online in August, 2023]. https://ejatlas.org/conflict/over-a-century-of-the-pollution-from-the-bor-mines-serbia

Element, C. A. S. (2007). Method 3051A microwave assisted acid digestion of sediments, sludges, soils, and oils. *Z. Für Anal. Chem*, *111*, 362-366.

Elghali, A., Benzaazoua, M., Bouzahzah, H., Bussi`ere, B., Villarraga-G´omez, H., (2018). Determination of the available acid-generating potential of waste rock, part I: mineralogical approach. Appl. Geochem. 99, 31–41. https://doi.org/10.1016/j. apgeochem.2018.10.021.

EPA (1994): *Acid Mine Drainage Prediction*. Environmental Protection Agency, Washington. Technical Document EPA530–R–94–036. Order Number: PB94–201 829 (NTIS).

Fanfani, L., Nunzi, A., Zanazzi, P.F., (1970). The crystal structure of roemerite. Am. Mineral. 55, 78–89.

Fernández-Ondoño, E., Bacchetta, G., Lallena, A. M., Navarro, F. B., Ortiz, I., & Jiménez, M. N. (2017). Use of BCR sequential extraction procedures for soils and plant metal transfer predictions in contaminated mine tailings in Sardinia. *Journal of Geochemical Exploration*, *172*, 133-141. https://doi.org/10.1016/j.gexplo.2016.09.013

Ferrer F.M., Dold B., Jerez O., (2021) Dissolution kinetics and solubilities of copper sulfides in cyanide and hydrogen peroxide leaching: Applications to increase selective extractions, Journal of Geochemical Exploration, Volume 230,106848 https://doi.org/10.1016/j.gexplo.2021.106848.

Ficklin, W.H., Plumlee, G.S., Smith, K. and McHugh, J.B. (1992) Geochemical classification of mine drainages and natural drainages in mineralized areas. In: Kharaka, Y.K. and Maest, A.S. (Eds.) Proceedings, 7th International *Water-Rock Interaction Conference, Park City*, pp. 381–384.

Filgueiras, A.V., Lavilla, I. and Bendicho, C. (2002) Chemical Sequential Extraction for Metal Partitioning in Environmental Solid Samples. *Journal of environmental monitoring*, 4, 823–857. https://doi.org/10.1039/B207574C

Filimon, M.N., Nica, D.V., Ostafe, V, Bordean, D.M., Borozan, A.B., Vlad D.C. and Popescu, R. (2013) Use of enzymatic tools for biomonitoring inorganic pollution in aquatic sediments: a case study (Bor, Serbia). *Chemistry Central Journal*, 7(59). https://doi.org/10.1186/1752-153X-7-59

Filimon, M.N., Popescu, R., Horhat, F.G. and Voia, O.S. (2016) Environmental impact of mining activity in Bor area as indicated by the distribution of heavy metals and bacterial population dynamics in sediment. *Knowledge and Management of Aquatic Ecosystems*, 417(30). https://doi.org/10.1051/kmae/2016017

Filipek, L.H. and Theobald Jr., P.K., (1981). Sequential extraction techniques applied to a porphyry copper deposit in the basin and range province. J. Geochem. Explor. 14, 155–174. https://doi.org/10.1016/0375-6742(81)90110-2.

Fosso-Kankeu, E., Manyatshe, A., and Waanders, F. (2017). Mobility potential of metals in acid mine drainage occurring in the Highveld area of Mpumalanga Province in South Africa: Implication of sediments and efflorescent crusts. International Biodeterioration & Biodegradation, 119, 661-670. https://doi.org/10.1016/j.ibiod.2016.09.018.

Frau, F. (2000). The formation–dissolution–precipitation cycle of melanterite at the abandoned pyrite mine of Genna Luas in Sardinia, Italy — environmental implications. Mineral. Mag. 64, 995–1006.

Galán, E., Gómez-Ariza, J. L., González, I., Fernández-Caliani, J. C., Morales, E., & Giráldez, I. (2003). Heavy metal partitioning in river sediments severely polluted by acid mine drainage in the Iberian Pyrite Belt. Applied Geochemistry, 18(3), 409-421 . https://doi.org/10.1016/S0883-2927(02)00092-6

Gammons, C.H., Nimick, D.A., Parker, S.R., Cleasby, T.E. and Mccleskey, R.B. (2005) Diel Behavior of Iron and Other Heavy Metals in a Mountain Stream with Acidic to Neutral pH: Fisher Creek, Montana, USA. *Geochimica et Cosmochimica Acta*, 69, 2505–2516. https://doi.org/10.1016/j.gca.2004.11.020

Gammons C. H., Duaime T. E., Parker S. R., Poulson S. R. and Kennelly P. (2010) Geochemistry and stable isotope investigation of acid mine drainage associated with abondoned coal mines in central Montana, USA. Chemical Geology 269, 100–112.

García-Lorenzo, M.L., Pérez-Sirvent, C., Martínez-Sanchez, M.J., Molina-Ruiz, J., (2012). Trace elements contamination in an abandoned mining site in a semiarid zone. J. Geochem. Explor. 113, 23–35.

Gardić, V.R., Petrović, J.V., Đurđevac-Ignjatoviić, L.V., Kolaković, S.R. and Vujović, S.R. (2015) Impact assessment of mine drainage water and municipal wastewater on the surface water near the city of Bor. *Hemijska Industrija*, 69(2),165–174. (in Serbian, English abstract). https://doi.org/10.2298/HEMIND140128031G

Gardić V.R., Marković, R., Masuda, N., Sokolović, J., Petrović, J., Đorđievski, S. and Bozić, D. (2017) The study of leachability and toxicity of sludge after neutralization of Saraka and Robule AMD wastewaters. *Journal of Mining and Metallurgy A: Mining*, 53, 17–29. https://doi.org/10.5937/JMMA1701017G

Gerding, J., Novoselov, A. A., and Morales, J. (2021). Climate and pyrite: two factors to control the evolution of abandoned tailings in Northern Chile. Journal of Geochemical Exploration, 221, 106686.https://doi.org/10.1016/j.gexplo.2020.106686.

Godin, B. (1991). 4.4 The Use of Sediment in Impact Evaluation of the Mining Industry. In Sediment Issues Workshop; April 24-26, 1990 Vancouver, BC (p. 56).

Gómez, A.A. and Ruiz, M.E.G (2023). Heavy Metal Speciation, and the Evaluation and Remediation of Polluted Mine Wastes and Soils. IntechOpen. 10.5772/intechopen.110412

González, I., Romero, A., Galán, E., Pecchio, M., Andrade, F. R. D., D'agostino, L. Z., ... and Tassinari, M. M. M. L. (2004). Environmental aspects of waste dumps at the Pena del Hierro Mine (Iberian Pyrite Belt SW Spain). Applied mineralogy: developments in science and technology. ICAM, Sao Paulo, 419-422.Gray, N.F., 1996. Field assessment of acid mine drainage contamination in surface and ground water. Environ. Geol. 27, 358–361.

Gray, N.F. (1998). Acid mine drainage composition and the implications for its impact on lotic systems. Water Res. 32, 2122–2134.

Gray, N.F. (1997) Environmental impact and remediation of acid mine drainage: a management problem. *Environ.Geol.* 30, 62-71.

Grover, B. P. C., Johnson, R. H., Billing, D. G., Weiersbye, I. G., and Tutu, H. (2016). Mineralogy and geochemistry of efflorescent minerals on mine tailings and their potential impact on water chemistry. Environmental Science and Pollution Research, 23, 7338-7348.. https://doi.org/10.1007/s11356-015-5870-z

Håkanson, L. (1980) An ecological risk index for aquatic pollution control - A sedimentological approach. *Water Research*, 14(8), 975-1001. https://doi.org/10.1016/0043-1354(80)90143-8

Hammarstrom JM, Seal II RR, Meier AL, Kornfeld JM (2005) Secondary sulfate minerals associated with acid drainage in the eastern US: recycling of metals and acidity in surficial environments. Chem Geol 215:407−431

Harris, D.L., Lottermoser, B.G., Duchesne, J. (2003). Ephemeral acid mine drainage at the Montalbion silver mine, North Queensland. Aust. J. Earth. Sci. 50, 797–809

Harrison, R.M., D.P.H. Laxe, and S.J. Wilson. 1981. Chemical associations of lead, cadmium, copper and zinc in street dusts and roadside soils. Environ. Sci. Technol. 15:1378–1383.

Hickey, M.G., and J.A. Kittrick. (1984). Chemical partitioning of Cd, Cu, Ni and Zn in soils and sediments containing high levels of heavy metals. *J. Environ. Qual.* 13:372–377.

Hudson-Edwards, K. A., Schell, C., & Macklin, M. G. (1999). Mineralogy and geochemistry of alluvium contaminated by metal mining in the Rio Tinto area, southwest Spain. Applied Geochemistry, 14(8), 1015-1030.

Hurowitz JA, Tosca NJ, Darby Dyar M (2009) Acid production by $FeSO_4 \cdot nH_2O$ dissolution and implications for terrestrial and martian aquatic systems. Am Mineral 94:409—414

Ishiyama, D., Kawaraya, H., Sato, H., Obradovic, L., Blagojevic, B., Petrovic, J., Gardic, V., Stevanovic, Z., Shibayama, A., Masuda, N. and Takasaki, Y. (2012). *Geochemical characteristics of mine drainage water and river water in Bor mining area, Serbia: results of study in 2011*. Scientific and Technical Reports of Graduate School of Engineering and Resource Science, Akita University, 33, 41– 49.

Islam, N., Rabha, S., Subramanyam, K. S. V., and Saikia, B. K. (2021). Geochemistry and mineralogy of coal mine overburden (waste): A study towards their environmental implications. *Chemosphere*, *274*, 129736. https://doi.org/10.1016/j.chemosphere.2021.129736

Jambor, J.L. and Traill, R.J. (1963) On rozenite and siderotil. Canadian Mineralogist, 7, 751–763.

Jambor, J.L., Nordstrom, D.K., Alpers, C.N., (2000a). Metal-sulfate salts from sulfide mineral oxidation. In: Alpers, C.N., Jambor, J.L., Nordstrom, D.K. (Eds.), Sulfate Minerals—Crystallography, Geochemistry, and Environmental Significance. Rev.Mineral. Geochem 40, pp. 303–350.

Jamieson, H.E., Robinson, C., Alpers, C.N., McCleskey, R.B., Nordstrom, D.K., Peterson, R.C., (2005). Major and trace element composition of copiapite-group minerals and coexisting water from the Richmond mine, Iron Mountain, California. Chem. Geol. 215, 387–405.

Janković, S. (1980): Metallogenic features of copper deposits in the volcanointrusive complexes of the Bor district, Yugoslavia. – Monograph European copper deposits. Janković, S. & Sillitoe, R.H. (Eds.): SGA – Spec. publ. No 1, Copper Mining, Smelting and Refining Corporation, Bor and Department for Economic Geology, Faculty of Mining and Geology, Belgrade University, Belgrade, 42–49.

Jelenković, R., Milovanović, D., Koželj, D., Banješević, M. (2016) The Mineral Resources of the Bor Metallogenic Zone: A Review. *Geologia Croatia*, 69(1), 143–155. https://doi.org/10.4154/GC.2016.11

Jeong, Y., Yang, J. and Park, K. (2014) Changes in Water Quality After the Construction of an Estuary Dam in the Geum River Estuary Dam System, Korea. *Journal of Coastal Research*, 30, 1278–1286. https://doi.org/10.2112/JCOASTRES-D-13-00081.1

Jerz, J.K., Rimstidt, J.D., 2003. Efflorescent iron sulfate minerals: paragenesis, relative stability, and environmental impact. Am. Mineral. 88, 1919–1932.

Johnson, R.H., Blowes, D.W., Robertson,W.D., Jambor, J.L., (2000). The hydrogeochemistry of the Nickel Rimmine tailings impoundment, Sudbury, Ontario. J. Contam. Hydrol. 141, 49–80.

Kaasalainen, H., Lundberg, P., Aiglsperger, T., & Alakangas, L. (2019). Impact of declining oxygen conditions on metal (loid) release from partially oxidized waste rock. Environmental Science and Pollution Research, 26, 20712-20730.https://doi.org/10.1007/s11356-019-05115-z

Karamata, S. & Djordjević, P. (1980): Origin of the Upper Cretaceous and Tertiary magmas in the eastern part of Yugoslavia.– Bulletin Academie des Serbe des Sciences et des Arts, Classe des Sciences Mathematiques et Sciences Naturalles, v. 32, 1–p.

Karamata, S. and Krstić, B. (1996) Terranes of Serbia and neighbouring areas. In: Knežević, V., Đorđević, P. and Krstić, B. (Eds.) *Terranes of Serbia*, Belgrade University and Serbian Academy of Science and Art, Belgrade, pp. 25–40

Karamata, S., Knežević-Djordjević, V. and Milovanović, D. (2002): A review of the evolution of Upper Cretaceous–Paleogene magmatism in the Timok Magmatic Complex and the associated mineralization. –In: Koželj, D. & Jelenković, R. (eds.): Geology and metallogeny of the copper and gold deposits in the Bor Metallogenic Zone, QWERTY, Bor,15–28.

Keith, D.C., Runnells, D.D., Esposito, K.J., Chermak, J.A., Hannula, S.R., (1999). Efflorescent Sulfate Salts—Chemistry, Mineralogy, and Effects on ARD Streams. Tailings and Mine Waste '99. Balkema, Rotterdam, pp. 573–579.

Keith, D.C., Runnells, D.D., Esposito, K.J., Chermak, J.A., Levy, D.B., Hannula, S.R., Watts, M., Hall, L., (2001). Geochemical models of the impact of acidic groundwater and evaporative sulfate salts on Boulder Creek at Iron Mountain, California. Appl. Geochem. 16, 947–961.

Kerolli–Mustafa, M., Fajković, H., Rončević, S., & Ćurković, L. (2015). Assessment of metal risks from different depths of jarosite tailing waste of Trepça Zinc Industry, Kosovo based on BCR procedure. *Journal of Geochemical Exploration*, *148*, 161-168. https://doi.org/10.1016/j.gexplo.2014.09.001

Khorasanipour, M., Tangestani, M.H., Naseh, R., Hajmohammadi, H. (2011) Hydrochemistry, mineralogy and chemical fractionation of mine and processing wastes associated with porphyry copper mines: a case study from the Sarcheshmeh mine, SE Iran. *Applied Geochemistry*, 26, 714–730. https://doi.org/10.1016/j.apgeochem.2011.01.030

Khorasanipour, M., Eslami, A., (2014). Hydrogeochemistry and contamination of trace elements in Cu-porphyry mine tailings: a case study from the Sarcheshmeh Mine, SE Iran. Mine Water Environ. http://dx.doi.org/10.1007/s10230-014-0272-x.

Khorasanipour, M., (2015). Environmental mineralogy of Cu-porphyry mine tailings, a case study of semi-arid climate conditions, Sarcheshmeh mine, SE Iran. J. Geochem. Explor. 153, 40–52. https://doi.org/10.1016/j.gexplo.2015.03.001.

Kirby, C. S., & Cravotta III, C. A. (2005). Net alkalinity and net acidity 1: theoretical considerations. Applied Geochemistry, 20(10), 1920-1940.

Klein, C., and Hurlbut Jr, C. S. (1996). Manual de Mineralogía. Reverté. ISBN 8429146067.

Komnitsas K, Xenidis A, Adam K (1995) Oxidation of pyrite and arsenopyrite in sulphidic spoils in Lavrion. Miner Eng 8(12):1443–1454

Kamberovic, Z. J. (2006). Characterization of wastewater streams from Bor site.

Korac, M. and Kamberović, Ž. (2007) Characterization of wastewater streams from Bor Site. *Metalurgija*, 13(1), 41–51.

Kossoff, D., Hudson-Edwards, K. A., Dubbin, W. E., & Alfredsson, M. A. (2011). Incongruent weathering of Cd and Zn from mine tailings: a column leaching study. *Chemical Geology*, *281*(1-2), 52-71. https://doi.org/10.1016/j.chemgeo.2010.11.028

Koželj, D. I. (2002) Epithermal Gold Mineralization in the Bor Metallogenic Zone – Morphogenetic types, structural-texture varieties and potentiality. Institut za Bakar Bor, Bor (in Serbian, English summary).

Kubota, R. A. N., Ohta, A., and Okai, T. (2014). Speciation of 38 elements in eight GSJ geochemical sedimentary reference materials determined using a sequential extraction technique. *Geochemical Journal*, *48*(2), 165-188. https://doi.org/10.2343/geochemj.2.0297

Lalinská-Voleková, B., Majerová, H., Kautmanová, I., Brachtýr, O., Szabóová, D., Arendt, D., Brčeková, J. and Šottník, P. (2022) Hydrous ferric oxides (HFO's) precipitated from contaminated waters at several abandoned Sb deposits – Interdisciplinary assessment. *Science of The Total Environment*, 821. https://doi.org/10.1016/j.scitotenv.2022.153248

Lapakko, K.A., (2002). Metal Mine Rock and Waste Characterization Tools: An Overview. Minnesota Department of Natural Resources (http://www.pubs.iied.org/pdfs/G00559.pdf).

Lee, G., Bigham, J. and Faure, G. (2002) Removal of trace metals by coprecipitation with Fe, Al and Mn from natural waters contaminated with acid mine drainage in the Ducktown Mining District, Tennessee. *Applied Geochemistry*, 17, 569–581. https://doi.org/10.1016/S0883-2927(01)00125-1

Levy, D.B., Custis, K.H., Casey,W.H., Rock, P.A., (1997). A comparison of metal attenuation in mine residue and overburden material from an abandoned copper mine. Appl. Geochem. 12, 03–211.

Li, W., Chen, G., (1990). Lishizhenite — a new zinc sulfate mineral. Acta Mineral. Sin. 10 (4), 299–305.

Loredo-Jasso, A. U., Villalobos, M., Ponce-Pérez, D. B., Pi-Puig, T., Meza-Figueroa, D., del Rio-Salas, R., & Ochoa-Landín, L. (2021). Characterization and pH neutralization products of efflorescent salts from mine tailings of (semi-)arid zones. *Chemical Geology*, *580*, 120370. https://doi.org/10.1016/j.chemgeo.2021.120370

Lottermoser, B.G., (2010) Mine wastes: characterization, treatment, and environmental impacts, 3rd edn. Springer, Berlin

Lottermoser, B.G., Ashley, P., (2006). Mobility and retention of trace elements in hardpan cemented cassiterite tailings, north Queensland, Australia. Environ.Geol. 50, 835–846.

Majzlan, J., Navrotsky, A. and Schwertmann, U. (2004) Thermodynamics of iron oxides: Part III. Enthalpies of formation and stability of ferrihydrite (~$Fe(OH)_3$), schwertmannite ~$FeO(OH)_{3/4}(SO4)_{1/8}$), and ε-Fe_2O_3. *Geochimica et Cosmochimica Acta*, 68, 1049–1059. https://doi.org/10.1016/S0016-7037(03)00371-5

Markovic, Z., Stirbanovic, Z., Pantovic, R. and Kongoli, F. (2014) Sustainable Mining Waste Management in Bor Basin, Serbia. In: Kongoli, F. (Ed.) Flogen 2014: *Sustainable Industrial Processing Summit/Shechtman International Symposium, Cancun*, 2.

Marin, B., Valladon, M., Polve, M. and Monaco, A. (1997) Reproducibility testing of a sequential extraction scheme for the determination of trace metal speciation in marine reference sediment by inductively coupled plasma-mass spectrometry. *Analytica Chimica Acta*, 342, 91–112. https://doi.org/10.1016/S0003-2670(96)00580-6

McGregor, R.G., Blowes, D.W., (2002). The physical, chemical and mineralogical properties of three cemented layers within sulfide-bearing mine tailings. J. Geochem. Explor. 76,195–207.

Milton, C. and Johnston, W.D. (1938) Sulphate minerals of the Comstock Lode, Nevada. Economic Geology, 33, 749–771.

Montecinos, M., Coquery, M., Alsina, M., Bretier, M., Gaillard, J., Dabrin, A. and Pastén, P. (2020) Partitioning of copper at the confluences of Andean rivers. *Chemosphere*, 259. https://doi.org/10.1016/j.chemosphere.2020.127318

Montecinos, M., Briso, A., Vega, A. and Pastén, P. (2022) Settling of copper-rich suspended particles from acid drainage neutralization as a function of chemical composition and particle size distribution. *Applied Geochemistry*, 139. https://doi.org/10.1016/j.apgeochem.2022.105239

Moses C.O, Nordstrom DK, Herman JS, Mills AL (1987). Aqueous pyrite oxidation by dissolved oxygen and ferric iron. Geochimica et Cosmochimica Acta 51: 1561-1571.

Mossop, K. F., & Davidson, C. M. (2003). Comparison of original and modified BCR sequential extraction procedures for the fractionation of copper, iron, lead, manganese and zinc in soils and sediments. *Analytica Chimica Acta*, *478*(1), 111-118. https://doi.org/10.1016/S0003-2670(02)01485-X

Nieva, N.E.; Garcia, M.G.; Borgnino, L.; Borda, L.G. (2021) The role of efflorescent salts associated with sulfide-rich mine wastes in the short-term cycling of arsenic: Insights from XRD, XAS, and _-XRF studies. J. Hazard. Mater. 404, 124158

Nordin, A. P., da Silva, J., de Souza, C. T., Niekraszewicz, L. A. B., Dias, J. F., da Boit, K., Oliveira, M. L. S., Grivicich, I., Garcia, A. L. H., Oliveira, L. F. S., & da Silva, F. R. (2018). In vitro genotoxic effect of secondary minerals crystallized in rocks from coal mine drainage. *Journal of hazardous materials*, *346*, 263–272. https://doi.org/10.1016/j.jhazmat.2017.12.026

Nordstrom, D.K., Southam, G., Nordstrom, D.K., Southam, G., (1997). Geomicrobiology of sulfide mineral oxidation, chap. 11. In: Banfield, J.F., Nealson, K.H. (Eds.), Geomicrobiology: Interactions Between Microbes and Minerals. Reviews in Mineralogy, Min. Soc. Am. vol. 35. Mineralogical Society of America, Washington, DC, pp. 361–390.

Nordstrom, D.K. and Alpers, C.N. (1999b): Negative pH, efflorescent mineralogy, and consequences for environmental restoration at the Iron Mountain Superfund site, California. *In* Geology, Mineralogy, and Human Welfare (J.V. Smith, P.R. Buseck & M. Ross, eds.). *Proc. Nat. Acad. Sci. USA* 96, 3455-3462.

Nordstrom, D.K., (2011). Hydrogeochemical processes governing the origin, transport and fate of major and trace elements from mine wastes and mineralized rock to surface waters. Appl. Geochem. 26, 1777–1791.

Ogawa, Y., Ishiyama, D., Shikazono, N., Iwane, K., Kajiwara, M. and Tsuchiya, N. (2012) The role of hydrous ferric oxide precipitation in the fractionation of arsenic, gallium, and indium during the neutralization of acidic hot spring water by river water in the Tama River watershed, Japan, *Geochimica et Cosmochimica Acta*, 86,367–383. https://doi.org/10.1016/j.gca.2012.03.009

Ogawa, Y., Ishiyama, D., Shikazono, N., Iwane, K., Kajiwara, M. and Noriyoshi, T. (2013) Fractionation and Deposition of Indium and Arsenic from the Kusatsu and Tamagawa Acidic Hot Springs, Japan: Possible Man-Made Analogues for Rare Metal Concentrations onto Lake Beds? *Economic Geology*, 108, 1641–1656. https://doi.org/10.2113/econgeo.108.7.1641

Ogawa, Y., Ishiyama, D., Shikazono, N., Suto, K., Inoue, C., Tsuchiya, N., Saini-Eidukat, B. and Wood, S.A. (2018) Factors controlling the fractionation and seasonal mobility variations of Ga

Olías, M., Nieto, J.M., Sarmiento, A.M., Cerón, J.C., and Cánovas, C.R. (2004). Seasonal water quality variations in a river affected by acid mine drainage: The Odiel River (South West Spain). *The Science of the total environment, 333 1-3*, 267-81.

Olías M, Cánovas CR, Macías F, Basallote MD, Nieto JM. (2020) The Evolution of Pollutant Concentrations in a River Severely Affected by Acid Mine Drainage: Río Tinto (SW Spain). *Minerals*.; 10(7):598. https://doi.org/10.3390/min10070598

Onac, B.P., Veres, D.Ş., Kearns, J., Chirienco, M.I., Minut, A., Breban, R., (2003). Secondary sulfates found in an old Adit from Rosia Montana, Romania. Geologia XLVIII. Studia Universitatis Babeş-Bolyai, pp. 29–44.

Osenyeng, O., Ishiyama, D., Đorđievski, S., Adamović, D. and Ogawa, Y. (2023) Environmental risk assessment of the contamination of river water and sediments from the Bor mining area, East Serbia—Secondary Cu enrichment at the reservoir site. Resource Geology, 73(1), e12314. Available from: https://doi.org/10.1111/rge.12314

Oyarzún, J., Carvajal, M. J., Maturana, H., Núñez, J., Kretschmer, N., Amezaga, J. M. and Oyarzún, R. (2013). Hydrochemical and isotopic patterns in a calc-alkaline Cu-and Au-rich arid Andean basin: the Elqui River watershed, North Central Chile. *Applied geochemistry*, *33*, 50-63.

Palache, C., Berman, H., and Frondel, C. (1951) Dana's System of Mineralogy, v. 2. J. Wiley

Parker, S., Gammons, C., Pedrozo, F. and Wood, S. (2008) Diel changes in metal concentrations in a geogenically acidic river: Rio Agrio, Argentina. *Journal of Volcanology and Geothermal Research*, 178, 213–223. https://doi.org/10.1016/j.jvolgeores.2008.06.029

Pascaud, G., Leveque, T., Soubrand, M., Boussen, S., Joussein, E., & Dumat, C. (2014). Environmental and health risk assessment of Pb, Zn, As and Sb in soccer field soils and sediments from mine tailings: solid speciation and bioaccessibility. *Environmental Science and Pollution Research, 21*, 4254-4264.

Paunović, P. (2010) Unsuccessful attempt of regulation of Timok in order to prevent destruction of the land from industrial waste from Bor copper mine. In: Marković, Z.S. (Ed.*) Proceedings of XVIII International Scientific and Professional Meeting "Ecological Truth" Eco-Ist'10, 1-4 June, Spa Junakovic, Apatin, Serbia*. University of Belgrade – Technical Faculty in Bor, Serbia, pp. 224–251

Pedersen, H. D., Postma, D., & Jakobsen, R. (2006). Release of arsenic associated with the reduction and transformation of iron oxides. *Geochimica et Cosmochimica Acta*, *70*(16), 4116-4129.

Pérez-López, R., Nieto, J.M., Alvarez-Valero, A.M., Almodovar, G.R. (2007). Mineralogy of the hardpan formation processes in the interface between sulfide-rich sludge and fly ash: Applications for acid mine drainage mitigation. Am. Mineral 92, 1966–1977.

Peterson, R., Hammarstrom, J. and Seal, R. (2006). Alpersite $(Mg,Cu)SO_4 \cdot 7H_2O$, a new mineral of the melanterite group, and cuprian pentahydrite: Their occurrence within mine waste. *American Mineralogist*, *91*(2-3), 261-269. https://doi.org/10.2138/am.2006.1911

Pi-Puig, T., Solé, J., & Gómez Cruz, A. (2020). Mineralogical Study and Genetic Model of Efflorescent Salts and Crusts from Two Abandoned Tailings in the Taxco Mining District, Guerrero (Mexico). Minerals, 10(10), 871. https://doi.org/10.3390/min10100871

Plant, J.A., Kinniburgh, D.G., Smedley, P.L., Fordyce, F.M. and Klinck, B.A. (2005) Arsenic and selenium. In: Sherwood, B.L. (Ed.) *Environmental Geochemistry: Treatise on Geochemistry* Vol. 9. Elsevier, pp.15-66.

Plumlee, G., Smith, K., Ficklin, W.H. and Briggs, P.H. (1992) Geological and geochemical controls on the composition of mine drainages and natural drainages in mineralized areas. In: Kharaka, Y.K and Maest, A.S.(Eds.) *Water-Rock Interaction, Proceedings of the 7th International Symposium on Water-Rock Interaction, Park City, Utah, July 13-18*. Rotterdam, A.A. Balkema, pp. 419–422.

Postma, D., Jessen, S., Hue, N. T. M., Duc, M. T., Koch, C. B., Viet, P. H., and Larsen, F. (2010). Mobilization of arsenic and iron from Red River floodplain sediments, Vietnam. *Geochimica et Cosmochimica Acta*, *74*(12), 3367-3381.

Prashant, M., Ghosh, C. N., & Mandal, P. K. (2010). Use of crushed and washed overburden for stowing in underground mines: A case study. *Journal of Mines, Metals & Fuels*, *58*(1,2), 7-12.

Quispea, D., Pérez-López a, Rafael, Acerob, P., Ayorac, C., Nieto, J.M., (2013). The role of mineralogy on element mobility in two sulfide mine tailings from the Iberian Pyrite Belt (SW Spain). Chem. Geol. 345, 119–129.

Rauret, G., López-Sánchez, J.F., Sahuquillo, A., Rubio, R., Davidson, C., Ure, A.M. and Quevauviller, Ph. (1999) Improvement of the BCR Three Step Sequential Extraction Procedure Prior to the Certification of New Sediment and Soil Reference Materials. *Journal of Environmental Monitoring*, 1, 57–61. https://doi.org/10.1039/A807854H

Redwan, M., Rammlmair, D., (2012). Influence of climate, mineralogy and mineral processing on the weathering behaviour within two, low-sulfide, high-carbonate, gold mine tailings in the Eastern Desert of Egypt. Environ. Earth Sci. 65, 2179–2193.

Romero, A., González Díez, I., Galán, E., (2006). The role of sulphates efflorescences in the storage of trace elements in stream waters polluted by acid mine drainage. The case of Peña del Hierro (SW Spain). Can. Mineral. 44, 1465–1480.

Rudnick, R.L. and Gao, S. (2003) Composition of the Continental Crust. In: Holland, H.D and Turekian, K.K. (Eds.) *Treatise on Geochemistry*, Vol. 3. Elsevier, pp. 1–64. https://doi.org/10.1016/B0-08-043751-6/03016-4

Sanchéz-España, J., Velasco, F., Yusta, I., (2000). Hydrothermal alteration of felsic volcanic rocks associated with massive sulfide deposition in the northern Siberian Pyrite Belt (SW Spain). Appl. Geochem., 1265–1290.

Sanchéz-España, J., López Pamo, E., Santofimia, E., Aduvire, O., Reyes, J., Barettino, D., (2005). Acid mine drainage in the Iberian Pyrite Belt (Odiel river watershed, Huelva, SW Spain): geochemistry, mineralogy and environmental implications. Appl. Geochem. 20, 1320–1356.

Sánchez España, J., López Pamo, E., Santofimia Pastor, E., Reyes Andrés, J.,Martín Rubí, J.A., (2006). The removal of dissolvedmetals by hydroxysulphate precipitates during oxidation and neutralization of acid mine waters, Iberian Pyrite Belt. Aquat. Geochem. 12, 269–298

Sanchez-España, J. (2007) The Behavior of Iron and Aluminum in Acid Mine Drainage: Speciation, Mineralogy, and Environmental Significance. In: Letcher, T.M. (Ed.) *Thermodynamics, Solubility and Environmental Issues*, Elsevier, pp. 137–150. https://doi.org/10.1016/B978-044452707-3/50009-4

Sanchéz-España, J., (2008). Acid mine drainage in the Iberian Pyrite Belt: an overview with special emphasis on generation mechanisms, aqueous composition and associated mineral phases. Macla 10, 34–43.

Schwertmann, U. T. R. M., & Taylor, R. M. (1989). Iron oxides. Minerals in soil environments, 1, 379-438.by Acidithiobacillus ferrooxidans. Hydrometallurgy 104, 424–431.

Seal II, R. R. and Piatak, N. M., (2012). Mineralogy and environmental geochemistry of historical iron slag, Hopewell Furnace National Historic Site, Pennsylvania, USA. *Applied geochemistry*, *27*(3), 623-643.

Serbula, S., Stanković, V., Zivkovic, D., Kamberović, Ž., Gorgievski, M. and Kalinovic, T. (2016) Characteristics of Wastewater Streams Within the Bor Copper Mine and Their Influence on Pollution of the Timok River, Serbia. *Mine Water and the Environment*, 35, 480–485. https://doi.org/10.1007/s10230-016-0392-6

Schemel, L.E., Kimball, B.A. and Bencala, K.E. (2000) Colloid formation and metal transport through two mixing zones affected by acid mine drainage near Silverton, Colorado. *Appl. Geochem*. 15, 1003-1018. https://doi.org/10.1016/S0883-2927(99)00104-3

Schemel, L., Kimball, B., Runkel, R. and Cox, M. (2007) Formation of mixed Al–Fe colloidal sorbent and dissolved-colloidal partitioning of Cu and Zn in the Cement Creek – Animas River Confluence, Silverton, Colorado. *Applied Geochemistry*, 22, 1467–1484. https://doi.org/10.1016/j.apgeochem.2007.02.010

Shim, M.J., Yang, Y.M., Oh, D.Y., Lee, S. and Yoon, Y. (2015) Spatial distribution of heavy metal accumulation in the sediments after dam construction. *Environmental Monitoring and Assessment*. 187. https://doi.org/10.1007/s10661-015-4967-7

Simić, D. & Mihajlović, B. (2006): Elaborat o rezervama bakra i pratećih elemenata u ležištu Borska reka [Elaborate of reserves of copper and accompanied elements in Borska reka deposit – in Serbian, English translated]. – Ministry of Mines and Energy, Serbia, Found of geological documentation, 147 p.

Singer, D.A., Berger, V.I., Moring, B.C., (2008). Porphyry Copper Deposits of the World-Database and Grade and Tonnage Models: U.S. Geological Survey Open-file Report 2008-1155.

Smith, K. S. (1999). Metal sorption on mineral surfaces: an overview with examples relating to mineral deposits. *Reviews in economic geology*, *6*, 161-182.

Stanković, S., Moric, I., Pavic, A., Vojnović, S., Vasiljevic, B. and Cvetković, V. (2015) Bioleaching of Copper from Old Flotation Tailings Samples (Copper Mine Bor, Serbia). *Journal of the Serbian Chemical Society*, 80, 391–405. https://doi.org/10.2298/JSC140411097S

Stanojlović, R. D., Sokolović, J. M., & Milosević, N. (2014). Integrated environmental protection and waste minimization in the area of Copper Mine Bor, Serbia. *Environmental Engineering & Management Journal (EEMJ)*, *13*(4).

Stevanović, Z., Obradović, L., Marković, R., Radojka, J., Ljiljana, A., Mile, B. and Stevanović, J. (2013) Mine Waste Water Management in the Bor Municipality in Order to Protect the Bor River Water. In: Einschlag, F.S.G. and Carlos, L. (Eds.) *Waste Water - Treatment Technologies and Recent Analytical Developments*. IntechOpen http://dx.doi.org/10.5772/51902

Stoffregen, R.E., Alpers, C.N., Jambor, J.L., 2000. Alunite–jarosite crystallography, thermodynamics and geochronology. In: Alpers, C.N., Jambor, J.L., Nordstrom, D.K. (Eds.), Sulfate Minerals: Crystallography, Geochemistry, and Environmental Significance. Mineralogical Society of America, Washington, DC, pp. 453–479.

Terry, R. D., Chilingar, G. V., & Hancock, A. (1955). Comparison charts for visual estimation of percentage composition. *J. sedim. Petrol*, *25*, 229-234.

Tessier, A.P., Campbell, P.G.C. and Bisson, M. (1979) Sequential Extraction Procedure for the Speciation of Trace Metals. *Analytical Chemistry*, Vol. 51, pp. 844–851. https://doi.org/10.1021/ac50043a017

Triantafyllidis S, Skarpelis N, Komnitsas K (2007) Environmental characterization and geochemistry of Kirki, Thrace, NE Greece, abandoned flotation tailing dumps. Environ Forensics 8(4):351–359

Urošević, Snežana & Milovan, Vukovic & Pejčić, Bojana & Štrbac, Nada. (2018). Mining-metallurgical sources of pollution in eastern serbia and environmental consciousness. Revista Internacional de Contaminación Ambiental. 34:103-115.

Ure, A.M., Quevauviller, Ph., Muntau, H. and Griepink, B. (1993) Speciation of Heavy Metals in Soils and Sediments. An Account of the Improvement and Harmonization of Extraction Techniques Undertaken under the Auspices of the BCR of the Commission of the European Communities. *International Journal of Environmental Analytical Chemistry*, 51, 135–151. http://dx.doi.org/10.1080/03067319308027619

Ushakova, E., Menshikova, E., Blinov, S., Osovetsky, B., & Belkin, P. (2022). Environmental assessment impact of acid mine drainage from Kizel coal basin on the Kosva bay of the Kama Reservoir (Perm Krai, Russia). *Water*, *14*(5), 727.. https://doi.org/10.3390/w14050727

Valente, T., Leal Gomes, C., (2009). Occurrence, properties and pollution potential of environmental minerals in acid mine drainage. Sci. Total Environ. 407, 1135–1152.

Valente, T., Antunes, M., Braga, M.A., Pamplona, J., (2011). Geochemistry and mineralogy of ochre-precipitates formed as waste products of passive mine water treatment. Geochem.: Explor., Environ., Anal. 11, 103–106.

Valente, T., Grande, J.A., de la Torre, M.L., Santisteban, M., Cerón, J.C., (2013) Mineralogy and environmental relevance of AMD-precipitates from the Tharsis mines, Iberian Pyrite Belt (SW, Spain). Appl. Geochem. 39, 11–25.

Von Quadt, A., Peytcheva, I., Kamenov, B., Fanger, L., Heinrich, C. A., and Frank, M. (2002). The Elatsite porphyry copper deposit in the Panagyurishte ore district, Srednogorie zone, Bulgaria: U-Pb zircon geochronology and isotope-geochemical investigations of magmatism and ore genesis. Geological Society, London, Special Publications, 204(1), 119-135.

Von Quadt, A., Moritz, R., Peytcheva, I., & Heinrich, C. A. (2005). 3: Geochronology and geodynamics of Late Cretaceous magmatism and Cu–Au mineralization in the Panagyurishte

region of the Apuseni–Banat–Timok–Srednogorie belt, Bulgaria. Ore Geology Reviews, 27(1-4), 95-126.

Webster, J. G., Swedlund, P. J., and Webster, K. S. (1998). Trace metal adsorption onto an acid mine drainage iron (III) oxy hydroxy sulfate. *Environmental Science & Technology*, *32*(10), 1361-1368.

Wei, L., Cai M., Du Y., Tang J., Wu Q., Xiao T., Luo D., Huang X., Liu Y., Fei Y. and Chen Y. (2019) Spatial Attenuation of Mining/Smelting-Derived Metal Pollution in Sediments from Tributaries of the Upper Han River, China. *Mine Water and the Environment,* 38, 410–420. https://doi.org/10.1007/s10230-018-00583-0

Weirsma C.L. and Rimstidt J.D. (1984). Rates of reaction of pyrite and marcasite with ferric iron at pH 2. Geochimica et Cosmochimica Acta 48: 85-92.

Williams, T. and Smith, B. (2000). Hydrochemical Characterization of Acute Acid Mine Drainage at Iron Duke Mine, Mazowe, Zimbabwe. Environmental Geology. 39. 272-278. http://dx.doi.org/10.1007/s002540050006

Wu, P., Tang, C.Y., Liu, C.Q., Zhu, L.J., Pei, T.Q., Feng, L.J., (2009). Geochemical distribution and removal of As, Fe, Mn and Al in a surface water systemaffected by acidmine drainage at a coalfield in southwestern China. Environ. Geol. 57 (7), 1457–1467.

Yang, G., Yao, Y., and Shen, M. (1994) A study on the stabilization conditions of chalcanthite and the way for its preservation. Bulletin of the Chinese Academy of Geological Sciences, 29, 79–86.

Ye, Z., Zhou, J., Liao, P., Finfrock, Y., Liu, Y., Shu, C. and Liu, P. (2022) Metal (Fe, Cu, and As) transformation and association within secondary minerals in neutralized acid mine drainage characterized using X-ray absorption spectroscopy. *Applied Geochemistry*, 139, https://doi.org/10.1016/j.apgeochem.2022.105242.

Yun-Guo, L. I. U., Zhang, H. Z., Guang-Ming, Z. E. N. G., Huang, B. R., & Xin, L. I. (2006). Heavy metal accumulation in plants on Mn mine tailings. *Pedosphere*, *16*(1), 131-136. https://doi.org/10.1016/S1002-0160(06)60035-0

Yurovskii, A.Z., (1960). Sulfur in Coal. Academy of Sciences of the USSR, Moscow (translated into English and published for U.S. Dept of Interior by Indian National Scientific Documentation Centre, New Delhi, 1974).

Zhai, Y., Liu, X., Chen, H., Xu, B., Zhu, L., Li, C., and Zeng, G. (2014). Source identification and potential ecological risk assessment of heavy metals in PM2. 5 from Changsha. *Science of the Total Environment*, *493*, 109-115.

Zhao, H., Xia, B., Qin, J., Zhang, J., (2012). Hydrogeochemical and mineralogical characteristics related to heavy metal attenuation in a stream polluted by acid mine drainage: a case study in Dabaoshan Mine, China. J. Environ. Sci. 24 (6), 979–989.

Zhao, Q., Ding, J., Hong, Z., Ji, X., Wang, S., Lu, M. and Jing, Y. (2021) Impacts of water-sediment regulation on spatial-temporal variations of heavy metals in riparian sediments along the middle and lower reaches of the Yellow River. *Ecotoxicology and Environmental Safety*, 227. https://doi.org/10.1016/j.ecoenv.2021.112943

Zheng, T., Yang, J., Huang, P., Tang, C., & Wan, J. (2018). Comparison of trace element pollution, sequential extraction, and risk level in different depths of tailings with different

accumulation age from a rare earth mine in Jiangxi Province, China. *Journal of soils and sediments*, *18*, 992-1002. https://doi.org/10.1007/s11368-017-1853-7

Zhuang, S., Lu, X., Yu, B., Fan, X. and Yang, Y. (2021) Ascertaining the pollution, ecological risk and source of metal(loid)s in the upstream sediment of Danjiang River, China. *Ecological Indicators*, 125. https://doi.org/10.1016/j.ecolind.2021.107502

Zodrow, E.L., Wiltshire, J. & Mccandlish, K. (1979): Hydrated sulfates from Sydney Coalfield, Cape Breton Island, Nova Scotia. II. Pyrite and its alteration products. *Can. Mineral*. 17, 63-70.

APPENDICES

Appendix 1 Physical parameters and concentrations of major cations and anions in filtered waters samples collected in August 2019

Sample ID	pH -	Eh mV	Na mg/L	K mg/L	Mg mg/L	Ca mg/L	F^- mg/L	NO_3^- mg/L	Cl^- mg/L	SO_4^{2-} mg/L	$^aHCO_3^-$ mg/L
RW1	2.85	655	56	8.7	112.5	356	6.2	0.0	32.5	2830	-
RW2	7.75	439	94.9	6.7	84.5	554	-	50.7	14.1	1800	134.1
RW3	8.31	400	5.5	2.7	6.1	95.4	0.01	6.2	4.6	27	243.8
RW4	3.09	635	58.7	7.4	90	374	3.6	14.8	23.1	2110	-
RW5	3.68	533	63.6	9.0	74.1	410	3.2	6.6	21.8	1810	-
RW6	3.14	652	53.1	8.2	80	416	3.1	6.8	25.7	1920	-
RW7	7.45	42	29.5	4.1	10	76.9	0.02	0.0	19.8	8.2	359.5
RW8	6.53	416	26.5	4.4	25.1	146.2	0.4	1.4	17.8	380	170.6

Appendix 2 Physical parameters and concentrations of major cations and anions in filtered waters samples collected in August 2015

Unit	Discharge (m^3/min)	pH	Eh mV	Na mg/L	K mg/L	Mg mg/L	Ca mg/L	Cl^- mg/L	SO_4^{2-} mg/L	HCO_3^- mg/L
LOD	–	–	–	0.005	0.03	0.002	0.7	0.03	0.03	–
RW1	35	4.17	697	54.5	8.6	83.4	291	32.3	1510	–
RW2	33.7	4.49	707	98.2	12.5	79.3	477	41.1	2060	–
RW3	6.6	8.41	636	8.4	3.5	10.4	76.4	5.5	42.2	249.9
RW4	43.4	4.45	687	71.1	10.5	78	343	33.1	1590	–
RW5	55.6	4.66	688	57.8	7.9	71.4	298	29.4	1360	–
RW6	44.1	4.46	815	54.5	7.7	62.4	276	30.8	1430	–
RW7	174	7.29	420	20	2.9	12.2	73.9	17.9	46.7	254
RW8	218	7.22	541	30.1	4.8	25.6	118	20.3	348	100.4
RW9	218	7.9	647	8.9	2.1	11	94.2	7.9	118	206.9
RW10	218	8.02	615	7.8	2.2	9.9	95.6	6.6	111	213.2

Appendix 3 Concentrations of metals and arsenic from filtered and unfiltered river water samples collected in August 2019

		Al	Fe	Cu	Mn	Zn	Ni	Co	Cd	As	Pb	Tl
Unit		µg/L	µg/L	µg/L	µg/L	µg/L	µg/L	µg/L	µg/L	µg/L	µg/L	µg/L
RW1	Unfilt	98,700	341,700	116,300	10,800	14,900	1430	235	841	2694	673	7.8
	Filt	97,700	270,000	109,300	10,600	11,000	1050	184	831	653	399	7.6
RW2	Unfilt	11,200	9190	3080	6960	156	77.6	138	1.5	3.1	4.38	0.07
	Filt	260	80	73.9	6480	32.3	41.3	101	1.2	1.6	0.04	0.04
RW3	Unfilt	167	127	4.2	5.6	10.1	4.4	0.27	0.02	1.8	0.17	0
	Filt	140	60	1.6	1.6	0.72	4.4	0.22	0.02	1.7	0.08	0
RW4	Unfilt	61,300	196,000	68,100	8610	7740	628	143	497	1548	306	4.5
	Filt	59,300	120,300	66,800	8210	7080	628	138	497	129	238	4.5
RW5	Unfilt	49,700	153,300	52,600	6740	6280	505	110	391	1350	296	3.9
	Filt	46,300	80,000	51,100	6520	5590	488	105	391	38	199	3.9
RW6	Unfilt	53,700	84,700	55,200	6810	6480	534	118	425	499	385	4
	Filt	52,700	39,700	54,700	6770	6130	531	114	422	16.6	354	4
RW7	Unfilt	180	100	10.1	22.6	10.3	3.6	0.33	0.22	2.7	0.53	0
	Filt	147	100	1.8	22.2	7.7	3.6	0.33	0.22	2.7	0.27	0
RW8	Unfilt	873	1170	2560	1300	1038	87.8	19.3	64.5	6.3	5.89	0.69
	Filt	187	140	1550	1240	772	85.6	18.8	61.9	3.6	0.75	0.65

Appendix 4 Concentrations of metals and arsenic from filtered and unfiltered river water samples collected in August 2015

Sample ID		Al	Fe	Cu	Mn	Zn	Ni	[a] Co	Cd	As	Pb
	Unit	µg/L	µg/L	µg/L	µg/L	µg/L	µg/L	µg/L	µg/L	µg/L	µg/L
RW1	Unfilt	17,100	79,800	26,300	7770	2500	392	112	21.9	352	54.9
	Filt	16,000	26,400	24,200	6650	3190	420	106	22.2	17.7	20.4
RW2	Unfilt	32,600	46,100	31,500	7460	714	93.7	213	5.9	60.2	1.2
	Filt	29,200	12,200	30,500	5880	998	107	225	6.4	1.3	0.45
RW3	Unfilt	46.2	<100	2.6	7.24	2.5	<0.6	0.087	<0.02	2.8	0.17
	Filt	<4	<100	<0.4	<0.2	<1	<0.6	0.01	<0.02	1.5	<0.02
RW4	Unfilt	32,400	32,000	39,900	8190	3160	265	168	18.1	1830	218
	Filt	14,900	19,300	24,200	6020	3014	280	141	15.1	28.6	9.4
RW5	Unfilt	14,300	48,900	21,000	5040	1680	215	136	13.7	395	62.8
	Filt	10,600	11,200	18,900	5530	1838	234	136	13.5	8.3	8.9
RW6	Unfilt	12,700	45,400	23,100	5010	1540	223	122	12.7	373	43.1
	Filt	7550	240	17,200	4620	2020	219	119	14.3	2.4	7.8
RW7	Unfilt	41	<100	4.5	38.3	3.6	<0.6	0.115	<0.02	2.3	0.26
	Filt	53.6	<100	3.8	34.9	10.7	<0.6	0.124	<0.02	2.4	1.2
RW8	Unfilt	120	670	535	1490	127	37.1	24.6	1.4	7.2	0.47
	Filt	50.4	<100	114	1100	87.5	31.5	19.9	2.5	2.9	0.77

Appendix 5 Mineralogical characteristics of the riverbed sediments obtained by X-ray diffraction. Data published by Đorđievski et al. (2018)

		RS1	RS2	RS3	RS4	RS5	RS6	RS7	RS8	RS9	RS10
Silicate minerals	Quartz	+	+	+	+	+	+	+	+	+	+
	Plagioclase		+	+		+	+	+	+	+	+
	Amphibole	+	+	+		+	+	+	+	+	+
Clay minerals	Illite		+	+	+	+	+	+	+	+	+
	Kaolinite	+			+						+
	Chlorite		+	+		+	+	+	+	+	
	Pyrophyllite		+		+	+	+				
Fe-rich minerals	Fayalite	+			+	+	+				
	Magnetite	+			+	+	+				
	Pyrite	+	+		+	+	+		+		
Sulfate minerals	Jarosite									+	+
	Alunite									+	+
	Gypsum								+		
Carbonate minerals	Calcite			+				+	+		

Appendix 6: Upstream-downstream variations in mobility of toxic metals during the 2019 and 2015 sampling campaigns

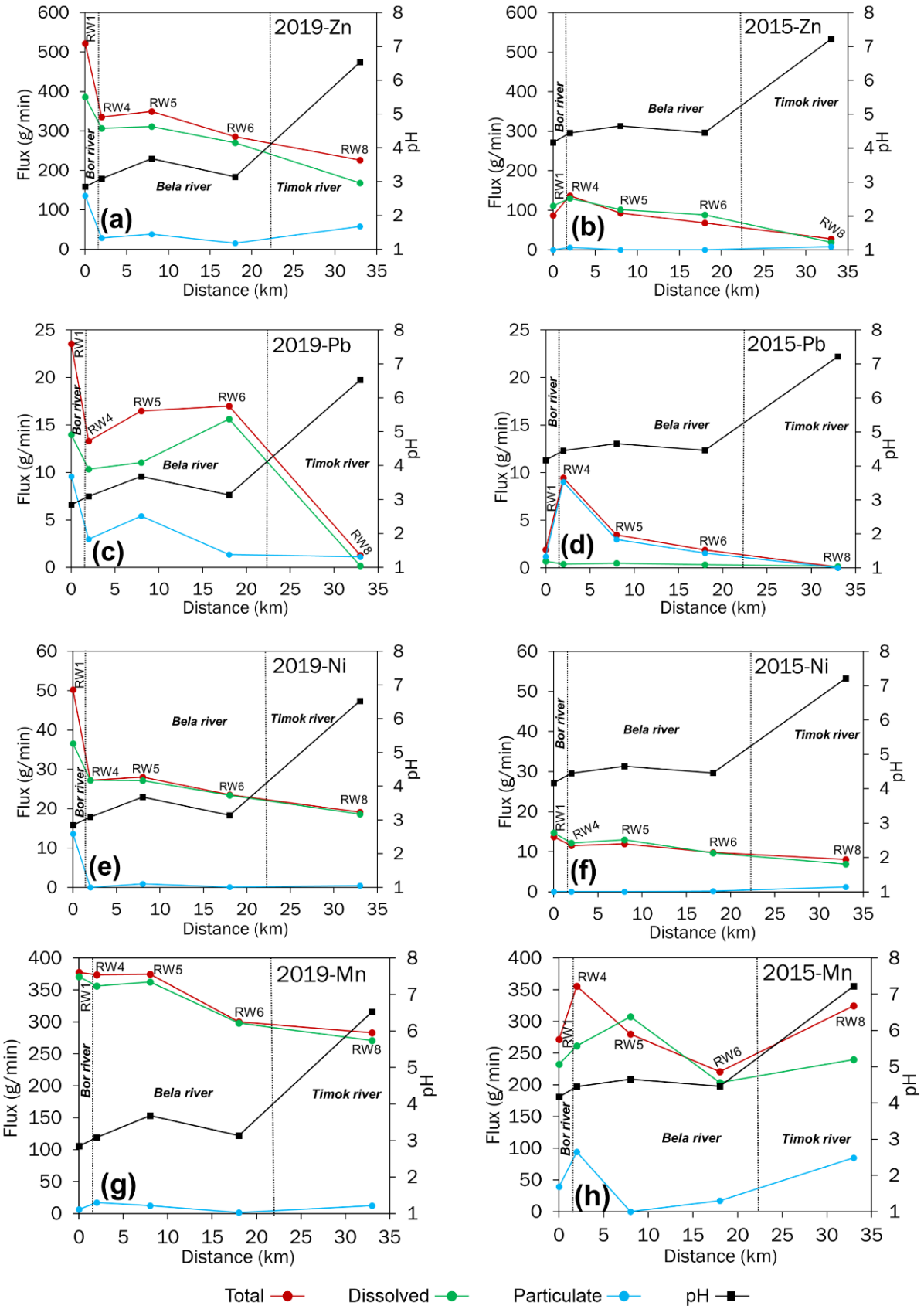

Appendix 7 Map of the study area showing sample locations of flotation tailings, overburden and evaporative salts precipitated from the mine wastes

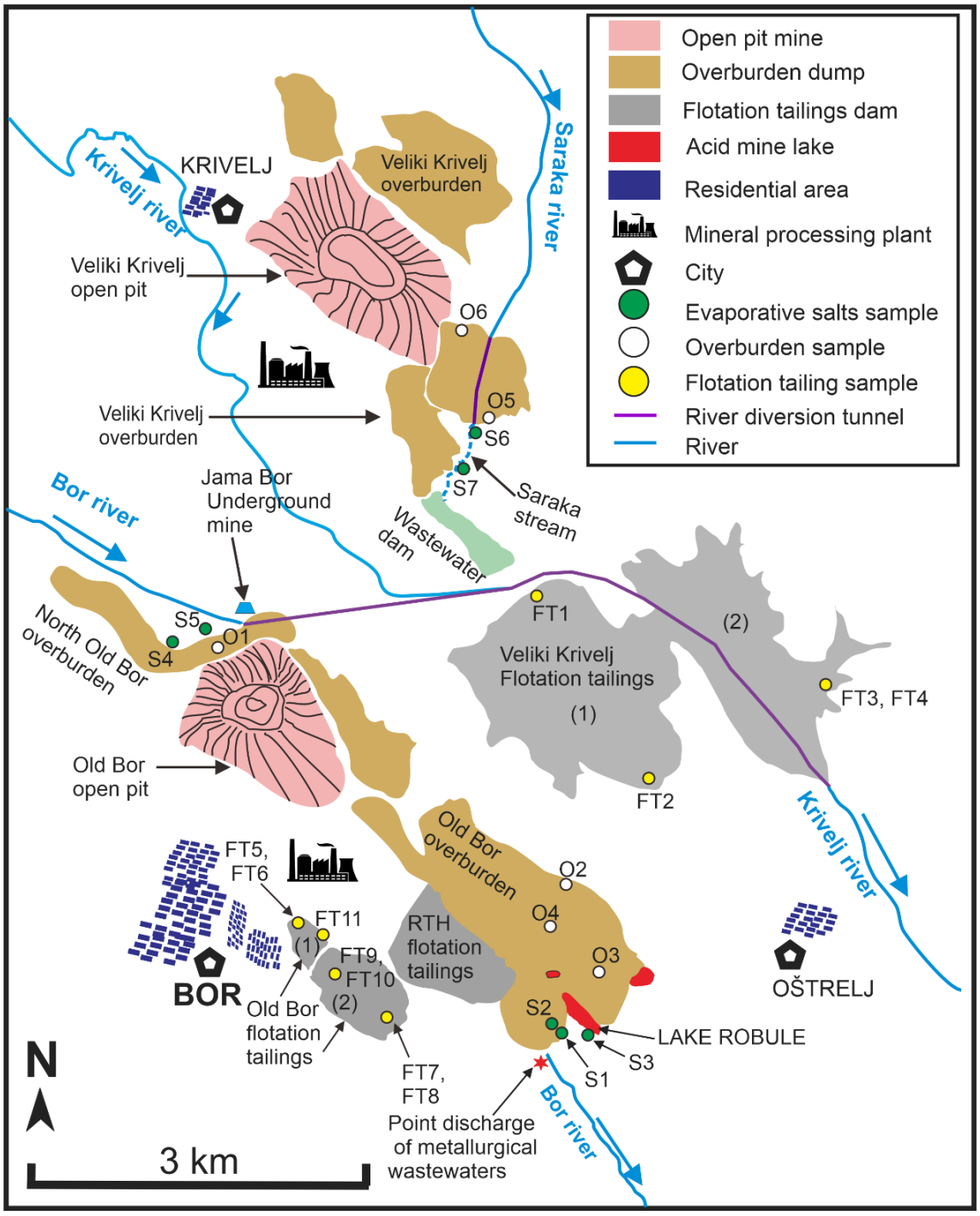

Appendix 8: Map of the study area showing sample locations of tailings on a floodplain near the confluence of Bela River and Timok River (Vrazogrnac village)

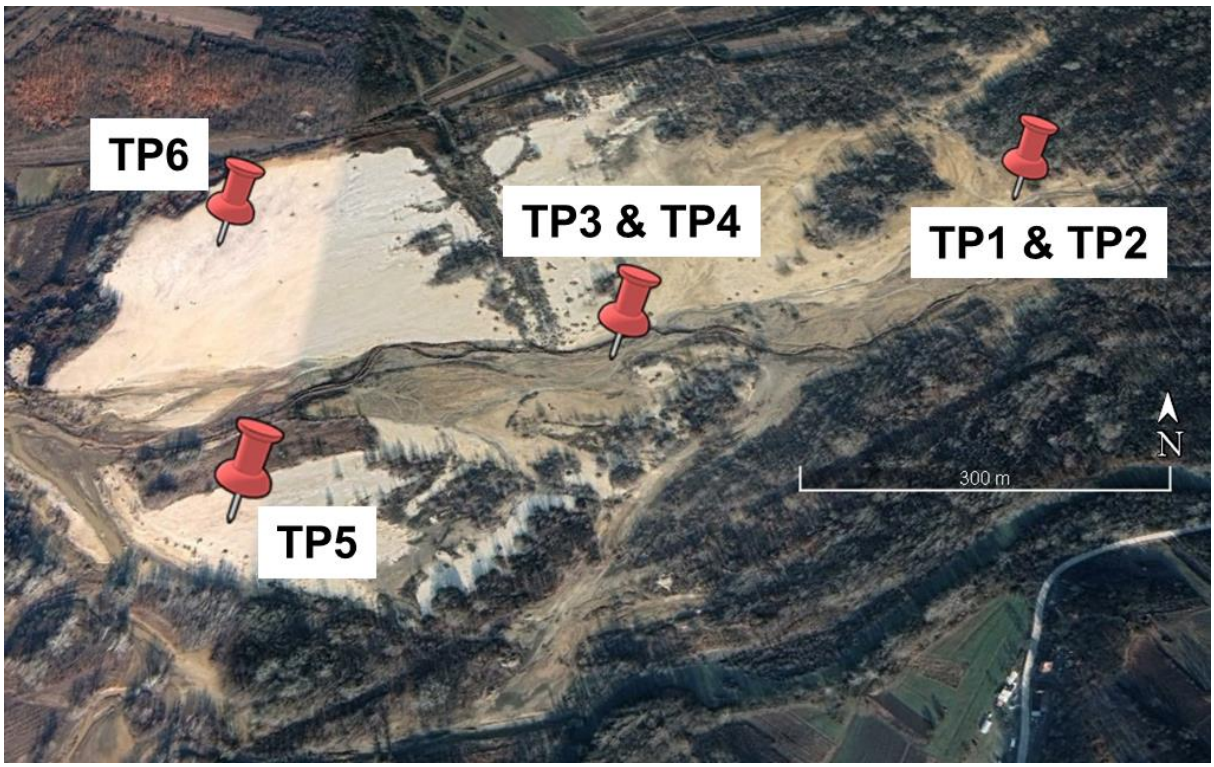

Appendix 9: Bulk XRD patterns of Veliki Krivelj waste rocks

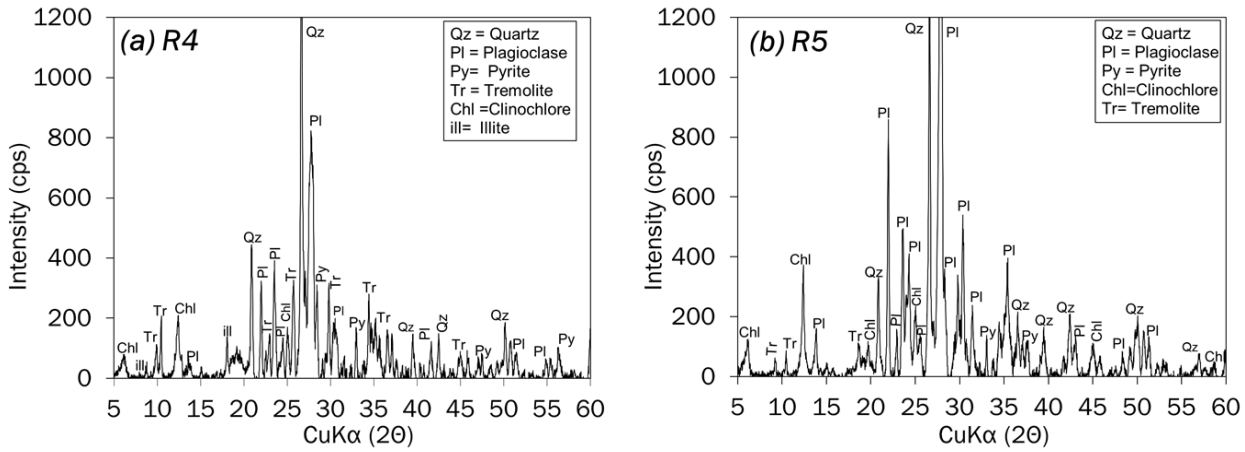

Appendix 10: Bulk XRD patterns of the evaporative salts from Old Bor and Veliki mine waste

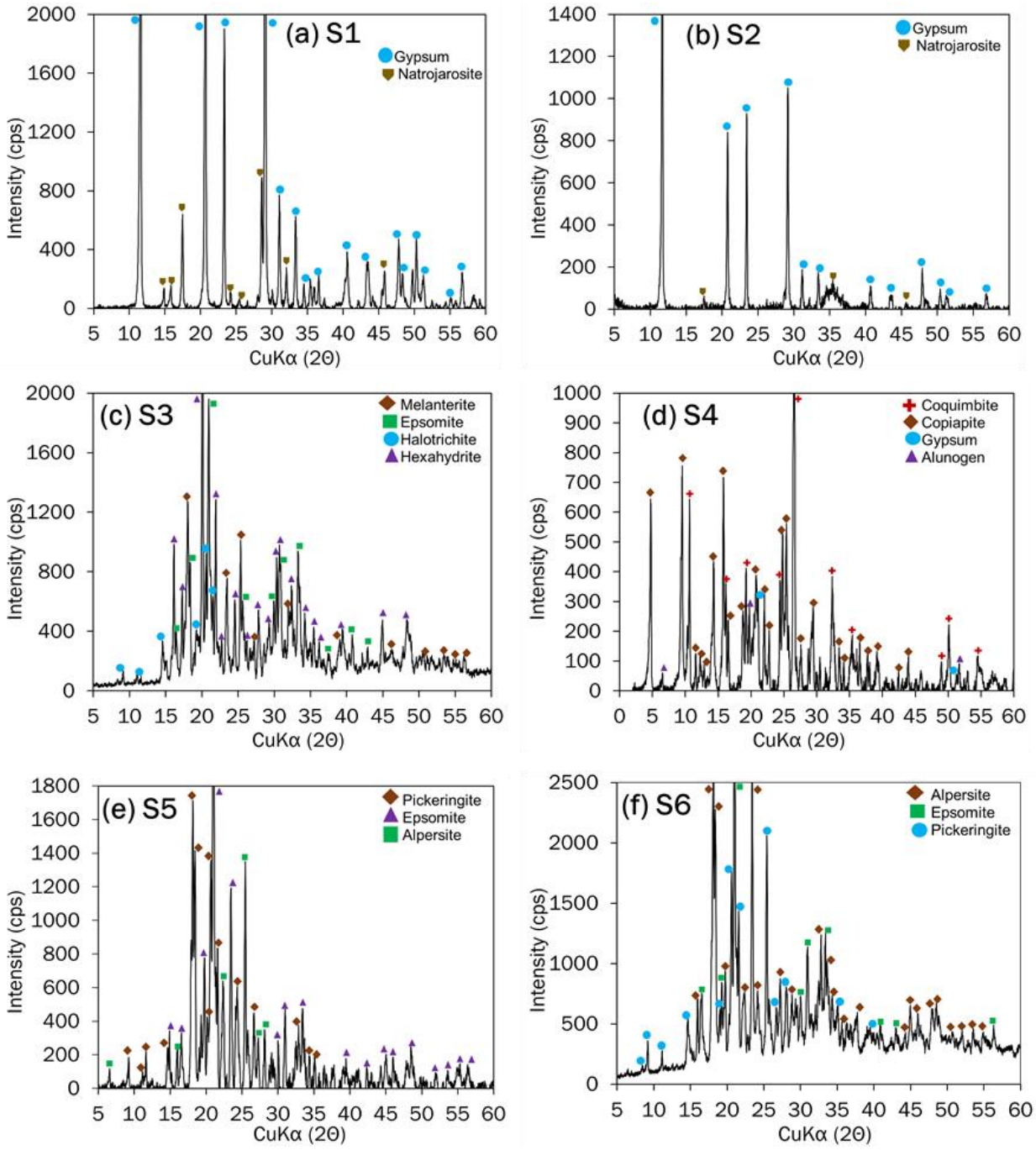

Appendix 11: SEM-EDS results of the efflorescent salts from Old Bor and Veliki Krivelj mine wastes. Back scattered electron (BSE) images on the right with corresponding EDS spectra on the left, showing elements present in the salt

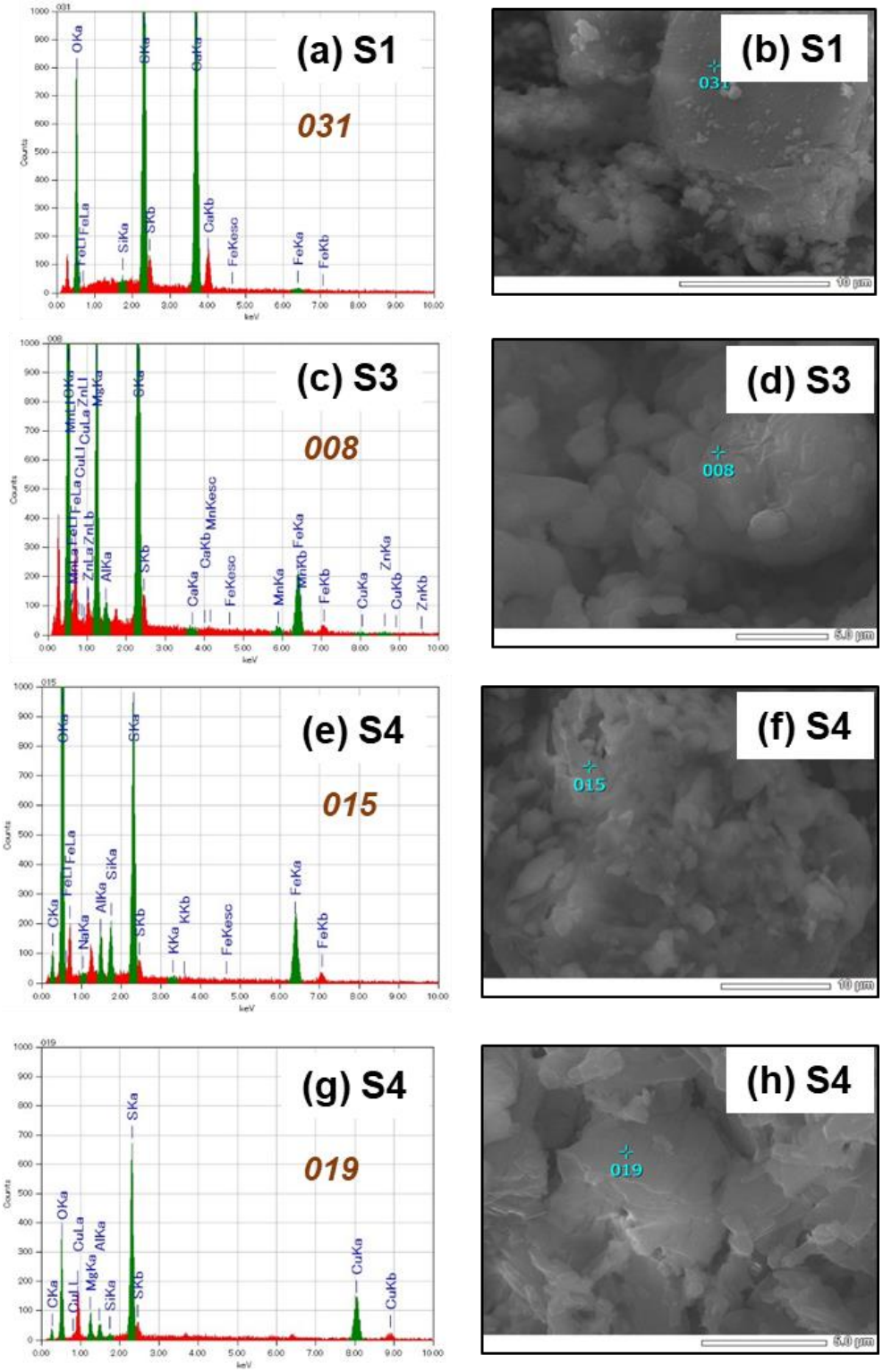

Appendix 12: Concentrations of dissolved metals and As released into solution during the 2-hour dissolution of evaporative salts with distilled water (pH 5.6)

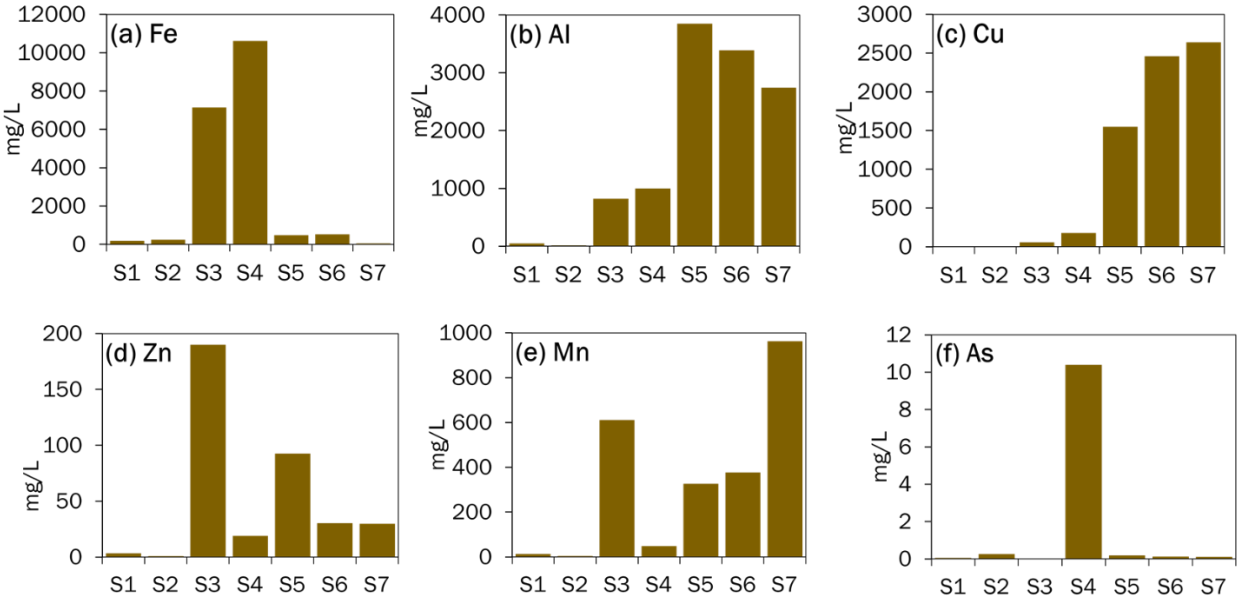

Appendix 13: pH and concentrations of dissolved Fe, Fe^{2+} and Fe^{3+} released into solution during the 2-hour dissolution of Old Bor and Veliki Krivelj evaporative salts with distilled water (pH 5.6)

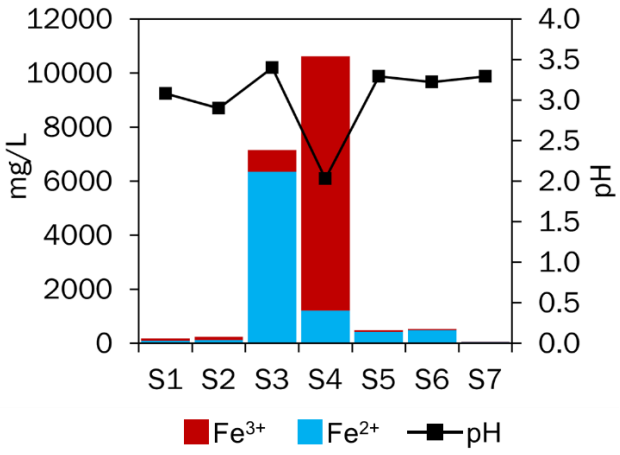

Appendix 14: Variations in pH and concentrations of dissolved metals and As released into solution during the 6-hour distilled water (pH 5.6) dissolution of flotation tailings (FTs) and overburden (OBs) after exposure to simulated weathering conditions

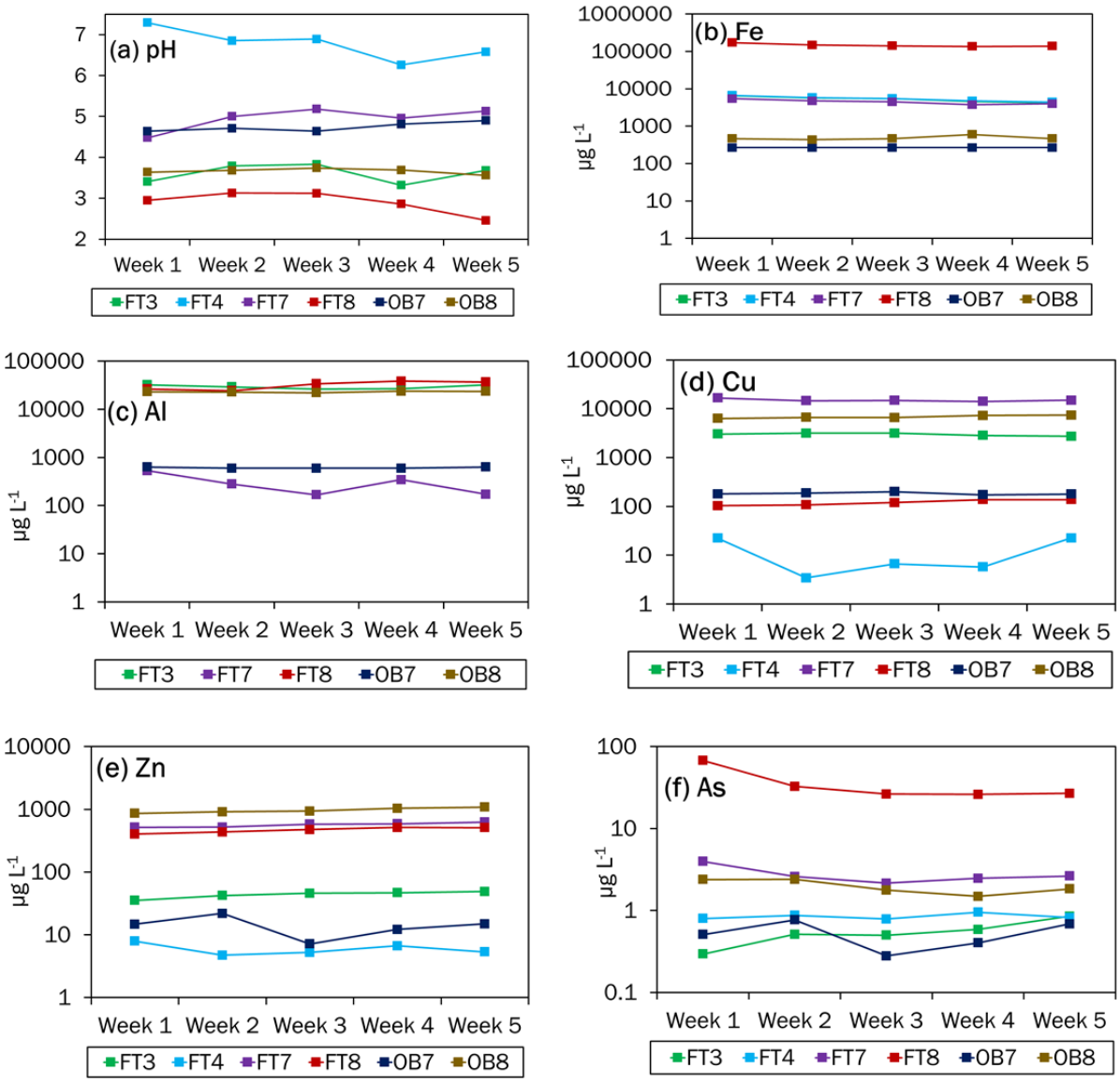

Appendix 15: Variations in pH after reacting riverbed sediments with distilled water **(a)**, HCO_3^- at different concentrations **(b)**, and H_2SO_4 solution at different pH condition **(c)**

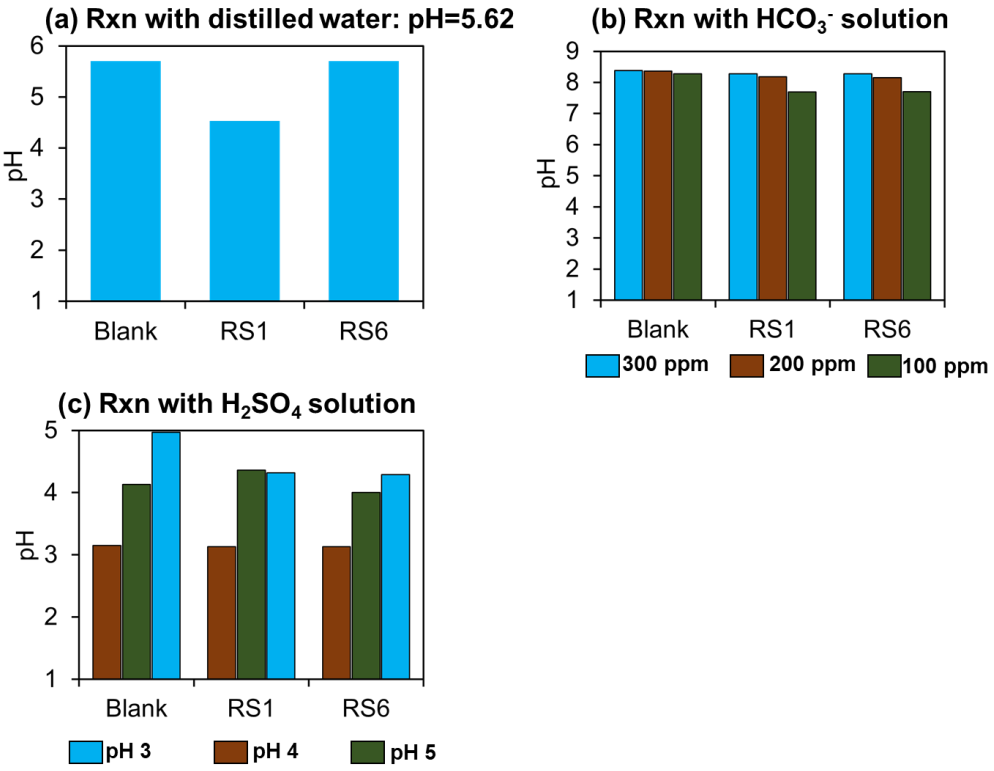

Appendix 16: Comparison in contents of toxic metals extracted by BCR Σ (Step 1+2+3) vs HCl extraction from riverbed sediments

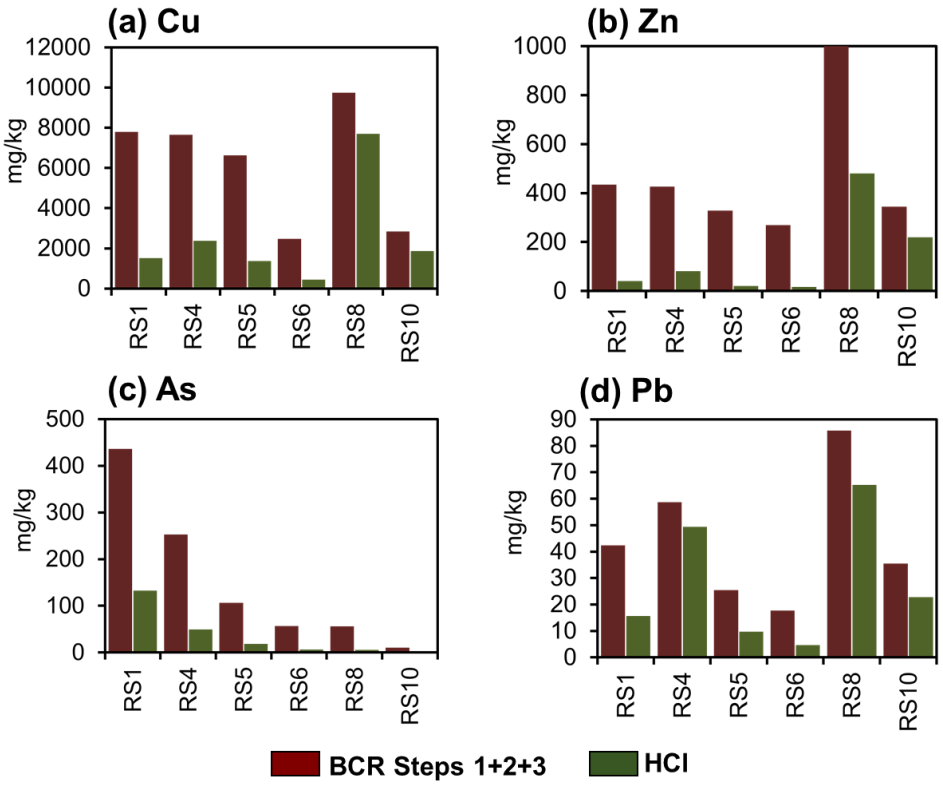

Appendix 17: Results from the five-step sequential extraction of waste rocks

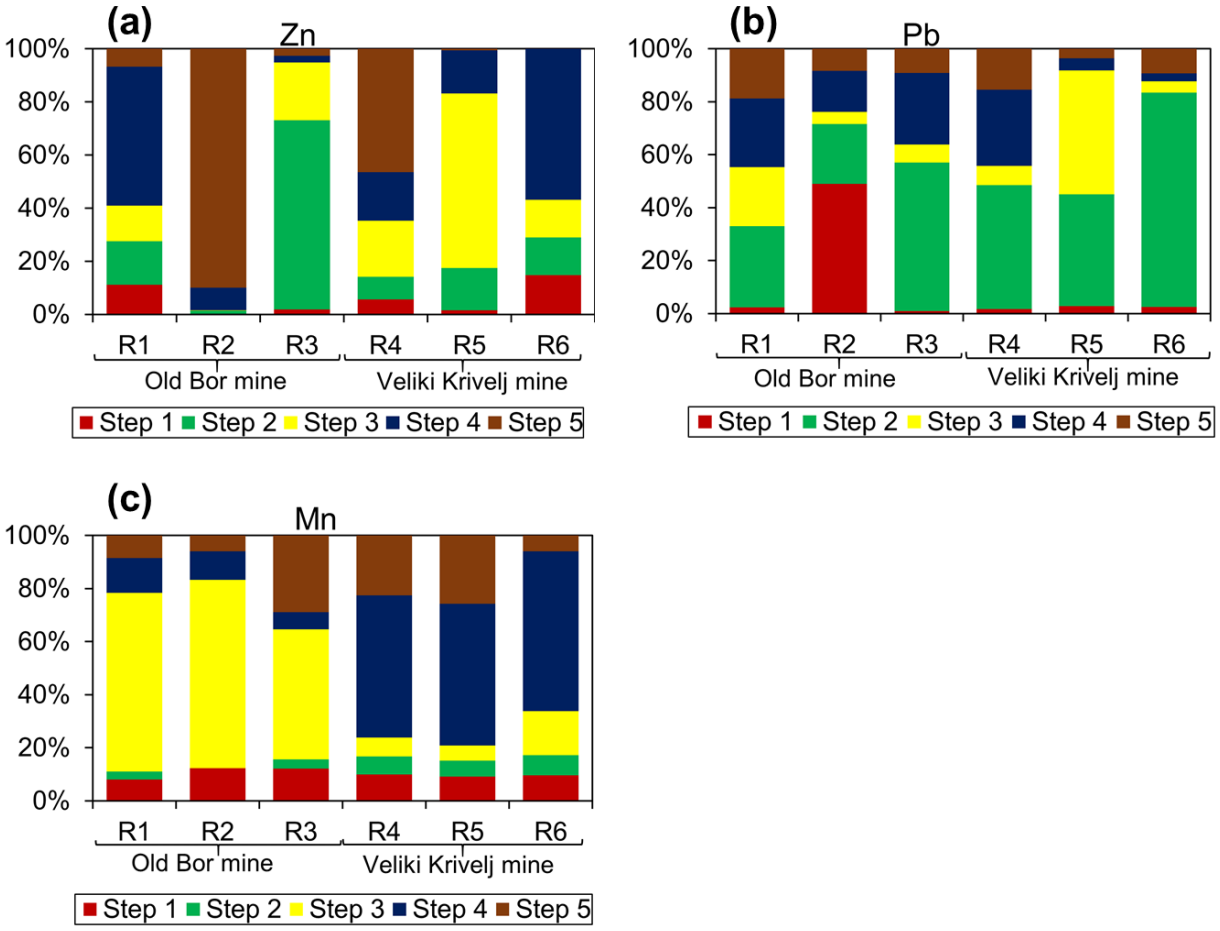

Appendix 18: Results from the five-step sequential extraction of overburden

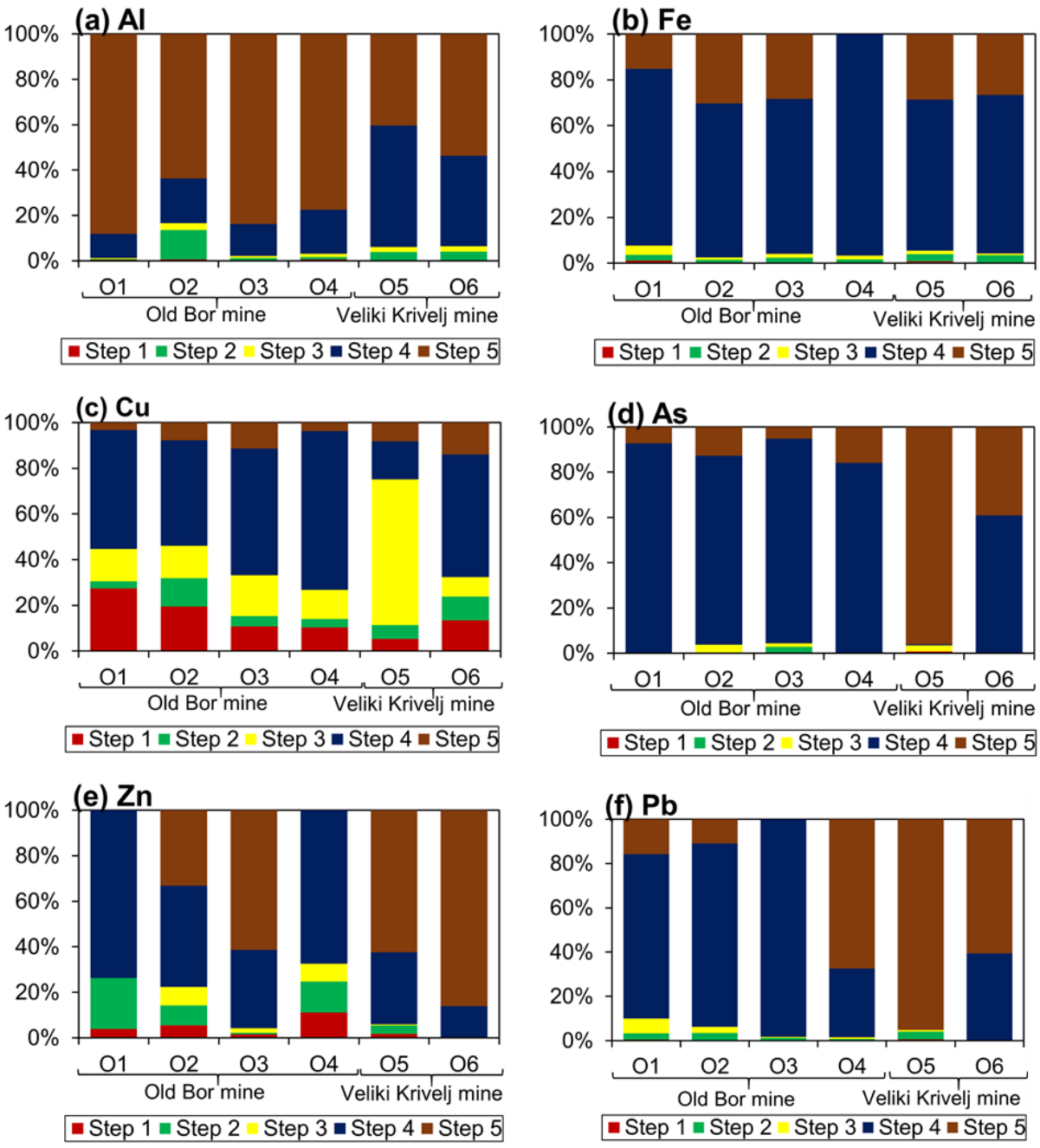

Appendix 19: Results from the five-step sequential extraction of flotation tailings

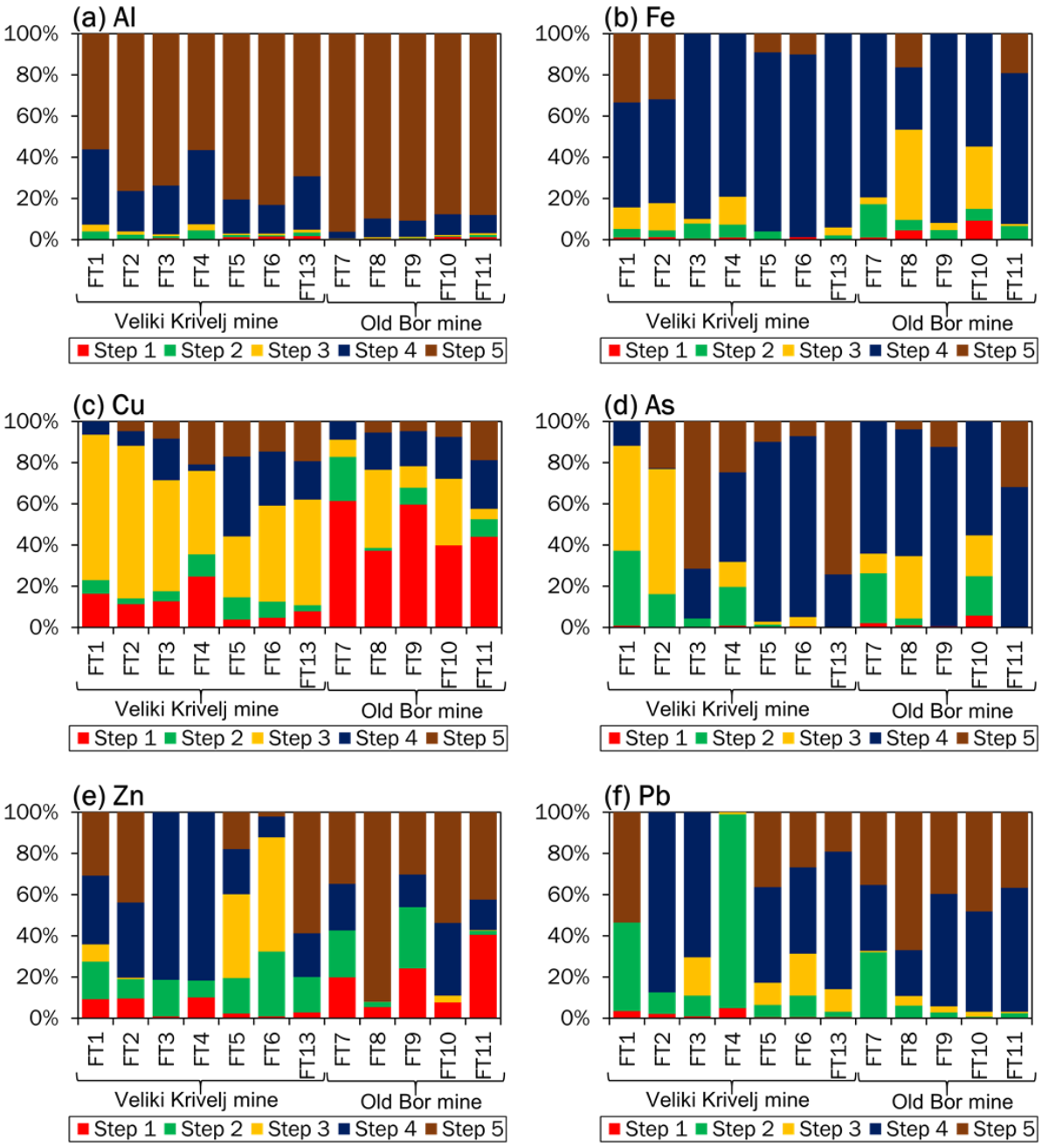

Appendix 20: Results from the five-step sequential extraction of tailings-covered river floodplains

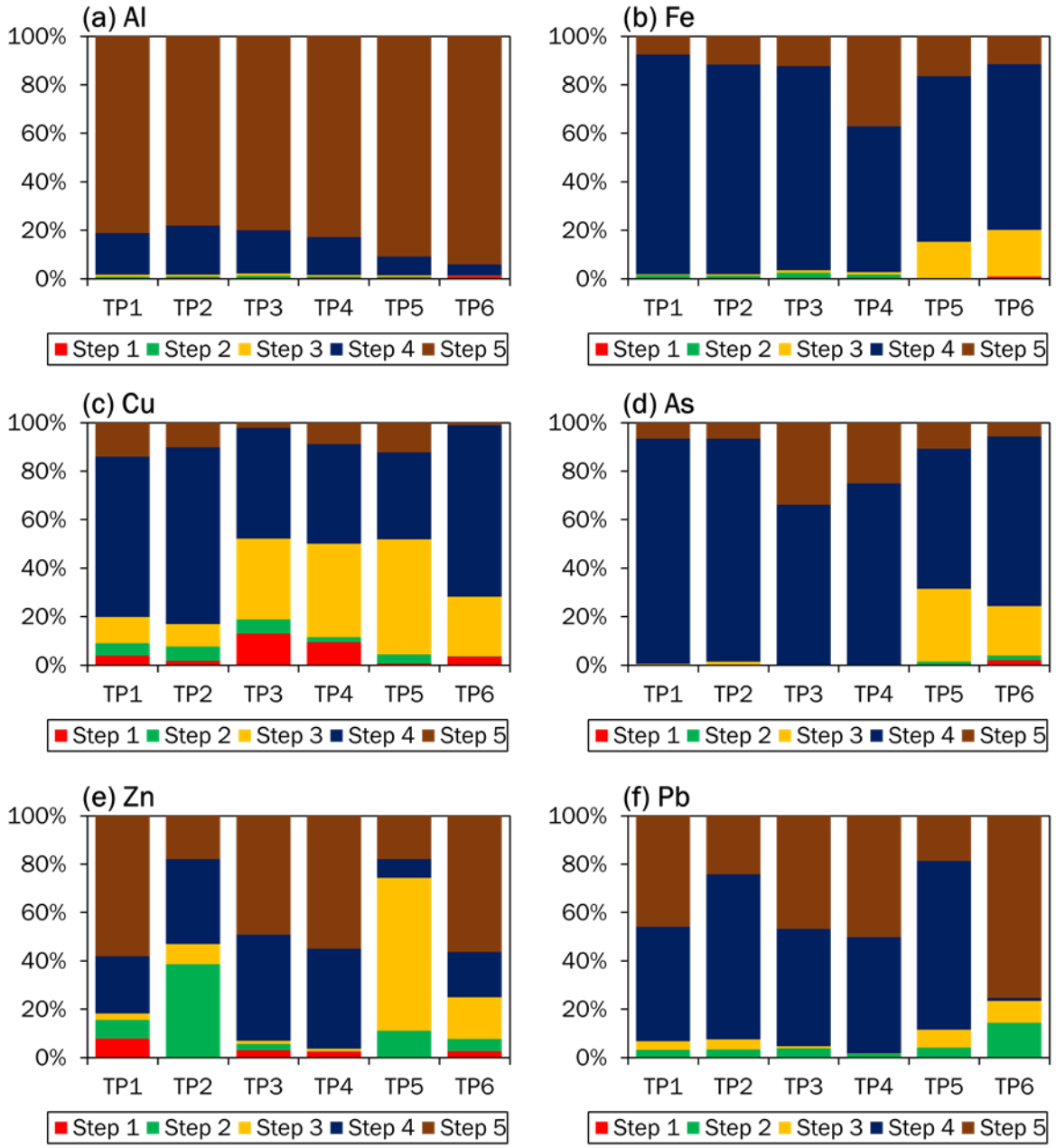

Appendix 21: BCR sequential extraction of toxic metals from the mainstream riverbed sediments

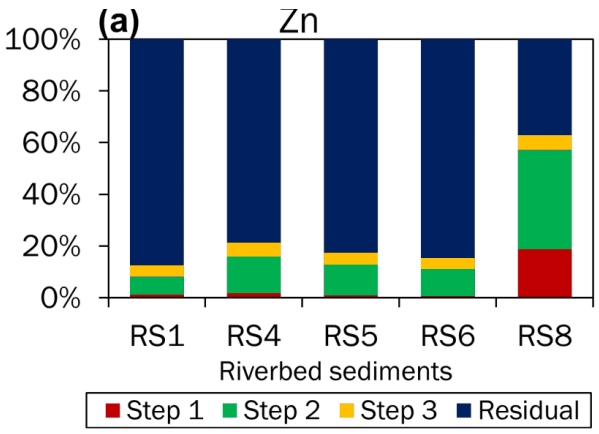

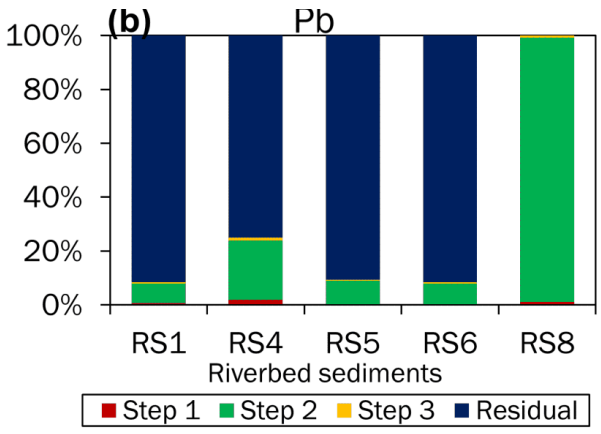

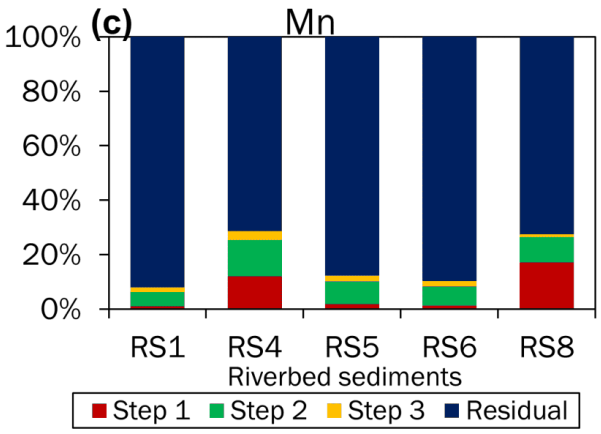

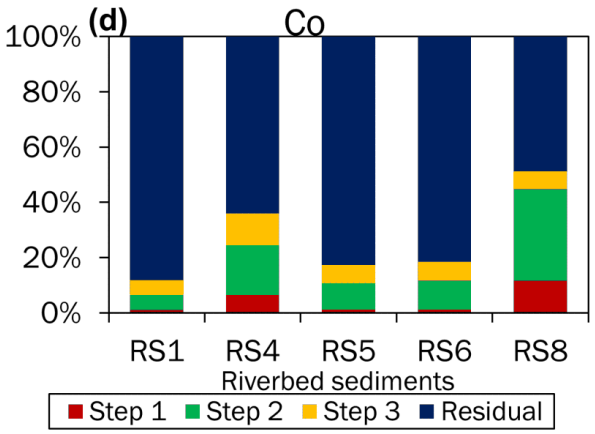

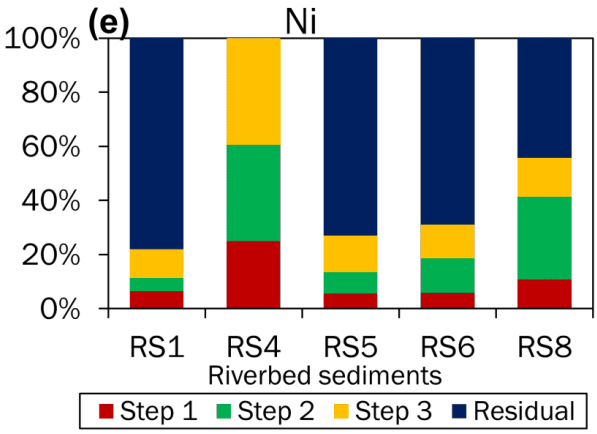

Appendix 22: 5-step modified BCR sequential extraction of toxic metals from the Krivelj River shallower floodplain (RS3) sample after exposure to weathering conditions for 5 weeks

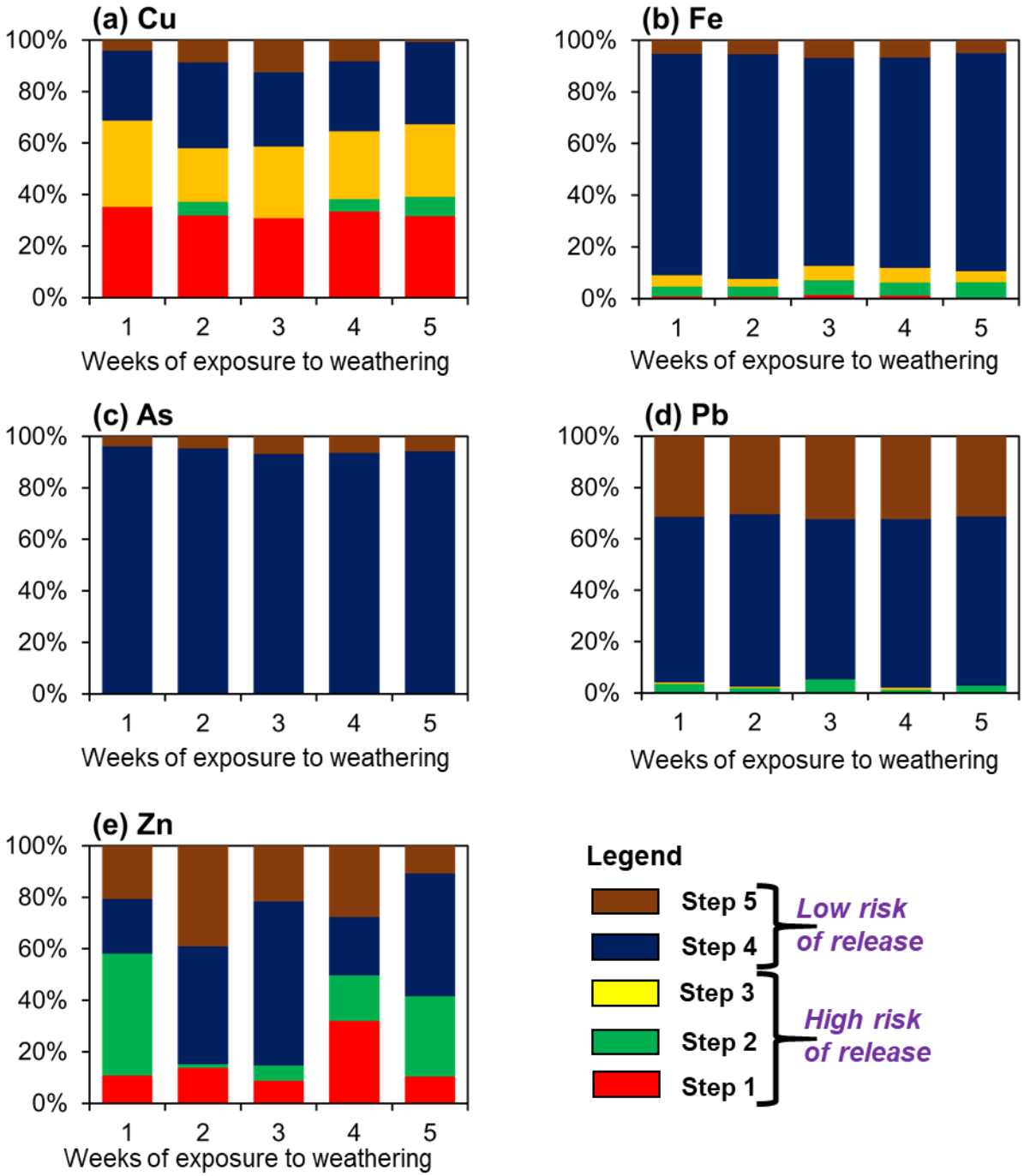

Appendix 23: 5-step modified BCR sequential extraction of toxic metals from the Krivelj River deeper floodplain (RS4) sample after exposure to weathering conditions for 5 weeks